The role of β-hairpins in protein aggregation

Inaugural-Dissertation

for the attainment of the title of doctor
in the Faculty of Mathematics and Natural Sciences
at the Heinrich-Heine-Universität Düsseldorf

presented by

Laetitia Françoise Heid

from Frankfurt am Main, Germany

Düsseldorf, September 2023

From the Institut für Physikalische Biologie at the Heinrich-Heine-Universität Düsseldorf

Published by permission of the Faculty of Mathematics and Natural Sciences at
Heinrich-Heine-Universität Düsseldorf

Supervisor:

1. Junior Prof. Dr. Wolfgang Hoyer
2. Prof. Dr. Thomas Kurz

Date of the oral examination: 18.12.2023

Declaration

I hereby declare under oath that I have compiled this dissertation independently and without any undue assistance by third parties under consideration of the “Fundamental principles for safeguarding good scientific practice at Heinrich-Heine-Universität Düsseldorf”. Furthermore, neither this dissertation, nor similar work, has been submitted to another faculty. I have not made any unsuccessful attempt to obtain a doctorate.

Düsseldorf,

Laetitia Françoise Heid

Acknowledgements

First and foremost, I want to thank Jun.-Prof. Dr. Wolfgang Hoyer as my first supervisor for giving me the opportunity to work on his projects and for his endless patience, support, opportunities to go to various conferences, explanations, discussions, and availability during my PhD time. He provided a working environment and especially a group with a relaxed atmosphere where one could have fun with science and discussions and as a whole group on various occasions and during times spend outside of the lab together with a lot of laughter.

Second, I would like to thank Prof. Dr. Thomas Kurz as my second supervisor who had an open ear for me during tough times, who was quickly available whenever it was necessary and ensured that I would stick to my point when I knew I was right.

Thank you also to the rest of the WolfGang current and former members for being such an open, fun and science loving group, where one could always ask for help no matter what it was or even just for a short talk.

A big thank you also goes my former colleagues and now good friends Dr. Nadine Rösener and Dr. Lisa Galle who laughed with me, helped me with questions concerning science but also life. Helped me to keep a clear head and let me rant if I needed it and took a lot of walks and pictures with me in the botanical garden and to just talk about any- and everything or having a nice coffee with some sweets on slower days or spending time together outside the lab.

Thank you to all former and current TAs of the lab Elke Reinartz, Barabara Schulten, Robin Backer, Linda Reinecke, and Joanna Zeyer for all the help with things in the lab, ordering and a lot more.

I am grateful to the whole IPB, current and former members, PIs, students, PhDs, and PostDocs I had a lot of fun over all these years not only during my PhD but also before that. It really feels a bit like the end of an era. I will miss the atmosphere, the science, the parties, and gatherings (spontaneous and planned) and the people.

Thank you, Prof. Dr. Dieter Willbold for letting me work for such a long time at your Institute.

A big thank you also to my parents and grandparents because without them this journey until here would not have been possible so easily. Thank you for your endless support and patience during this, not always easy journey, and for always listening.

Another big thank you goes to my dancing teachers, especially Gabi, who kept me fit and provided an excellent distraction when I had too much to think about and just wanted to relax and clear my mind. Thank you for all the fun in classes, giving me confidence in myself, keeping me motivated and showing me that I can still do it.

Of course, thank you also to my other friends, the ones in Frankfurt and Schwerte.

Finally, I am sure there are many more people that I need to thank but I could not possibly write down all of you. So, whoever I did not list thank you!

“Everything that is real was imagined first.”

– The velveteen Rabbit

“Le monde est un livre dont chaque pas ouvre une page.”

– Alphonse de Lamartine

List of Publications and Manuscripts

Agerschou E D, Flagmeier P, Saridaki T, Galvagnion C, Komnig D, Heid L, Prasad V, Shaykhalishahi H, Willbold D, Dobson C M, Voigt A, Falkenburger B, Hoyer W, Buell A K, *An engineered monomer binding-protein for α-synuclein efficiently inhibits the proliferation of amyloid fibrils*, eLife, Volume 8:e46112, Published August 2019, https://doi.org/10.7554/eLife.46112

Heid L F, Agerschou A D, Orr A A, Kupreichyk T, Schneider W, Wördehoff M W, Schwarten M, Willbold D, Tamamis P, Stoldt M, Hoyer W, *Sequence-based identification of amyloidogenic β-hairpins reveals a prostatic acid phosphatase fragment promoting semen amyloid formation*, submitted to Computational and Structural Biotechnology Journal, August 31st 2023

Heid L F, Kupreichyk T, Schützmann M P, Stoldt M, Hoyer W, *Nucleation of α-synuclein amyloid fibrils induced by cross-interaction with β-hairpin peptides derived from immunoglobulin light chains*, submitted to International Journal of Molecular Sciences, September 15st 2023

Summary

The β-hairpin is a common motif in protein folds and represents the smallest possible β-sheet. It consists of two β-strands that are connected by a turn and align in an antiparallel fashion, which allows formation of backbone hydrogen bonds as well as interactions among side chains in the neighboring strands. β-hairpins are spread throughout all living species and building blocks of larger β-sheets. β-hairpins have gained interest in the research field of the diseases that involve amyloids. If two or more β-strands form hydrogen bonds between each other β-sheets begin to build. In amyloid diseases, such β-sheets grow in length along the fibril axis until they form extremely stable fibrils that, despite the involvement of different proteins with widely different sequences, have a highly consistent morphology consisting of a cross-β-structure where the parallel β-strands run perpendicular to the fibril axis. Such amyloid fibrils are linked to many diseases, in particular neurodegenerative diseases and non-neuropathic systemic amyloidosis.

In the projects of this thesis, different β-hairpins were identified and characterized, with regard to their role in amyloid formation and to their interaction with engineered binding proteins. One project explores how widespread amyloidogenic β-hairpins are in the human proteome. The second project aims to explore if amyloidogenic β-hairpins interfere with amyloid formation of sequence-unrelated proteins, to test if β-hairpins might contribute to the cross-interaction and cross-seeding phenomena previously described for different amyloid systems. In a third project the aim was to optimize compounds that bind β-hairpins and can inhibit the amyloid formation on the protein and small molecule level. On the protein level that meant to optimize the β-wrapin AS69, that can bind α-synuclein in a coupled-folded binding mode and optimize it via molecular dynamics simulation and characterize those new constructs via isothermal titration calorimetry. On the other hand, to approach the inhibition of α-synuclein aggregation with small molecules first steps to develop a high throughput screening assay have been taken to be able to identify the correct molecules that can bind the α-synuclein β-hairpin. In a fourth project the expression and purification of two model proteins for light-chain amyloidosis was established with sequences that also carry a β-hairpin motif with the same characteristics as those found in for example α-synuclein. With an established expression and purification protocol the next step was to find the correct conditions for those two proteins to aggregate and to test the potential of β-wrapin AS10 to inhibit aggregation.

The overall aim of this thesis is to further elucidate the role of β-hairpins in amyloid formation and delineate their potential to serve as targets in anti-amyloid inhibition approaches.

Contents

General Introduction

The β-hairpin is one of several secondary structure motifs a protein can take, apart from the other known ones like α-helices and unstructured motifs. [24, 26] The β-hairpin is known also as β-sheet, one β-hairpin is the smallest possible β-sheet. [1] It is the simplest motif but one that is stable and spread throughout all living species and is a building block of larger β-sheets. [1] Structurally a β-hairpin consists of two β-strands connected by a short turn. [1] If formed in proteins and peptides, the β-hairpin is often found in its antiparallel form, where the two involved β-strands are neighboring each other and connected by a short loop in the primary sequence of the protein. [1, 23, 24, 25] The antiparallel motif is also the energetically more favorable one, as the hydrogen bonds can form in perfect alignment, the so-called registry. [3, 12, 26] The two β-strands involved in the antiparallel β-hairpin are mainly stabilized non-covalently by hydrogen bonding, which can happen in different patterns also called registries depending on the sequence of the protein or peptide. [12, 24, 25] Other interactions that help stabilize β-hairpins are hydrophobic, electrostatic and van der Waals interactions between the two β-strand sequences. [24, 25] As these interactions are additive, the stability of an isolated β-hairpin depends on the length of the two β-strands. While β-hairpins are often found in folded proteins, they will usually not retain their structure in aqueous solutions if only the sequence part that contains the β-hairpin is extracted from the protein. [3] Until today it requires certain sequences or specialized mimics to form stable β-hairpins in short peptides. Despite being one of the simplest secondary structure motifs in proteins and peptides β-hairpins are stable once formed, can be highly adaptable and can be widely functionalized. [5] In their natural environment, they are involved in a wide range of biological functions, like protein-protein interactions, forming larger structures (β-barrels) or even in smaller formats as antimicrobial peptides. [5] This makes them also interesting for engineering purposes and further uses in the already mentioned antimicrobial peptides or even in material sciences. [5] Designed β-hairpins could maybe even be used as mini-receptors or as a pharmacophore display scaffold for drug discovery. [5] Thus, β-hairpins, despite their simplicity, make an interesting object to study.

β-hairpins also gained interest in another research field, namely that of the diseases that involve amyloids. [12] As already mentioned at the very beginning, β-hairpins are building blocks of β-sheets. If two or more β-strands form hydrogen bonds between each other β-sheets begin to

build. [23, 24] The β-sheets are, like the β-hairpin, stabilized by non-covalent interactions with hydrogen bonds, electrostatics, hydrophobic and van der Waals interactions plus, if aromatic amino acids are involved, by the stacking of the π-π electron systems of the aromatic rings. [23, 24, 25] In amyloid diseases, such β-sheets grow in length along the fibril axis until they form extremely stable fibrils that, despite the involvement of different proteins with widely different sequences, have a highly consistent morphology consisting of a cross-β-structure where the parallel β-strands run perpendicular to the fibril axis. [4, 5, 12, 13] In the following, the focus will be primarily on the most known amyloidogenic diseases and what is known about the involvement of β-hairpins in the fibril formation of Alzheimer's disease (AD), Parkinson's disease (PD), and Diabetes type II (DTII). [12]

Different studies over the years, experimental and simulations, showed that the β-hairpin plays a role in aggregation in two directions, either to inhibit aggregation or to accelerate it. [2, 4, 5]

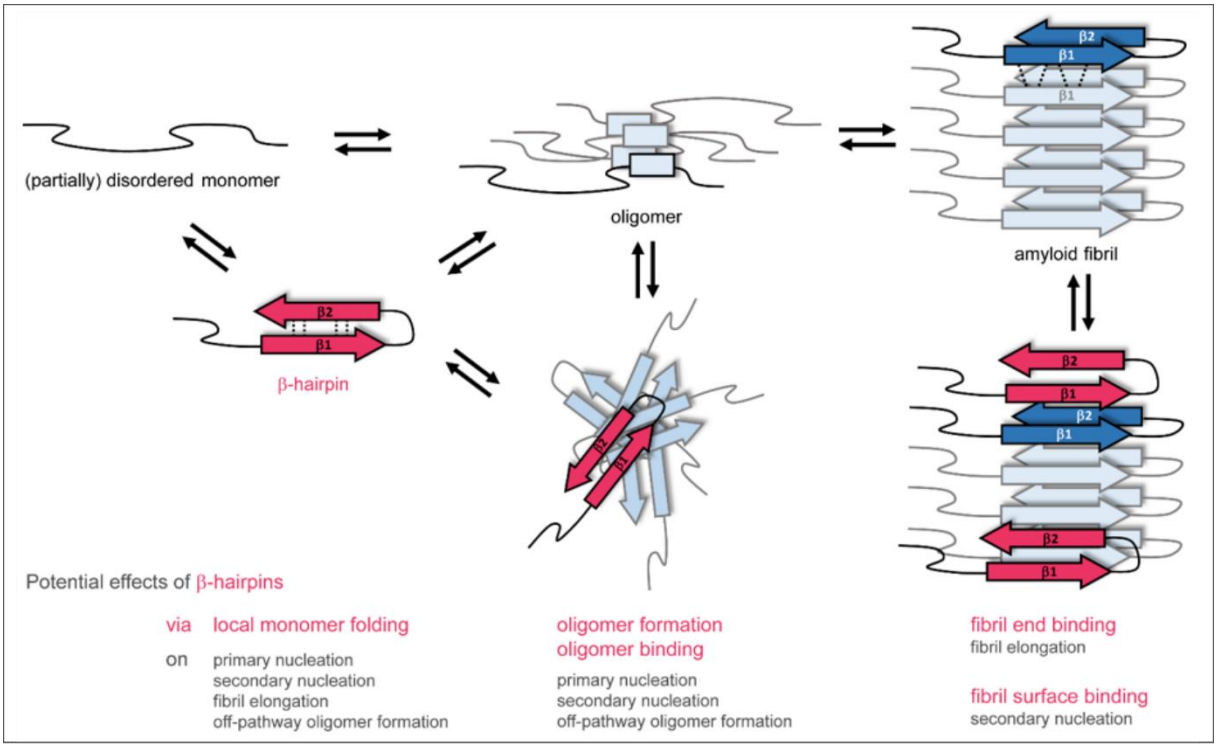

Figure 1: Schematic of the potential involvement of β-hairpin conformers (red) in the amyloid formation reaction. Dashed lines indicate backbone hydrogen bonds in antiparallel (β-hairpin) or parallel (amyloid fibril) β-sheets.

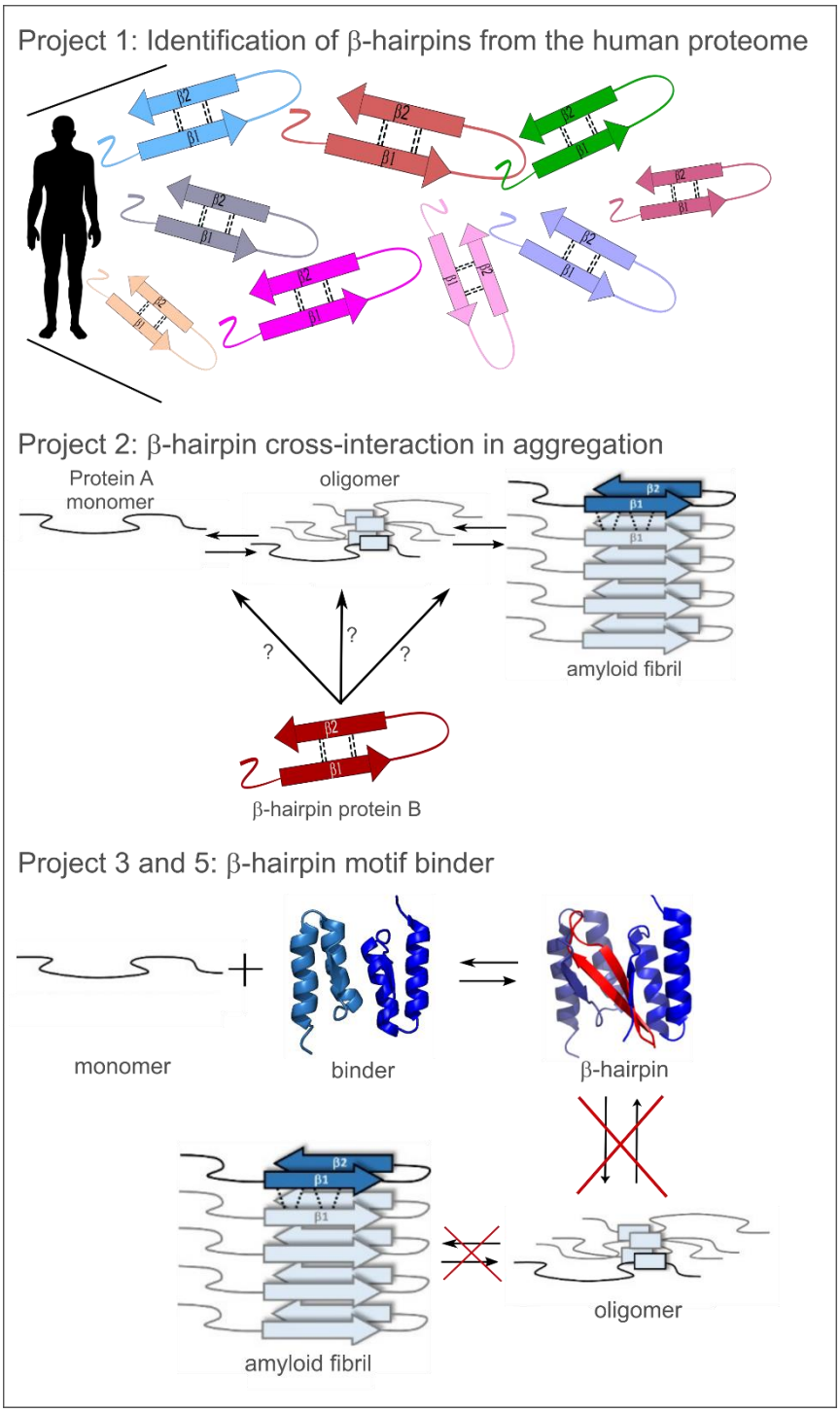

Figure 2: Schematic of the involvement of β-hairpins in the different projects of this thesis.

The β-hairpins seem to be a relatively short-lived structural motif in amyloid diseases but an important one not only for the build-up to fibrils but also to the structures that come before the oligomers, which in some cases are discussed to be more cytotoxic than the mature fibrils. [4] It has been shown that also oligomers seem to be built from β-sheets, but possibly from antiparallel ones and are folded in a more compact format. [12] Monomers folding into

β-hairpins seem to be a very important starting step in amyloid formation, especially considering that at least the most common neurodegenerative amyloidogenic diseases (AD, PD, DTII) are all caused by intrinsically disordered proteins (IDPs), meaning that in their natural state and without outside interference they do not have a fixed folded state. [4] If this first folding step is the β-hairpin which then leads to more compact structures, it would mean that when this first step was stabilized in a way, the further growth into more compact structures should be inhibited. [4, 5, 13] On the other hand, if a β-hairpin structure is encouraged without stabilizing it in that structure, it could also very well accelerate the aggregation of the involved proteins. [4, 5]

A prime example of how different the impact of a β-hairpin can be was shown in several studies on the Aβ protein (involved in AD) and several different peptide versions. [6, 7, 10, 14, 15, 20] It was shown over the years that during the formation of higher-ordered structures (oligomers and fibrils) the β-sheet content rises. [10, 14] It was furthermore shown that an engineered binding protein called ZAβ$_3$ can bind Aβ at a very specific position. [7, 20] Aβ folds into a β-hairpin upon the binding to that protein, and that hairpin is stabilized within a tunnel-like cavity of ZAβ$_3$, inhibiting aggregation. [7, 20] Taken together, this means that folding into a β-hairpin motif is possible for the protein and can be stabilized and exploited as a drug discovery approach [7, 20]. In another study, it was shown that it is already enough to stabilize the protein in a β-hairpin structure with a disulfide bond to slow down aggregation. [15] Simulations of an Aβ peptide demonstrated that the β-hairpin only forms while the peptide is still in its monomer form and not in later stages and it is seemingly triggered when those monomers attach themselves to a growing β-sheet to form or elongate the fibril. [10] During that time, the β-hairpin seems to primarily have the role of stabilizing the existing β-sheet before it changes its conformation from a β-hairpin into a stretched β-strand that can fully be incorporated into the growing β-sheet. [10] According to this, the monomer that can fold into a β–hairpin would be essential for the growth of the β-sheet and, in turn, the growth of the fibril. This would require the β-hairpin to be quite flexible to be able to change conformation. [10] It would also mean that this is a weakness of the growing fibril that could potentially be exploited. If the monomer were to be stabilized in this β-hairpin conformation it would mean that the β-sheets could no longer grow.[10] Different ways to probe this weakness where already been tried, either by capturing the monomer with an engineered binding protein that binds exactly the β-hairpin forming sequence parts (ZAβ$_3$) or in the form of mimics that contain small recognition sides to

inhibit aggregation. [10, 15, 20] With similar approaches, it was shown that it is also possible to reduce or inhibit the aggregation of IAPP, the protein involved in type II diabetes. [11, 17, 21] Also, here it could be shown that a β-hairpin is involved in the formation of aggregates. [21] The IAPP sequence, just like the Aβ sequence, has parts that are prone to fold into a β-hairpin under the right conditions. [11, 17, 21] Additionally, the same is true for the protein α-synuclein, which is involved in Parkinson's Disease. The α-synuclein sequence, too, has a sequence stretch that can form a β-hairpin which can be stabilized by either introducing cysteines to form a disulfide bond or by an engineered binding protein (AS69). [5, 8, 9, 16, 18, 19, 22]

In summary, the β-hairpin motif in proteins and peptides is an interesting object to study especially in the context of amyloid diseases. The fold into a β-hairpin seems to be a critical step at the beginning of aggregation in the commonly most known neurodegenerative diseases AD, PD, and DTII [5, 19]. It was shown that a β-hairpin could accelerate the aggregation if the folding into a hairpin structure is enhanced. [2, 4] Still, on the other hand, it can be used to inhibit the aggregation of the involved proteins. [2, 4] This can either happen by introducing stabilized β-hairpins that block the growing ends of larger structures or by forcing the involved proteins to fold into a β-hairpin with a specialized binding protein. [4, 19] Taken together, the studies also showed that, despite not being similar in sequence at all, the proteins Aβ, IAPP, and α-synuclein share properties that make it possible for them to aggregate and that the final product, the fibril, is morphologically quite similar. These commonalities could make it possible to find a way to treat these not yet treatable, diseases similarly.

Aims of the thesis

In the following projects of this thesis, different aspects of different β-hairpins were studied, with regard to their role in amyloid formation and to their interaction with engineered binding proteins. One such project explores just how widespread are amyloidogenic β-hairpins in a proteome-wide study. For that a set of β-hairpins, found by a bioinformatic approach, from across the whole human proteome were characterized and tested in their ability to be bound by an engineered binding protein that was previously able to bind Aβ, IAPP, and α-synuclein.

Another project aims to further explore if amyloidogenic β-hairpins interfere with amyloid formation of sequence-unrelated proteins to see if cross-interaction is possible. In detail this means that there is an aggregation prone protein A, in this case α-synuclein, and two different, unrelated to α-synuclein, sequences with a β-hairpin motif also found with the bioinformatic approach from project one. While adding the two β-hairpins to an α-synuclein aggregation assay in different concentrations and in conditions, the aggregation kinetics were monitored via ThT-fluorescence and the endpoints looked at with atomic force microscopy.

In a third part the aim was to optimize compounds that bind β-hairpins and can inhibit the amyloid formation on the protein and small molecule level. On the protein level that meant to optimize the β-wrapin AS69, that can bind α-synuclein in a coupled-folded binding mode and optimize it via molecular dynamics simulation and phage display and characterize those new constructs via isothermal titration calorimetry. On the other hand, to approach the inhibition of α-synuclein aggregation with small molecules first steps to develop a high throughput screening assay have been taken to be able to identify the correct molecules that can bind the α-synuclein β-hairpin.

In a fourth project the expression and purification of two model proteins for light-chain amyloidosis was established with sequences that also carry a β-hairpin motif with the same characteristics as those found in for example α-synuclein. With an established expression and purification protocol the next step was to find the correct conditions for those to proteins to aggregate and if possible, to add in β-wrapin AS10 as possible inhibitor.

The overall aim is to further elucidate the role of β-hairpins in amyloid formation and delineate their potential to serve as targets in anti-amyloid inhibition approaches.

References

1. Maynard, A. J., Sharman, G. J. & Searle, M. S. Origin of β-hairpin stability in solution: Structural and thermodynamic analysis of the folding of a model peptide supports hydrophobic stabilization in water. *J. Am. Chem. Soc.* **120**, 1996–2007 (1998).
2. Kar, K. *et al.* Backbone engineering within a latent β-hairpin structure to design inhibitors of polyglutamine amyloid formation. *J. Mol. Biol.* **429**, 308 (2017).
3. Li, X., Sabol, A. L., Wierzbicki, M., Salveson, P. J. & Nowick, J. S. An Improved Turn Structure for Inducing β-Hairpin Formation in Peptides. *Angew. Chemie Int. Ed.* **60**, 22776–22782 (2021).
4. Gill, A. C. b-Hairpin-Mediated Formation of Structurally Distinct Multimers of Neurotoxic Prion Peptides. *PLoS One* (2014) doi:10.1371/journal.pone.0087354.
5. Huggins, K. N. L. *et al.* Designed hairpin peptides interfere with amyloidogenesis pathways: Fibril formation and cytotoxicity inhibition, interception of the preamyloid state. *Biochemistry* **50**, 8202–8212 (2011).
6. Pellegrino, S. *et al.* β-Hairpin mimics containing a piperidine-pyrrolidine scaffold modulate the β-amyloid aggregation process preserving the monomer species. *Chem. Sci.* **8**, 1295–1302 (2017).
7. Hoyer, W., Grönwall, C., Jonsson, A., Ståhl, S. & Härd, T. Stabilization of a β-hairpin in monomeric Alzheimer's amyloid-β peptide inhibits amyloid formation. *Proc. Natl. Acad. Sci. U. S. A.* **105**, 5099–5104 (2008).
8. Mirecka, E. A. *et al.* Sequestration of a β-hairpin for control of α-synuclein aggregation. *Angew. Chemie - Int. Ed.* **53**, 4227–4230 (2014).
9. Agerschou, E. D., Borgmann, V., Wördehoff, M. M. & Hoyer, W. Inhibitor and substrate cooperate to inhibit amyloid fibril elongation of α-synuclein. *Chem. Sci.* **11**, 11331–11337 (2020).
10. Larini, L. & Shea, J. E. Role of β-Hairpin Formation in Aggregation: The Self-Assembly of the Amyloid-β(25–35) Peptide. *Biophys. J.* **103**, 576 (2012).
11. Lesma, J. *et al.* β-Hairpin Peptide Mimics Decrease Human Islet Amyloid Polypeptide (hIAPP) Aggregation. *Front. Cell Dev. Biol.* **9**, (2021).
12. Kreutzer, A. G. & Nowick, J. S. Elucidating the Structures of Amyloid Oligomers with Macrocyclic β-Hairpin Peptides: Insights into Alzheimer's Disease and other Amyloid Diseases. *Acc. Chem. Res.* **51**, 706 (2018).

13. Gill, A. C. b-Hairpin-Mediated Formation of Structurally Distinct Multimers of Neurotoxic Prion Peptides. *PLoS One* (2014) doi:10.1371/journal.pone.0087354.
14. Cruz, L., Rao, J. S., Teplow, D. B. & Urbanc, B. Dynamics of metastable β-hairpin structures in the folding nucleus of amyloid β-protein. *J. Phys. Chem. B* **116**, 6311–6325 (2012).
15. Sandberg, A. *et al.* Stabilization of neurotoxic Alzheimer amyloid-β oligomers by protein engineering. *Proc. Natl. Acad. Sci. U. S. A.* **107**, 15595–15600 (2010).
16. Shaykhalishahi, H. *et al.* Contact between the β1 and β2 Segments of α-Synuclein that Inhibits Amyloid Formation. *Angew. Chemie Int. Ed.* **54**, 8837–8840 (2015).
17. Mirecka, E. A. *et al.* β-Hairpin of Islet Amyloid Polypeptide Bound to an Aggregation Inhibitor. *Sci. Rep.* **6**, (2016).
18. Mirecka, E. A. *et al.* Sequestration of a β-hairpin for control of α-synuclein aggregation. *Angew. Chemie - Int. Ed.* **53**, 4227–4230 (2014).
19. Shaykhalishahi, H. *et al.* A β-Hairpin-Binding Protein for Three Different Disease-Related Amyloidogenic Proteins. *ChemBioChem* **16**, 411–414 (2015).
20. Hoyer, W., Grönwall, C., Jonsson, A., Ståhl, S. & Härd, T. Stabilization of a β-hairpin in monomeric Alzheimer's amyloid-β peptide inhibits amyloid formation. *Proc. Natl. Acad. Sci. U. S. A.* **105**, 5099–5104 (2008).
21. Dupuis, N. F., Wu, C., Shea, J. E. & Bowers, M. T. Human islet amyloid polypeptide monomers form ordered β-hairpins: A possible direct amyloidogenic precursor. *J. Am. Chem. Soc.* **131**, 18283–18292 (2009).
22. Yu, H., Han, W., Ma, W. & Schulten, K. Transient β -hairpin formation in α -synuclein monomer revealed by coarse-grained molecular dynamics simulation. *J. Chem. Phys.* **143**, (2015).
23. Rudra, J. S. & Collier, J. H. Self-assembling biomaterials. *Compr. Biomater.* **2**, 77–94 (2011).
24. Rudra, J. S., Kelly, S. H. & Collier, J. H. 2.4 Self-Assembling Biomaterials. *Compr. Biomater. II* 67–89 (2017) doi:10.1016/B978-0-12-803581-8.10210-3.
25. Banerjee, J., Radvar, E. & Azevedo, H. S. Self-assembling peptides and their application in tissue engineering and regenerative medicine. *Pept. Proteins as Biomater. Tissue Regen. Repair* 245–281 (2018) doi:10.1016/B978-0-08-100803-4.00010-3.
26. DuPai, C. D., Davies, B. W. & Wilke, C. O. A systematic analysis of the beta hairpin motif in the Protein Data Bank. *Protein Sci.* **30**, 613–623 (2021).

Project 1 [submitted Manuscript]:

Sequence-based identification of amyloidogenic β-hairpins reveals a prostatic acid phosphatase fragment promoting semen amyloid formation

Content

Article information

Title of the manuscript: Sequence-based identification of amyloidogenic β-hairpins reveals a prostatic acid phosphatase fragment promoting semen amyloid formation

Authors: Laetitia F. Heid[1], Emil Dandanell Agerschou[1], Asuka A. Orr[2], Tatsiana Kupreichyk[1,3], Walfried Schneider[1], Michael M. Wördehoff[1], Melanie Schwarten[3], Dieter Willbold[1,3], Phanourios Tamamis[2,4], Matthias Stoldt[3], Wolfgang Hoyer[1,3]

Journal: Computational and Structural Biotechnology Journal (CSBJ)

Status: Submitted, under review

Data availability: Code and output sequences of the prediction of amyloidogenic β-hairpins are available on zenodo under doi:10.5281/zenodo.8264535. Structure coordinate files of the AS10 complexes of PAP(185-208), CYP2W1(176-204), and NDUFS7(104-129) are available in the supplementary material of this article.

Author contributions: Conceptualization, LFH, EDA, WH; Investigation and Methodology, LFH, EDA, AAO, TK, WS, MMW, MSc, PT, MSt; Software, EDA; Funding acquisition and supervision, PT, WH; Project administration, WH; Writing - original draft, LFH, EDA, AAO, PT, WH; and Writing - review & editing, LFH, EDA, AAO, TK, WS, MMW, MSc, DW, PT, MSt, WH.

[1]Institut für Physikalische Biologie, Heinrich Heine University Düsseldorf, 40204 Düsseldorf, Germany
[2]Artie McFerrin Department of Chemical Engineering, Texas A&M University, College Station, Texas 77843-3122, United States
[3]Institute of Biological Information Processing (IBI-7) and JuStruct: Jülich Center for Structural Biology, Forschungszentrum Jülich, 52425 Jülich, Germany
[4]Department of Materials Science and Engineering, Texas A&M University, College Station, Texas 77843-3033, United States

Correspondence and requests for materials should be addressed to W.H. (email: wolfgang.hoyer@hhu.de)

Declarations of interest: none

Abstract

β-Structure-rich amyloid fibrils are hallmarks of several diseases, including Alzheimer's (AD), Parkinson's (PD), and type 2 diabetes (T2D). While amyloid fibrils typically consist of parallel β-sheets, the anti-parallel β-hairpin is a structural motif accessible to amyloidogenic proteins in their monomeric and oligomeric states. Here, to investigate implications of β-hairpins in amyloid formation, potential β-hairpin-forming amyloidogenic segments in the human proteome were predicted based on sequence similarity with β-hairpins previously observed in Aβ, α-synuclein, and islet amyloid polypeptide, amyloidogenic proteins associated with AD, PD, and T2D, respectively. These three β-hairpins, established upon binding to the engineered binding protein β-wrapin AS10, are characterized by proximity of two sequence segments rich in hydrophobic and aromatic amino acids, with high β-aggregation scores according to the TANGO algorithm. Using these criteria, 2505 potential β-hairpin-forming amyloidogenic segments in 2098 human proteins were identified. Characterization of a test set of eight protein segments showed that seven assembled into Thioflavin T-positive aggregates and four formed β-hairpins in complex with AS10 according to NMR. One of those is a segment of prostatic acid phosphatase (PAP) comprising amino acids 185-208. PAP is naturally cleaved into fragments, including PAP(248-286) which forms functional amyloid in semen. We find that PAP(185-208) strongly decreases the protein concentrations required for fibril formation of PAP(248-286) and of another semen amyloid peptide, SEM1(86-107), indicating that the β-hairpin-prone PAP segment promotes nucleation of semen amyloids. In conclusion, β-hairpin-forming amyloidogenic protein segments could be identified in the human proteome with potential roles in functional or disease-related amyloid formation.

1.1 Introduction

1

Amyloid fibrils are a structural key feature of several prevalent diseases including Alzheimer's disease (AD), Parkinson's disease (PD), and type 2 diabetes (T2D), but also fulfill functional roles in biology [1-4]. Their principal framework is the cross-β structure, in which β-strands oriented perpendicular to the fibril axis form long β-sheets, stabilized by backbone hydrogen bonds (Fig. 1). Amyloid fibrils consist of two or more such β-sheets that pack against each other, supported by interactions between their side chains. In the fibrils of disease-related amyloidogenic proteins a parallel in-register β-sheet organization is commonly established, i.e., identical side chains of neighboring monomer units stack on top of each other [1, 4]. Fibrils grow by stepwise addition of monomers, which form multiple β-strand-kink-β-strand motifs. The different β-strand forming segments of one monomer can make contact with each other via side chain-side chain interactions (Fig. 1). This β-strand-kink-β-strand conformation is not stable in free monomers, but is stabilized in the amyloid fibril by the hydrogen bond network and side chain interactions within the highly ordered intermolecular β-sheets.

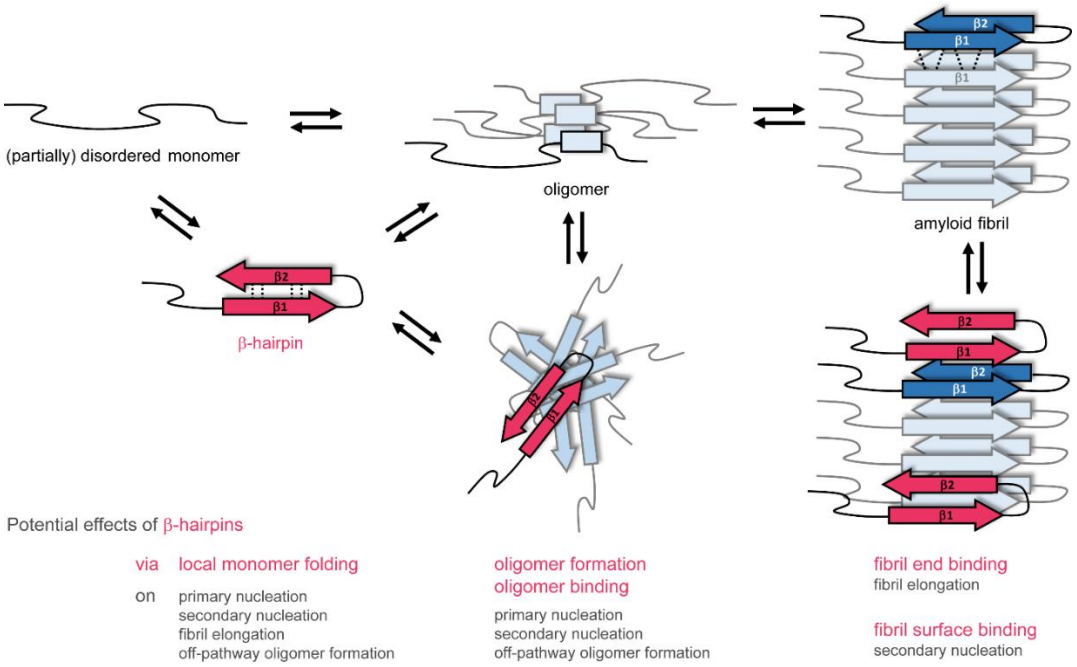

Figure 1: Schematic of the potential involvement of β-hairpin conformers (red) in the amyloid formation reaction. Dashed lines indicate backbone hydrogen bonds in antiparallel (β-hairpin) or parallel (amyloid fibril) β-sheets.

A related structural motif is the β-hairpin (Figure 1, pink red) [5, 6]. In contrast to the β-strand-kink-β-strand conformation in amyloid fibrils, the β-hairpin features intramolecular backbone hydrogen-bonding within an antiparallel β-sheet. The β-hairpin conformation is readily accessible in monomeric peptides provided there is a sequence segment with turn-forming propensity connecting two stretches of residues with β-sheet propensity. The kinetic stability of a β-hairpin is largely determined by the side chain interactions among the β-sheet residues. Even in optimized β-hairpin peptides, the hairpin conformation is not persistent but folds and unfolds on the microsecond timescale [7]. Nevertheless, molecular dynamics (MD) simulations have identified a substantial fraction of β-hairpin-containing structures in the conformational ensembles of monomeric amyloidogenic intrinsically disordered proteins (IDPs), confirmed by experimental evidence [8-23]. This observation can be explained by the presence of sequence segments with high β-sheet propensity, a determinant of high amyloidogenicity. Due to its preferred occurrence in amyloidogenic proteins, the β-hairpin conformation might affect several steps of the amyloid formation reaction (Fig. 1): β-Hairpins may (i) constitute basic components of oligomers (on-pathway or off-pathway) and therefore trigger or suppress the nucleation of amyloid fibrils, (ii) bind to other types of oligomers and affect primary and/or secondary nucleation, (iii) bind to fibril ends and block fibril elongation, or (iv) bind to fibril surfaces and affect secondary nucleation. Many such aggregation-promoting or -inhibiting functions have been described for β-hairpins of several amyloidogenic proteins in the literature [8, 9, 14, 15, 17, 22, 24-36].

We have previously observed β-hairpins in amyloid-β (Aβ), α-synuclein (αSyn), and islet amyloid polypeptide (IAPP), amyloidogenic proteins associated with AD, PD, and T2D, respectively (Fig. 2) [37-39]. These β-hairpins are established upon binding to engineered binding proteins termed β-wrapins. β-Wrapins are selected from protein libraries based on ZAβ3, an affibody with high affinity for monomeric Aβ [37, 39-42]. β-Hairpin structures of Aβ, αSyn and IAPP have been determined by NMR spectroscopy of their complexes with ZAβ3 and the β-wrapins AS69 and HI18, respectively (Fig. 2A) [37-39]. The β-hairpins are stabilized in the complexes by formation of an intermolecular β-sheet with two short β-stands contributed by the binding proteins, and by coverage of the their mostly hydrophobic side chains as the binding proteins wrap around the β-hairpins. Importantly, the β-hairpins of Aβ, αSyn and IAPP are established in sequence regions that according to MD simulations also populate β-hairpin conformation in the free state (Fig. 2B) [8, 11, 13, 23]. Interestingly, a single β-wrapin, denoted

AS10, can bind all three amyloidogenic targets Aβ, αSyn and IAPP with sub-micromolar affinity, emphasizing the similarity of their β-hairpin regions [43].

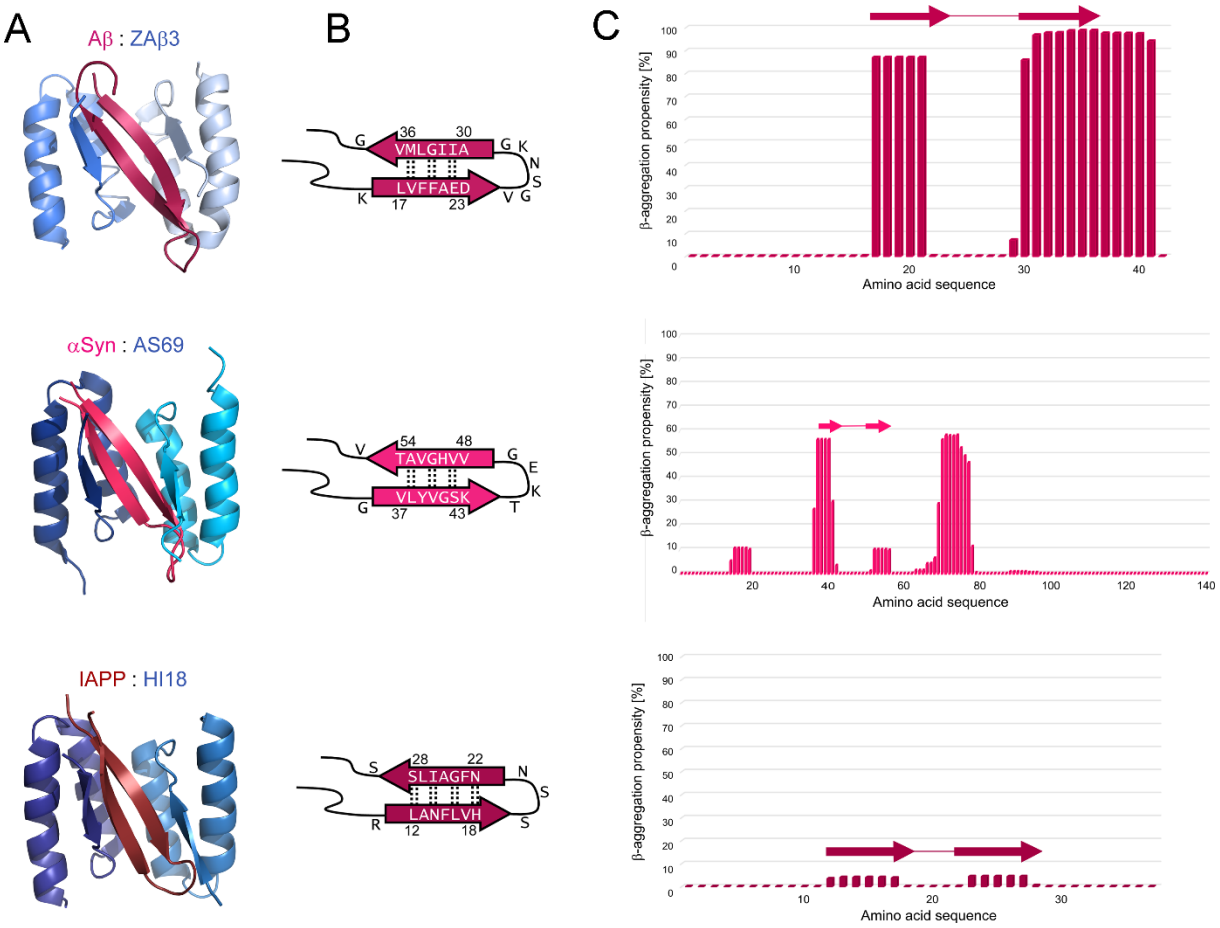

Figure 2: β-Hairpins of Aβ (top row), αSyn (middle row), and IAPP (bottom row). (A) NMR structures of local β-hairpin folds of Aβ (pdb 2OTK), αSyn (pdb 4BXL), and IAPP (pdb 5K5G), established upon coupled folding-binding to ZAβ3 or the β-wrapins AS69 and HI18, respectively [37-39]. (B) Corresponding β-hairpin registries. (C) β-Aggregation propensities of the amino acid sequences. The positions of the observed β-hairpins are indicated by arrows (β-strands) connected by a line (turn).

Here, we aimed to identify further human proteins containing β-hairpin regions similar to Aβ, αSyn and IAPP. Such proteins might form oligomers or amyloid fibrils by themselves or they might affect oligomer or fibril formation of other proteins. β-Hairpin forming segments in the human proteome were predicted by sequence comparison with Aβ, αSyn and IAPP. Out of 2505 potential β-hairpin-forming amyloidogenic segments a test set of eight segments was characterized in peptide format, proving Thioflavin T (ThT)-positive aggregation for seven and β-hairpin formation for four of the candidates. Further analysis of one segment, which stems

from prostatic acid phosphate (PAP), demonstrated a promoting effect on physiologically relevant PAP semen amyloid formation.

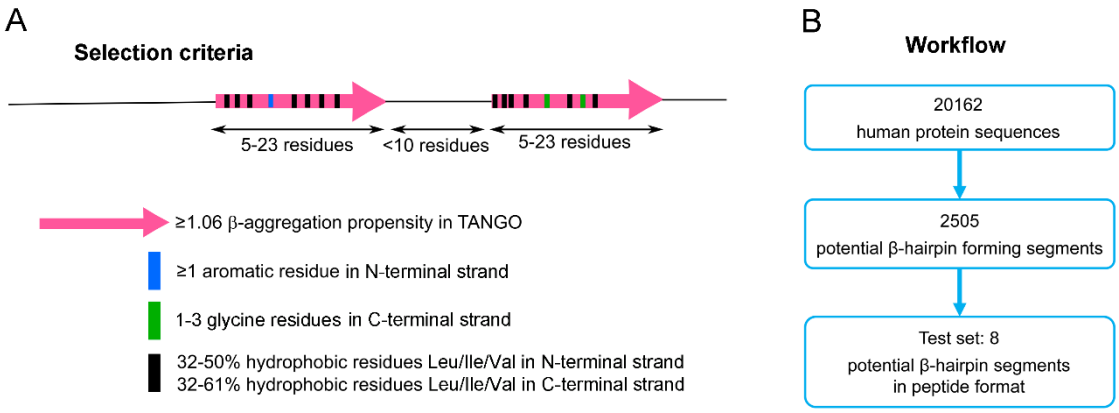

Figure 3: Criteria and workflow for prediction of amyloidogenic β-hairpins. (A) Protein segments were searched for that contained two segments of high β-aggregation propensity and an amino acid composition similar to the β-hairpins of Aβ, αSyn, and IAPP. (B) Numbers of protein sequences screened, predicted, and tested.

1.2 Materials and Methods

1.2.1 Bioinformatics

The 64-bit Linux binary of the TANGO algorithm 2.3.1 [44-46] was downloaded from http://tango.crg.es. The annotated human proteome was acquired on the February 21st 2017 from Uniprot [47] using the query: *reviewed:yes AND organism:"Homo sapiens (Human) [9606]" AND proteome:up000005640* and downloading the amino acid sequences as a FASTA file (20,162 protein sequences). The sequences were then prepared for the TANGO algorithm by creating files with up to one thousand lines (TANGO limit) all having the following structure: "uniprot ID" N N 7 298 0.1 "aa_sequence", corresponding to running the TANGO algorithm on all sequences assuming no modifications of termini, T = 298 K, and an ionic strength of 0.1 M (default parameters of TANGO). These batch files were then supplied to a locally running instance of TANGO. For unknown reasons some sequences resulted in errors, both when run locally as well as when the amino acid sequences were supplied to the online version of TANGO, and they were therefore excluded from any analysis. The Uniprot IDs of the error causing sequences were: Q8NHP1, P22352, P59796, P18283, P07203, Q9C0D9, P36969, Q8IZQ5, Q9BVL4, Q9BQE4, Q8WWX9, P49908, P62341, P59797, Q9NZV5, P63302, Q9Y6D0, O60613, Q99611, Q9NNW7, Q86VQ6, Q8WZ42, P49895, Q92813, P55073, Q9NZV6, Q16881. A filter was applied based on the length of aggregation prone β-stretches, the length of the turn between the stretches, presence of aromatic residues, presence of hydrophobic residues, and the presence of glycine. The parameters were based on three previously identified aggregation-prone β-hairpins in Aβ, αSyn, and IAPP [37-39]. In particular, the following filter was developed and applied to the output from TANGO:

1. Only amino acids with a TANGO aggregation propensity >1.06 were considered to be in β-stretch.
2. Only β-stretches between 5 and 23 amino acids long were considered for further analysis.
3. Only β-stretches connected to other β-stretches by 9 or fewer amino acids (i.e potential turns) were considered for further analysis.
4. Only β-stretches where the first (i.e. N-terminal strand) had the following properties were considered:
4.1. At least one aromatic residue.
4.2. A fractional content of the residues isoleucine, leucine, and valine between 0.32 and 0.5.

5. Only β-stretches where the second (i.e. C-terminal strand) had the following properties were considered:
5.1. Between 1 and 3 glycine residues.
5.2. A fractional content of the residues isoleucine, leucine, and valine between 0.32 and 0.61.
This resulted in 2505 potentially aggregation prone β-hairpins from 2098 protein sequences. The entire workflow is available as a Jupyter Notebook except the TANGO binary which should be obtained from the above mentioned source. Code and output sequences are available on zenodo under doi:10.5281/zenodo.8264535.

1.2.2 Peptides

Synthetic peptides were obtained either from peptides & elephants or from CASLO. To fully monomerize the peptides, 1 mg aliquots were solubilized in 1 ml hexafluoroisopropanol (HFIP), aliquoted in smaller amounts, lyophilized and stored at -20 °C.

1.2.3 Cloning of the fusion constructs

Like other β-wrapins derived from the affibody ZAβ3, AS10 is a dimer of two identical subunits [43]. In the fusion constructs the two AS10 subunits and the β-hairpin-forming peptides were linked via flexible glycine-serine linkers in the following format: N-His_6-AS10(subunit1)-$(G_4S)_3$-AS10(subunit2)-$(G_4S)_3$-HairpinPeptide-C. DNA fragments containing the sequence of the fusion constructs were obtained from Thermo Fisher Scientific and cloned into vector pET302/NT-His using In-Fusion HD EcoDry Cloning Kit (Takara Bio). The success of the cloning was verified by sequencing.

1.2.4 Expression and purification of the fusion constructs

Expression of the fusion constructs was done in *E. coli* JM109 DE3 cells. An overnight pre-culture was grown in 2YT medium supplemented with 100 µg/L ampicillin at 37 °C and 180 rpm. For a subsequent overnight pre-culture, M9 minimal medium supplemented with 100 µg/L ampicillin was inoculated with the 2YT pre-culture at an optical density of 0.05 and grown at the same conditions as the previous culture. An expression culture in M9 minimal medium supplemented with 100 µg/L ampicillin, ^{15}N-NH_4Cl (1 g/l) and $^{13}C_6$-glucose (2 g/l) was inoculated with the M9 pre-culture at an optical density of 0.05 and grown at 37 °C and 140 rpm until induction with Isopropyl-β-D-thiogalactopyranosid (IPTG), then incubated at 20 °C, 120 rpm for additional 20 hours before harvesting. Cells were harvested by centrifugation at

5000 rpm for 10 min at 4 °C and frozen in loading buffer (50 mM Tris(hydroxymethyl)aminomethane (Tris), pH 8, 500 mM NaCl, 20 mM imidazole) with protease inhibitor (cOmplete EDTA-free Protease Inhibitor Cocktail, Roche). After thawing, cells were sonicated on ice twice for 5 min with the sonication probe MS-72, with an amplitude of 35 % and a cycle of 3 s pulse and 5 s pause. Next, the cell debris was removed by centrifugation and the supernatant was applied to a NiNTA HisTrap FF column (GE Healthcare) in loading buffer. Protein was eluted with a mixture of loading buffer and elution buffer (50 mM Tris, pH 8, 500 mM NaCl, 500 mM imidazole) into a final concentration of 250 mM imidazole. The eluate was concentrated and applied to a size exclusion chromatography column (SEC Superdex 200 Increase 10/300 GL, GE Healthcare) in a sodium phosphate buffer (20 mM NaPi, pH 7.4, 50 mM NaCl). The purified fusion protein was frozen in liquid nitrogen and stored at -80 °C.

1.2.5 Thioflavin T (ThT) aggregation assay

All ThT aggregation assays were done in Greiner 96-well half-area, clear bottom, low-binding plates. The measurements themselves were done in a BMG CLARIOstar plate reader at 37 °C and 300 rpm shaking with one glass bead (0.75-1 mm, Roth) per well. Wells with samples were always surrounded by wells filled with liquid, either other samples or 150 µl water, to counter potential artefacts due to evaporation. For characterization of the aggregation of the peptide test set, peptides were dissolved in 20 mM NaPi, pH 7.4, 50 mM NaCl, and added to the wells at final concentrations or 20 µM (CYP2W1, FibA, 3-PGDH, MIC26), 25 µM (TTC5, NDUFS7), 500 µM (NBPF1) or 550 µM (PAP) in triplicate samples of 80 µl. Final concentrations of 25 µM ThT and 0.04% sodium azide (NaN_3) were added. The plate was sealed with sealing tape and put into the plate reader, heated to 37 °C, and ThT fluorescence was read in 1000 cycles of 300 s each. To investigate the effect of PAP(185-206) on the aggregation of PAP(248-286) and SEM1(86-107), the prepared peptides were dissolved in 50 mM Tris, pH 8.5. PAP(248-286) and SEM1(86-107) were kept at constant concentrations of 500 and 300 µM, respectively. The final concentration of PAP(185-206) was varied between 25 and 100 µM. Samples contained 40 µM ThT and 0.04% NaN_3.

1.2.6 Atomic force microscopy (AFM)

For AFM imaging, 2 µl samples were taken out of the wells at the end of the ThT aggregation assays, put onto a freshly cleaved muscovite mica surface and dried during incubation for 10 minutes under the clean bench. Subsequently, the samples were washed with 100 µl ddH_2O in three steps and dried with a stream of N_2 gas. Imaging was performed in intermittent contact mode (AC mode) in a JPK NanoWizard 3 atomic force microscope using a silicon cantilever with silicon tip (OMCL-AC160TS-R3, Olympus) with a typical tip radius of 9 ± 2 nm, a force constant of 26 N/m and resonance frequency around 300 kHz. The images were processed using JPK DP Data Processing Software (version spm-5.0.84).

1.2.7 Isothermal titration calorimetry (ITC)

ITC was performed at 30°C using a Microcal iTC200 calorimeter (GE Healthcare). AS10 was filled into the cell at a concentration of 30 µm in 20 mM sodium phosphate, pH 7.4, 50 mM NaCl. Peptides were titrated from the syringe in approximately10-fold higher concentrations. Heats of post-saturation injections were averaged and subtracted from each injection to correct for heats of dilution and mixing. Dissociation constants were obtained from a nonlinear least-squares fit to a 1:1 binding model using MicroCal Origin.

1.2.8 NMR spectroscopy

The NMR spectra were acquired at 25 °C using VNMRS instruments (Varian) at proton frequencies of 800 and 900 MHz, each equipped with a cryogenically cooled Z-axis pulse-field-gradient (PFG) triple resonance probe. The sample buffer was 20 mM sodium phosphate, pH 7.4, 50 mM NaCl, supplemented with 10% D_2O. For detection of complex formation, samples contained 100 µM ^{15}N-labeled AS10, expressed and purified as described [39, 43], and a 20% excess of the unlabeled peptide. For determination of β-sheet registries, NMR samples contained $^{13}C^{15}N$-labeled fusion constructs in concentrations between 360-700 µM. Backbone assignments were obtained using BEST-TROSY experiments [48]. Nuclear Overhauser effect (NOE) based distance restraints for β-sheet registry determination were derived from 3D (^{1}H-^{1}H-^{15}N)-NOESY-HSQC (120 ms mixing time) and (^{1}H-^{13}Cali-^{1}H)-HSQC-NOESY (100 ms mixing time) experiments. NMR data were processed using NMRPipe [49] and analyzed with CcpNMR [50].

1.2.9 Structure modeling

The structures of AS10 in complex with NDUFS7(104-129), PAP(185-208), or CYP2W1(176-204) were initially modeled using the structure of the AS10:Aβ complex [51] as a template. The residues of Aβ forming β-sheets with AS10 were first mutated to the residues of the investigated β-hairpin peptides forming β-sheets with AS10 according to the experimentally derived β-sheet registries. Subsequently, the loop residues of Aβ (VGSNKG) were deleted, and the loop residues of the peptides were modeled using Modeller [52]. The resulting structures were used as initial structures for 5-replicate MD simulations, which were performed using the same methods as in our previous studies on AS10 binding to Aβ, αSyn, and IAPP [51, 53]. Structural analysis comparing the simulated complex structures with experimental β-sheet registries and hydrogen atom distance constraints suggested that the MD simulations efficiently modeled the complex structures.

1.3 Results

1.3.1 Prediction of amyloidogenic β-hairpins

To identify potential β-hairpin-forming amyloidogenic segments in the human proteome, we aimed to search for protein segments with sequence properties similar to those of the β-hairpins of Aβ, αSyn and IAPP established in their complexes with the engineered binding proteins (Fig. 2). We therefore looked for commonalities among these three β-hairpin sequences that might serve as criteria in the search for further amyloidogenic β-hairpins. When comparing the sequences of the Aβ, αSyn and IAPP β-hairpins directly, no obvious sequence similarity exists (Fig. 2B). Moreover, secondary structure prediction did not reveal a common theme among the three sequences that could be used as a search pattern (Fig. S1). As we are specifically interested in β-hairpins capable of amyloid formation, amyloid propensity predictors are of interest. The TANGO algorithm predicts secondary structure and also calculates amyloid propensity, or β-aggregation propensity as TANGO denotes it, enabling identification of aggregation-prone regions (APRs) [44-46]. When applying TANGO to Aβ, αSyn and IAPP, a consistent pattern was observed where most of residues in the β-strands of the β-hairpins had high β-aggregation propensity scores and the parts corresponding to the turns had scores of zero (Fig. 2C). Hence, a first search criterion was the presence of two regions with nonzero β-aggregation propensity scores separated by a segment of zero β-aggregation propensity. More specifically, sequences covering two stretches with between 5 and 23 consecutive residues with β-aggregation propensity scores ≥1.06 separated by maximally nine residues with a β-aggregation propensity score of zero were searched for (Fig. 3A). This resulted in 26,715 potential β-hairpins forming amyloidogenic regions distributed over 10,711 proteins out of a total of 20,162 analyzed human protein sequences. In other words, 53% of all sequences contained an average of 2.5 potential β-hairpin regions as judged by the TANGO search criterion. This high number is in line with the observation that the majority of human proteins contain multiple aggregation-prone regions (APRs) as assessed by computational predictions [54].

For a more stringent search pattern, additional requirements were imposed on the type of amino acids in the β-aggregation propensity-positive stretches, based on the specific sequence compositions of the Aβ, αSyn and IAPP β-hairpins. In particular, hydrophobicity and aromaticity were considered, as aromatic and hydrophobic amino acids have been implicated in amyloid formation [55, 56]. Slightly different requirements were placed on the N-terminal and C-terminal β-aggregation propensity-positive stretch to reflect the known properties of the

Aβ, αSyn and IAPP β-hairpins. In the N-terminal stretch, at least one aromatic residue and a fractional content of the large aliphatic residues leucine, isoleucine, and valine between 0.32 and 0.5 of all residues were required. In the C-terminal stretch, between 1 and 3 glycine residues and a fractional content of the large aliphatic residues between 0.32 and 0.61 of all residues were required (Fig. 3A). The use of these additional requirements resulted in a reduction of hits to 2505 potential β-hairpin regions distributed over 2098 proteins (Fig. 3B). In other words, 10% of the human protein sequences contained an average of 1.2 potential β-hairpins. Code and output sequences of the prediction of amyloidogenic β-hairpins are available on zenodo under doi:10.5281/zenodo.8264535.

1.3.2 Characterization of a test set of potential amyloidogenic β-hairpin protein fragments

To evaluate whether the identified protein segments are indeed aggregation-prone and able to adopt β-hairpin conformation a test set of eight segments was investigated in peptide format (see Fig. 4A for source proteins, peptide names and sequences, and an overview of characterization results). Apart from the predicted β-hairpin sequences, the peptides included up to three additional, mostly charged or polar amino acids at their termini, in accordance with the sequences of the source proteins, with the aim to a) increase peptide hydrophilicity and b) ensure that β-hairpin formation is not impeded by insufficient peptide length. In the sequence context of their source proteins, the segments adopt diverse secondary and tertiary structures (Fig. 4B). In one case, TTC5(335-361), the segment forms a β-hairpin in the source protein's native fold. Here, we investigated the segments' behavior when excised from the source protein.

A

Segment peptide	Protein name Peptide sequence	UniProt entry	pI	Soluble	ThT	NMR β-hairpin	Affinity to AS10 [μM]
TTC5(335-361)	Tetratricopeptide repeat protein 5 AVILGKVVFSLTTEEKVPFTFGLVDSD	Q8N0Z6	4.3	+	+	+	4.7 ± 0.9
NDUFS7(104-129)	NADH dehydrogenase [ubiquinone] iron-sulfur protein 7, mitochondrial DRFGVVFRASPRQSDVMIVAGTLTNK	O75251	10.7	+	+	+	4.7 ± 0.5
PAP(185-208)	Prostatic acid phosphatase KDFIATLGKLSGLHGQDLFGIWSK	P15309	8.5	+	+	+	39 ± 5
CYP2W1(176-204)	Cytochrome P450 2W1 SNITFALLFGRRFDYRDPVFVSLLGLIDE	Q8TAV3	4.7	-	+	+	n.d.
NBPF1(928-946)	Neuroblastoma breakpoint family member 1 RSAFYILEQQRVGWALDMD	Q3BBV0	4.6	+	-	-	-
FibA(655-678)	Fibrinogen alpha chain SSKIFSVYSDQETSLGGWLLIQQR	P02671	5.8	-	+	-	n.d.
3-PGDH(298-319)	D-3-phosphoglycerate dehydrogenase EIAVQFVDMVKGKSLTGVVNAQ	O43175	6.2	-	+	-	n.d.
MIC26(153-178)	MICOS complex subunit MIC26 QQAIVFAQVSGERLYDWGLRGYIVIE	Q9BUR5	4.7	-	+	-	n.d.

B

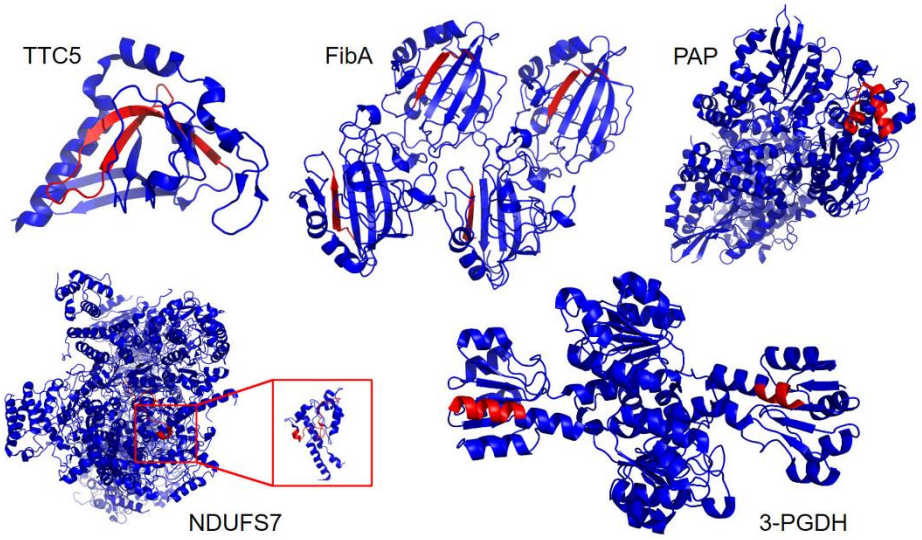

Figure 4: Test set of eight protein segments. (A) List of the investigated peptides. Underlined stretches in the peptide sequences correspond to the predicted amyloidogenic β-hairpins. A peptide was considered 'soluble' when no visible precipitation occurred upon dissolution of the lyophilized peptide in 20 mM NaPi, pH 7.4, 50 mM NaCl, to a final concentration of 20 μM. Affinities were not determined ('n.d.') for peptides exhibiting precipitation. (B) Conformations of investigated segments (red) in the context of their source proteins. PDB codes 2XVS (TTC5), 1FZD (FibA), 1ND6 (PAP), 5XTB (NDUFS7), 6RJ3 (3-PGDH).

When dissolved in aqueous buffer at μM concentrations at neutral pH, four of the eight peptides exhibited extensive precipitate formation indicative of low solubility (Fig. 4A). To test if any of the eight peptides form amyloid, the dye Thioflavin T (ThT), which shows dramatically increased fluorescence upon binding to amyloid fibrils [57], was added to the peptides and time courses of ThT fluorescence were recorded (Fig. 5). Only in one case, NBPF1(928-946), no increase in fluorescence intensity was detected (Fig. 5E). For five peptides, ThT fluorescence was initially low but increased rapidly after a lag-time, which is characteristic of amyloid formation (Fig. 5A,B,D,F,G). Two of these five peptides, FibA(655-678) and 3-PGDH(298-319), belonged to the group showing immediate precipitate formation upon dissolution, indicating that they can form both ThT-positive as well as ThT-negative aggregates. For two further peptides exhibiting immediate precipitation, CYP2W1(176-204) and MIC26(153-178), ThT fluorescence was high from the beginning, indicating that ThT-positive structures had formed directly upon sample preparation (Fig. 5C,H). We aspired to image the aggregates at the end of the aggregation assays by AFM, but the amount of material on the substrate was typically sparse, which we attribute to a poor interaction of the comparatively hydrophobic peptides with the hydrophilic mica substrate. Nevertheless, fibrillar aggregates confirming amyloid formation were detected of NDUFS7(104-129), PAP(185-208), CYP2W1(176-204), and MIC26(153-178) (Fig. 5). Collectively, these initial experiments showed that only one of the eight peptides remained soluble, whereas the other seven formed aggregates with features typical for amyloids.

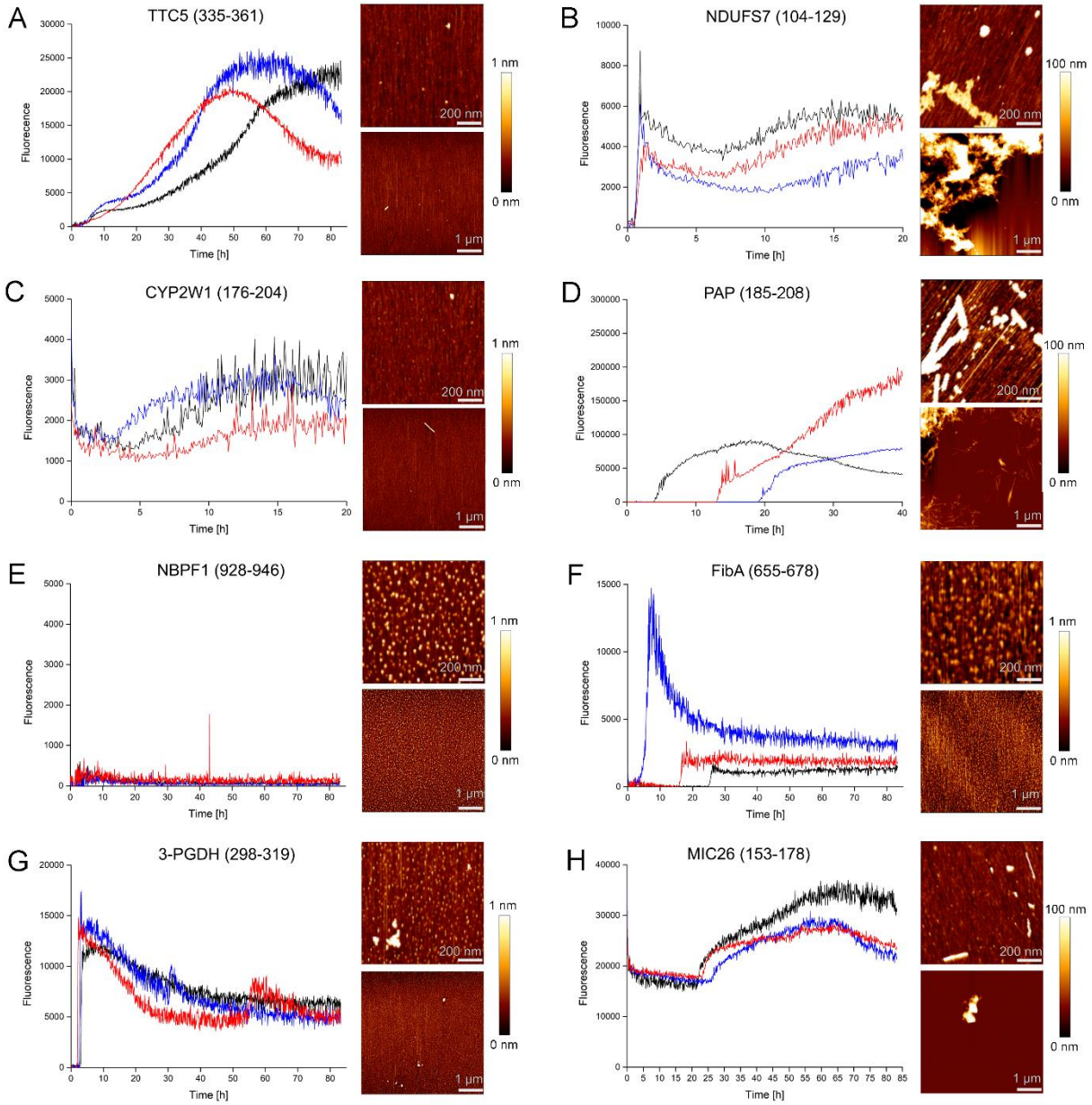

Figure 5: ThT aggregation assay and AFM. Left in panel, Time courses of ThT fluorescence upon incubation of the peptides at concentrations of 20 µM (CYP2W1, FibA, 3-PGDH, MIC26), 25 µM (TTC5, NDUFS7), 500 µM (NBPF1), or 550 µM (PAP), respectively, in 20 mM NaPi, pH 7.4, 50 mM NaCl. Three replicates per peptide are shown in black, blue, and red, respectively. Right in panel, AFM images of samples at the end of the aggregation assay.

We next applied ITC to test if the peptides have affinity for β-wrapin AS10, which binds Aβ, αSyn and IAPP each with sub-micromolar affinity and concomitantly induces β-hairpin conformation [43]. This was investigated only for the four peptides that did not precipitate in aqueous buffer at neutral pH, as heats resulting from precipitate formation or dissolution would superpose the ITC signal that stems from binding. For the three peptides that exhibited an increase in ThT fluorescence in the course of the aggregation assays, TTC5(335-361),

NDUFS7(104-129), and PAP(185-208), heat signals in agreement with 1:1 binding were observed, yielding dissociation constants of 4.7±0.9 µM, 4.7±0.5 µM, and 39±5 µM, respectively (Figs. 4A and 6). In contrast, heat signals were not observed for the peptide NBPF1(928-946) that was soluble and did not show ThT fluorescence.

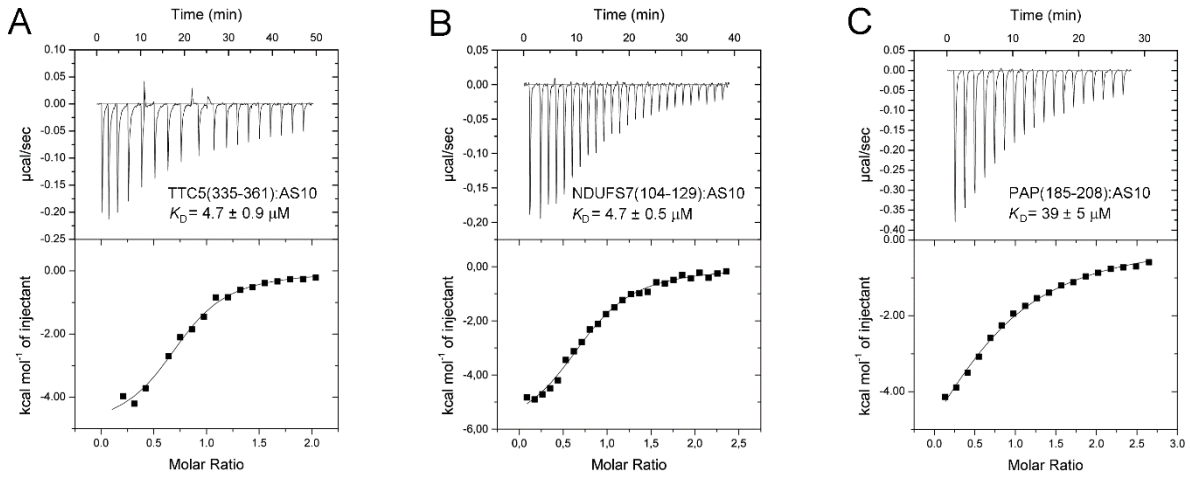

Figure 6: Binding of peptides to β-wrapin AS10 observed by ITC. Titrations of (A) 500 µM TTC5(335-361), (B) 300 µM NDUFS7(104-129), or (C) 300 µM PAP(185-208) into 30 µM AS10. The upper panels show the baseline-corrected instrumental response. The lower panels show the integrated data (filled squares) and the best fit of the parameters of a 1:1 binding model (continuous line).

To test for β-hairpin formation in the peptides upon binding to AS10 we performed NMR spectroscopy. ^{1}H-^{15}N HSQC NMR spectroscopy using ^{15}N-labeled AS10 (^{15}N-AS10) and unlabeled binding partner leads to characteristic changes upon β-hairpin folding coupled to binding. These include a great increase in resonance dispersion, appearance of four amide proton resonances in the glycine region (^{15}N chemical shift <110 ppm) stemming from Gly-13 and Gly-14 in the two AS10-subunits, as well as appearance of amide proton resonances with shift values typical for β-sheet conformation (high ^{1}H and high ^{15}N chemical shifts) [43]. This signature was observed here for the three peptides TTC5(335-361), NDUFS7(104-129), and PAP(185-208) with affinity for AS10 according to ITC (Fig. 7A-C). Interestingly, this signature was also observed for CYP2W1(176-204), which formed precipitates upon dissolution, indicating that this peptide can also partition into a 1:1 complex with AS10 (Fig. 7D). In contrast, no change in the ^{1}H-^{15}N HSQC NMR spectrum of ^{15}N-AS10 was observed upon addition of the other four peptides, which is in line with the absence of AS10 affinity for

NBPF1(928-946) demonstrated by ITC and with the insolubility of FibA(655-678), 3-PGDH(298-319), and MIC26(153-178).

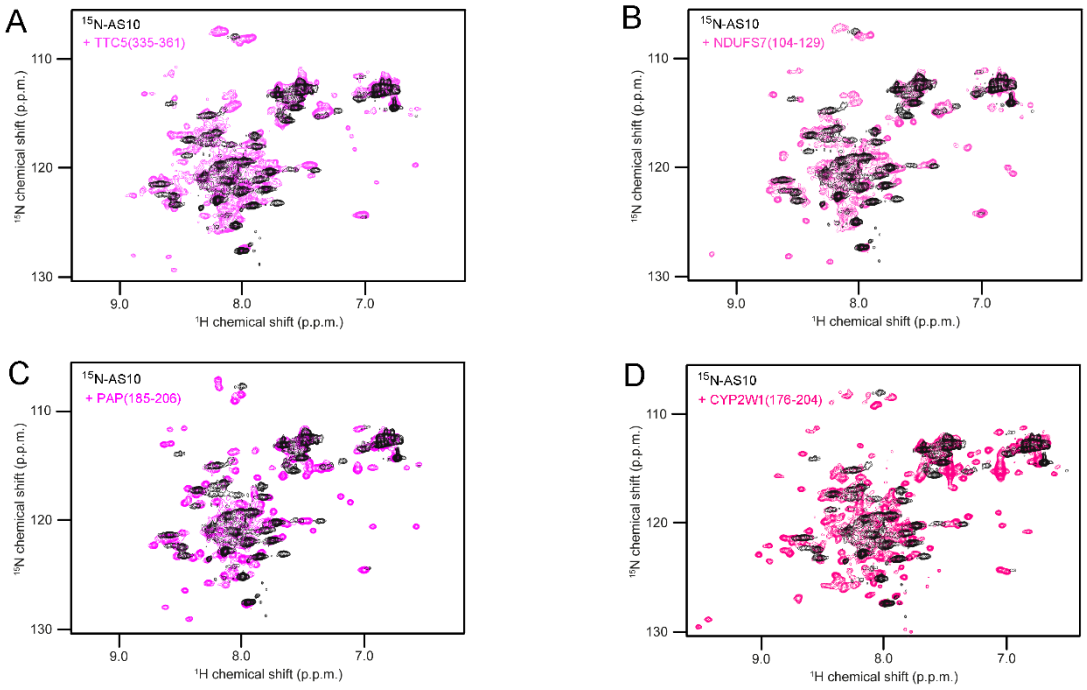

Figure 7: NMR spectroscopy indicates β-hairpin formation upon AS10 binding. ^{1}H-^{15}N HSQC NMR spectra of ^{15}N-AS10 in the absence (black) or presence (magenta to pink red color range) of a slight excess of unlabeled (A) TTC5(335-361), (B) NDUFS7(104-129), (C) PAP(185-208), or (D) CYP2W1(176-204), respectively.

To determine the registries of the β-hairpins of TTC5(335-361), NDUFS7(104-129), PAP(185-208), and CYP2W1(176-204) formed in complex with AS10, we performed NMR spectroscopy on the ^{13}C,^{15}N-labeled complexes of peptides with AS10. To circumvent cost-intensive chemical synthesis of isotopically labeled peptides, fusion constructs of AS10 at the N-terminus and the respective peptide at the C-terminus, linked via a flexible $(G_4S)_3$ linker, were produced recombinantly. For NDUFS7(104-129), PAP(185-208), and CYP2W1(176-204), the backbone amide resonances of ^{15}N-labeled AS10 bound to the unlabeled peptides (Fig. 7B-D) were recovered in the ^{13}C,^{15}N-labeled fusion constructs, demonstrating that the structure of the complex is not affected by the fusion (Fig. 8A). In contrast, this was not true for the AS10 fusion construct of TTC5(335-361), which prohibited determination of the β-hairpin registry in this case. For registry determination, the resonances stemming from the β-hairpin motif were assigned by standard triple resonance heteronuclear NMR techniques and characteristic NOE

contacts involving NH and Hα protons in the backbones of the peptides and of AS10 were identified. For all three peptides, the NOE contacts were compatible with only one unique β-hairpin registry (Figs. 8B and S2). The β-hairpin registries determined for PAP(185-208), CYP2W1(176-204), and NDUFS7(104-129) are shown in Fig. 8C-E along with those of Aβ, αSyn and IAPP (Fig. 8F).

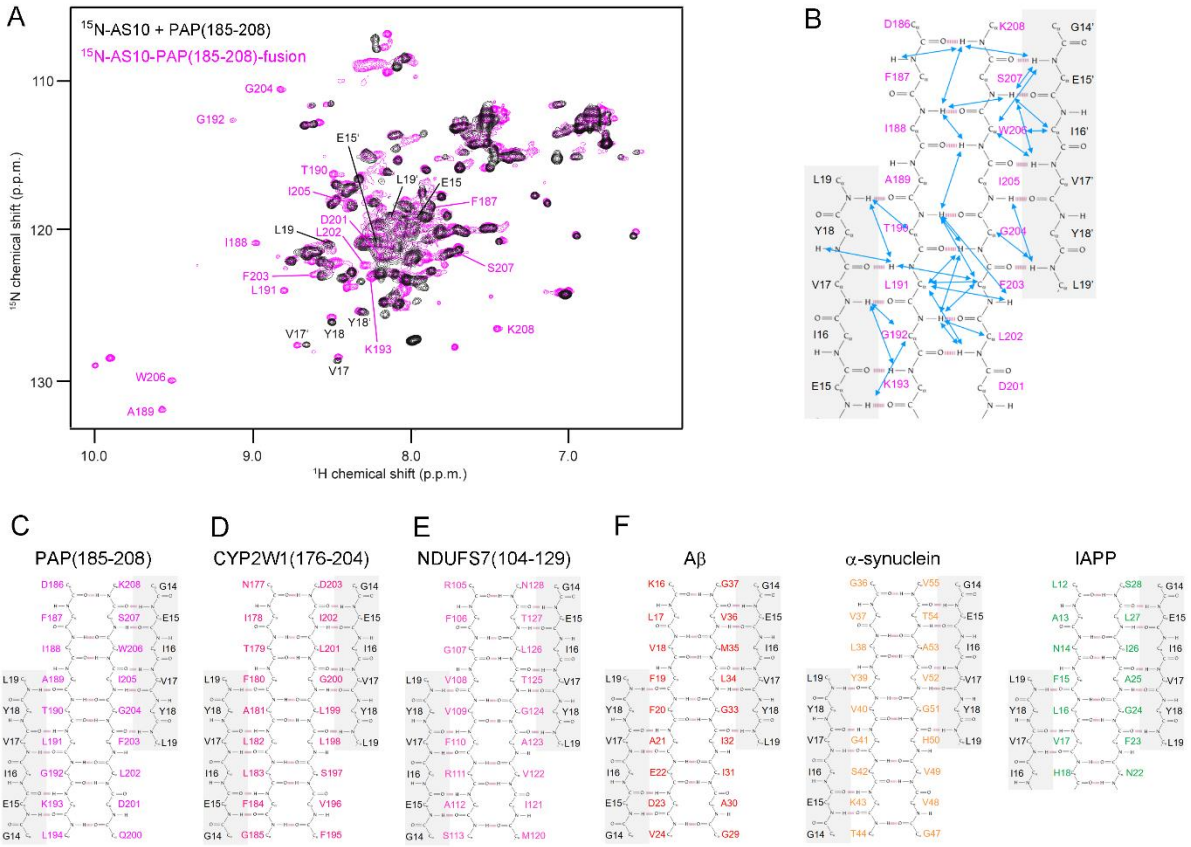

Figure 8: Determination of β-sheet registries. (A) Overlay of the ^{1}H-^{15}N HSQC NMR spectra of ^{15}N-AS10 in the presence of unlabeled PAP(185-208) (black) and of the ^{13}C,^{15}N-labeled AS10-PAP(185-208) fusion construct (magenta). Assignments of backbone amide resonances stemming from the β-sheet were obtained by NMR spectroscopy of the fusion construct and are displayed in black for AS10 residues and in magenta for PAP(185-208) residues. (B) NOE contacts (blue arrows) involving backbone NH and Hα protons allow identification of the β-sheet registry in the PAP(185-208):AS10 complex. Two AS10 β-strands (gray background, black residue labels) flank the β-hairpin formed by PAP(185-208) (white background, magenta residue labels). (C)-(F) Comparison of β-hairpin registries determined in this work (C-E) with those identified previously in Aβ, αSyn, and IAPP (F) [37-39].

As the general architecture of all six intermolecular β-sheets was identical in all the cases (Fig. 8C-F), we modeled the structures of the AS10 complexes of PAP(185-208), CYP2W1(176-204), and NDUFS7(104-129) using the known structures of β-wrapins with Aβ, αSyn and IAPP as starting point. Specifically, the template used for initial modeling of the AS10 complexes of the peptides was the structure of the Aβ:AS10 complex [51]. We first mutated the Aβ residues that form the two β-strands to the residues of the peptides at the corresponding position in the experimentally derived β-sheet registries. Subsequently, the loop residues of Aβ (VGSNKG) were replaced by the loop residues of the individual peptides, modeled using Modeller [52]. The resulting structures were used as initial structures for MD simulations performed analogous to our previous studies [51, 53], yielding snapshots of the AS10 complexes of PAP(185-208), CYP2W1(176-204), and NDUFS7(104-129) which were generally in agreement with the experimental constraints (Fig. 9). Files containing coordinates of the ten snapshots of lowest energy for each complex are available in the supplementary material of this article.

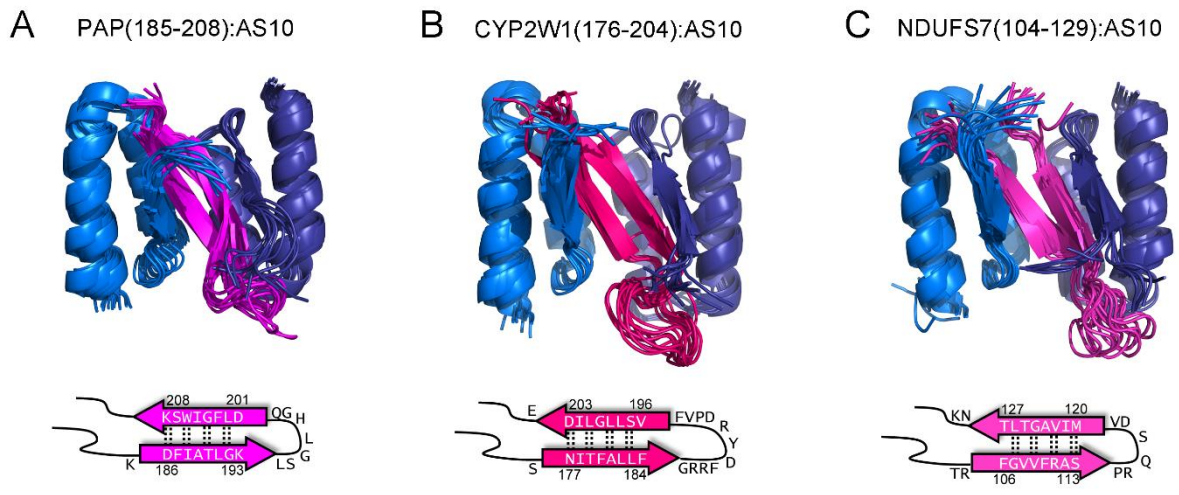

Figure 9: Computationally predicted structural models of β-hairpins in complex with AS10. Models were initially built based on the common β-sheet architecture of the newly identified β-hairpin complexes and the known β-hairpin complexes of Aβ, αSyn and IAPP. The 10 structures of lowest energy in subsequent MD simulations are displayed. The corresponding coordinate files are available in the supplementary material.

Taken together, the characterization of the test set of eight protein segments identified in the prediction showed that the majority of them formed ThT-positive structures. For four of the eight segments, β-hairpin formation in complex with AS10 analogous to that observed for Aβ, αSyn and IAPP was confirmed.

1.3.3 PAP(185-208) triggers semen amyloid formation

The herein identified protein segments with capacity to adopt β-hairpin conformation are usually incorporated into the native fold of their source protein, which prohibits amyloid formation (Fig. 4B). However, when liberated from the native fold, they might be able to form amyloid and gain new biological activities. For example, prostatic acid phosphatase (PAP) is synthesized in the prostatic gland and secreted into the semen, where it is proteolytically cleaved into many fragments [58]. Two of these fragments, PAP(248-286) and PAP(85-120) are known to exist as amyloids in the seminal plasma [59, 60]. Similarly, semenogelin-1 (SEM1) and semenogelin-2 (SEM2) are cleaved into fragments that also form semen amyloids [61, 62]. The semen amyloids belong to the class of functional amyloid, as they fulfill beneficial roles in the selection of healthy sperms [63].

Here we tested if the β-hairpin-forming PAP segment PAP(185-208) identified above can modulate amyloid formation of PAP(248-286) or SEM1(86-107), as these interactions might occur in the seminal plasma. PAP(185-208) at concentrations up to 100 μM did not exhibit ThT fluorescence in the time frame of the aggregation assay (Fig. 10A); concentrations >0.5 mM, however, were sufficient for amyloid formation (Fig. 5D). PAP(248-286) and SEM1(86-107) did not exhibit ThT fluorescence in the time frame of the aggregation assays at concentrations of 500 μM and 300 μM, respectively (Fig. 10B,C), in line with the high concentrations (>1 mM) applied in previous studies of *in vitro* amyloid formation of these fragments [60, 61]. Nevertheless, even in the absence of ThT fluorescence at moderate peptide concentrations, aggregates of amorphous shape were detected by AFM of PAP(185-208), PAP(248-286), and SEM1(86-107) (Fig. 10D-F). When low concentrations of PAP(185-208) were added to aggregation assays of 500 μM PAP(248-286) or 300 μM SEM1(86-107), ThT time traces featuring a lag-time and a phase of rapid growth indicative of amyloid formation were obtained (Fig. 10B,C). The corresponding AFM demonstrated a shift to fibrillar aggregate morphology (Fig. 10G,H). The data indicates that PAP(185-208) can trigger the formation of semen amyloids, at concentrations where PAP(185-208) alone does not form amyloid. We conclude that cross-interaction of the herein identified β-hairpin forming segment PAP(185-208) with PAP(248-286) and SEM1(86-107) can promote semen amyloid formation.

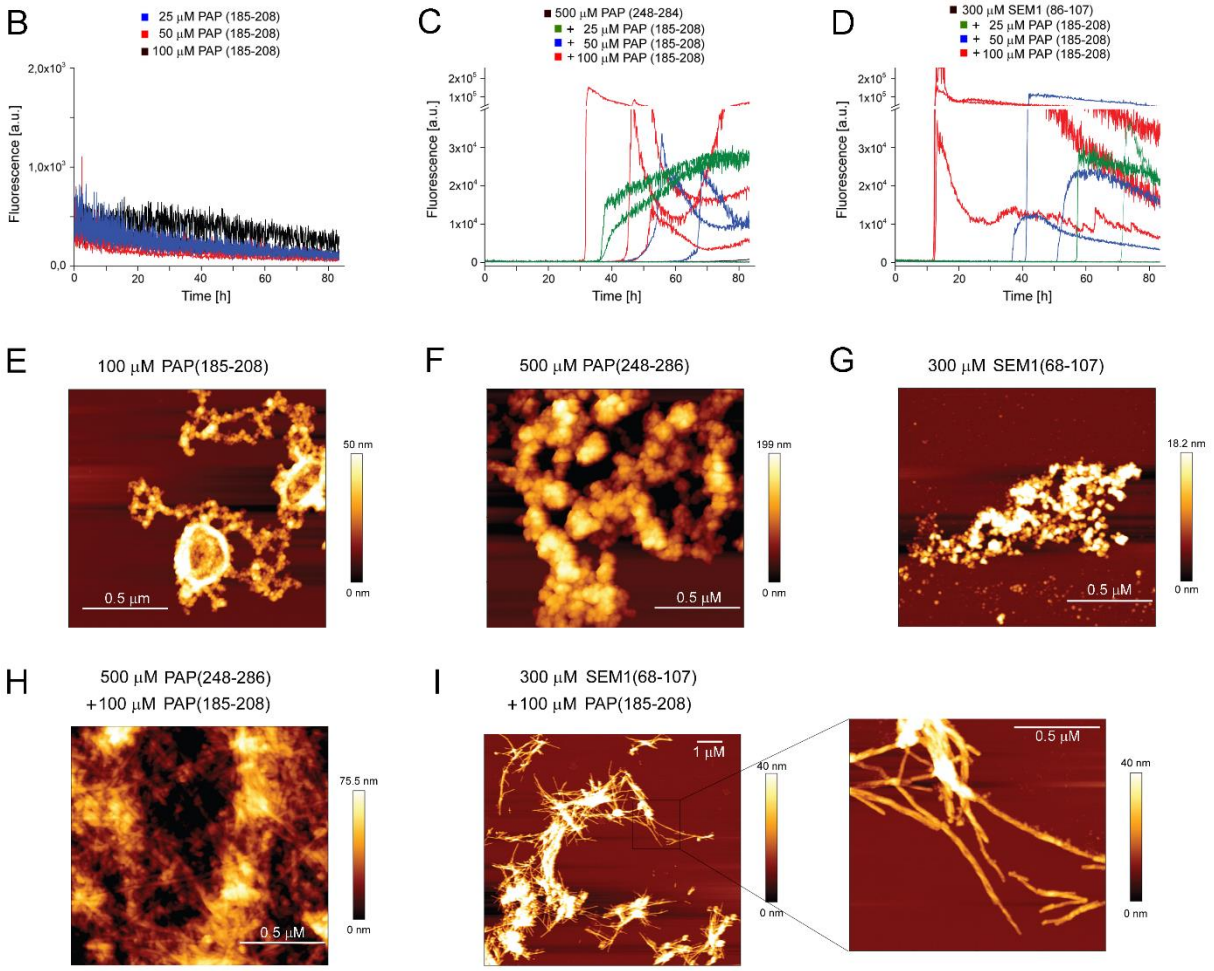

Figure 10: PAP(185-208) triggers semen amyloid formation. (A) Amino acid sequences of the identified β-hairpin-forming amyloidogenic segment PAP(185-208) and the semen amyloid fragments PAP(248-286) and SEM1(86-107). (B)-(D) Time courses of ThT fluorescence of (B) PAP(185-208) alone, (C) PAP(248-286) in absence and presence of PAP(185-208), and (D) SEM1(86-107) in absence and presence of PAP(185-208). (E)-(I) AFM images at the end of the aggregation assays of the individual peptides (E-G) and of the co-incubations of PAP(185-208) with (H) PAP(248-286) or (I) SEM1(86-107).

1.4 Discussion

In this study we aimed to identify protein segments with similarity to Aβ, αSyn and IAPP, three highly amyloidogenic proteins with important roles in protein misfolding diseases. Starting point was the common formation of β-hairpins in all three proteins in regions that are critical for amyloid formation [37-39]. These β-hairpins are stabilized upon binding to engineered binding proteins, have a common architecture, and one binding protein, β-wrapin AS10, binds all three proteins with sub-micromolar affinity [43]. The search for proteins with propensity to form similar β-hairpins might identify further molecules that contribute to disease processes and may improve our understanding of the roles of β-hairpins in amyloid formation. By combining the capacity of the TANGO algorithm to predict APRs with the general architecture of β-hairpins and some specific features of the amino acid composition of the Aβ, αSyn and IAPP β-hairpins, we filtered the human proteome and obtained 2505 potential β-hairpin regions distributed over 2098 proteins. The characterization of the test set of eight protein segments showed that this approach could indeed identify protein segments that form amyloid and can adopt β-hairpin conformation. The test set included one peptide, NBPF1(928-946), that did not form amyloid and remained soluble, showing that the filtered sequences have to be analyzed case-by-case. The test data set was not large enough to derive further factors deciding if or if not a sequence will form ThT-positive aggregates and bind to AS10 in a β-hairpin conformation. However, the wide range of pI values of the identified peptides indicates that no specific charge state is required (Fig. 4A). The peptides within the test set with highest affinity for AS10 achieved a K_D of 5 μM, which is an order of magnitude higher than the K_Ds of Aβ, αSyn and IAPP [43]. The higher affinity of Aβ and αSyn is not surprising, as the generation of AS10 included steps for selection for Aβ binding and affinity maturation for αSyn. The high affinity of IAPP, on the other hand, is remarkable, as it was not involved in the selection [43].

A potential relevance of the identified β-hairpin segments has to be evaluated case-by-case. The segments are usually incorporated into the source protein structure, lacking that conformational flexibility that is required for folding into a β-hairpin or into an amyloid structure (Fig. 1). However, the segments may gain this flexibility during their lifetimes, as described above for PAP, which is cleaved into fragments by proteases in the seminal fluid. PAP fragments that include the segment PAP(185-208) are likely present in the seminal fluid, where they may trigger the formation of semen amyloids built from PAP(248-286) and SEM1(86-107), as

suggested by the aggregation assay data (Fig. 10). In conclusion, this study has identified a large number of potential β-hairpin-forming amyloidogenic protein segments in the human proteome which may have important roles in amyloid formation.

Acknowledgments

This project has received funding from the European Research Council under the European Union's Horizon 2020 research and innovation program, grant agreement No. 726368 (W.H.), and from the National Institute on Aging, NIH, R03 AG058100 (P.T.). We acknowledge access to the Jülich-Düsseldorf Biomolecular NMR Center. All MD simulations and energy calculations were performed using computational resources available to P.T. provided by the Texas A&M High Performance Research Computing Facility, the College of Engineering and the Artie McFerrin Department of Chemical Engineering. We acknowledge Nina Kirchgässler for support with CD spectroscopy. We acknowledge discussions with Joseph M. Jakubowski.

1.5 References

1. M.G. Iadanza, M.P. Jackson, E.W. Hewitt, N.A. Ranson, S.E. Radford, A new era for understanding amyloid structures and disease, Nat. Rev. Mol. Cell Biol., 19 (2018) 755-773.
2. T.P. Knowles, M. Vendruscolo, C.M. Dobson, The amyloid state and its association with protein misfolding diseases, Nat. Rev. Mol. Cell Biol., 15 (2014) 384-396.
3. D. Otzen, R. Riek, Functional Amyloids, Cold Spring Harb. Perspect. Biol., 11 (2019).
4. D. Willbold, B. Strodel, G.F. Schröder, W. Hoyer, H. Heise, Amyloid-type protein aggregation and prion-like properties of amyloids, Chem. Rev., 121 (2021) 8285-8307.
5. M.A. Jimenez, Design of monomeric water-soluble β-hairpin and β-sheet peptides, Methods Mol. Biol., 1216 (2014) 15-52.
6. Q. Shao, J. Wang, J. Shi, W. Zhu, The universality of β-hairpin misfolding indicated by molecular dynamics simulations, J. Chem. Phys., 139 (2013) 165103.
7. V. Munoz, P.A. Thompson, J. Hofrichter, W.A. Eaton, Folding dynamics and mechanism of beta-hairpin formation, Nature, 390 (1997) 196-199.
8. N.F. Dupuis, C. Wu, J.E. Shea, M.T. Bowers, Human islet amyloid polypeptide monomers form ordered β-hairpins: a possible direct amyloidogenic precursor, J. Am. Chem. Soc., 131 (2009) 18283-18292.
9. A.C. Gill, β-hairpin-mediated formation of structurally distinct multimers of neurotoxic prion peptides, PLoS One, 9 (2014) e87354.
10. G. Reddy, J.E. Straub, D. Thirumalai, Influence of preformed Asp23-Lys28 salt bridge on the conformational fluctuations of monomers and dimers of Aβ peptides with implications for rates of fibril formation, J. Phys. Chem. B, 113 (2009) 1162-1172.
11. D.J. Rosenman, C.R. Connors, W. Chen, C. Wang, A.E. Garcia, Aβ monomers transiently sample oligomer and fibril-like configurations: ensemble characterization using a combined MD/NMR approach, J. Mol. Biol., 425 (2013) 3338-3359.
12. S. Mitternacht, I. Staneva, T. Härd, A. Irbäck, Monte Carlo study of the formation and conformational properties of dimers of Abeta42 variants, J. Mol. Biol., 410 (2011) 357-367.

13. H. Yu, W. Han, W. Ma, K. Schulten, Transient β-hairpin formation in α-synuclein monomer revealed by coarse-grained molecular dynamics simulation, J. Chem. Phys., 143 (2015) 243142.

14. L. Cruz, J.S. Rao, D.B. Teplow, B. Urbanc, Dynamics of metastable β-hairpin structures in the folding nucleus of amyloid β-protein, J. Phys. Chem. B, 116 (2012) 6311-6325.

15. N.D. Lazo, M.A. Grant, M.C. Condron, A.C. Rigby, D.B. Teplow, On the nucleation of amyloid β-protein monomer folding, Protein Sci., 14 (2005) 1581-1596.

16. L. Xu, R. Nussinov, B. Ma, Allosteric stabilization of the amyloid-β peptide hairpin by the fluctuating N-terminal, Chem. Commun., 52 (2016) 1733-1736.

17. R. Halfmann, S. Alberti, R. Krishnan, N. Lyle, C.W. O'Donnell, O.D. King, B. Berger, R.V. Pappu, S. Lindquist, Opposing effects of glutamine and asparagine govern prion formation by intrinsically disordered proteins, Mol. Cell, 43 (2011) 72-84.

18. W. Zheng, M.Y. Tsai, M. Chen, P.G. Wolynes, Exploring the aggregation free energy landscape of the amyloid-β protein (1-40), Proc. Natl. Acad. Sci. U. S. A., 113 (2016) 11835-11840.

19. K.A. Ball, A.H. Phillips, D.E. Wemmer, T. Head-Gordon, Differences in β-strand populations of monomeric Aβ40 and Aβ42, Biophys. J., 104 (2013) 2714-2724.

20. B. Tarus, T.T. Tran, J. Nasica-Labouze, F. Sterpone, P.H. Nguyen, P. Derreumaux, Structures of the Alzheimer's wild-type Aβ1-40 dimer from atomistic simulations, J. Phys. Chem. B, 119 (2015) 10478-10487.

21. M. Grabenauer, C. Wu, P. Soto, J.E. Shea, M.T. Bowers, Oligomers of the prion protein fragment 106-126 are likely assembled from β-hairpins in solution, and methionine oxidation inhibits assembly without altering the peptide's monomeric conformation, J. Am. Chem. Soc., 132 (2010) 532-539.

22. S. Singh, C.C. Chiu, A.S. Reddy, J.J. de Pablo, α-helix to β-hairpin transition of human amylin monomer, J. Chem. Phys., 138 (2013) 155101.

23. A.S. Reddy, L. Wang, S. Singh, Y.L. Ling, L. Buchanan, M.T. Zanni, J.L. Skinner, J.J. de Pablo, Stable and metastable states of human amylin in solution, Biophys. J., 99 (2010) 2208-2216.

24. W. Hosia, N. Bark, E. Liepinsh, A. Tjernberg, B. Persson, D. Hallen, J. Thyberg, J. Johansson, L. Tjernberg, Folding into a β-hairpin can prevent amyloid fibril formation, Biochemistry, 43 (2004) 4655-4661.

25. K.L. Sciarretta, D.J. Gordon, A.T. Petkova, R. Tycko, S.C. Meredith, Aβ40-Lactam(D23/K28) models a conformation highly favorable for nucleation of amyloid, Biochemistry, 44 (2005) 6003-6014.

26. E.D. Agerschou, V. Borgmann, M.M. Wördehoff, W. Hoyer, Inhibitor and substrate cooperate to inhibit amyloid fibril elongation of α-synuclein, Chem. Sci., 11 (2020) 11331-11337.

27. E.D. Agerschou, M.P. Schützmann, N. Reppert, M.M. Wördehoff, H. Shaykhalishahi, A.K. Buell, W. Hoyer, β-Turn exchanges in the α-synuclein segment 44-TKEG-47 reveal high sequence fidelity requirements of amyloid fibril elongation, Biophys. Chem., 269 (2021) 106519.

28. D. Bhowmik, K.R. Mote, C.M. MacLaughlin, N. Biswas, B. Chandra, J.K. Basu, G.C. Walker, P.K. Madhu, S. Maiti, Cell-membrane-mimicking lipid-coated nanoparticles confer Raman enhancement to membrane proteins and reveal membrane-attached amyloid-β conformation, ACS Nano, 9 (2015) 9070-9077.

29. S. Maity, M. Hashemi, Y.L. Lyubchenko, Nano-assembly of amyloid β peptide: role of the hairpin fold, Sci. Rep., 7 (2017) 2344.

30. T.M. Doran, E.A. Anderson, S.E. Latchney, L.A. Opanashuk, B.L. Nilsson, An azobenzene photoswitch sheds light on turn nucleation in amyloid-β self-assembly, ACS Chem. Neurosci., 3 (2012) 211-220.

31. C. Lendel, M. Bjerring, A. Dubnovitsky, R.T. Kelly, A. Filippov, O.N. Antzutkin, N.C. Nielsen, T. Härd, A hexameric peptide barrel as building block of amyloid-β protofibrils, Angew. Chem. Int. Ed., 53 (2014) 12756-12760.

32. A. Sandberg, L.M. Luheshi, S. Sollvander, T. Pereira de Barros, B. Macao, T.P. Knowles, H. Biverstal, C. Lendel, F. Ekholm-Petterson, A. Dubnovitsky, L. Lannfelt, C.M. Dobson, T. Härd, Stabilization of neurotoxic Alzheimer amyloid-β oligomers by protein engineering, Proc. Natl. Acad. Sci. U. S. A., 107 (2010) 15595-15600.

33. A.I. Ilitchev, M.J. Giammona, C. Olivas, S.L. Claud, K.L. Lazar Cantrell, C. Wu, S.K. Buratto, M.T. Bowers, Hetero-oligomeric amyloid assembly and mechanism: Prion fragment PrP(106-126) catalyzes the islet amyloid polypeptide β-hairpin, J. Am. Chem. Soc., 140 (2018) 9685-9695.

34. N. Izuo, C. Kasahara, K. Murakami, T. Kume, M. Maeda, K. Irie, K. Yokote, T. Shimizu, A Toxic Conformer of Aβ42 with a Turn at 22-23 is a Novel Therapeutic Target for Alzheimer's Disease, Sci. Rep., 7 (2017) 11811.

35. L. Yu, R. Edalji, J.E. Harlan, T.F. Holzman, A.P. Lopez, B. Labkovsky, H. Hillen, S. Barghorn, U. Ebert, P.L. Richardson, L. Miesbauer, L. Solomon, D. Bartley, K. Walter, R.W. Johnson, P.J. Hajduk, E.T. Olejniczak, Structural characterization of a soluble amyloid β-peptide oligomer, Biochemistry, 48 (2009) 1870-1877.

36. M. Khaled, I. Rönnbäck, L.L. Ilag, A. Gräslund, B. Strodel, N. Österlund, A hairpin motif in the amyloid-β peptide is important for formation of disease-related oligomers, J. Am. Chem. Soc., (2023).

37. W. Hoyer, C. Grönwall, A. Jonsson, S. Ståhl, T. Härd, Stabilization of a β-hairpin in monomeric Alzheimer's amyloid-β peptide inhibits amyloid formation, Proc. Natl. Acad. Sci. U. S. A., 105 (2008) 5099-5104.

38. E.A. Mirecka, S. Feuerstein, L. Gremer, G.F. Schröder, M. Stoldt, D. Willbold, W. Hoyer, β-Hairpin of islet amyloid polypeptide bound to an aggregation inhibitor, Sci. Rep., 6 (2016) 33474.

39. E.A. Mirecka, H. Shaykhalishahi, A. Gauhar, S. Akgül, J. Lecher, D. Willbold, M. Stoldt, W. Hoyer, Sequestration of a β-hairpin for control of α-synuclein aggregation, Angew. Chem. Int. Ed., 53 (2014) 4227-4230.

40. C. Grönwall, A. Jonsson, S. Lindström, E. Gunneriusson, S. Stahl, N. Herne, Selection and characterization of Affibody ligands binding to Alzheimer amyloid β peptides, J. Biotechnol., 128 (2007) 162-183.

41. E.A. Mirecka, L. Gremer, S. Schiefer, F. Oesterhelt, M. Stoldt, D. Willbold, W. Hoyer, Engineered aggregation inhibitor fusion for production of highly amyloidogenic human islet amyloid polypeptide, J. Biotechnol., 191 (2014) 221-227.

42. C.S.R. Grüning, E.A. Mirecka, A.N. Klein, E. Mandelkow, D. Willbold, S.F. Marino, M. Stoldt, W. Hoyer, Alternative conformations of the Tau repeat domain in complex with an engineered binding protein, J. Biol. Chem., 289 (2014) 23209-23218.

43. H. Shaykhalishahi, E.A. Mirecka, A. Gauhar, C.S. Gruning, D. Willbold, T. Härd, M. Stoldt, W. Hoyer, A β-hairpin-binding protein for three different disease-related amyloidogenic proteins, ChemBioChem, 16 (2015) 411-414.

44. A.M. Fernandez-Escamilla, F. Rousseau, J. Schymkowitz, L. Serrano, Prediction of sequence-dependent and mutational effects on the aggregation of peptides and proteins, Nat. Biotechnol., 22 (2004) 1302-1306.

45. R. Linding, J. Schymkowitz, F. Rousseau, F. Diella, L. Serrano, A comparative study of the relationship between protein structure and β-aggregation in globular and intrinsically disordered proteins, J. Mol. Biol., 342 (2004) 345-353.

46. F. Rousseau, J. Schymkowitz, L. Serrano, Protein aggregation and amyloidosis: confusion of the kinds?, Curr. Opin. Struct. Biol., 16 (2006) 118-126.

47. C. The UniProt, UniProt: the universal protein knowledgebase, Nucleic Acids Res., 45 (2017) D158-D169.

48. Z. Solyom, M. Schwarten, L. Geist, R. Konrat, D. Willbold, B. Brutscher, BEST-TROSY experiments for time-efficient sequential resonance assignment of large disordered proteins, J. Biomol. NMR, 55 (2013) 311-321.

49. F. Delaglio, S. Grzesiek, G.W. Vuister, G. Zhu, J. Pfeifer, A. Bax, NMRPipe: a multidimensional spectral processing system based on UNIX pipes, J. Biomol. NMR, 6 (1995) 277-293.

50. W.F. Vranken, W. Boucher, T.J. Stevens, R.H. Fogh, A. Pajon, M. Llinas, E.L. Ulrich, J.L. Markley, J. Ionides, E.D. Laue, The CCPN data model for NMR spectroscopy: development of a software pipeline, Proteins, 59 (2005) 687-696.

51. A.A. Orr, M.M. Wördehoff, W. Hoyer, P. Tamamis, Uncovering the binding and specificity of β-wrapins for amyloid-β and α-synuclein, J. Phys. Chem. B, 120 (2016) 12781-12794.

52. B. Webb, A. Sali, Protein structure modeling with MODELLER, Methods Mol. Biol., 1137 (2014) 1-15.

53. A.A. Orr, H. Shaykhalishahi, E.A. Mirecka, S.V.R. Jonnalagadda, W. Hoyer, P. Tamamis, Elucidating the multi-targeted anti-amyloid activity and enhanced islet amyloid polypeptide binding of β-wrapins, Comput. Chem. Eng., 116 (2018) 322-332.

54. R. Prabakaran, D. Goel, S. Kumar, M.M. Gromiha, Aggregation prone regions in human proteome: Insights from large-scale data analyses, Proteins, 85 (2017) 1099-1118.

55. K.E. Marshall, K.L. Morris, D. Charlton, N. O'Reilly, L. Lewis, H. Walden, L.C. Serpell, Hydrophobic, aromatic, and electrostatic interactions play a central role in amyloid fibril formation and stability, Biochemistry, 50 (2011) 2061-2071.

56. F.T. Senguen, N.R. Lee, X. Gu, D.M. Ryan, T.M. Doran, E.A. Anderson, B.L. Nilsson, Probing aromatic, hydrophobic, and steric effects on the self-assembly of an amyloid-β fragment peptide, Mol. Biosyst., 7 (2011) 486-496.

57. H. LeVine, 3rd, Quantification of β-sheet amyloid fibril structures with thioflavin T, Methods Enzymol., 309 (1999) 274-284.

58. A. Röcker, N.R. Roan, J.K. Yadav, M. Fändrich, J. Münch, Structure, function and antagonism of semen amyloids, Chemical Communications (Cambridge), 54 (2018) 7557-7569.

59. F. Arnold, J. Schnell, O. Zirafi, C. Stürzel, C. Meier, T. Weil, L. Ständker, W.G. Forssmann, N.R. Roan, W.C. Greene, F. Kirchhoff, J. Münch, Naturally occurring fragments from two distinct regions of the prostatic acid phosphatase form amyloidogenic enhancers of HIV infection, J. Virol., 86 (2012) 1244-1249.

60. J. Münch, E. Rücker, L. Ständker, K. Adermann, C. Goffinet, M. Schindler, S. Wildum, R. Chinnadurai, D. Rajan, A. Specht, G. Gimenez-Gallego, P.C. Sanchez, D.M. Fowler, A. Koulov, J.W. Kelly, W. Mothes, J.C. Grivel, L. Margolis, O.T. Keppler, W.G. Forssmann, F. Kirchhoff, Semen-derived amyloid fibrils drastically enhance HIV infection, Cell, 131 (2007) 1059-1071.

61. N.R. Roan, H. Liu, S.M. Usmani, J. Neidleman, J.A. Müller, A. Avila-Herrera, A. Gawanbacht, O. Zirafi, S. Chu, M. Dong, S.T. Kumar, J.F. Smith, K.S. Pollard, M. Fandrich, F. Kirchhoff, J. Münch, H.E. Witkowska, W.C. Greene, Liquefaction of semen generates and later degrades a conserved semenogelin peptide that enhances HIV infection, J. Virol., 88 (2014) 7221-7234.

62. N.R. Roan, J.A. Müller, H. Liu, S. Chu, F. Arnold, C.M. Stürzel, P. Walther, M. Dong, H.E. Witkowska, F. Kirchhoff, J. Münch, W.C. Greene, Peptides released by physiological cleavage of semen coagulum proteins form amyloids that enhance HIV infection, Cell Host Microbe, 10 (2011) 541-550.

63. N.R. Roan, N. Sandi-Monroy, N. Kohgadai, S.M. Usmani, K.G. Hamil, J. Neidleman, M. Montano, L. Ständker, A. Rocker, M. Cavrois, J. Rosen, K. Marson, J.F. Smith, C.D. Pilcher, F. Gagsteiger, O. Sakk, M. O'Rand, P.V. Lishko, F. Kirchhoff, J. Münch, W.C. Greene, Semen amyloids participate in spermatozoa selection and clearance, Elife, 6 (2017).

1.6 Supporting information

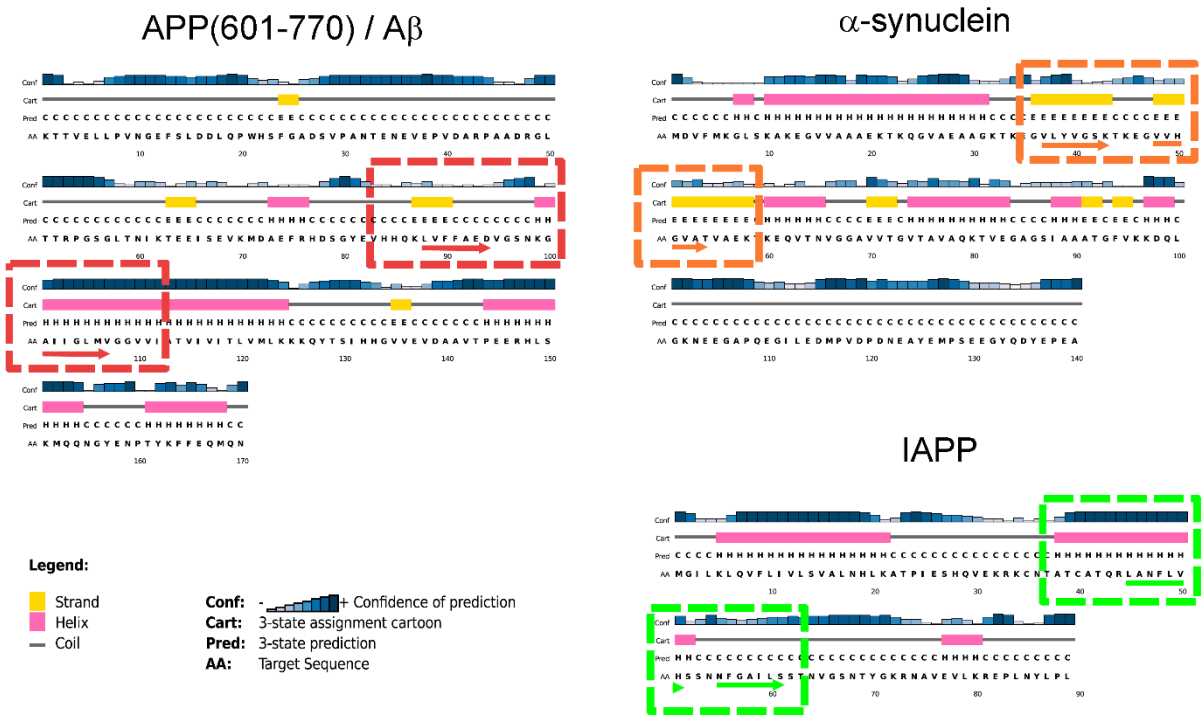

Figure S1: Secondary structure prediction does not suggest commonalities between the β-hairpin regions of Aβ, αSyn and IAPP. Secondary structure prediction was performed with the algorithm PSIPRED, for Aβ and IAPP in the sequence context of their precursor proteins. The β-hairpin-forming regions are highlighted in dashed boxes and β-strand positions are indicated by arrows. For αSyn, β-strand propensity was lining up well with the β-strands in its β-hairpin. In contrast, this was not observed for Aβ and IAPP.

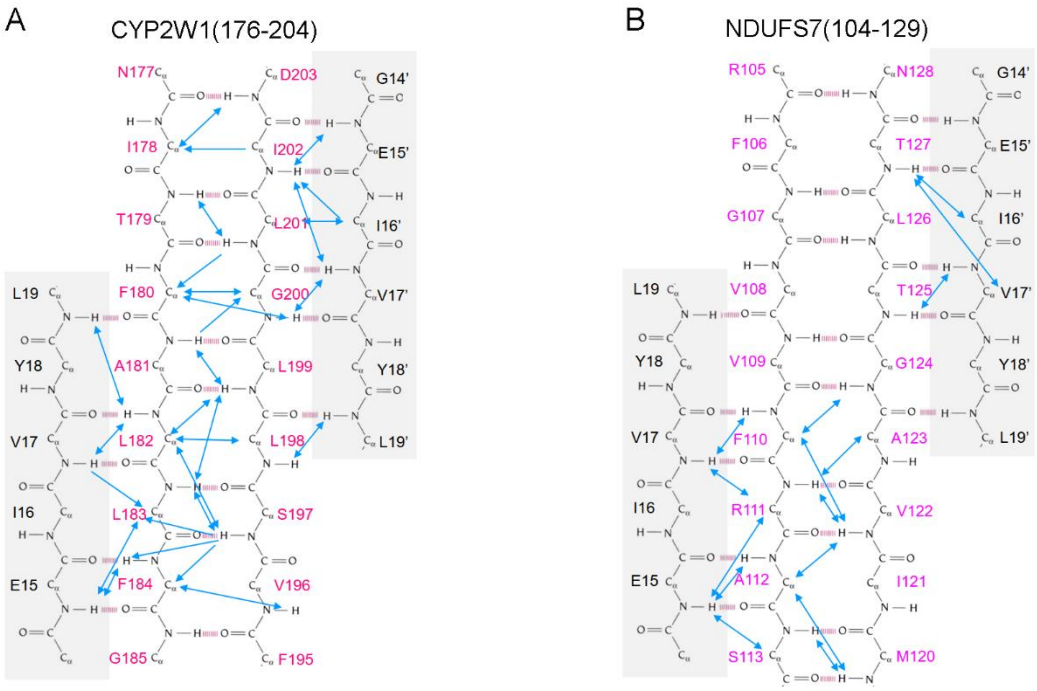

Figure S2: β-Sheet registries of CYP2W1(176-204) and NDUFS7(104-129). β-Sheet registries were determined from NOE contacts involving backbone NH and Hα protons (blue arrows). Two AS10 β-strands (gray background, black residue labels) flank the β-hairpins formed by (A) CYP2W1(176-204) (white background, pink red residue labels) or (B) NDUFS7(104-129) (white background, magenta residue labels).

1.7 List of Figures

1.8 List of Abbreviations

°C	Degrees Celsius
3-PGDH	D-3-phosphoglycerate dehydrogenase
AD	Alzheimer's Disease
APR	Aggregation-prone region
Aβ	Amyloid beta
CYP2W1	Cytochrome P450 2W1
FibA	Fibrinogen alpha chain
HFIP	Hexafluoroisopropanol
IAPP	Islet amyloid polypeptide
IDPs	intrinsically disordered proteins
IPTG	Isopropyl-β-D-thiogalactopyranosid
MD	Molecular dynamics simulations
MHz	Megahertz
MIC26	MICOS complex subunit MIC26
mM	Millimolar
NBPF1	Neuroblastoma breakpoint family member 1
NDUSF7 mitochondrial	NADH dehydrogenase [ubiquinone] iron-sulfur protein 7,
PAP	Prostatic acid phosphatase
PD	Parkinson’s Disease
T2D	Type 2 Diabetes
ThT	Thioflavin T
Tris	Tris(hydroxymethyl)aminomethane
TTC5	Tetratricopeptide repeat protein 5
αSyn	α-synuclein
µg	Mikrogramm
µL	Mikroliter
µM	Mirkomolar

Project 2 [submitted Manuscript]:

Nucleation of α-synuclein amyloid fibrils induced by cross-interaction with β-hairpin peptides derived from immunoglobulin light chains

Content

Article information

Title of the manuscript: Nucleation of a-synuclein amyloid fibrils induced by cross-interaction with b-hairpin peptides derived from immunoglobulin light chains

Authors: Laetitia F. Heid[1], Tatsiana Kupreichyk[1,2], Marie P. Schützmann[1], Matthias Stoldt[2], Wolfgang Hoyer[1,2]

Journal: International Journal of Molecular Science

Status: Submitted

Data Availability Statement: Data is contained within the article.

Author contributions: Conceptualization, LFH and WH; investigation, LFH, TK, MS and WH; writing, LFH and WH. All authors have read and agreed to the published version of the manuscript.

[1]Institut für Physikalische Biologie, Heinrich Heine University Düsseldorf, 40204 Düsseldorf, Germany

[2]Institute of Biological Information Processing (IBI-7) and JuStruct: Jülich Center for Structural Biology, For-schungszentrum Jülich, 52425 Jülich, Germany

Correspondence: wolfgang.hoyer@hhu.de

Funding: This research was funded by the European Research Council, grant number 726368

Acknowledgments: We acknowledge access to the Jülich-Düsseldorf Biomolecular NMR Center.

Conflicts of Interest: The authors declare no conflict of interest.

Abstract

Heterologous interactions between different amyloid-forming proteins, also termed cross-interactions, may have critical impact on disease-related amyloid formation. β-Hairpin conformers of amyloid-forming proteins have been shown to affect the homologous interactions in the amyloid self-assembly process. Here, we applied two β-hairpin-forming peptides derived from immunoglobulin light chains as models to test how heterologous β-hairpins modulate fibril formation of the Parkinson's disease-associated protein α-synuclein (αSyn). The peptides SMAhp and LENhp comprise the β-strands C and C' of the κ4 antibodies SMA and LEN, which are associated with light chain amyloidosis and multiple myeloma, respectively. SMAhp and LENhp bind with high affinity to the β-hairpin-binding protein β-wrapin AS10 according to isothermal titration calorimetry and NMR spectroscopy. Addition of SMAhp and LENhp affects the kinetics of αSyn aggregation monitored by Thioflavin T (ThT) fluorescence, with the effect depending on assay conditions, salt concentration, and applied β-hairpin peptide. In the absence of agitation, sub-stoichiometric concentrations of the hairpin peptides strongly reduce the lag-time of αSyn aggregation, suggesting that they support nucleation of αSyn amyloid fibrils. The effect is also observed for aggregation of αSyn fragments lacking the N-terminus or lacking the C-terminus indicating that promotion of nucleation involves the interaction of hairpin peptides with the hydrophobic NAC region.

2.1 Introduction

2

The assembly of proteins into amyloid fibrils with cross-β architecture is associated with a wide range of diseases, in particular neurodegenerative diseases such as Parkinson's disease (PD) and non-neuropathic systemic amyloidoses such as AL amyloidosis [1]. PD belongs to the group of synucleinopathies, which are characterized by aggregates of the protein α-synuclein (αSyn) localized in the brain, whose spreading has been linked to pathogenesis [2-4]. In AL amyloidosis, the most prevalent systemic amyloidosis in the Western world, proliferation of monoclonal plasma cells that secrete high concentrations of immunoglobulin light chains leads to deposition of light chain amyloid fibrils in various organs, in particular heart, kidney, and liver, which is ultimately fatal [5,6].

The nucleation of amyloid fibrils is incompletely understood [7,8]. In the case of αSyn, heterogeneous nucleation processes are thought to dominate, with surfaces of membranes or of preexisting amyloid fibrils acting as plausible *in vivo* nucleation sites [9-11]. Similar to homologous interactions with αSyn fibrils [10], αSyn monomers can cross-interact with other amyloid proteins such as amyloid-β (Aβ) or islet amyloid polypeptide (IAPP), which may result in cross-seeding of αSyn aggregation [12-15].

The β-hairpin is a structural motif consisting of two β-strands that are connected by a turn and together form an antiparallel β-sheet [16,17]. As β-hairpins and amyloid fibrils are both built from β-strands, β-hairpin conformers are enriched in the conformational ensembles of amyloid-forming proteins [18-33]. Such β-hairpins may affect amyloid formation, either by forming oligomeric or fibrillar assemblies themselves, or by interacting with other oligomers or fibrils [18,19,24,25,27,32,34-47]. β-Hairpins may be of particular importance for amyloid formation of proteins with Greek key fold, including light chains, as these contain anti-parallel β-hairpin loops that are susceptible to diffusion, which may lead to exposure of sites that subsequently trigger amyloid formation [48]. An interesting case is the β-hairpin formed by the C and C' β-strands of the light chains SMA and LEN [48-52]. C-C' β-hairpins in immunoglobulins are only present in the variable domains of light chains (VLs). SMA and LEN are κ4 antibodies that differ in only eight amino acid residues [49]. While SMA is associated with light chain amyloidosis, LEN is not involved in amyloidosis but connected to multiple myeloma. In line with this, LEN requires harsher conditions including partial chemical denaturation for amyloid formation in vitro [49,50]. Interestingly, introduction of a single SMA residue into the LEN

sequence, namely the P40L mutation, is enough to regain the amyloidogenicity of SMA [50]. The P40L mutation is located in the turn connecting the C and C' β-strands (Figure 1A) [48]. Virtually all human light-chain sequences contain proline at position 40, and all those known to have a hydrophobic substitution at position 40 are amyloidogenic [53].

Figure 1: The C-C' β-hairpin in the light chain variable domain and β-hairpin binding by β-wrapins. (A) Structure of the LEN VL domain (pdb:1LVE) [54]. The C-C' β-hairpin is highlighted in orange, apart from the sites that differ between SMA and LEN, which are shown in red. Residue P40 in the turn of the C-C' β-hairpin is displayed as red spheres. (B) Sequences of hairpin peptides investigated in this study, with differences between SMAhp and LENhp highlighted in red. Amino acid residue 40 regulating amyloid formation is printed in bold. (C) Structure of β-wrapin AS69 (the two sub-units displayed in light grey and dark grey, respectively) in complex with the β-hairpin formed by αSyn (orange) (pdb:4BXL) [55]. AS69 binds β-hairpins in the same way as AS10 does [56,57].

Due to their roles in regulating amyloid formation, we chose the C-C' β-hairpins of SMA and LEN as models to investigate cross-interactions of β-hairpins and αSyn. The β-hairpins were applied as peptides, termed SMAhp and LENhp (Figure 1B). The potential of SMAhp and LENhp to adopt β-hairpin structure was confirmed by char-acterization of their complexes with the β-hairpin binding protein β-wrapin AS10 (Figure 1C) [57]. Subsequently, the effects of SMAhp and LENhp on αSyn fibril for-mation were investigated. Our data indicates that the β-hairpin peptides support the nucleation of αSyn amyloid fibrils.

2.2 Results

2.1. SMAhp and LENhp bind to the β-hairpin-binding protein β-wrapin AS10

The peptides SMAhp and LENhp comprise residues 29-54 of the respective VL domains (Figure 1B). To confirm that these VL segments can indeed adopt β-hairpin structure in peptide format, we tested their binding to the engineered binding protein β-wrapin AS10. AS10 stems from phage display selection of a β-wrapin library against the target αSyn and stabilizes a β-hairpin conformation of αSyn (Figure 1C) [55-57]. AS10 was found to bind each of the three disease-related amyloid proteins αSyn, Aβ, and IAPP with sub-micromolar affinity, stabilizing related β-hairpins [56-58]. AS10 may therefore serve as a tool for the identification of □-hairpins that can affect amy-loid formation.

In isothermal titration calorimetry (ITC), titration of SMAhp or LENhp into AS10 solutions demonstrated 1:1 binding with dissociation constants of 1.35±0.33 μM or 0.30±0.07 μM, respectively (Figure 2A). These affinities for AS10 are in the same range as those of αSyn (KD = 0.38 μM), Aβ (KD = 0.15 μM), and IAPP (KD = 0.91 μM) [57]. The 4.5-fold higher affinity of LENhp can be explained by the presence of proline residue P40, which is expected to support turn and β-hairpin formation. For both SMAhp and LENhp endothermic post-transition heat signals were observed, indicating that dilu-tion of the concentrated peptide solutions (c ≈ 0.6 mM) into the ITC cell leads to heat consumption. A plausible explanation is that the peptides form assemblies at high concentrations that (partially) disassemble upon dilution, which would result in detec-tion of heat of the disassembly reaction.

The structural basis of the interaction of SMAhp and LENhp with AS10 was investigated by 1H-15N HSQC NMR spectroscopy. Upon addition of unlabeled SMAhp or LENhp to 15N-labeled AS10 the resonance dispersion greatly increased, indicative of coupled folding and binding (Figure 2B). Four amide proton resonances appeared in the glycine region, which originate from Gly-13 and Gly-14 in the two AS10 subunits (Figure 2C). In addition, amide proton resonances were detected in the downfield region of the spectrum with shift values typical for β-sheet conformation (Figure 2C). The same pattern has been observed before for the interaction of AS10 with αSyn, Aβ, and IAPP (Figure 2C) [57]. The NMR data indicates that SMAhp and LENhp adopt β-hairpin conformation in complex with AS10 analogous to αSyn, Aβ, and IAPP.

2.2. LENhp and SMAhp promote nucleation of αSyn amyloid fibrils

We next tested the effects of SMAhp and LENhp on αSyn fibril formation by recording the kinetics of amyloid formation via fluorescence of the dye Thioflavin T (ThT) [59]. As nucleation of αSyn amyloid fibrils is slow at neutral pH, in vitro assays are usually performed under agitation and in the presence of glass beads, which en-hances nucleation at the air-water interface and promotes the proliferation of fibrils by increasing the number of fibril ends through fibril fragmentation [11,60,61]. Here, we performed αSyn fibril formation assays both under agitation (Figure 3) and under qui-escent conditions (Figures 4 and 5).

In the agitation assay, 25 μM αSyn exhibited the characteristic sigmoidal time trace of amyloid formation with a lag-time of approximately 10 hours (Figure 3A,D). In contrast, SMAhp and LENhp alone did not cause an increase in ThT fluorescence (Figure 3A,D). Addition of both SMAhp and LENhp to 25 μM αSyn showed concentration-dependent effects on the ThT time traces. Low concentrations of SMAhp led to a reduction of the lag-time, whereas addition of 50 μM SMAhp resulted in a prolonged lag-time (Figure 3A,B). In contrast, LENhp reduced the lag-time also at high concentrations (Figure 3D,E). Biphasic time traces observed for certain concentrations of the hairpin peptides suggest that complex (co-)assembly mechanisms are active. Atomic force microscopy (AFM) showed that αSyn in the absence of the hairpin peptides formed long amyloid fibrils with a tendency to cluster (Figure 3C, top row left), whereas imaging of the ThT-negative SMAhp and LENhp samples in the absence of αSyn showed some oligomeric assemblies (Figure 3C,F, top rows right). Incubation of αSyn with increasing concen-trations of SMAhp and LENhp led to decreased fibril lengths and reduced fibrillar morphology (Figure 3C,F, bottom rows).

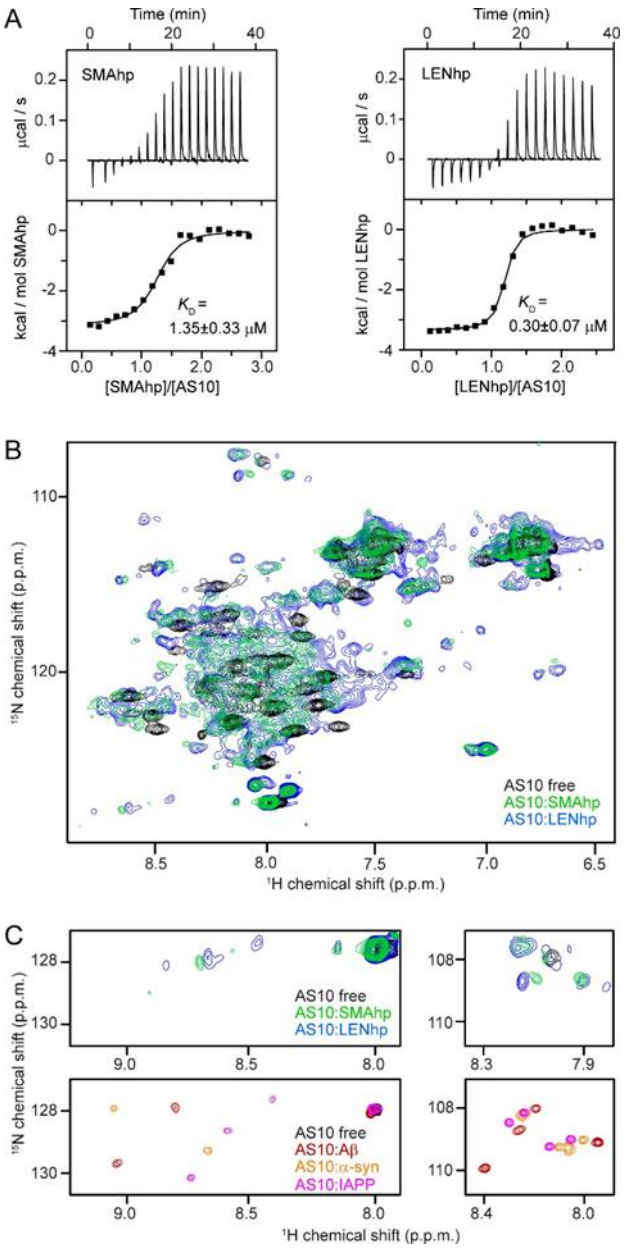

Figure 2: β-Hairpin conformation of SMAhp and LENhp upon complex formation with β-wrapin AS10. (A) Isothermal titration calorimetry data showing (top) the baseline-corrected instrumental response and (bottom) the integrated data (filled squares) and best fit of the parameters of a 1:1 binding model (continuous line), upon titration of 656 µM SMAhp (left) or 600 µM LENhp (right) into 30 µM AS10. (B) 1H-15N HSQC NMR spectrum of 15N-AS10 in the absence (black) and presence of a slight molar excess of unlabeled SMAhp (green) or unlabeled LENhp (blue). (C) Downfield (left) and glycine (right) regions of the 1H-15N HSQC NMR spectra of 15N-AS10 in the absence or presence of unlabeled SMAhp (green), LENhp (blue), Aβ (red), αSyn (yellow), or IAPP (magenta).

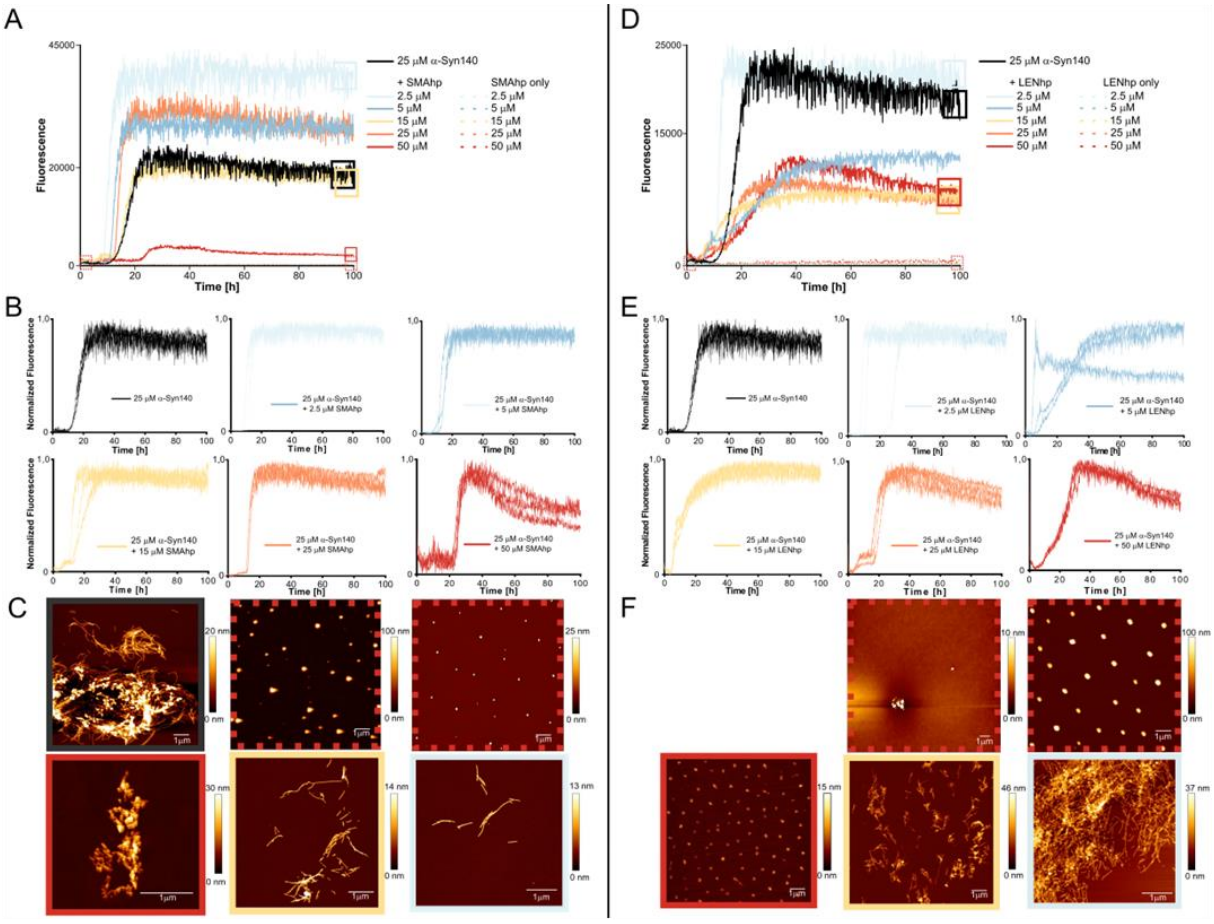

Figure 3: Modulation of αSyn aggregation by SMAhp (left) and LENhp (right) in ThT assay with agitation. Samples contained one glass bead per microtiter plate well and were continuously shaken at 300 rpm. Buffer, 30 mM Tris-HCl, pH 7.4, 50 mM NaCl. (A,B,D,E) Time course of ThT fluorescence of 25 µM αSyn in absence (black) and presence of SMAhp (A,B) or LENhp (D,E). Panels A and D show one trace per peptide concentration, panels B and E give triplicate traces to illustrate reproducibility. (C,F) AFM images of the ThT samples, typically at the end of the aggregation assay. Frames around the images correspond to the frames in panels A and D for indication of sample and incubation time. AFM images of samples of SMAhp and LENhp in the absence of αSyn are given in dashed frames, both for samples at the beginning (C,F, middle image in top row) and at the end (C,F, right image in top row) of the aggregation assay.

To reduce the impact of fibril fragmentation in the kinetics assays, they were repeated under quiescent conditions (Figure 4). Under these conditions, αSyn fibril formation is usually not observed on the hours-to-days timescale that is commonly covered in in vitro aggregation assays [61]. In line with this, we observed an increase in ThT fluorescence within 100 hours only for one of nine samples of αSyn in the absence of hairpin peptides, with high fluorescence occurring after ~60 hours in this one case (Figure 4E). The assays were performed for three different salt concentrations ranging from 5 to 250 mM NaCl in order to identify a potential impact of electrostatic interactions. For all salt concentrations addition of β-hairpin peptides resulted in several time courses with increases in ThT fluorescence, with the exception of SMAhp addition in 5 mM NaCl. The effect was dependent on the peptide concentration, as 2.5 μM pep-tide was usually not sufficient to induce αSyn fibril formation (Figure 4, light blue time traces).

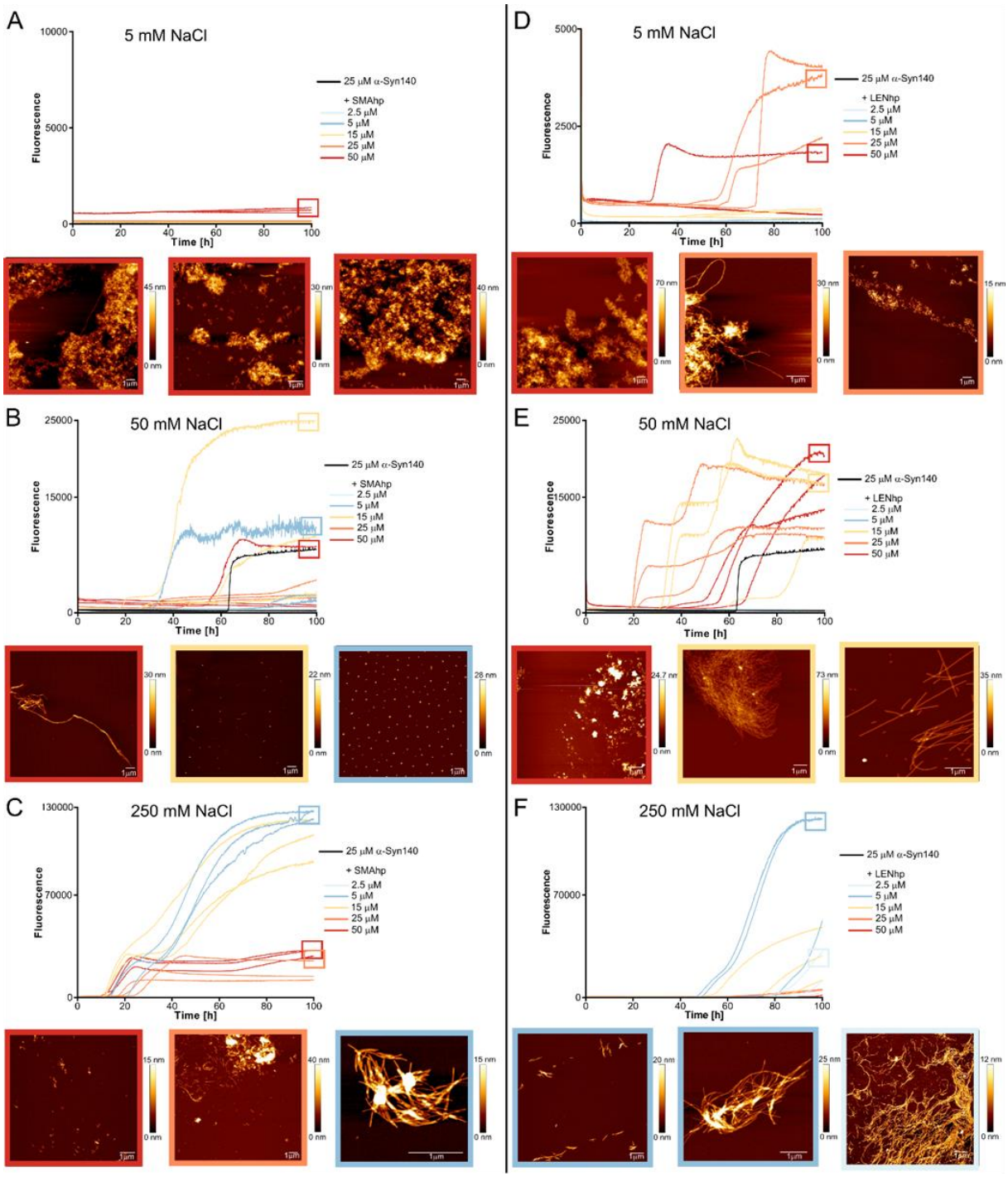

Figure 4: Modulation of αSyn aggregation by SMAhp (left) and LENhp (right) in ThT assay under quiescent conditions. Buffer, 30 mM Tris-HCl, pH 7.4, with indicated salt concentration. ThT time course and AFM images of 25 µM αSyn in absence (black) and presence of SMAhp (A-C) or LENhp (D-F). Frames around the AFM images correspond to the frames in the kinetics diagrams for indication of sample and incubation time.

Over all peptide-salt combinations, excluding SMAhp in 5 mM NaCl, the fraction of aggregation time traces with strong increases in ThT fluorescence at peptide concentrations ≥ 5 μM ranged between 33% (5 mM NaCl, LENhp, Figure 4D) and 100% (250 mM, SMAhp, Figure 4D). This indicates that the hairpin peptides promote αSyn fibril nucleation. The extent of aggregation promotion showed a complex dependency on salt concentration, peptide concentration, and nature of the peptide, with stronger promotion at 5 and 50 mM NaCl observed for LENhp and at 250 mM NaCl for SMAhp.

AFM imaging of the end points of the ThT assays frequently detected fibrils but also amorphous material (Figure 4). As for the assay under agitation, increased concentrations of the hairpin peptides correlated with a transition from fibrillar to amorphous aggregates. For example, co-incubation of 25 μM αSyn with 50 μM SMAhp in 5 mM NaCl resulted in largely amorphous material with comparatively low ThT fluorescence (Figure 4A).

2.3. Promotion of nucleation involves the hydrophobic NAC segment and the acidic C-terminus of αSyn

The dependence of aggregation promotion on salt concentration suggests that electrostatic interactions are involved. At neutral pH, the basic N-terminus of αSyn is positively charged while the highly acidic C-terminus is negatively charged. SMAhp and LENhp both contain four basic but no acidic residues and could therefore engage in electrostatic interactions with the αSyn C-terminus. To evaluate to what extent such interactions account for the observed effects on αSyn aggregation, we investigated the aggregation of truncated αSyn variants lacking the C-terminus, αSyn(1-95), or lacking the N-terminus, αSyn(61-140).

αSyn(1-95) contains N-terminus and NAC region of αSyn. SMAhp and LENhp reduced the lag-time of fibril formation of αSyn(1-95) in presence of 250 mM NaCl, an effect that was strongly dependent on the hairpin peptide concentration (Figure 5A,C). At low salt concentrations, only LENhp addition led to a late increase in ThT fluorescence accompanied by fibril formation according to AFM (Figure 5C). This indicates that the aggregation-promoting effects of the hairpin peptides are indeed reduced in the absence of the αSyn C-terminus.

αSyn(61-140) contains NAC region and C-terminus of αSyn. SMAhp and LENhp strongly promote aggregation of αSyn(61-140) according to ThT fluorescence (Figure 5B,D). Interestingly, at low salt concentrations ThT fluorescence intensity is already high at the start of the aggregation assay and increases with the concentration of the hairpin peptide. This indicates that under the conditions that favor electrostatic interactions the β-hairpin peptides instantly form ThT-positive assemblies together with αSyn(61-140). Subsequent increases in ThT fluorescence later in the aggregation assay suggest that alternative fibril assemblies with increased thermodynamic stability are formed. As further test for the importance of electrostatic interactions, we added the polyamine spermine to αSyn(61-140). Spermine has a net charge of +4 at neutral pH, just like SMAhp and LENhp, and was shown to promote αSyn fibril formation in as-says employing agitation conditions [62]. Under the quiescent conditions applied here spermine at concentrations up to 50 μM (i.e., in the same concentration range covered for SMAhp and LENhp) did not lead to any increase in ThT fluorescence (data not shown). This suggests that it is not just the presence of charges, but also the interplay between polypeptide chains that govern the consequences of this cross-interaction for αSyn assembly.

The data obtained for the truncated αSyn variants suggest that both the hydro-phobic NAC region and the acidic C-terminus of αSyn are involved in the promotion of αSyn nucleation by SMAhp and LENhp.

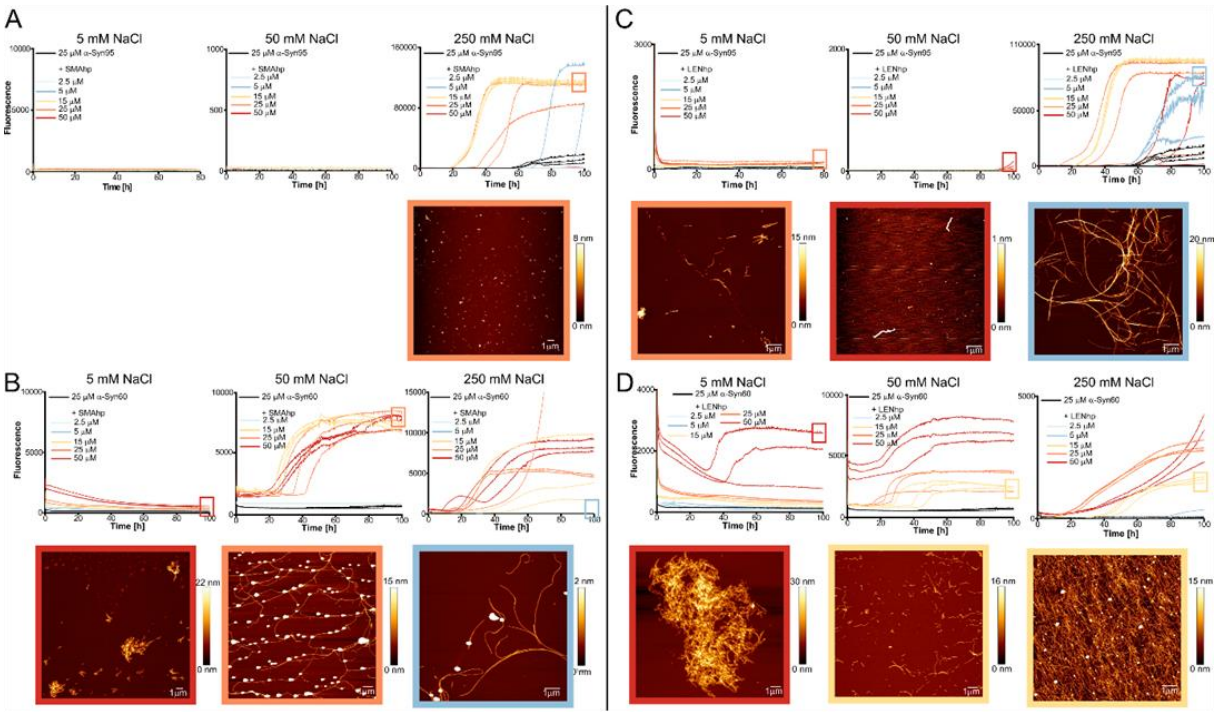

Figure 5: Modulation of aggregation of truncated αSyn variants by SMAhp (left) and LENhp (right) in ThT assay under quiescent conditions. Buffer, 30 mM Tris-HCl, pH 7.4, with indicated salt concentration. ThT time course and AFM images of (A,C) 25 µM αSyn(1-95) or (B,D) 25 µM αSyn(61-140) in absence (black) and presence of SMAhp (A,B) or LENhp (C,D). Frames around the AFM images correspond to the frames in the kinetics diagrams for indication of sample and incubation time.

2.3 Discussion

In this work, we chose to investigate the C-C' β-hairpins of the SMA and LEN light chains as models to test for a potential cross-interaction of β-hairpins with αSyn fibril formation. The choice was based on the observation that hairpin formation in SMA and LEN might be critical for their involvement in AL amyloidosis vs. multiple myeloma, as the identity of the turn residue at position 40 regulates amyloidogenicity [50]. Interestingly, LENhp, which contains the turn-promoting proline at position 40, binds to the β-hairpin-binding protein AS10 with similar sub-micromolar affinity as αSyn, Aβ, and IAPP. The affinity of SMAhp is weaker with a 4.5-fold higher KD. Importantly, affinity to AS10 is not a sequence-unspecific property of any disordered polypeptide. For example, neither the four-repeat-domain tau protein construct K18ΔK280/AA nor the Y145Stop variant of human prion protein huPrP(23–144) exhibited affinity for AS10 [57]. Thus, with regard to AS10 binding, SMAhp and LENhp have similar properties as the β-hairpin regions involved in oligomer and fibril for-mation of αSyn, Aβ, and IAPP.

Different activities of β-hairpins with respect to amyloid formation have been described based on simulations and experiments. β-Hairpins may act as on-pathway intermediates, possibly even as primary nuclei [19,32,35]. On the other hand, they may also prevent fibril formation [34,36,37,39,40,42]. With regard to cross-interactions, experimental evidence was obtained for a key role of β-hairpins in cross-seeding of IAPP fibril formation by a prion protein fragment and by a Tau fragment [43,47]. In line with this, we find here that the light chain β-hairpin peptides SMAhp and LENhp promote αSyn fibril nucleation, resulting in αSyn fibril formation under quiescent conditions at neutral pH where it is usually not observed. Our data indicates that both the hydrophobic NAC region and the acidic C-terminus are responsible for this activity. However, a detailed understanding of the mechanism is not achieved based on the present data. SMAhp and LENhp might act as monomers, since they are available as monomers as demonstrated by the formation of their 1:1 complexes with AS10 in ITC. On the other hand, the post-transition heats of dilution in ITC suggest that the peptides can form oligomers, which is supported by the observation of oligomeric structures by AFM. Therefore, it may also be oligomeric assemblies of the β-hairpin peptides that provide the interaction surface for heterogeneous nucleation of αSyn fibrils. In conclusion, we find that model β-hairpin peptides derived from disease-related immunoglobulin light chains can cross-interact with αSyn to promote αSyn fibril nucleation.

2.4 Materials and Methods

2.4.1. Peptides

SMAhp and LENhp were obtained as synthetic peptides from CASLO. To fully monomerize the peptides, 1 mg aliquots were solubilized in 1 ml hexafluoroisopropa-nol (HFIP), aliquoted in smaller amounts, lyophilized and stored at -20 °C.

2.4.2. Proteins

Full-length αS was exressed and purified as described previously, yielding N-terminally acetylated protein [59,63].

αSyn(1-95) and αSyn(61-140) were expressed from codon-optimized gene sequences in pT7-7 vector in Escherichia coli BL21DE3, without N-terminal acetylation. Expression and purification were performed as for full-length αSyn, with the differ-ence that for αSyn(1-95) the anion exchange chromatography step was replaced by cation exchange chromatography, using a 5 ml HiTrap SP FF column (Cytiva) and 10 mM sodium acetate buffer, pH 5, with elution in a NaCl gradient from 0-500 mM.

β-Wrapin AS10 with or without isotope labels for NMR spectroscopy was expressed and purified as previously described [55,57].

4.3. Isothermal titration calorimetry

ITC was performed on a Microcal iTC200 calorimeter (GE Healthcare) at a temperature of 30°C. AS10 was filled into the cell at a concentration of 30 μM in 20 mM sodium phosphate, pH 7.4, 50 mM NaCl. The syringe was filled with 656 μM SMAhp or 600 μM LENhp followed by titration of the β-hairpin peptide solutions into the cell. Heats of post-saturation injections were averaged and subtracted from each injection to correct for heats of dilution and mixing. Dissociation constants were obtained from a nonlinear least-squares fit to a 1:1 binding model using MicroCal Origin.

4.4. NMR spectroscopy

NMR spectroscopy was performed at 25 °C on a VNMRS instrument (Varian) at a proton frequency of 800 MHz, equipped with a cryogenically cooled Z-axis pulse-field-gradient (PFG) triple resonance probe. SMAhp and LENhp were not iso-topically labeled and added in a slight excess to 15N-labeled AS10. The sample buffer was 20 mM sodium phosphate, pH 7.4, 50 mM NaCl, supplemented with 10% D2O. NMR data were processed using NMRPipe [64] and analyzed with CcpNMR [65].

4.5. Thioflavin T aggregation assay

Aggregation kinetics were monitored in Greiner 96-well half-area, clear bottom, low-binding plates by ThT fluorescence in a BMG CLARIOstar plate reader at 37 °C. Wells with samples were always surrounded by wells filled with liquid, either other samples or 150 µl water, to counter potential artefacts due to evaporation. The assays done under agitation were performed with continuous orbital shaking at 300 rpm and with addition of one glass bead (0.75-1 mm, Roth) per sample well. αSyn, αSyn(1-95), and αSyn(61-140) were applied at a constant concentration of 25 µM in 30 mM Tris-HCl, pH 7.4, 25 µM ThT, 0.04% NaN_3 and 5, 50 or 250 mM NaCl. SMAhp and LENhp were dissolved at high concentration in 30 mM Tris-HCl, pH 7.4, 50 mM NaCl and added to the sample wells to achieve final concentrations between 2.5 and 50 µM. Samples were prepared in triplicates. Plates were covered with sealing tape, placed into the plate reader, heated to 37 °C, and ThT fluorescence was read using bottom optics.

4.6. Atomic force microscopy

For AFM imaging the samples were taken out of the 96-well plates after the ThT aggregation assay. 5 µl of each sample were put onto a freshly cleaved muscovite mica surface and incubated for 2 min. Subsequently, the samples were washed with 100 µl ddH2O three times and dried with a stream of N2 gas. Imaging was performed in in-termittent contact mode (AC mode) in a JPK NanoWizard 3 atomic force microscope (JPK) using a silicon cantilever with silicon tip (OMCL-AC160TS-R3, Olympus) with a typical tip radius of 9 ± 2 nm, a force constant of 26 N/m and resonance frequency around 300 kHz. The images were processed using JPK DP Data Processing Software (version spm-5.0.84).

2.5 References

1. Iadanza, M.G.; Jackson, M.P.; Hewitt, E.W.; Ranson, N.A.; Radford, S.E. A new era for understanding amyloid structures and disease. Nat. Rev. Mol. Cell Biol. 2018, 19, 755-773, doi:10.1038/s41580-018-0060-8.

2. Lashuel, H.A.; Overk, C.R.; Oueslati, A.; Masliah, E. The many faces of a-synuclein: from structure and toxicity to therapeutic target. Nat. Rev. Neurosci. 2013, 14, 38-48, doi:10.1038/nrn3406.

3. Oliveira, L.M.A.; Gasser, T.; Edwards, R.; Zweckstetter, M.; Melki, R.; Stefanis, L.; Lashuel, H.A.; Sulzer, D.; Vekrellis, K.; Halliday, G.M.; et al. Alpha-synuclein research: defining strategic moves in the battle against Parkinson's disease. NPJ Parkinsons Disease 2021, 7, 65, doi:10.1038/s41531-021-00203-9.

4. Volpicelli-Daley, L.; Brundin, P. Prion-like propagation of pathology in Parkinson disease. Handb. Clin. Neurol. 2018, 153, 321-335, doi:10.1016/B978-0-444-63945-5.00017-9.

5. Blancas-Mejia, L.M.; Ramirez-Alvarado, M. Systemic amyloidoses. Annual Reviews of Biochemistry 2013, 82, 745-774, doi:10.1146/annurev-biochem-072611-130030.

6. Ramirez-Alvarado, M. Amyloid formation in light chain amyloidosis. Curr. Top. Med. Chem. 2012, 12, 2523-2533, doi:10.2174/1568026611212220007.

7. Buell, A.K. The Nucleation of Protein Aggregates - From Crystals to Amyloid Fibrils. Int. Rev. Cell Mol. Biol. 2017, 329, 187-226, doi:10.1016/bs.ircmb.2016.08.014.

8. Chatani, E.; Yamamoto, N. Recent progress on understanding the mechanisms of amyloid nucleation. Biophys. Rev. 2018, 10, 527-534, doi:10.1007/s12551-017-0353-8.

9. Galvagnion, C.; Buell, A.K.; Meisl, G.; Michaels, T.C.; Vendruscolo, M.; Knowles, T.P.; Dobson, C.M. Lipid vesicles trigger a-synuclein aggregation by stimulating primary nucleation. Nat. Chem. Biol. 2015, 11, 229-234, doi:10.1038/nchembio.1750.

10. Kumari, P.; Ghosh, D.; Vanas, A.; Fleischmann, Y.; Wiegand, T.; Jeschke, G.; Riek, R.; Eichmann, C. Structural insights into a-synuclein monomer-fibril interactions. Proc. Natl. Acad. Sci. U. S. A. 2021, 118, doi:10.1073/pnas.2012171118.

11. Campioni, S.; Carret, G.; Jordens, S.; Nicoud, L.; Mezzenga, R.; Riek, R. The presence of an air-water interface affects formation and elongation of a-synuclein fibrils. J. Am. Chem. Soc. 2014, 136, 2866-2875, doi:10.1021/ja412105t.

12. Bassil, F.; Brown, H.J.; Pattabhiraman, S.; Iwasyk, J.E.; Maghames, C.M.; Meymand, E.S.; Cox, T.O.; Riddle, D.M.; Zhang, B.; Trojanowski, J.Q.; et al. Amyloid-beta (Ab) plaques promote seeding and spreading of alpha-synuclein and tau in a mouse model of Lewy body disorders with Ab pathology. Neuron 2020, 105, 260-275 e266, doi:10.1016/j.neuron.2019.10.010.

13. Mandal, P.K.; Pettegrew, J.W.; Masliah, E.; Hamilton, R.L.; Mandal, R. Interaction between Ab peptide and a synuclein: molecular mechanisms in overlapping pathology of Alzheimer's and Parkinson's in dementia with Lewy body disease. Neurochem. Res. 2006, 31, 1153-1162, doi:10.1007/s11064-006-9140-9.

14. Horvath, I.; Wittung-Stafshede, P. Cross-talk between amyloidogenic proteins in type-2 diabetes and Parkinson's disease. Proc. Natl. Acad. Sci. U. S. A. 2016, 113, 12473-12477, doi:10.1073/pnas.1610371113.

15. Martinez-Valbuena, I.; Amat-Villegas, I.; Valenti-Azcarate, R.; Carmona-Abellan, M.D.M.; Marcilla, I.; Tunon, M.T.; Luquin, M.R. Interaction of amyloidogenic proteins in pancreatic b cells from subjects with synucleinopathies. Acta Neuropathol. 2018, 135, 877-886, doi:10.1007/s00401-018-1832-0.

16. Jimenez, M.A. Design of monomeric water-soluble b-hairpin and b-sheet peptides. Methods Mol. Biol. 2014, 1216, 15-52, doi:10.1007/978-1-4939-1486-9_2.

17. Shao, Q.; Wang, J.; Shi, J.; Zhu, W. The universality of b-hairpin misfolding indicated by molecular dynamics simulations. J. Chem. Phys. 2013, 139, 165103, doi:10.1063/1.4826461.

18. Dupuis, N.F.; Wu, C.; Shea, J.E.; Bowers, M.T. Human islet amyloid polypeptide monomers form ordered b-hairpins: a possible direct amyloidogenic precursor. J. Am. Chem. Soc. 2009, 131, 18283-18292, doi:10.1021/ja903814q.

19. Gill, A.C. b-hairpin-mediated formation of structurally distinct multimers of neurotoxic prion peptides. PLoS One 2014, 9, e87354, doi:10.1371/journal.pone.0087354.

20. Reddy, G.; Straub, J.E.; Thirumalai, D. Influence of preformed Asp23-Lys28 salt bridge on the conformational fluctuations of monomers and dimers of Ab peptides with implications for rates of fibril formation. J. Phys. Chem. B 2009, 113, 1162-1172, doi:10.1021/jp808914c.

21. Rosenman, D.J.; Connors, C.R.; Chen, W.; Wang, C.; Garcia, A.E. Ab monomers transiently sample oligomer and fibril-like configurations: ensemble characterization using a combined MD/NMR approach. J. Mol. Biol. 2013, 425, 3338-3359, doi:10.1016/j.jmb.2013.06.021.

22. Mitternacht, S.; Staneva, I.; Härd, T.; Irbäck, A. Monte Carlo study of the formation and conformational properties of dimers of Abeta42 variants. J. Mol. Biol. 2011, 410, 357-367, doi:10.1016/j.jmb.2011.05.014.

23. Yu, H.; Han, W.; Ma, W.; Schulten, K. Transient b-hairpin formation in a-synuclein monomer revealed by coarse-grained molecular dynamics simulation. J. Chem. Phys. 2015, 143, 243142, doi:10.1063/1.4936910.

24. Cruz, L.; Rao, J.S.; Teplow, D.B.; Urbanc, B. Dynamics of metastable b-hairpin structures in the folding nucleus of amyloid b-protein. J. Phys. Chem. B 2012, 116, 6311-6325, doi:10.1021/jp301619v.

25. Lazo, N.D.; Grant, M.A.; Condron, M.C.; Rigby, A.C.; Teplow, D.B. On the nucleation of amyloid b-protein monomer folding. Protein Sci. 2005, 14, 1581-1596, doi:10.1110/ps.041292205.

26. Xu, L.; Nussinov, R.; Ma, B. Allosteric stabilization of the amyloid-b peptide hairpin by the fluctuating N-terminal. Chem. Commun. 2016, 52, 1733-1736, doi:10.1039/c5cc08107f.

27. Halfmann, R.; Alberti, S.; Krishnan, R.; Lyle, N.; O'Donnell, C.W.; King, O.D.; Berger, B.; Pappu, R.V.; Lindquist, S. Opposing effects of glutamine and asparagine govern prion formation by intrinsically disordered proteins. Mol. Cell 2011, 43, 72-84, doi:10.1016/j.molcel.2011.05.013.

28. Zheng, W.; Tsai, M.Y.; Chen, M.; Wolynes, P.G. Exploring the aggregation free energy landscape of the amyloid-b protein (1-40). Proc. Natl. Acad. Sci. U. S. A. 2016, 113, 11835-11840, doi:10.1073/pnas.1612362113.

29. Ball, K.A.; Phillips, A.H.; Wemmer, D.E.; Head-Gordon, T. Differences in b-strand populations of monomeric Ab40 and Ab42. Biophys. J. 2013, 104, 2714-2724, doi:10.1016/j.bpj.2013.04.056.

30. Tarus, B.; Tran, T.T.; Nasica-Labouze, J.; Sterpone, F.; Nguyen, P.H.; Derreumaux, P. Structures of the Alzheimer's wild-type Ab1-40 dimer from atomistic simulations. J. Phys. Chem. B 2015, 119, 10478-10487, doi:10.1021/acs.jpcb.5b05593.

31. Grabenauer, M.; Wu, C.; Soto, P.; Shea, J.E.; Bowers, M.T. Oligomers of the prion protein fragment 106-126 are likely assembled from b-hairpins in solution, and methionine oxidation inhibits assembly without altering the peptide's monomeric conformation. J. Am. Chem. Soc. 2010, 132, 532-539, doi:10.1021/ja905595k.

32. Singh, S.; Chiu, C.C.; Reddy, A.S.; de Pablo, J.J. a-helix to b-hairpin transition of human amylin monomer. J. Chem. Phys. 2013, 138, 155101, doi:10.1063/1.4798460.

33. Reddy, A.S.; Wang, L.; Singh, S.; Ling, Y.L.; Buchanan, L.; Zanni, M.T.; Skinner, J.L.; de Pablo, J.J. Stable and metastable states of human amylin in solution. Biophys. J. 2010, 99, 2208-2216, doi:10.1016/j.bpj.2010.07.014.

34. Hosia, W.; Bark, N.; Liepinsh, E.; Tjernberg, A.; Persson, B.; Hallen, D.; Thyberg, J.; Johansson, J.; Tjernberg, L. Folding into a b-hairpin can prevent amyloid fibril formation. Biochemistry 2004, 43, 4655-4661, doi:10.1021/bi036248t.

35. Sciarretta, K.L.; Gordon, D.J.; Petkova, A.T.; Tycko, R.; Meredith, S.C. Ab40-Lactam(D23/K28) models a conformation highly favorable for nucleation of amyloid. Biochemistry 2005, 44, 6003-6014, doi:10.1021/bi0474867.

36. Agerschou, E.D.; Borgmann, V.; Wördehoff, M.M.; Hoyer, W. Inhibitor and substrate cooperate to inhibit amyloid fibril elongation of a-synuclein. Chem. Sci. 2020, 11, 11331-11337, doi:10.1039/d0sc04051g.

37. Agerschou, E.D.; Schützmann, M.P.; Reppert, N.; Wördehoff, M.M.; Shaykhalishahi, H.; Buell, A.K.; Hoyer, W. b-Turn exchanges in the a-synuclein segment 44-TKEG-47 reveal high sequence fidelity requirements of amyloid fibril elongation. Biophys. Chem. 2021, 269, 106519, doi:10.1016/j.bpc.2020.106519.

38. Bhowmik, D.; Mote, K.R.; MacLaughlin, C.M.; Biswas, N.; Chandra, B.; Basu, J.K.; Walker, G.C.; Madhu, P.K.; Maiti, S. Cell-membrane-mimicking lipid-coated

nanoparticles confer Raman enhancement to membrane proteins and reveal membrane-attached amyloid-b conformation. ACS Nano 2015, 9, 9070-9077, doi:10.1021/acsnano.5b03175.

39. Maity, S.; Hashemi, M.; Lyubchenko, Y.L. Nano-assembly of amyloid b peptide: role of the hairpin fold. Sci. Rep. 2017, 7, 2344, doi:10.1038/s41598-017-02454-0.

40. Doran, T.M.; Anderson, E.A.; Latchney, S.E.; Opanashuk, L.A.; Nilsson, B.L. An azobenzene photoswitch sheds light on turn nucleation in amyloid-b self-assembly. ACS Chem. Neurosci. 2012, 3, 211-220, doi:10.1021/cn2001188.

41. Lendel, C.; Bjerring, M.; Dubnovitsky, A.; Kelly, R.T.; Filippov, A.; Antzutkin, O.N.; Nielsen, N.C.; Härd, T. A hexameric peptide barrel as building block of amyloid-b protofibrils. Angew. Chem. Int. Ed. 2014, 53, 12756-12760, doi:10.1002/anie.201406357.

42. Sandberg, A.; Luheshi, L.M.; Sollvander, S.; Pereira de Barros, T.; Macao, B.; Knowles, T.P.; Biverstal, H.; Lendel, C.; Ekholm-Petterson, F.; Dubnovitsky, A.; et al. Stabilization of neurotoxic Alzheimer amyloid-b oligomers by protein engineering. Proc. Natl. Acad. Sci. U. S. A. 2010, 107, 15595-15600, doi:10.1073/pnas.1001740107.

43. Ilitchev, A.I.; Giammona, M.J.; Olivas, C.; Claud, S.L.; Lazar Cantrell, K.L.; Wu, C.; Buratto, S.K.; Bowers, M.T. Hetero-oligomeric amyloid assembly and mechanism: Prion fragment PrP(106-126) catalyzes the islet amyloid polypeptide b-hairpin. J. Am. Chem. Soc. 2018, 140, 9685-9695, doi:10.1021/jacs.8b05925.

44. Izuo, N.; Kasahara, C.; Murakami, K.; Kume, T.; Maeda, M.; Irie, K.; Yokote, K.; Shimizu, T. A Toxic Conformer of Ab42 with a Turn at 22-23 is a Novel Therapeutic Target for Alzheimer's Disease. Sci. Rep. 2017, 7, 11811, doi:10.1038/s41598-017-11671-6.

45. Yu, L.; Edalji, R.; Harlan, J.E.; Holzman, T.F.; Lopez, A.P.; Labkovsky, B.; Hillen, H.; Barghorn, S.; Ebert, U.; Richardson, P.L.; et al. Structural characterization of a soluble amyloid b-peptide oligomer. Biochemistry 2009, 48, 1870-1877, doi:10.1021/bi802046n.

46. Khaled, M.; Rönnbäck, I.; Ilag, L.L.; Gräslund, A.; Strodel, B.; Österlund, N. A hairpin motif in the amyloid-b peptide is important for formation of disease-related oligomers. J. Am. Chem. Soc. 2023, doi:10.1021/jacs.3c03980.

47. Arya, S.; Claud, S.L.; Cantrell, K.L.; Bowers, M.T. Catalytic prion-like cross-talk between a key Alzheimer's disease tau-fragment R3 and the type 2 diabetes peptide IAPP. ACS Chem. Neurosci. 2019, 10, 4757-4765, doi:10.1021/acschemneuro.9b00516.

48. Davis, P.D.; Raffen, R.; Dul, L.J.; Vogen, M.S.; Williamson, K.E.; Stevens, J.F.; Argon, Y. Inhibition of amyloid fiber assembly by both BiP and its target peptide. Immunity 2000, 13, 433-442, doi:10.1016/s1074-7613(00)00043-1.

49. Stevens, P.W.; Raffen, R.; Hanson, D.K.; Deng, Y.L.; Berrios-Hammond, M.; Westholm, F.A.; Schiffer, M.; Stevens, F.J.; Murphy, C.; Solomon, A.; et al. Recombinant immunoglobulin variable domains generated from synthetic genes provide a system for in vitro characterization of light-chain amyloid proteins. Protein Sci. 1995, 4, 421-432, doi:10.1002/pro.5560040309.

50. Raffen, R.; Dieckman, L.J.; Szpunar, M.; Wunschl, C.; Pokkuluri, P.R.; Dave, P.; Wilkins Stevens, P.; Cai, X.; Schiffer, M.; Stevens, F.J. Physicochemical consequences of amino acid variations that contribute to fibril formation by immunoglobulin light chains. Protein Sci. 1999, 8, 509-517, doi:10.1110/ps.8.3.509.

51. Souillac, P.O.; Uversky, V.N.; Millett, I.S.; Khurana, R.; Doniach, S.; Fink, A.L. Effect of association state and conformational stability on the kinetics of immunoglobulin light chain amyloid fibril formation at physiological pH. J. Biol. Chem. 2002, 277, 12657-12665, doi:10.1074/jbc.M109230200.

52. Khurana, R.; Souillac, P.O.; Coats, A.C.; Minert, L.; Ionescu-Zanetti, C.; Carter, S.A.; Solomon, A.; Fink, A.L. A model for amyloid fibril formation in immunoglobulin light chains based on comparison of amyloidogenic and benign proteins and specific antibody binding. Amyloid 2003, 10, 97-109, doi:10.3109/13506120309041731.

53. Bellotti, V.; Mangione, P.; Merlini, G. Review: immunoglobulin light chain amyloidosis--the archetype of structural and pathogenic variability. J. Struct. Biol. 2000, 130, 280-289, doi:10.1006/jsbi.2000.4248.

54. Huang, D.B.; Chang, C.H.; Ainsworth, C.; Johnson, G.; Solomon, A.; Stevens, F.J.; Schiffer, M. Variable domain structure of kappaIV human light chain Len: high homology to the murine light chain McPC603. Mol. Immunol. 1997, 34, 1291-1301, doi:10.1016/s0161-5890(98)00002-9.

55. Mirecka, E.A.; Shaykhalishahi, H.; Gauhar, A.; Akgül, S.; Lecher, J.; Willbold, D.; Stoldt, M.; Hoyer, W. Sequestration of a b-hairpin for control of a-synuclein aggregation. Angew. Chem. Int. Ed. 2014, 53, 4227-4230, doi:10.1002/anie.201309001.

56. Orr, A.A.; Wördehoff, M.M.; Hoyer, W.; Tamamis, P. Uncovering the binding and specificity of b-wrapins for amyloid-b and a-synuclein. J. Phys. Chem. B 2016, 120, 12781-12794, doi:10.1021/acs.jpcb.6b08485.

57. Shaykhalishahi, H.; Mirecka, E.A.; Gauhar, A.; Gruning, C.S.; Willbold, D.; Härd, T.; Stoldt, M.; Hoyer, W. A b-hairpin-binding protein for three different disease-related amyloidogenic proteins. ChemBioChem 2015, 16, 411-414, doi:10.1002/cbic.201402552.

58. Orr, A.A.; Shaykhalishahi, H.; Mirecka, E.A.; Jonnalagadda, S.V.R.; Hoyer, W.; Tamamis, P. Elucidating the multi-targeted anti-amyloid activity and enhanced islet amyloid polypeptide binding of b-wrapins. Comput. Chem. Eng. 2018, 116, 322-332, doi:10.1016/j.compchemeng.2018.02.013.

59. Wördehoff, M.M.; Hoyer, W. a-Synuclein aggregation monitored by Thioflavin T fluorescence assay. Bio Protocols 2018, 8, doi:10.21769/BioProtoc.2941.

60. Giehm, L.; Otzen, D.E. Strategies to increase the reproducibility of protein fibrillization in plate reader assays. Anal. Biochem. 2010, 400, 270-281, doi:10.1016/j.ab.2010.02.001.

61. Buell, A.K.; Galvagnion, C.; Gaspar, R.; Sparr, E.; Vendruscolo, M.; Knowles, T.P.; Linse, S.; Dobson, C.M. Solution conditions determine the relative importance of nucleation and growth processes in a-synuclein aggregation. Proc. Natl. Acad. Sci. U. S. A. 2014, 111, 7671-7676, doi:10.1073/pnas.1315346111.

62. Antony, T.; Hoyer, W.; Cherny, D.; Heim, G.; Jovin, T.M.; Subramaniam, V. Cellular polyamines promote the aggregation of a-synuclein. J. Biol. Chem. 2003, 278, 3235-3240, doi:10.1074/jbc.M208249200.

63. Wordehoff, M.M.; Shaykhalishahi, H.; Gross, L.; Gremer, L.; Stoldt, M.; Buell, A.K.; Willbold, D.; Hoyer, W. Opposed Effects of Dityrosine Formation in Soluble and Aggregated alpha-Synuclein on Fibril Growth. J. Mol. Biol. 2017, 429, 3018-3030, doi:10.1016/j.jmb.2017.09.005.

64. Delaglio, F.; Grzesiek, S.; Vuister, G.W.; Zhu, G.; Pfeifer, J.; Bax, A. NMRPipe: a multidimensional spectral processing system based on UNIX pipes. J. Biomol. NMR 1995, 6, 277-293.

65. Vranken, W.F.; Boucher, W.; Stevens, T.J.; Fogh, R.H.; Pajon, A.; Llinas, M.; Ulrich, E.L.; Markley, J.L.; Ionides, J.; Laue, E.D. The CCPN data model for NMR spectroscopy: development of a software pipeline. Proteins 2005, 59, 687-696, doi:10.1002/prot.20449.

2.6 List of Figures

2.7 List of Abbreviations

°C	Degrees Celsius
AL amyloidosis	Light chain amyloidosis
HFIP	Hexafluoroisopropanol
ITC	Isothermal titration calorimetry
LENhp	LEN hairpin
mM	milli Molar
NAC region	Non-amyloid-β-component region
nm	Nanometer
PD	Parkinson's Disease
SMAhp	SMA hairpin
ThT	Thioflavin T
VL	Variable light chain domain
αSyn	α-synuclein
αSyn(1-95)	α-synuclein (1-95)
αSyn(61-140)	α-synuclein (61-140)
κ	kappa
µL	mikro Liter
µM	micro Molar

Project 3: *Optimization of β-wrapin AS69 and set-up of an HTS assay*

Content

3 Introduction

For the longest time, antibodies were the only known source of affinity proteins that could be tailored to fit any given target. [11] Today they are still the most used affinity proteins used in the life sciences, as roughly 20 years ago the immune system, from which the antibodies were discovered, was the only known source for affinity proteins, especially affinity proteins that could be engineered to become binders to specific targets. [11] Since then, it has become possible to produce and isolate an antibody to virtually any given target with only a few exceptions. [11] Antibodies have the advantage that they can be engineered to have a high affinity and specificity with the added perk that they can also be highly selective. [41] The most frequently used antibody type for engineering is the IgG-type molecule. [41] The IgG-type antibody is the most abundant in human blood serum. If partly proteolytically cleaved by papain the antibody is fragmented into three major parts where each is about 50 kDa in size. [40, 41] Two of those parts can bind antigens and are called F_{ab} (Fragment antigen binding) and the third part crystallizes easily and was thus called F_C. [41] Some IgG F_C can bind F_C receptors for example on monocytes, neutrophils, macrophages, and B cells. [40, 41] The IgG antibody consists of two peptide chains of the so-called “light-chain” (LC) and two peptide chains that are called the “heavy-chain” (HC). The LCs are usually around 25 kDa and the HCs around 50 kDa. [41] Each of the LCs is connected to an HC via a disulfide bond as are the HCs among each other. When looking at the overall structure of IgGs they strongly resemble a “Y”, with the two “arms” being where the LCs are, those LCs have two homologous domains, and each “arm” can bind one antigen and are very flexible. [40, 41] This also corresponds to the F_{ab} and F_C fragments, where the latter consists purely of the amino-terminus (N-terminus) of the two HCs, while F_{ab} consists of the full-length LCs and the carboxy-terminus (C-terminus) of the HCs. Since the antigen-binding “arms” are very flexible and each IgG can bind two antigens, it is also easy for this type of antibody to interconnect several antigens among each other. [40, 41]

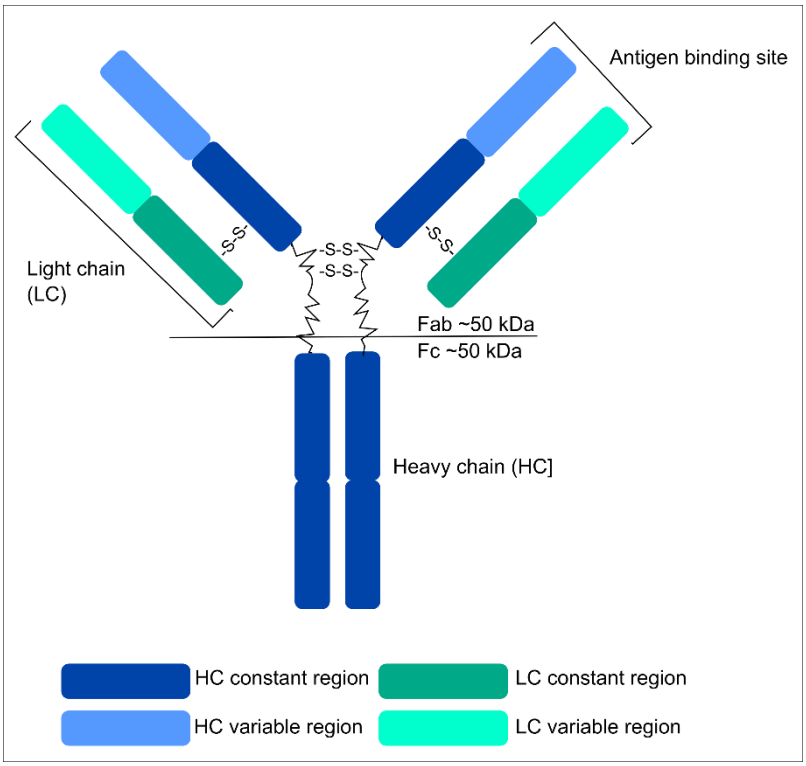

Figure 1: Schematic representation of an IgG antibody.

Although antibodies have many positive aspects, and many different usages across the different sciences, and are very well established they also have a few drawbacks. [12, 15] The IgG-type antibody is rather large which can be a problem when it is delivered to certain parts of the human body, like the brain, antibodies cannot easily pass the blood-brain barrier (BBB). [4, 7, 15] Another point is that antibodies have poor heat stability, which can cause problems with shelf life and handling. [4, 12] The manufacturing process of an antibody, especially if it is a newly engineered one, is expensive, because that laboratory animal immunization, which is often combined with hybridoma technologies, is necessary and lengthy. [4, 12, 15] Another drawback is that only a tiny portion of an antibody's large molecule size is involved in antigen recognition. [4, 12, 15] Considering all this the search for and generation of new *in vitro* non-antibody repertoires began. Synthetic combinatorial libraries and *in vitro* selections systems (phage display and others) were established to search and engineer so-called alternative scaffold proteins that had to follow certain desired criteria, among them being a small size, high stability, high heat stability, the absence of cysteines as far as possible and a high yield in bacterial expression. [3, 4, 11, 15] Along with these criteria, the new class of affinity proteins should have some preferable abilities, of course, the most important being the ability to bind a given

molecular structure with high affinity. [4, 10, 11] Other preferable abilities depend on the application, to give a few examples of therapeutic potentials: in imaging techniques the new affinity proteins need to be small, thermostable, and functional even under harsh chemical conditions; on the other hand, for *in vitro* diagnostics, it is essential, that the proteins have a minimal background, overall low manufacturing costs and long shelf life is desired for all possible fields of application. [1, 3, 4, 7, 9, 10, 11, 13, 14, 15, 17] Here, I want to focus on the development of only one type of non-antibody affinity proteins called affibody molecules or simply affibodies. [1, 3, 4, 10] The original affibody molecule was derived from the B-domain in the immunoglobulin-binding region of protein A (6.5 kDa) in the bacterium *Staphylococcus aureus*. [1, 3, 4, 6, 11] The derived domain has the structure of a three-helix bundle and has most of the desired criteria covered, it has one of the fastest folding properties known, high solubility and stability, also thermal stability, it cannot only be produced by bacteria but also via chemical peptide synthesis. [1, 2, 4, 5] The first engineered variant was then called the Z-domain and all later derived and engineered affibody molecules are derived from this Z-domain. [1, 3, 4, 5, 11] Theoretically, this molecule can be engineered with specific binding to any given target, one of the examples important for this project was the affibody called Zaβ$_3$ against the peptide Aβ$_{1\text{-}40}$ which is heavily involved in the pathogenesis of Alzheimer's disease. [8] The development timeline of the affibody molecules is briefly as follows: The protein A from *Staphylococcus aureus*, from which all affibody molecules are derived, was sequenced in 1984. [4] The first affibody molecules were selected by phage display in 1997. [4] In 2003 the Affibody molecules showed that they could specifically target a xenograft tumor in mice, and in 2005 the first clinical data on tumor imaging was published using a HER2-binding Affibody molecule (HER2 (human epidermal growth factor receptor2) involved in breast cancer). [4, 5, 16]

In this project, the focus is on a special type of affibody molecules or a subgroup of these, the so-called β-wrapins (Figure 2). [18, 22] As the name suggests these molecules "wrap" around their target which takes the structure of a β-hairpin upon binding or has the potential for a β-hairpin in certain regions. [18, 22] The sequences of the β-wrapins are based on the affibody sequence but are further selected by phage display. [18, 22] Here instead of one Z-domain, two of them are linked by cysteines at position 28 in the second helix of each of the subunits and thus build a disulfide-linked homodimer. This is the basis of the first β-wrapin called ZAβ3 (14 kDa) selected against the target Aβ$_{1\text{-}40,}$ the protein involved in Alzheimer's disease (AD). [18, 19, 20] Both the β-wrapin and Aβ$_{1\text{-}40}$ fold upon binding to each other and the Aβ peptide

adopts an antiparallel β-hairpin structure. [18, 19, 20] By now for each of the major neurodegenerative diseases one β-wrapin was selected, HI18 (14 kDa) that binds IAPP or amylin that is involved in Type II Diabetes, AS69 (14kDa) that targets α-synuclein (αSyn) involved in Parkinson's disease (PD) and one β-wrapin called AS10 (14 kDa) that can bind all three targets, albeit with different K_d-values. [22, 23, 24, 26, 27] In this project the focus will be solely on AS69 against αSyn. [22, 23, 27]

All three targets mentioned above play a significant role in neurodegenerative diseases that mostly only ail the elderly. Since society is steadily growing older, those diseases play an important role and are a significant problem. To this day no therapy can heal AD, PD, or type II diabetes or even diagnose them in an early enough stage to prevent major problems because when there are symptoms, it is often too late to rescue the already comprised brain cells.

PD is a neurodegenerative disease, with the main hallmark being Lewy bodies and Lewy neurites. [43, 44, 45] These amyloid plaques can be made of more than one protein or peptide, but mostly there is one dominant species or even only one. [43, 44, 45] The processes of how these plaques come into existence are still largely unknown. [43, 44, 45] It is also unclear if the plaques themselves or species that are on their way to forming plaques are the cytotoxic species. [43, 44, 45] The result, in the end, is that neurons, in PD especially, the dopaminergic neurons die. [43,44, 45] The most abundant protein in the plaques of PD is αSyn. [29, 42, 44] The protein αSyn can aggregate over several different species into amyloid fibrils, which are the main component of the amyloid plaques found postmortem in the brain of PD patients. [28, 29, 42] This phenomenon is replicable *in vitro*, although αSyn needs agitation and being in contact with another surface like a glass bead to successfully aggregate in relatively a short timeframe. This aggregation can be monitored by measuring the fluorescence of the dye Thioflavin-T (ThT) as it binds to amyloid fibrils. Now the curious thing is that these three disease-related proteins/peptides all have the potential to fold into a β-hairpin at specific positions in their sequence. As was found first with the here described β-wrapins, if this β-hairpin is formed and stabilized, the proteins lose their ability to form amyloid fibrils. The same concept is applied to αSyn, despite having the most significant size (with 140 amino acids) among these three disease-related proteins. [29] The potential β-hairpin forming region of αSyn can be found in its N-terminal part in the residues 36 to 55, along with most of its familial mutations. [28, 29] The N-terminal part of αSyn is also the most conserved throughout all synucleins and has an amphipathic character. [28, 29] Then there is a middle part of the protein from residues 61 to 95 called the NAC region for non-amyloid-β-component, which is the most aggregation-prone

part and the C-terminal end from residues 96 to 140 which incorporates mostly anionic residues which results in an acidic character for this part of the protein. [29] Like most amyloidogenic proteins, αSyn is a so-called IDP or intrinsically disordered protein that does not favor any fixed secondary structure but fluctuates between different structures and is primarily in a random coil structure as long as the protein is monomeric. [29] As soon as aggregation starts and the monomers start to form oligomeric species or larger aggregates, the structure could become and slowly develop into the final cross-β structure typical of amyloid fibrils. [29]

As already mentioned, the β-wrapins are based on the affibody sequence and then further developed by phage display and later by a bacterial display system. [18, 22] Here I want to briefly introduce phage display used to develop the β-wrapins. [3, 6] Phages, or rather bacteriophages, are viruses that are pathogens for bacteria. [37, 38, 39] The phages use the bacteria for their own reproduction, and either are lethal to the cell when they lyse the cell to find a new host or severely impair the cell's own production but do not kill the cell. [37, 38, 39] Phage display as a method was discovered in 1985 by George Smith and by now has become a fundamental method in research. [37, 38, 39] The advantage of phages is that they display proteins on their surface, and it is easy to integrate new gene sequences into their genome at the points of these surface proteins. [37] With this ability, it is possible to generate so-called phage libraries where, millions of fragments are displayed, each with a unique sequence. [37, 38] This makes it possible to screen for many target molecules to these displayed proteins simultaneously and quickly discern which is the best. [37, 38, 39] Furthermore, they can be used for a wide variety of targets: proteins, peptides, bacteria, cancer cells, viruses, and even non-organic substances. [37, 38, 39] As already mentioned, desired nucleotide sequences can be easily integrated into a phage genome since the phage genome is on the one hand small and on the other hand well known. [37, 38, 39] In the most commonly used phage display system, the desired target DNA is fused to a gene encoding for one of the M13 phage structural proteins (such as protein III or protein VIII) cloned into a phagemid vector. [37, 38, 39] It is important to note that when the target is displayed it will not be displayed alone but always as a fusion protein together with the rest of the originally displayed protein. [37, 38, 39] The phage display system is still the most well-known and most used display system, especially in combination with antibody development, but there are other display systems. [37, 38, 39] The β-wrapins $ZA\beta_3$, AS69 and HI18 were selected with phage display against three of the most prominent neurodegenerative diseases AD, PD and TIID respectively ($ZA\beta_3$ was selected by a group in Stockholm; AS69 and HI18 were selected in our own lab). [22, 23, 26]

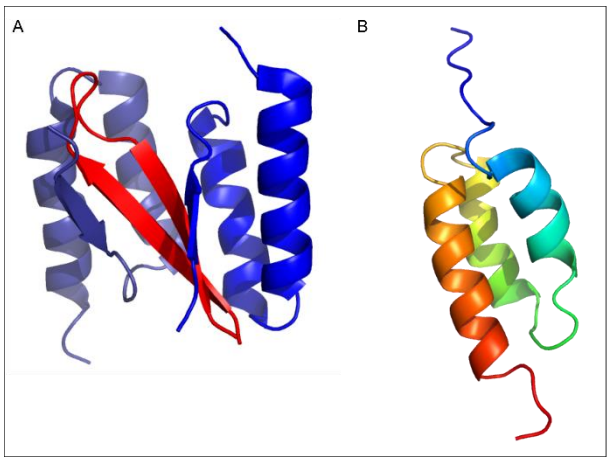

Figure 2: (A) Structure of the β-wrapin AS69 (blue) and the bound αSyn (red), (B) the *Staphylococcus aureus* protein A, immunoglobulin-binding B domain from which the β-wrapin sequence is derived.

This work is focused on the β-wrapin AS69 that binds αSyn monomer in its wildtype form with a K_d of 240 nM. AS69 was successfully designed, engineered, and displayed with the phage display system, as it was first done with $ZA\beta_3$. The measured K_d value is already good but can be further optimized; this was here approached through molecular dynamics simulations. Here, two strategies were explored. One was to enhance the binding enthalpy, the other to enhance the binding entropy. The molecular dynamics simulations and sequence generation was done by Professor Phanourios Tamamis, while the cloning into, and expression, purification with *E. coli* and isothermal titration calorimetry measurements of the resulting sequences was done by me (Figure 3 and 4).

```
                    10         20         30         40         50
AS69 WT    -VDNKFNKEMASADGEIFYLPNLNPDQLCAFFHSVHDDPSQSANLLAEAKKLNDAQAPK-
AS69 2x    -VDNKFNKEMASADGEIFYLPNLNPDQLCAFFHSVHDDPKQSDNLLAEAKKLNDAQAPK-
AS69 3x    -VDNKFNKEMASADGEIFYLPNLNADQLCAFFRSVEDDPSQSANLLAEAKKLNDAQAPK-
AS69 4x    -VDNKFNKEMASADGEIFYLPNLKADQLCAFFRSVEDDPSQSANLLAEAKKLNDAQAPK-
AS69 5x    -VDNKFNKEMASADGEIFYLPNLNADQLCAFFRSVEDDPKQSDNLLAEAKKLNDAQAPK-
AS69 6x    -VDNKFNKEMASADGEIFYLPNLKADQLCAFFRSVEDDPKQSDNLLAEAKKLNDAQAPK-
AS69 R8-2  -VDNKFNKEMASADGEIFYLPNLDPRQLCAFFESVRDDPKQSDNLLAEAKKLNDAQAPK-
```

Figure 3: The sequences of AS69 of the MD simulated mutants compared to the WT sequence, mutations indicated in bold.

In following will be a short overview of molecular dynamics simulations (MD simulations). The first MD simulation of a protein was done in the late 1970s, but the technique is already older; in the late 1950s, MD simulations were already used on gasses. [30] MD simulation makes it possible to predict and analyze the structure and movements of molecules down to the atomic level during a defined timeframe. [30] What MD simulations enable is to study how a protein, molecule, or biological system moves when parameters are changed, and the system is perturbed. [30] On the other hand, MD simulation is employed to investigate biological processes that are hard or impossible to visualize experimentally. [30] In the case of this project, the MD simulation was used to optimize a binder to its target. In general, the setup of an MD simulation is mostly the same at the very beginning. Most frequently, the MD simulations start from a known structure of the molecule or a homolog, by which a so-called molecular system must be built, and therefore, a suitable kind of force-field must be chosen to use. [30] The force-field is a model in which environment the simulation is run, they assimilate the forces that can influence the molecule, for example, electrostatic interactions between atoms, the solvent, and its ions. [30] It is important to note that different force-fields exist, each tailored to a specific set of molecules or interactions that they simulate, but still they remain incomplete, and imperfect compared to natural systems, which must be kept in mind for the final analysis. [30] Furthermore, the molecular system that needs to be built up, missing atoms, also hydrogen atoms, lipids, ions, and what else is required must be embedded before starting a simulation. [30] For the simulation itself, it must be decided which to perform since each simulation

accumulates a massive amount of data, as position of each atom at timepoint X can theoretically be simulated. [30] Experiments can often be designed and performed according to the results of such simulations or to validate the predicted results. Overall, today MD simulations are used for quite a few applications, from the refinement of structures to drug design, responses of biological systems to disruptions of any kind and connected, to watch biological systems while working/functioning in their native way and when, for example, mutations are introduced. [30] Specifically, in this project, MD simulations were used to optimize the binder AS69 to its target αSyn, through mutations of key amino acids with the final goal of improving the enthalpy of binding, by pre-forming the hairpin binding tunnel-like cavity of the β-wrapin and thus stabilizing the hairpin. [22, 23, 27, 39] This was achieved by mutating different amino acids in the second helix of each subunit of the β-wrapin by either mutating only one amino acid or up to six, but always symmetrical, meaning in both subunits, the same amino acids were mutated. Those were then experimentally tested first with isothermal titration calorimetry (ITC) to derive a K_d and the enthalpy (ΔH) and entropy (ΔS) and compare them to the simulated values, before performing further experiments.

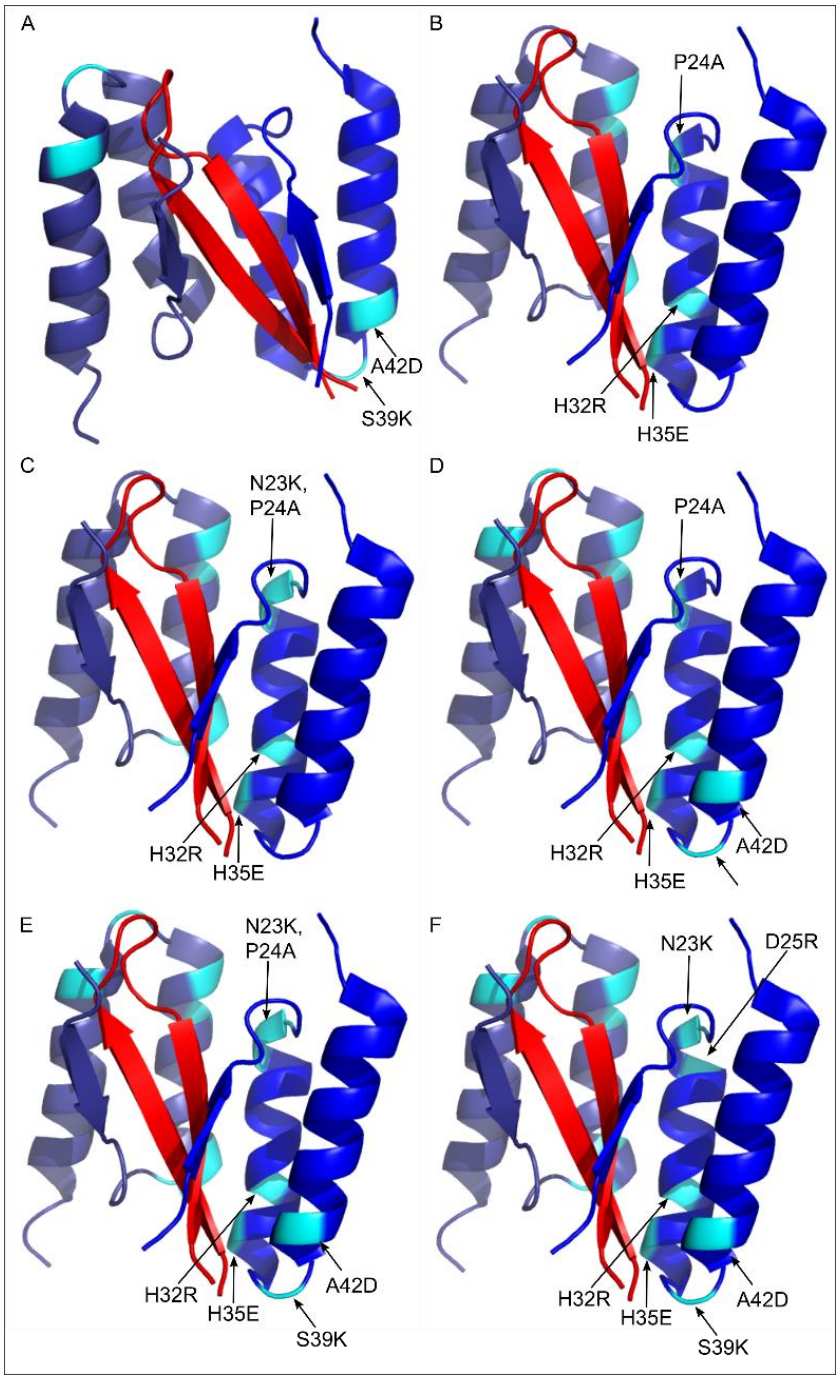

Figure 4: AS69 with indicated mutations selected by MD simulations, (A) AS69 2x, (B) AS69 3x, (C) AS69 4x, (D) AS69 5x, (E) AS69 6x and (F) AS69 R8-2.

In this section, an overview of the ITC method will be given. ITC is the abbreviation for "isothermal titration calorimetry", a technique that is used to determine thermodynamic parameters like entropy, enthalpy, free energy and K_d-values of molecular interactions, often between two binding partners, by measuring the heat differences between a sample and a

control. [31] The first theoretical approach on ITC, the equations that are used today and how it could work was done by Keily and Hume in 1956. [31] In 1961 the first experimental approach was made by Bricker et al., and the principle has barely changed since then. Every ITC machine contains two cells, one a reference cell for the buffer, the second the sample cell, and an injection syringe. [31] While measuring the differences in heat between the two cells are measured, or rather the power that needs to be applied to keep the reference cell and the sample cell at the same temperature. [31] Here, one can differentiate between exothermic and endothermic reactions between two partners taking place in the sample cell; in case of the exothermic reaction, the temperature of the sample cell increases, so the machine has to apply more power to keep both cells at the same temperature. [31] The other way around with endothermic reactions, here the temperature in the sample cell decreases, so the machine needs to reduce power to keep the cells at the same temperature. [31] These differences can be measured. Now, titrating one of the two components into the sample cell with the injection syringe to the second molecule, results in a signal change, which can be used to calculate ΔS (entropy) and ΔG (free energy), while ΔH (enthalpy) and K_a (association constant), K_d and the binding stoichiometry can be directly read out of an ITC titration curve. [31] The equations for calculating ΔS and ΔG are depicted in below. [31]

$$\Delta G = -RTln(K_a)$$

$$\Delta S = \frac{(\Delta H - \Delta G)}{T}$$

R being the gas constant and T the temperature in Kelvin.

Finally, as a side project to this main one, the first steps towards a high throughput screening (HTS) assay were taken. For this purpose, fluorescence polarization (FP) technique was used. FP is a tool to help determine the interactions between different molecules and, today, a favored technique used for HTS since today it is possible to do the assay in a well-plate format which allows for the screening of many molecules at the same time. [35, 36] Moreover, the application's application is today much higher than in the past. [35] FP can show changes in the molecular weight of a fluorescent dye (tracer) when brought together with another molecule by measuring the emission intensity of different polarized planes. [35]

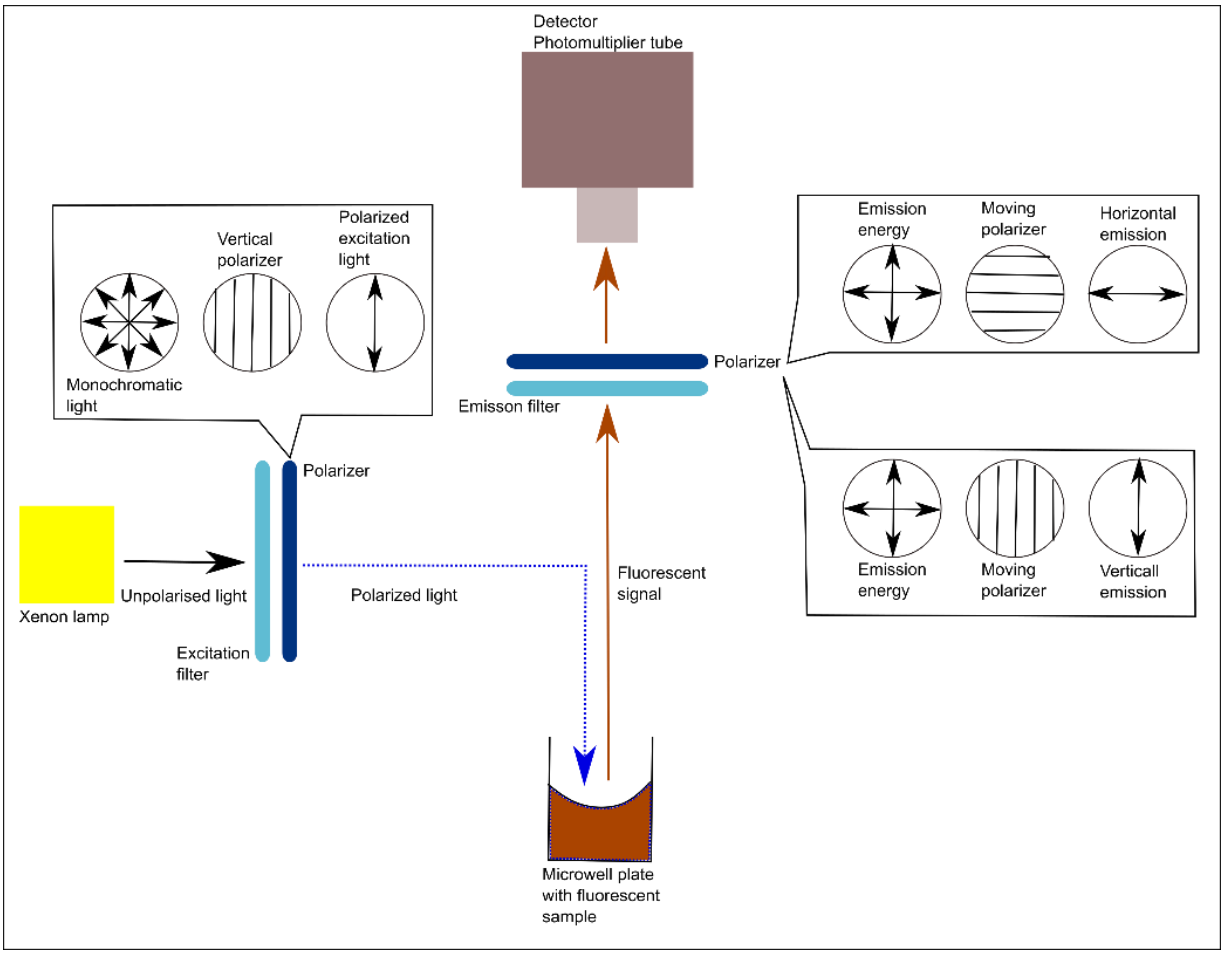

Figure 5: Schematic of an FP measurement and its light path.

The theoretical approach to FP was already published in 1926 by Francis Perrin, and in 1996, Jolley was one of the first to do FP in a well-plate screening, while it was formerly done in quartz cuvettes. [35, 36] FP was used before, mostly in diagnostics starting in the 1960s as an immunoassay. [35, 36] As mentioned earlier, the principle of FP is that the emission of a fluorescent dye, conjugated to one of the studied molecules (usually the smaller one), is measured which can be affected by the interaction of the fluorescently-labeled molecule with another unlabled molecule. [35, 36] First, to explain the method itself (Figure 4 and 5). Natural light, like sunlight randomly fluctuates in all directions without a set direction. [35, 36] It is possible to direct light in such a way that the light only oscillates in one direction, which means it can be polarized, this is, for example, common in lasers. [35, 36] Special filters can polarize light in a linear, circular, and elliptical fashion. [35, 36] Here for FP, the light needs to be linear polarized. [35, 36] The linear polarization happens perpendicular to the propagation direction of the light. [35] One can then chose any oscillation plane (Figure 4 top left) and measure the

intensity of this plane. [35, 36] The reference intensity is then the plane perpendicular to the measured plane. [35, 36] If the polarization declines and when fully gone the intensities in both planes will be the same. [35, 36] To detect differences in molecular weight through an FP assay, one utilizes the fact that the tumbling rate of a fluorophore is inversely related to the degree of polarization. [35, 36] In addition, fluorophores show different intensities in different polarization planes at different time points, or if they are bound or not; those different planes are usually parallel and perpendicular. [35, 36] This means the following: a small peptide or molecule (< 1.5 kDa) conjugated with a fluorescent dye and alone in solution is very flexible and tumbles fast. [35, 36] If the tumbling is fast, the peptide or molecule moves a lot between the excitation and emission time, and the emission light is often no longer in the same plane as the light used for excitation, this results in low FP values. [35, 36] On the other hand, when a second molecule (>10 kDa) binds the peptide or molecule with the fluorophore, the tumbling is much slower. [35, 36] Consequently, the molecule complex does not move much between the excitation and emission time, and the emission light is more often in the same plane as the light used for excitation, resulting in high FP values. [35, 36] These differences in tumbling of the molecule in the time between excitation light and emission light are what an FP experiment measures. [35, 36]

$$P = \frac{(F \parallel - F \perp)}{(F \parallel + F \perp)}$$

The formula above is how FP values are calculated. It calculates the difference between the emission fluorescence intensity of parallel (F∥) and perpendicular light (F⊥) to the excitation light, which is then divided by the total fluorescence emission intensities. [35, 36] FP values in general, are dimensionless, as they are ratios between light intensities. [35, 36] Often mP (millipolarization) is used and for biological samples mP-values between 10 and 300 mP are typical. [35, 36] In the plate reader it works as follows: the sample is excited at the needed wavelength by parallel polarized light, the light source most used is a xenon lamp, where the light is filtered by a filter before passing through the polarizer. [35, 36] The emission light is filtered again by a filter to remove unwanted wavelengths and then separated into parallel and perpendicular polarized light and quantified separately by using again polarizers, the intensities are quantified by a detector, commonly a photomultiplier tube. [35, 36] This technique was used as steppingstone for an HTS assay to screen for possible small molecules to block the fibrillation of αSyn (Figure 5). [35, 36] For this, a peptide was designed which contained the hairpin region of αSyn, where AS69 also binds, and the conjugated dye TAMRA (5-

carboxytetramethylrodamin) a red fluorescent dye. This peptide is supposed to be part of a competition assay, as described in the following. [35, 36]

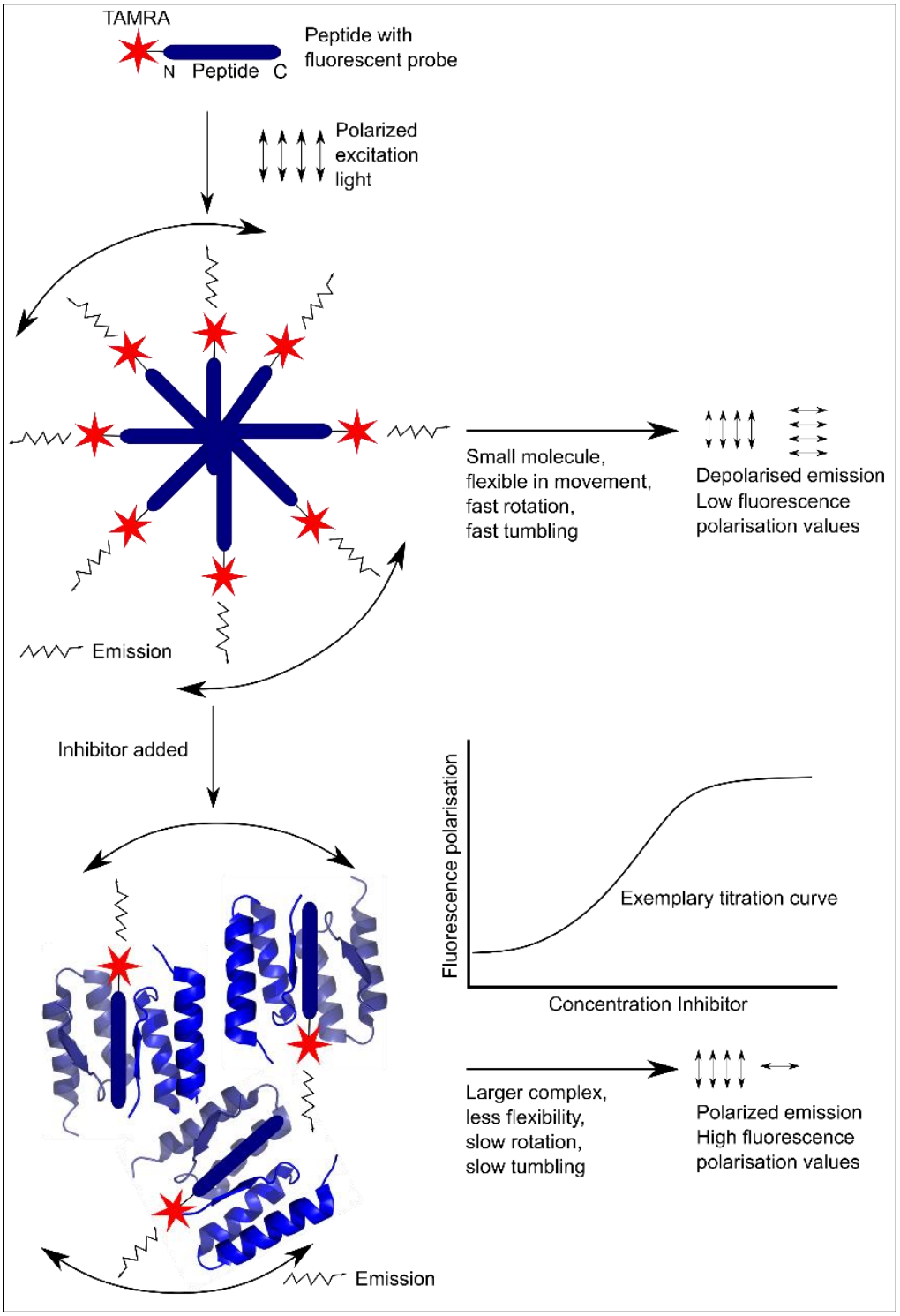

Figure 6: Schematic of a FP measurement.

If there are high polarization values the peptide is bound by AS69, if there are low polarization values the peptide is unbound which could either mean the peptide is bound by small molecule (correct positive) or the AS69 binding site is blocked by the small molecule (false positive).

3.2 Objective

The first and foremost object of this project is the optimization of the β-wrapin AS69, through MD simulations (Dr. Phanourios Tamamis) and followed by experimental testing of the new sequences with ITC. Promising candidates will be tested in aggregation inhibition assays. The second objective of this project is to set up a fluorescence polarization assays to test for the possibility or the development of a high throughput screening assay to test small molecules against αSyn in a competition assay. Here, the hairpin region with a fluorescent dye is being used where AS69 and the small molecule candidate compete for the binding of the peptide. From there on further steps could be developed.

3.3 Material and Methods

3.3.1 Material

Chemicals

Chemicals	Supplier
10x TGS-buffer (Tris-Glycin-SDS-buffer)	BioRad
2YT (Yeast extract tryptone)	AppliChem
Acetic acid	Merck
Acrylamid/Bisacrylamid (Rotiphorese Gel 30 (37:1))	Roth
Ammonium persulfate (APS)	Roth
Ammonium sulfate $(NH_4)_2SO_4$	Merck, Sigma-Aldrich
Ampicillin sodium salt	Roth
Bacto agar	Dickinson and Company, BD
Bromophenol Blau	Merck
Comassie Brillant Blue G-250	Sigma
cOmplete™, Mini, EDTA-free Protease Inhibitor Cocktail	Roche
Deoxynucleotide triphosphates (dNTPs)	Thermo Scientific
Disodium hydrogen phosphate (Na_2HPO_4)	Honeywell
Glycerol	VWR Chemicals
HF 5x Phusion reaction buffer	New England BioLabs
Hydrochloric acid (HCl)	Fisher Chemical
Imidazole	Honeywell
Isopropyl-β-D-thiogalactopyranosid (IPTG)	Roth
Lysogeny broth (LB)	AppliChem
Methanol	Merck
Phusion® High-Fidelity DNA Polymerase	New England BioLabs
Sealing tape (Polyolefin Acrylate)	Thermo Scientific
Sodium dihydrogen phosphate (NaH_2PO_4)	Applichem, Sigma-Aldrich
Sodium dodecyl sulfate (SDS)	Merck
Sodiumchloride (NaCl)	Merck
Streptomycin sulfate	Serve

Tetramethylethylenediamine (TEMED)	Merck
Thioflavin T (ThT)	Sigma
Tris(hydroxymethyl)-aminomethan (Tris)	VWR Chemicals
β-Mercaptoethanol	Roth

Plasmids

pMA-RQ [Invitrogen by Thermo Fisher Scientific]
pET 302 nt/HIS [in house]
pT7-7 [in house]

Cells

Stellar competent cells, chemically competent from Takara Clontech
Genotype: F–, endA1, supE44, thi-1, recA1, relA1, gyrA96, phoA, Φ80d lacZΔ M15, Δ (lacZYA - argF) U169, Δ (mrr - hsdRMS - mcrBC), ΔmcrA, λ–

Jm109 (DE3), chemically competent [in house]
Genotype: endA1 glnV44 thi-1 relA1 gyrA96 recA1 mcrB+ Δ(lac-proAB) e14- [F' traD36 proAB+ lacIq lacZΔM15] hsdR17(rK-mK+) and λ(DE3 [lacI lacUV5-T7p07 ind1 sam7 nin5]) [malB+]K-12(λS)

Oligonucleotides

Linearization of the vector pET 302 nt/HIS from Sigma-Aldrich, now Merck
Forward 5'-GTGATGATGATGATGATGCATATG-3'
Reverse 5'-CCTAGGTATAATCGGATCCGG-3'

Fusion constructs from Sigma-Aldrich, now Merck
Forward 5'-CATATGCATCATCATCATCATCAC-3'
Reverse 5'-CCGGATCCGATTATACCTAGG-3'

Gene strings fusion constructs

Gene strings from Invitrogen by Thermo Fisher Scientific

AS69 S39K, A42D (2x)

-GTAGATAACAAATTCAACAAAGAAATGGCGAGTGCGGATGGGGAGATCTTTTATTTACCTA
ACTTAAACCCGGATCAACTGTGCGCCTTCTTCCATAGTGTACATGATGACCCAAAACAAAGCGATA
ACTTGCTAGCAGAAGCTAAAAAGCTAAATGATGCTCAGGCGCCGAAA-

AS69 P24A, H32R, H35E (3x)

-GTAGATAACAAATTCAACAAAGAAATGGCGAGTGCGGATGGGGAGATCTTTTATTTACCTA
ACTTAAACGCGGATCAACTGTGCGCCTTCTTCCGTAGTGTAGAAGATGACCCAAGCCAAAGCGCGA
ACTTGCTAGCAGAAGCTAAAAAGCTAAATGATGCTCAGGCGCCGAAA-

AS69 N23K, P24A, H32R, H35E (4x)

-GTAGATAACAAATTCAACAAAGAAATGGCGAGTGCGGATGGGGAGATCTTTTATTTACCTA
ACTTAAAAGCGGATCAACTGTGCGCCTTCTTCCGTAGTGTAGAAGATGACCCAAGCCAAAGCGCGA
ACTTGCTAGCAGAAGCTAAAAAGCTAAATGATGCTCAGGCGCCGAAA-

AS69 P24A, H32R, H35E, S39K, A42D (5x)

-GTAGATAACAAATTCAACAAAGAAATGGCGAGTGCGGATGGGGAGATCTTTTATTTACCTA
ACTTAAACGCGGATCAACTGTGCGCCTTCTTCCGTAGTGTAGAAGATGACCCAAAACAAAGCGATA
ACTTGCTAGCAGAAGCTAAAAAGCTAAATGATGCTCAGGCGCCGAAA-

AS69 N23K, P24A, H32R, H35E, S39K, A42D (6x)

-GTAGATAACAAATTCAACAAAGAAATGGCGAGTGCGGATGGGGAGATCTTTTATTTACCTA
ACTTAAAAGCGGATCAACTGTGCGCCTTCTTCCGTAGTGTAGAAGATGACCCAAAACAAAGCGATA
ACTTGCTAGCAGAAGCTAAAAAGCTAAATGATGCTCAGGCGCCGAAA-

AS69 R8-2 (N23D, D25R, H32E, H35R, S39K, A42D)

-GTAGATAACAAATTCAACAAAGAAATGGCGAGTGCGGATGGGGAGATCTTTTATTTACCTA
ACTTAGATCCGCGTCAACTGTGCGCCTTCTTCGAAAGTGTACGTGATGACCCAAAACAAAGCGATA
ACTTGCTAGCAGAAGCTAAAAAGCTAAATGATGCTCAGGCGCCGAAA-

Proteins and Peptides

AS69 WT

-MHHHHHHVDN KFNKEMASAD GEIFYLPNLN PDQLCAFFHS VHDDPSQSAN LLAEAKKLND AQAPK-

AS69 S39K, A42D (2x)

-MHHHHHHVDN KFNKEMASAD GEIFYLPNLN PDQLCAFFHS VHDDP**K**QS**D**N LLAEAKKLND AQAPK-

AS69 P24A, H32R, H35E (3x)

-MHHHHHHVDN KFNKEMASAD GEIFYLPNLN **A**DQLCAFF**R**S V**E**DDPSQSAN LLAEAKKLND AQAPK-

AS69 N23K, P24A, H32R, H35E (4x)

-MHHHHHHVDN KFNKEMASAD GEIFYLPNL**K** **A**DQLCAFF**R**S V**E**DDPSQSAN LLAEAKKLND AQAPK-

AS69 P24A, H32R, H35E, S39K, A42D (5x)

-MHHHHHHVDN KFNKEMASAD GEIFYLPNLN **A**DQLCAFF**R**S V**E**DDP**K**QS**D**N LLAEAKKLND AQAPK-

AS69 N23K, P24A, H32R, H35E, S39K, A42D (6x)

-MHHHHHHVDN KFNKEMASAD GEIFYLPNL**K** **A**DQLCAFF**R**S V**E**DDP**K**QS**D**N LLAEAKKLND AQAPK-

AS69 R8-2 (N23D, D25R, H32E, H35R, S39K, A42D)

-MHHHHHHVDN KFNKEMASAD GEIFYLPNL**D** P**R**QLCAFF**E**S V**R**DDP**K**QS**D**N LLAEAKKLND AQAPK-

α-synuclein (1-140)

-MDVFMKGLSK AKEGVVAAAE KTKQGVAEAA GKTKEGVLYV GSKTKEGVVH GVATVAEKTK EQVTNVGGAV VTGVTAVAQK TVEGAGSIAA ATGFVKKDQL GKNEEGAPQE GILEDMPVDP DNEAYEMPSE EGYQDYEPEA-

α-synuclein TAMRA peptide

30-GKTKEGVLYVGSKTKEGVVHGVATVAEKT-60

α-synuclein CC peptide

H-KEGVLYV**C**SKTKEG**C**VHGVATVAE-OH

Media

LB (Lysogeny broth) -Agar for 1 L

5 g/L NaCl

10 g/L Tryptone

5 g/L Yeast extract

100 mg/ml Ampicillin

15 g/L Bacto agar

2YT (Yeast extract tryptone)

5 g/L NaCl

16 g/L Tryptone

10 g/L Yeast extract

100 mg/ml Ampicillin

Buffers

AS69 and mutants purification buffers

Loading buffer Ni-NTA

50 mM Tris-HCl, pH 8

500 mM NaCl

20 mM imidazole

Elution buffer Ni-NTA

50 mM Tris-HCl, pH 8.0

500 mM NaCl

500 mM imidazole

SEC-buffer

20 mM NaPi, pH 7.4

50 mM NaCl

α-synuclein purification buffers

Thawing and heating

150 mM NaCl

1 tablet cOmplete™, Mini, EDTA-free Protease Inhibitor Cocktail

DNA precipitation

10 mg/ml Streptomycin sulfate

Protein precipitation

3.5 M Ammonium sulfate

Dialysis buffer

25 mM Tris-HCl, pH 8.0

Loading buffer IEC

25 mM Tris-HCl, pH 8.0

Elution buffer IEC

25 mM Tris-HCl, pH 8.0

800 mM NaCl

SEC buffer

20 mM NaPi, pH 7.4

50 mM NaCl

ITC buffer

20 mM NaPi, pH 7.4

50 mM NaCl

FP-assay buffer

20 mM NaPi, pH 7.4

50 mM NaCl

SDS-Page

Separating gel buffer

1.5 M Tris-HCl, pH 8.8

14 mM SDS

Stacking gel buffer

0.5 M Tris-HCl, pH 6.8

4% (w/v) SDS

Separating gel 15% (2 gels)

4000 µl Acrylamid/Bisacrylamid (Rotiphorese Gel 30 (37:1))

1600 µl ddH_2O

400 µl Glycerin (99%)

2000 µl separating gel buffer

4 µl TEMED

40 µl 10% APS

Stacking gel (2 gels)

532 µl Acrylamid/Bisacrylamid (Rotiphorese Gel 30 (37:1))

2468 µl ddH_2O

1000 µl stacking gel buffer

3.2 µl TEMED

32 µl 10% APS

4x Læmmli reducing loading buffer

16% (v/v) SDS

38% (v/v) Glycerin

200 mM Tris-HCl, pH 6.8

0.04% (w/v) Bromophenol Blau

8% (v/v) β-Mercaptoethanol

TGS buffer (10x)

25 mM Tris-HCl

192 mM Gylcin

0.1% (w/v) SDS

Coomassie Brilliant Blue

Coomassie Brillant Blue R-250

45% (v/v) Methanol

10% (v/v) Acetic acid

45% (v/v) ddH_2O

Kits

Kit	Supplier
In-Fusion® HD EcoDry™ Cloning Kit	Takara Bio
NucleoSpin Gel and PCR Clean-up	Macherey-Nagel
Plasmid DNA purification NucleoSpin®Plasmid	Macherey-Nagel

Devices

Device	Supplier
5 ml HisTrap FF	GE-Healthcare
5 ml HiTrap Q FF	Cytiva life science
Agarose gel documentation G:Box	Syngene
Agarose gel electrophoresis device Mini-Sub® Cell GT	BioRad
Beckman Coulter Avanti J-26S XP	Beckman Coulter
BMG Labtech CLARIOstar	BMG
Centrifuge 5415 R	Eppendorf
Centrifuge 5804 R	Eppendorf
GE Äkta Purifier	GE-Healthcare
Geldocumentation System	BioRad
Heatblock Ori Block 0B-3	Techne
Infors HT Multitron Standard	Infors
Innova 40	New Brunswick Scientific
Mastercycler ep gradient S	Eppendorf
Microcal iTC200 calorimeter	GE Healthcare
Mini Protean Tetra System	BioRad
Nanodrop 2000 Spectrophotometer	Thermo Scientific
pH-meter PB-11	Sartorius
Power source 300 V	VWR
Rotor JLA 10.500	Beckman Coulter
Sonicator Sonoplus	Bandelin
Sonotrode MS72	Bandelin]
Spectrophotometer V-650	Jasco
Superdex 200 increase 10/300 GL	GE-Healthcare
Thermomixer compact/comfort	Eppendorf

Software

Name	Supplier
CLARIOstar 5.40 R	BMG
CLARIOstar Mars Data Analysis 3.31	BMG
GeneSnap	Syngene
Image Lab	BioRad
MicroCal Origin	Origin
Nanodrop 2000/2000s 1.5	Thermo scientific
Origin Pro 9.0G	Origin
Pymol 2.0.6	Origin
SnapGene Viewer 3.1.3	SnapGene
Unicorn 5.2	GE-Healthcare

3.3.2 Methods

Molecular dynamics simulation fully done by Prof Phanourios Tamamis and his group

To investigate the stability of the unbound β-wrapins we employed triplicate MD simulations of the unbound β-wrapins. We performed RMSF (root-mean-square-fluctuations) calculations on the resulting MD simulation snapshots and simulated residues 12 to 56 of each β-wrapin subunit for 24 ns. The β-wrapins were solvated in a 72x72x72 explicit water box with a potassium chloride concentration of 0.15 M. The charge-solvated systems are neutralized through the addition of potassium or chloride ions. Simulation of each β-wrapin was run in triplicates to ensure the reproducibility of their work.

Following the MD simulations, solvent molecules were stripped from the simulation snapshots and the trajectories from all three triplicate runs were combined for each β-wrapin variant. The RMSF calculations per C_α atoms for residues 21 to 56 were calculated. The C_α atoms for residues 12 through 20 were excluded in these calculations as this region is disordered in the unbound state of the β-wrapins. RMSF calculations per C_α atom were performed through Wordom using the following equation:

$$RMSF_i = \sqrt{\frac{\sum_j^N ((x_i(j) - \bar{x}_i)^2 + (y_i(j) - \bar{y}_i)^2 + (z_i(j) - \bar{z}_i)^2)}{N}}$$

Where *i* is the C_α atom, *j* is the simulation snapshot, *N* is the total number of simulation snapshots. We subsequently summed the RMSFs of the C_α atoms of both β-wrapin subunits (residues 21 through 56) and divided by the total number of C_α atoms in both β-wrapin subunits (residues 21 through 56) to obtain the average RMSF over the triplicate runs.

Linearization of pET 302 nt/His vector

For the linearization of the pET302 nt/HIS vector the Phusion polymerase was used in the following PCR-program:

Step	Temperature	Time	Number of cycles
Initial denaturation	98 °C	30 sec	
Denaturation	98°C	10 sec	x35
Annealing	69 °C	30 sec	
Elongation	72 °C	1 min	
Final elongation	72 °C	5 min	
Storage	10 °C	∞	

After the PCR the product was cleaned up with the Macherey-Nagel PCR clean-up kit.

InFusion cloning reaction for AS69 mutants

The sequences of the AS69 mutants were ordered as GeneArt Strings DNA fragments from Invitrogen [ThermoFisher Scientific] and delivered as a lyophilized powder. The DNA fragments/inserts were dissolved in water to a final concentration of 35 ng/µl to 40 ng/µl. In 5 µl final volume the inserts were mixed with the linearized vector, the 5x enzyme premix from the In-Fusion® HD Cloning Kit from Takara Bio USA, Inc. and water if the volume was not reached by the other components. The mixture was incubated according to the user manual at 50°C for 15 min before setting on ice. The mutant R8-2 was done with the In-Fusion® HD EcoDry™ Cloning Kit from Takara Bio USA, Inc.. To prepare the cloning reaction, the lyophilized enzyme pellet was resuspended into a mixture of the insert, linearized vector, and water, (in the total volume of 10 µl). The mixture is then incubated first at 50°C for 15 min followed by another 15 min at 37°C according to the manual. Afterwards the reaction is put on ice until further use. Part of the reactions was immediately transformed into Stellar™ competent cells, and the remaining was stored at -20°C.

Transformation of AS69 mutants into *E. coli* Stellar™ competent cells and JM109 DE3 cells

The In-Fusion reactions were all transformed into the chemically competent *E. coli* Stellar™ competent cells. 50-µl aliquot cells were thawed on ice and then 1 µl of the In-Fusion reaction was added. Then, the mixture was kept on ice for an additional 30 min before performing a 45-sec heat shock at 42°C. Heat shock was followed by additional 2-min incubation on ice before adding 450 µl of pre-warmed SOC medium without antibiotics. The cells were then incubated at 37°C for 1 h at 800 rpm before being plated on an LB-agar plate supplemented with 100 µg/ml Ampicillin final concentration and then grown at 37°C overnight. The success of the transformation and the correct sequence of the protein was verified by sequencing.

The verified plasmids were all transformed into the chemically competent cells *E. coli* JM109 DE3. 50-µl aliquots of the cells were thawed on ice and then 2 µl of the DNA was added and the mixture left to incubate for 10 min on ice before performing a 60 sec heat shock at 42°C, another 2 min incubation on ice before adding 450 µl 2YT medium without antibiotics. The cells are left to incubate at 37°C for 1 h at 800 rpm before being plated on a LB-agar plate supplemented with 100 µg/ml Ampicillin final concentration and then grown at 37°C overnight. The success of the transformation and the correct sequence of the protein was verified by sequencing.

Expression of AS69 mutants

The expression of the fusion constructs was done in *E. coli* JM109 DE3 cells using 2YT supplemented with 100 µg/L ampicillin. An overnight 2YT preculture was grown at 37 °C and 180 rpm. A 2YT expression culture was inoculated from the preculture at an optical density of 0.05 and grown at 37°C and 140 rpm until induction with Isopropyl-β-D-thiogalactopyranosid (IPTG) at an optical density of 0.6-0.8, then incubated at 37°C, 130 rpm for additional 4 hours before harvesting. The cells were harvested by centrifuging at 5000 rpm for 10 min at 4 °C.

Purification of AS69 mutants

All AS69 mutants could be purified as according to the same protocol used for the AS69 wild type. Harvested cells were frozen overnight in loading buffer (50 mM Tris(hydroxymethyl)aminomethane (Tris), pH 8, 500 mM sodium chloride (NaCl), 20 mM imidazole with a protease inhibitor (cOmplete^{TM}, Mini, EDTA-free Protease Inhibitor Cocktail, Roche). After thawing the cells, they were sonicated on the ice twice for 5 min with the sonication probe MS-72, with an amplitude of 35 % and a cycle of 3 s pulse and 5 s pause. The next step was to spin down the cell debris at 10000 xg for 20 min at 4°C, and the supernatant was run over a NiNTA-column (GE-healthcare, 5 ml HisTrap FF, column) in the loading buffer. Protein was eluted with a mixture of loading buffer and elution buffer (50 mM Tris, pH 8, 500 mM NaCl, 500 mM imidazole) into a final concentration of 250 mM imidazole. The eluate is then concentrated and kept at 4°C over night. The next day the protein was run over a size exclusion chromatography column (SEC Superdex^{TM} 200 Increase 10/300 GL GE healthcare) in a sodium phosphate buffer (20 mM NaPi, pH 7.4, 50 mM NaCl). The correct fractions were collected, pooled, concentrated and protein concentration measured with a spectrophotometer. Afterwards, the protein was aliquoted, frozen in liquid nitrogen and stored at -80 °C. SDS tris-glycine gels were run as controls for expression and later purity.

Expression of α-synuclein

αSyn is expressed in E. coli BL21 DE3 cells with ampicillin resistance. The cells were kindly provided as a glycerol stock by Dr. Emil Dandanell-Agerschou. A preculture is grown overnight at 37 °C and 180 rpm shaking in 2YT supplemented with 100 µg/ml Ampicillin as the final concentration. From the preculture fresh glycerol stocks were derived. The cells were put into 80% autoclaved glycerol, flash-frozen in liquid nitrogen and stored at -80°C. The main culture, also grown in 2YT with the same final concentration of antibiotics, was inoculated to an optical density of 0.05 and then grown at 37°C and 110 rpm until an optical density of 1 was reached. The cells were then induced with IPTG (Isopropyl-β-D-thiogalactopyranosid) to a final concentration of 1mM IPTG. The cultures were incubated for 4 h at 37°C and 110 rpm after induction. The cells were harvested by centrifugation at 4°C for 10 min at 5000 xg. The harvested cells are transferred into fresh 50 ml falcon tubes before frozen at -20°C.

Purification of α-synuclein

The harvested cell pellet is frozen over night at -20 °C in a 50 ml falcon tube. While thawing the cell pellet 150 mM Natrium chloride (NaCl) is added until the 20 ml mark on the falcon tube is reached and an EDTA-free protease inhibitor tablet (cOmplete^{TM}, Mini, EDTA-free Protease Inhibitor Cocktail, Roche) is added. The mixture is vortexed until the pellet is fully thawed, and the tablet dissolved. The cells are then placed in a heating block, pre-heated to 100 °C, and heated for 10 min with interspaced with short vortexing. The lysate is cooled in ice-water, interspaced with vortexing. The cooled lysate is centrifuged at 8000 xg, for 15 min at 4 °C. The supernatant is transferred to a fresh 50 ml Falcon tube, 10 mg/ml Streptomycin sulfate was added to the supernatant and the mixture was incubated for 10 min on a tilt/roller mixer (TAMIRO) at 10°C. After incubation the mixture was centrifuged again for 15 min. at 8000 xg and 4°C; again the supernatant was decanted into a fresh 50 ml Falcon tube, and the pellet was discarded. The volume of the supernatant was noted, and an equivalent volume was of saturated (3.5 M) Ammonium sulfate solution was added into the solution until there was a precipitate visible. The mixture was centrifuged again for 15 min at 8000 xg at 4 °C. In the next step the supernatant was discarded, and the pellet dissolved in 25 mM Tris(hydroxymethyl)aminomethane (Tris-HCl), pH 8.0 and dialyzed over night against 25 mM Tris, pH 8. A 5 ml HiTrap Q FF (Cytiva life science) ion exchange column was equilibrated with 25 mM Tris, pH 8.0 and the dialyzed protein was loaded on the column. Elution was done with the elution buffer 25 mM Tris-HCl pH 8.0 and 800 mM NaCl by eluting first for 5 min with 160 mM NaCl at 3 ml/min, followed by a gradient from 160-480 mM NaCl. The protein fractions were pooled and precipitated again with Ammonium sulfate, as described above. The pellet was resuspended in the size exclusion buffer (SEC-buffer) 20 mM Natrium-phosphate pH 7.4, 50 mM NaCl and run over a size exclusion chromatography column the Superdex 75 increase 10/300 GL (GE-Healthcare) and the corresponding peak was collected. The fractions corresponding to the protein peak were collected, pooled, and then concentrated. Purity was checked via SDS gel electrophoresis.

Isothermal titration calorimetry of AS69 mutants

ITC was performed at 30°C using a Microcal iTC200 calorimeter (GE Healthcare). aSyn was filled into the cell at a concentration of 50 µM in 20 mM sodium phosphate, pH 7.4, and 50 mM NaCl. AS69 mutants were titrated from the syringe in approximately 10-fold higher concentrations. Heats of post-saturation injections were averaged and subtracted from each injection to correct for heats of dilution and mixing. Dissociation constants were obtained from a nonlinear least-squares fit to a 1:1 binding model using MicroCal Origin.

Analysis of TAMRA-αSyn peptide with high performance liquid chromatography (HPLC) and size exclusion chromatography (SEC)

The fluorescent dye TAMRA was N-terminally bound to β-hairpin forming region of αSyn (residues 31-59) TAMRA-GKTKEGVLYVGSKTKEGVVHGVATVAEKT-. TAMRA has an excitation maximum at 543 nm and an emission maximum at 576 nm. An analytical HPLC (Agilent) was run at 80°C using a Zorbax C8 column (Agilent) to check whether the dye was still attached to the peptide. The following method was used for the run:

Time [min]	Buffer A [%]	Buffer B [%]	Flow [ml/min]	Max. Pressure [bar]
0.00	75.00	25.00	0.250	300
0.00	75.00	25.00	1.000	300
3.00	75.00	25.00	1.000	300
23.00	0.00	100.00	1.000	300
27.00	0.00	100.00	1.000	300
27.10	75.00	25.00	1.000	300
34.00	75.00	25.00	1.000	300

Buffer A is fresh distilled water with 0.1% Trifluoroacetic acid (TFA), and buffer B is 80% Acetonitrile. From the TAMRA-peptide 100 µl with a concentration of 10 µM were used for the analytical run. Measured were the wavelengths at 214.2 nm, 254.2 nm, 276.2 nm, 543.2 nm and 570.2 nm.

For the SEC the TAMRA-peptide was mixed 1:2 with β-wrapin AS69 to determine if peptide and dye are still bound to one another. For that 150 µl of the AS69 mixed with the TAMRA-

peptide mixture were injected on a Superdex 75 inc. 10/300 GL (GE Healthcare), while measuring the wavelengths at 215 nm, 275 nm and 543 nm. The run was done in 20 mM NaPi pH 7.4 and 50 mM NaCl.

Fluorescence polarization of AS69 and TAMRA-α-synuclein

Fluorescence polarization (FP) measurements were done at 37°C in a Greiner Bio-One, black, non-binding 384-well plates. As buffer 20 mM Natrium Phosphate, pH 7.4, 50 mM Natrium Chloride was used. The fluorescent dye TAMRA, with excitation at 543 nm and emission at 576 nm, was N-terminally conjugated to a peptide containing a sequence stretch of αSyn that encompassed the whole β-hairpin region made from 29 amino acids (residues 31-59). For FP measurements, the concentration of the TAMRA-peptide was kept the same throughout the measurements and the concentrations of the additives (AS69 WT, αSyn CC, αSyn WT) were varied. The volume pipetted into the plate was reduced to 24 µl per well. In all experiments, measurements were done with 3 cycles, a cycle time of 95 sec, and 200 flashes per well and cycle. The gain and focal height were determined using one of the wells as a reference. The plate was shaken at 300 rpm for 10 s and settled for 0.2 s before each cycle. The measurements were done with the top optic. This measurement was done once immediately after pipetting the plate, once 5 min after the first measurement, and after 30, 60 and 90 min and if possible after overnight or 2 days of storage protected from light at 4°C. In other experiments, competitors to the TAMRA-αSyn peptide were added in different concentrations. The competitors were full length αSyn and an αSyn CC variant.

3.4 Results

ITC measurements of AS69 mutants

After the successful expression and purification of the mutant AS69 versions they were subjected to an ITC measurement with α-synuclein (αSyn). The AS69 wild type (WT) values are known from the literature. The objective of the MD simulation of the following mutations was to improve either the binding enthalpy or the binding entropy. This was modeled with the idea that the hairpin of αSyn should be stabilized by preforming and stabilizing the binding area of the β-wrapin AS69. The AS69 S39K and A42D (AS69 2x) mutant was tested as, according to the computational simulations, these two amino acid changes stabilize the hairpin with salt bridges formed between AS69 and the hairpin. This variant showed a K_d of 198 nM and binding enthalpy and entropy values of -125.5 kJ/mol and -87 kJ/mol*K respectively. These two mutations are also present in two other simulated mutants, in the AS69 P24A, H32R, H35E, S39K, and A42D (AS69 5x), and in AS69 N23K, P24A, H32R, H35E, S39K, and A42D (AS69 6x). (Figure 3 and 10, Table 1) The additional mutations in that combination should also, according to the simulation results, help make the β-wrapin more rigid as they allow for more salt bridges, and hydrogen bonds in varying strengths between the wrapin subunits. The measured values for the AS69 5x from ITC are a K_d of 520 nM, a binding enthalpy of -37.2 kJ/mol, and a binding entropy of -0.9 kJ/mol*K and for AS69 6x a K_d of 440 nM, and -54.4 kJ/mol and -17.6 kJ/mol*K for binding enthalpy and entropy respectively (Table 1, Figure 7 and 10). Two additional mutants explored the number of mutations needed for the more rigid β-wrapin. The mutant with three mutations, P24A, H32R, and H35E (AS69 3x), showed a K_d value of 420 nM with the enthalpy being at -26.7 kJ/mol and entropy at 10.3 kJ/mol*K (Table 1). Similar values for the enthalpy and entropy were measured for the AS69 N23K, P24A, H32R and H35E (AS69 4x) with a K_d of 860 nM and -24.2 kJ/mol as value for enthalpy and 11 kJ/mol*K for the entropy (Table 1).

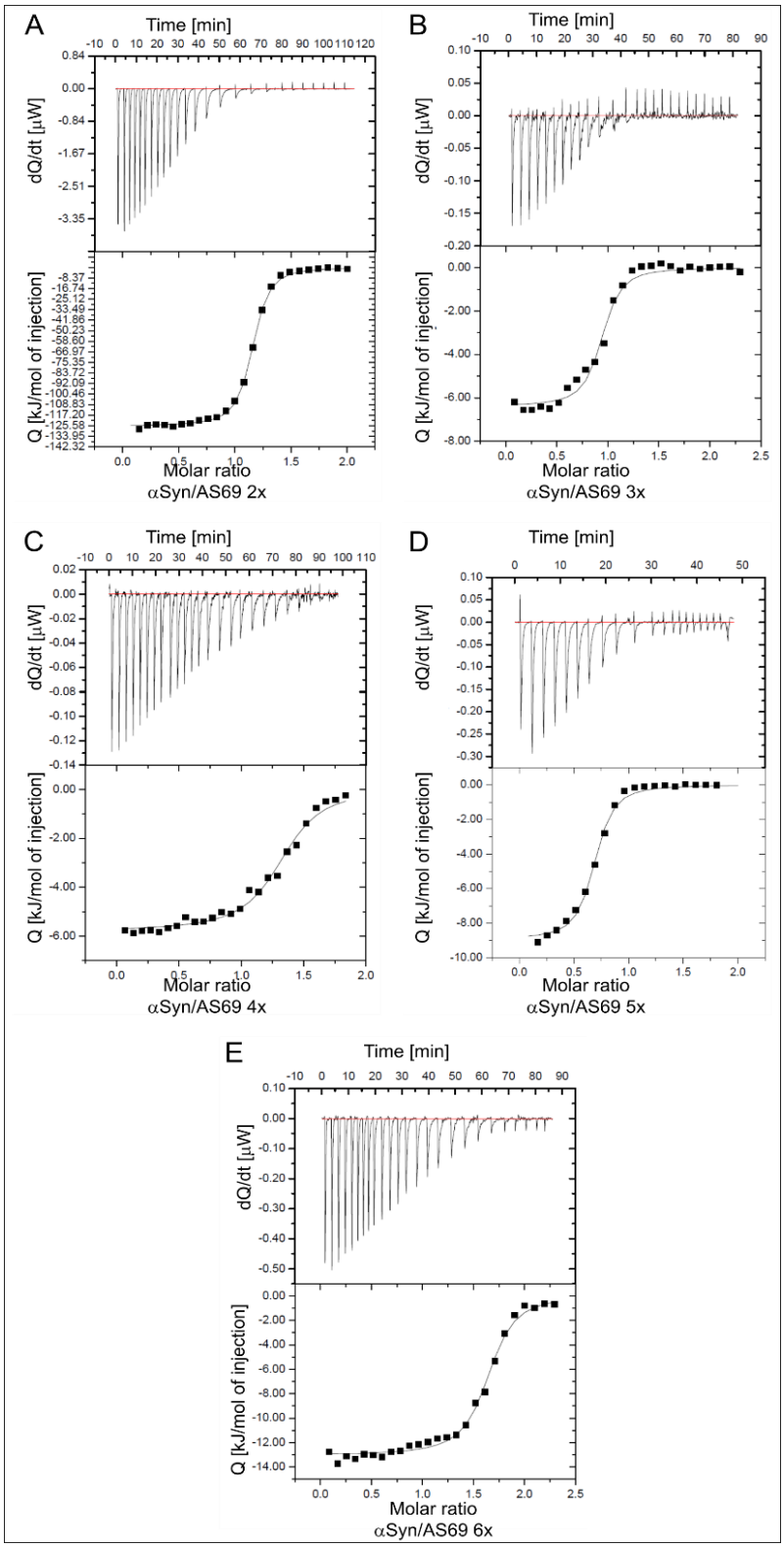

Figure 7: ITC measurements of the MD simulated AS69 mutants (A) AS69 2x, (B) AS69 3x, (C) AS69 4x, (D) AS69 5x and (E) AS69 6x.

A further mutant derived from the MD simulations, AS69 R8-2 (N23D, D25R, H32E, H35R, S39K and A42D), investigated a partially reversed placement of the side chain charges compared to the previous variants. However, the ITC measurements for this mutant were not successful.

Table 1: Calculated K_ds, binding enthalpy, and binding entropy of the ITC measurements of the MD simulation-derived mutants of AS69 and the WT from literature.

AS69 Variant	**K_d [nM]**	**ΔH [kJ*mol^{-1}]**	**ΔS [kJ*mol^{-1}*K^{-1}]**
WT	240	-75,3	-37,3
S39K, A42D (2x)	198	-125,5	-87,0
P24A, H32R, H35E (3x)	420	-26,7	10,3
N23K, P24A, H32R, H35E (4x)	860	-24,2	11,0
P24A, H32R, H35E, S39K, A42D (5x)	520	-37,2	-0.9
N23K, P24A, H32R, H35E, S39K, A42D (6x)	440	-54,4	-17,6

Fluorescence polarization

Before the fluorescence polarization assay was attempted it was first checked if the peptide-dye complex was still intact. The first experiment was an analytical run with the HPLC system to analyze if the dye is still in working order and still attached to the peptide. The TAMRA dye has an excitation wavelength of 543 nm and an emission wavelength of 576 nm, together with the wavelengths typically measured when peptides and proteins are involved, meaning 215 nm, 254 nm and 275 nm in this case, it would be possible to see if dye and peptide are still bound to each other, as they should have the same retention times. The analytic run showed two distinct peaks (Figure 8), where all measured wavelengths overlapped, of roughly the same intensity that eluted close to each other, which means that the dye is still active and usable but could also mean that there are two different populations of the TAMRA conjugated peptide (TAMRA-peptide). Since both peaks are also visible in the dye-corresponding wavelengths, it

is unclear which contains the whole TAMRA-peptide, and the other peak could contain TAMRA with only parts of the peptide. To elucidate further if the TAMRA-peptide complex is still intact, the HPLC run was followed by an SEC of the dye-peptide complex with AS69. Since the peptide attached to TAMRA is the β-hairpin region of aSyn, it could also bind to β-wrapin AS69 which was also a component of the fluorescence polarization assay (FP-assay). It should be possible to see in a mixture of the dye-peptide and AS69 if the dye is still attached to the peptide and if the peptide is still intact otherwise AS69 should not bind to it. In this experiment, a 1:2 concentration of TAMRA-peptide and AS69 was used, meaning here 80 µM of the TAMRA-peptide and 160 µM AS69. The mixture was left at room temperature until the column was equilibrated. In the end, 150 µl of the mixture was injected, and the column was wrapped partially in foil to avoid the dye photobleaching too much. A part of the dye was stuck on top of the column and did not flow through the column, unless 0.5 M Natrium hydroxide (NaOH) was applied as washing buffer. It could not be elucidated if what stayed on top of the column was just free dye or attached to the peptide. The wavelengths used here were 215 nm, 275 nm and for the dye 543 nm. In the SEC profile (Figure 8), only one peak was visible that overlapped in all wavelength channels. Since only one peak was visible despite using the fully formed β-wrapin (AS69 dimer) it indicated that the concentration of the TAMRA-peptide as given was not correct. If the concentration was truly 1:2 with more AS69, free AS69 should also be visible in the SEC profile. After this experiment what can be said is the following the TAMRA-peptide should be intact and can be bound by AS69 and measured, but the concentration of the TAMRA-peptide needed to be reevaluated.

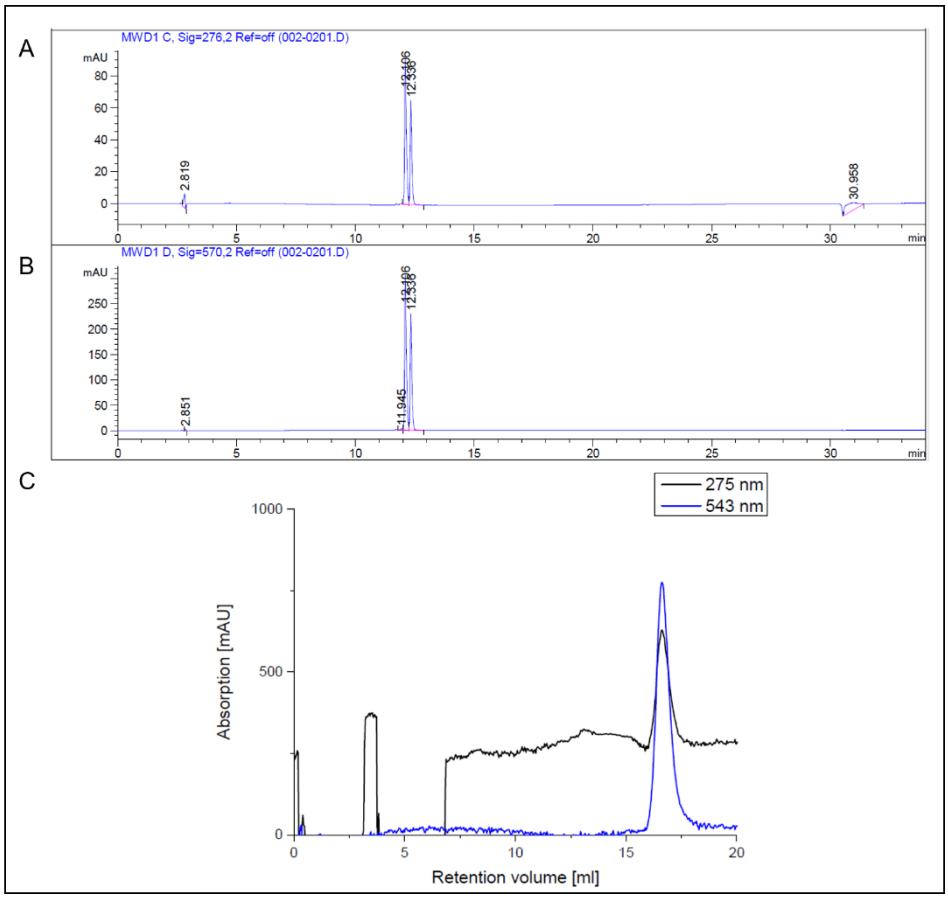

Figure 8: HPLC run of the TAMRA-peptide alone with two exemplary wavelengths 275 nm (A) for the peptide and 570 nm (B) close to the emission maximum of the TAMRA dye and SEC run (C) to control if the peptide can still be bound by β-wrapin AS69 shown by two wavelengths 275 nm (black) for peptide and protein and 543 nm (blue) for the TAMRA dye.

Following validation of the TAMRA-peptide functionality, FP measurements were performed. The trials measurements were optimized for the components volume and concentration in order to be used in a high throughput format. The assay was done in a 384-well plate in the first trial with 40 µl volume. In a first experiment two different ratios were chosen, the TAMRA-peptide and AS69 in a 1:1 ratio and the TAMRA-peptide and AS69 in a 1:5 ratio. As controls the TAMRA-peptide alone and buffer alone were also included. Each of the conditions was done as a duplicate. The concentration of the TAMRA-peptide was kept the same over all the experiments with 10 µM, AS69 depending on the chosen ratio, and was adjusted accordingly. The conditions that included AS69 and the TAMRA-peptide showed stable mFP values for the duplicates. With only the TAMRA peptide present, the FP values were about 35 mFP while in the 1:1 ratio it was about 55-58 mFP and in the 1:5 ratio at 144 mFP. The only thing that was

not used in any further experiments were the wells filled only with buffer, which were supposed to be control wells, as these gave very high mFP values; instead, empty wells were used as blank. In the second assay, the volume was varied to lower values, 16 µl and 24 µl instead of 40 µl. Both volumes are still measurable, but with 24 µl, the measurement were more stable than with only 16 µl. In the end, in all further experiments 24 µl volume per well was used. In a third experiment, different concentrations of the TAMRA-peptide were tested, as the stock solution (concentration 1 mM) of it is the limiting factor in this assay. First, as already described, 10 µM of the TAMRA-peptide was used, which worked without any problem and yielded very stable values. The same setup was also followed with 5 µM and 1 µM TAMRA-peptide, and the amount of AS69 in the assay was adjusted as necessary (ratios 1:1 and 1:5). Both concentrations still gave stable values in the FP assay, so concentrations between 1 and 10 µM TAMRA-peptide could be used but in the subsequent experiments the concentration of the TAMRA-peptide was kept at 10 µM. In the end the following conditions were used: the volume in the 384-well plates was kept at 24 µl, and the concentration of the TAMRA-peptide at 10 µM and the parameters for the measurement itself were always the same as described in the methods section. One further test was performed with the conditions described before. After the volume and concentration were defined for all further experiments, the plate containing the samples was wrapped in foil and kept over the weekend in a refigerator at 4 °C. After the weekend, the plate was removed from the fridge and warmed again to room temperature before being measured again at 37 °C with the same settings to see how stable the TAMRA-peptide with or without AS69 is. The mFP values barely changed after a weekend at 4 °C.

In the following experiment a titration of the TAMRA-peptide with AS69 was done (Figure 7). As already mentioned, the buffer, volume, TAMRA-peptide concentration, and measurement settings are fixed, here the concentration of AS69 was varied from 0 µM to 100 µM and the whole titration was done in duplicates. The plate was measured five times in total, once directly after pipetting when the plate was not yet warmed to the 37 °C of the machine, 5 minutes after the first measurement, 30, 60 and 90 minutes after the first measurement. During that time, the plate was kept in the plate reader. Within one measurement the duplicates were almost the same and stayed stable until 90 minutes after the first measurement. The FP values increased the more AS69 is added until it became a plateau around a ratio of 1:5. This showed that the stock concentration of the TAMRA-peptide is probably not correct, as already mentioned above, as a plateau should be reached already at a 1:1 molar ratio, with the assumption that every AS69 molecule can only bind one β-hairpin region in αSyn. This was adjusted in the following

experiments. On the other hand, the FP values never reach zero when there is no AS69 present; it comes only close to that value when the plate is left 60 to 90 minutes in the reader.

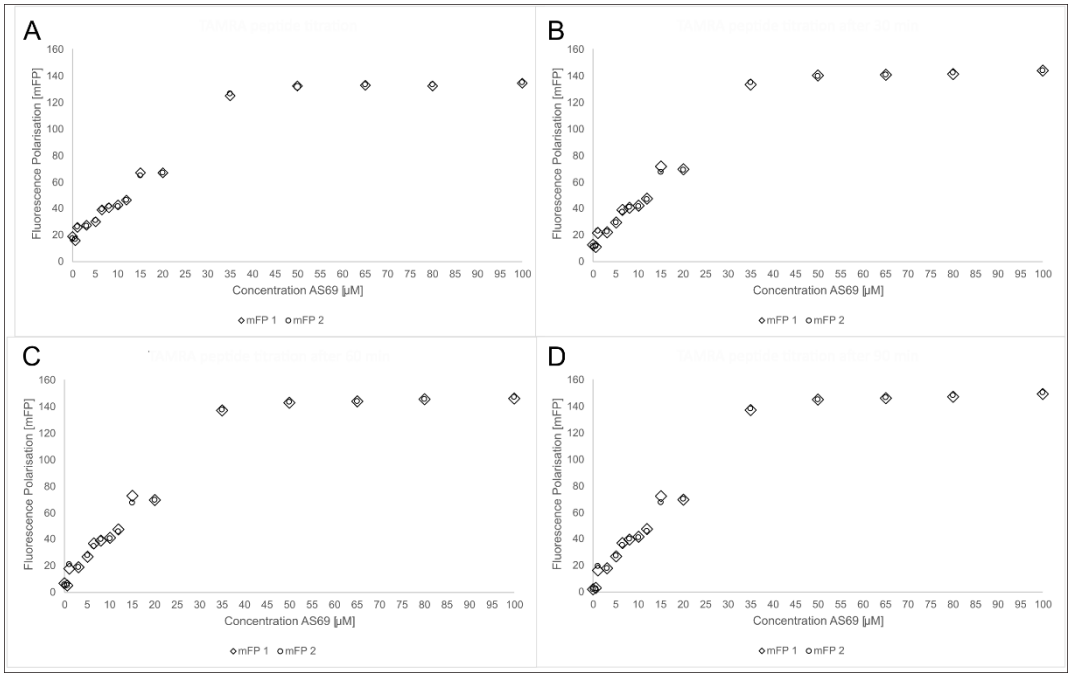

Figure 9: FP-measurements of AS69 (varied 0-100 µM) with the TAMRA-peptide (constant 10 µM) (A) directly after pipetting, (B) 30 min after the first measurement, (C) 60 min after the first measurement and (D) 90 min after the first measurement, showing that the measurement is stable even over a more extended time period.

In the next experiment, a competitor for the TAMRA-peptide was added, αSyn CC, also a β-hairpin fragment of αSyn where two residues were exchanged for cysteines to stabilize the hairpin by itself (Figure 8). AS69 can still bind to this aSyn CC version the same way as the TAMRA-peptide (αSyn CC: H-KEGVLYV**C**SKTKEG**C**VHGVATVAE-OH). Here the settings of the reader, as well as the volume per well and the concentration of TAMRA-peptide, and AS69 were kept the same as the former experiments. Since the plateau was reached in a 1:5 ratio to the TAMRA-peptide (50 µM AS69), the αSyn CC was added in concentrations from 0-100 µM. The plate was this time left in the reader at 37 °C, so that it already is, at least roughly, at the correct temperature. Every sample was pipetted as a duplicate and measured directly after pipetting with 3 cycles and then every 30 minutes for 2.5 hours for 3 cycles each. The resulting mFP values from each measurement were averaged and then displayed, as seen in figure 9. Again, the measurement remained stable, and the mFP values were in the same

range for all time points. One outlier at 15 µM aSyn CC was observed over all the measurements. Unlike the previous measurements, this time, the mFP values started with high values (for example, about ~57 mFP), and the more aSyn CC was added, the lower the value became until they reached the minimum at 80 µM aSyn CC (~8 mFP) and increased slightly at 100 µM aSyn CC.

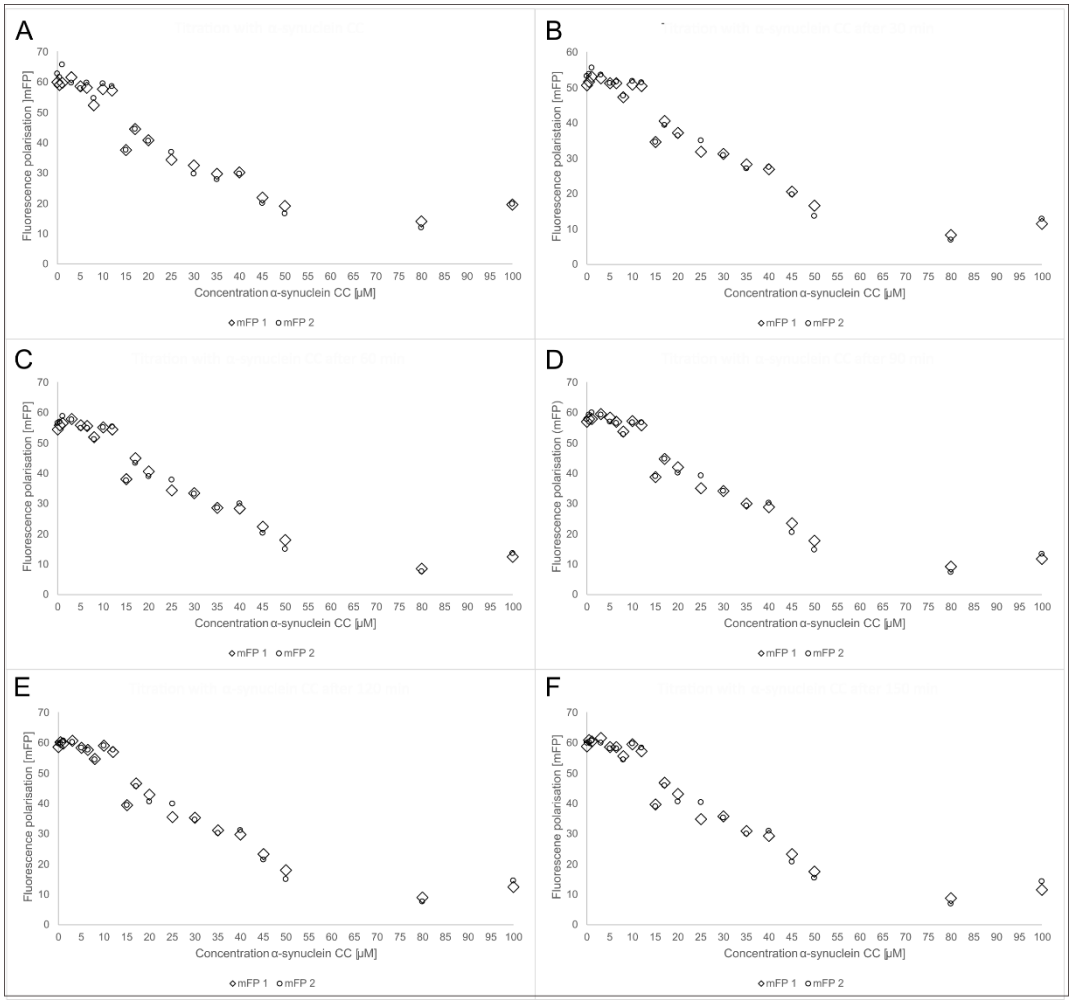

Figure 10: FP-measurements of AS69 (constant 50 µM) and TAMRA peptide (constant 10 µM) and aSyn CC (varied 0-100 µM) as a competitor for the binding with AS69. (A) Directly after pipetting, (B) 30 min after the first measurement, (C) 60 min, (D) 90 min, (E) 120 min, and (F) 150 min after the first measurement. From the first to last measurement, there is barely any change, indicating the reaction is fast and stable afterward, and αSyn CC can out-compete the TAMRA-peptide in the coupled-folded binding with AS69.

Since the FP assay worked nicely with the αSyn CC as a competitor for the TAMRA-peptide for the AS69, the subsequent trial was with αSyn full-length WT (Figure 9).

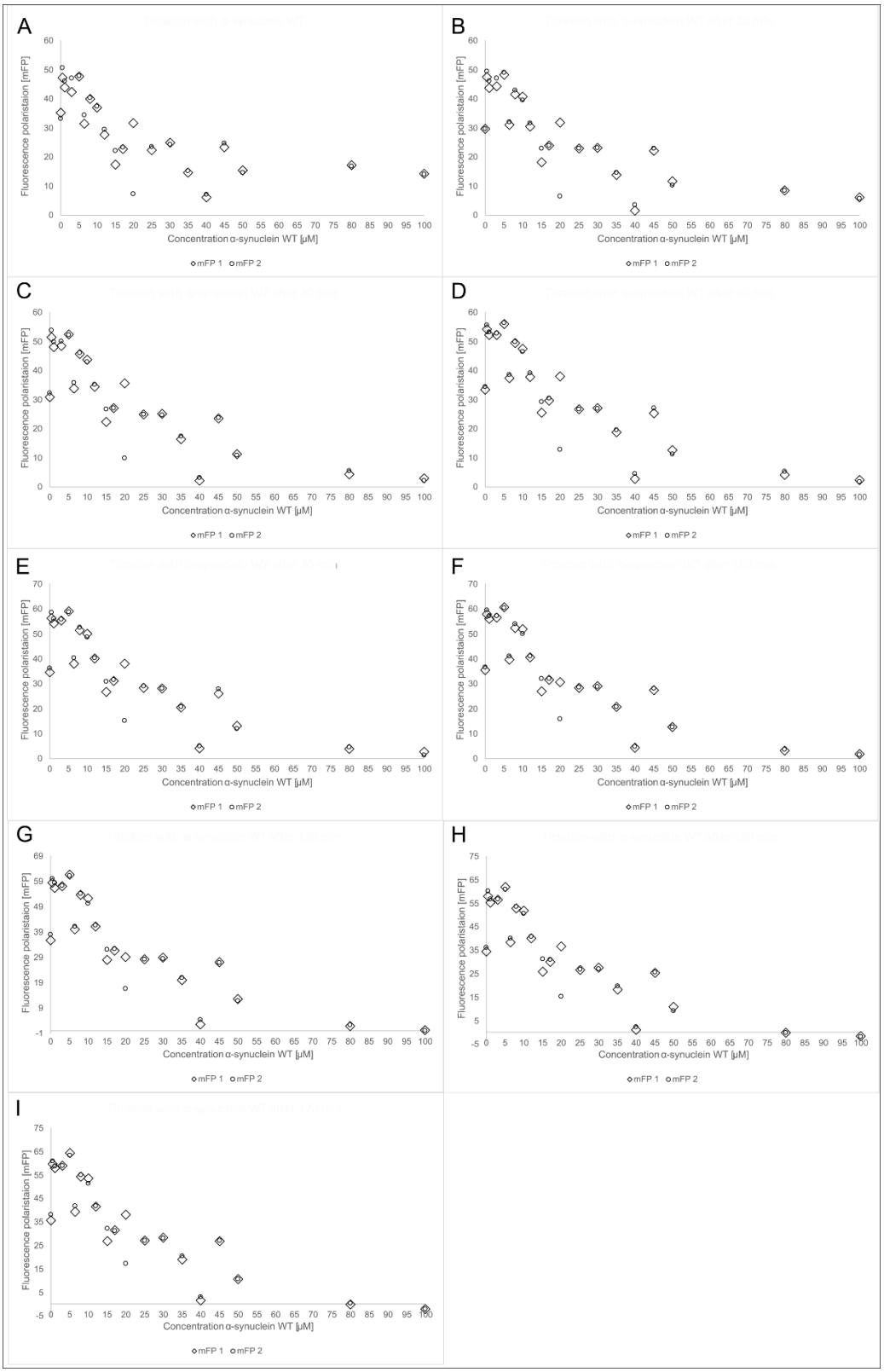

Figure 11: FP-measurements of AS69 and the TAMRA-peptide (both at fixed concentrations) with αSyn WT full-length as a competitor for the binding with AS69. (A) Directly after pipetting, (B) 20 min, (C) 40 min, (D) 60 min, (E) 80 min, (F) 100 min, (G) 120 min, (H) 150 min and (I) 170 min after the first measurement.

It was setup the same way as the αSyn CC experiment, though it was measured every 20 min for in total of 170 min after the first, freshly pipetted measurement. In this experiment the measured values, especially in the first measurements, were more scattered. Some of the duplicates showed significantly different values. Overall, the FP values decreased with higher αSyn WT concentrations, a trend that did not change with incubation time. The data showed that this type of is suited to identify compounds that compete for a component of the TAMRA-peptide:AS69 complex.

3.5 Discussion

The buildup of αSyn fibrils in the brain and subsequent death of dopaminergic neurons is a hallmark of Parkinson's disease. [45] The engineered β-wrapin AS69 can inhibit the growth of amyloid fibrils by literally wrapping around a specific sequence stretch in αSyn, which folds into a β-hairpin and can no longer aggregate or be added to a growing fibril. [22, 23] The original β-wrapin AS69 has a K_d value of 240 nM. [22, 23] The goal was to optimize this value by optimizing the enthalpy or entropy of binding. As already mentioned, this work was done by MD simulations by Dr. Phanourios Tamamis.

To further optimize β-wrapin AS69 two strategies in MD simulations were used. One strategy was to improve the binding enthalpy the other to improve the binding entropy. To improve the binding enthalpy the β-wrapin was made more rigid with mutations that allow for more salt bridges and hydrogen bonds between the two subunits of the AS69 dimer. The different mutations had different goals on their own before being combined. First there is the AS69 2x mutant, here the goal was to improve the binding enthalpy. The prognosis of the MD simulations was in this case correct the binding enthalpy is improved and the complex is more stable. The affinity on the other hand barely got improved compared to the AS69 WT. This can be explained by the fact that the binding entropy lessens, and this leads to an enthalpy-entropy-compensation meaning that there a more enthalpic interaction which hinders the flexibility of the complex. [32, 33, 34] In the second strategy the binding entropy should be improved, this was simulated in the AS69 3x and 4x mutants. Again, the prognosis of the MD simulations held true in the experiments the binding entropy was improved but the affinity got much worse compared to AS69 WT. On the other hand, the affinity got worse which can be explained by the binding enthalpy decreases. Like in the case of improving the binding enthalpy this is the result of the enthalpy-entropy-compensation, with the used mutations AS69 becomes too rigid which in turn leads to less flexibility even if the enthalpic interactions are optimally used. [32, 33, 34] In the cases of AS69 5x and 6x those two mutants are combinations of, in case of the 5x mutant the AS69 2x combined with AS69 3x and in the case of the 6x mutant AS69 2x combined with AS69 4x. This combines both approaches improved binding enthalpy and improved binding entropy. This combination is mirrored in the experimental results of both mutants. The binding enthalpy, binding entropy and affinity of AS69 5x and 6x is exactly in between those of AS69 2x and AS69 3x and AS69 2x and AS69 4x respectively. This leads to

the conclusion that the design of the AS69 optimization worked as intended but because of the enthalpy-entropy-compensation no binder with a higher affinity could be gained. [32, 33, 34]

The FP assay is supposed to be part of a future HTS assay to screen small molecules inhibitors against αSyn. [35, 36] To do so, the part of αSyn that can form the β-hairpin was used coupled with the red fluorescent rhodamine dye TAMRA. Together with the peptide the β-wrapin AS69 is in the assay to later be the competition to the small molecule. Eventually, it is supposed to be the first step in the HTS to distinguish reliably the actual positive and false positive signals with the help of a competition assay. If the peptide is alone in solution, it rotates quickly and freely; thus, the polarization values are low. On the contrary, when AS69 is also included in the solution, the β-wrapin binds the αSyn peptide, slowing down the dye rotation in complex with AS69, which consequently leads to higher polarization values. In competition with a small molecule compound, low polarization values in the assay are supposed to show that the peptide is not bound to AS69 but by a small molecule compound that blocks the binding of AS69 would be yielding an actual positive FP signal. Since the small molecule is supposed to be even smaller than the peptide, it should not influence the polarization resulting in the previously mentioned low polarization results. It is essential to mention that a small molecule capable of binding to AS69 could also lead to lower FP signals by release of the TAMRA-peptide from its AS69-complex, which would then be considered a false positive signal. In principle, high polarization values indicate the peptide binding to AS69. After optimizing the volume in the wells to a minimum as well as the concentrations of the TAMRA-peptide and AS69, the first experiments were performed. As predicted by AS69 titration, the more AS69 was added the more FP values increased the FP values increased until the signal reached a plateau at the 1:5 molar ratio (TAMRA-peptide:AS69) indicating that all TAMRA-labelled peptide molecules were bound to AS69. In a second experiment a competitor, αSyn CC, was added to the TAMRA-peptide. This construct should compete with the TAMRA-peptide for the AS69 binding site, especially considering in the fact that αSyn CC the β-hairpin is already pre-formed. The TAMRA-peptide and AS69 ratio in the solutions was 1:5, in order to have all TAMRA-peptide molecules bound to AS69 as mentioned above. This approach was used as no competitor for AS69 was available, and it would show if AS69 prefers a more fixed β-hairpin conformation to a more flexible one. While the FP values went down when the αSyn CC concentration was higher it cannot be used as a measure that AS69 prefers αSyn CC. But it seems that at 50 μM αSyn CC and 50 μM AS69 (Figure 10) the αSyn CC freed most AS69 binding pockets from the TAMRA-peptide, causing it to be free and thus rotate freely once again. Thereby, it could be said that this is an

equilibrium, the AS69:TAMRA-peptide complex is in equilibrium with the monomeric components, when αSyn CC is added there are more AS69: αSyn CC complexes formed. This data shows very nicely the principle of this competition assay. A similar experiment was performed using full-length αSyn instead of αSyn CC. The idea was the same as for the αSyn CC experiment. Here, the mFP values were showing a consistent trend but the scattering was much higher than in the previous experiments. At the highest concentration of full-length αSyn, the mFP value was low which could indicate that AS69 is more bound to the full-length aSyn than to the TAMRA-peptide. If AS69 prefers to bind to the full-length αSyn rather than the peptide cannot be assessed through this experiment and added the data with the full-length protein is less consistent as with the αSyn CC construct. Here, it is also noteworthy that, in contrast to the other measurements, the values do not remain approximately the same after 30 min or 180 min and continue to decrease in every measurement until they are firmly in the negative range. This is data that was not used for further analysis. An explanation could be that the full-length αSyn somehow interferes with the measurement. The assay system works but further work is needed to reduce the scattering when it occurs as it happened with full-length αSyn.

In conclusion, although only one of the MD-simulated AS69 mutants showed minor improvement in affinity compared to the original, the basis concepts of the computational design, improvement of binding enthalpy or binding entropy, could be confirmed in the *in vitro* experiments. The FP assay for an HTS assay also shows great promise to be at least a first step in such an HTS assay to filter out the small molecules that are not suitable at all. However, it can still give false positives in the form that AS69 can also be blocked; at least one step should be added after the FP assay to ensure that only actual positives are chosen for further experiments. It gives the possibility of an easy-to-use assay that can be scaled up from a 384-well format to a 1536-well format. It does not need high sample volumes or concentrations per well, and it is an easy to read the output in this HTS assay.

3.6 References

1. Nygren, P. Å. Alternative binding proteins: Affibody binding proteins developed from a small three-helix bundle scaffold. *FEBS Journal* vol. 275 2668–2676 (2008).
2. Jonsson, A., Dogan, J., Herne, N., Abrahmsén, L. & Nygren, P. Å. Engineering of a femtomolar affinity binding protein to human serum albumin. *Protein Eng. Des. Sel.* **21**, 515–527 (2008).
3. Grönwall, C. & Ståhl, S. Engineered affinity proteins-Generation and applications. *Journal of Biotechnology* vol. 140 254–269 (2009).
4. Löfblom, J. *et al.* Affibody molecules: Engineered proteins for therapeutic, diagnostic and biotechnological applications. *FEBS Lett.* **584**, 2670–2680 (2010).
5. Feldwisch, J. *et al.* Design of an Optimized Scaffold for Affibody Molecules. *J. Mol. Biol.* **398**, 232–247 (2010).
6. Lindborg, M. *et al.* High-affinity binding to staphylococcal protein A by an engineered dimeric Affibody molecule. *Protein Eng. Des. Sel.* **26**, 635–644 (2013).
7. Sexton, K. *et al.* Fluorescent Affibody Peptide Penetration in Glioma Margin Is Superior to Full Antibody. *PLoS One* **8**, (2013).
8. De Genst, E. & Muyldermans, S. Development of a high affinity Affibody-derived protein against amyloid β-peptide for future Alzheimer's disease therapy. *Biotechnology Journal* vol. 10 1668–1669 (2015).
9. Vazquez-Lombardi, R. *et al.* Challenges and opportunities for non-antibody scaffold drugs. *Drug Discovery Today* vol. 20 1271–1283 (2015).
10. Frejd, F. Y. & Kim, K. T. Affibody molecules as engineered protein drugs. *Experimental and Molecular Medicine* vol. 49 306 (2017
11. Ståhl, S. *et al.* Affibody Molecules in Biotechnological and Medical Applications. *Trends in Biotechnology* vol. 35 691–712 (2017).
12. Simeon, R. & Chen, Z. In vitro-engineered non-antibody protein therapeutics. *Protein Cell* **9**, 3 (2018).
13. Tolmachev, V. & Orlova, A. Affibody molecules as targeting vectors for PET imaging. *Cancers* vol. 12 (2020).
14. Meister, S. W. *et al.* An affibody molecule is actively transported into the cerebrospinal fluid via binding to the transferrin receptor. *Int. J. Mol. Sci.* **21**, (2020).

15. Barozzi, A., Ashton Lavoie, R., Day, K. N., Prodromou, R. & Menegatti, S. Affibody-binding ligands. *Int. J. Mol. Sci.* **21**, (2020).
16. Altunay, B. *et al.* HER2-directed antibodies, affibodies and nanobodies as drug-delivery vehicles in breast cancer with a specific focus on radioimmunotherapy and radioimmunoimaging. *Eur. J. Nucl. Med. Mol. Imaging* **48**, 1371 (2021).
17. Morito, T. *et al.* Synthesis and pharmacokinetic characterisation of a fluorine-18 labelled brain shuttle peptide fusion dimeric affibody. *Sci. Rep.* **11**, 2588 (2021).
18. Hoyer, W., Gronwall, C., Jonsson, A., Stahl, S. & Hard, T. Stabilization of a -hairpin in monomeric Alzheimer's amyloid- peptide inhibits amyloid formation. *Proc. Natl. Acad. Sci.* **105**, 5099–5104 (2008).
19. Hoyer, W. & Härd, T. Interaction of Alzheimer's Aβ Peptide with an Engineered Binding Protein-Thermodynamics and Kinetics of Coupled Folding-Binding. *J. Mol. Biol.* **378**, 398–411 (2008).
20. Luheshi, L. M. *et al.* Sequestration of the Aβ peptide prevents toxicity and promotes degradation in vivo. *PLoS Biol.* **8**, (2010).
21. Malm, M. *et al.* Inhibiting HER3-Mediated Tumor Cell Growth with Affibody Molecules Engineered to Low Picomolar Affinity by Position-Directed Error-Prone PCR-Like Diversification. *PLoS One* **8**, (2013).
22. Gauhar, A., Shaykhalishahi, H., Gremer, L., Mirecka, E. A. & Hoyer, W. Impact of subunit linkages in an engineered homodimeric binding protein to -synuclein. *Protein Eng. Des. Sel.* **27**, 473–479 (2014).
23. Mirecka, E. A. *et al.* Sequestration of a β-hairpin for control of α-synuclein aggregation. *Angew. Chemie - Int. Ed.* **53**, 4227–4230 (2014).
24. Shaykhalishahi, H. *et al.* A b-hairpin-binding protein for three different disease-related amyloidogenic proteins. *ChemBioChem* **16**, 411–414 (2015).
25. Orr, A. A., Wördehoff, M. M., Hoyer, W. & Tamamis, P. Uncovering the Binding and Specificity of β-Wrapins for Amyloid-β and α-Synuclein. *J. Phys. Chem. B* **120**, 12781–12794 (2016).
26. Orr, A. A. *et al.* Elucidating the multi-targeted anti-amyloid activity and enhanced islet amyloid polypeptide binding of β-wrapins. *Comput. Chem. Eng.* **116**, 322–332 (2018).
27. Agerschou, E. D. *et al.* An engineered monomer binding-protein for α-synuclein efficiently inhibits the proliferation of amyloid fibrils. *Elife* **8**, (2019).

28. Szegő, É. M. *et al.* A β-Wrapin Targeting the N-Terminus of α-Synuclein Monomers Reduces Fibril-Induced Aggregation in Neurons. *Front. Neurosci.* **15**, (2021).
29. Bisi, N. *et al.* α-Synuclein: An All-Inclusive Trip Around its Structure, Influencing Factors and Applied Techniques. *Front. Chem.* **9**, (2021).
30. Hospital, A., Goñi, J. R., Orozco, M. & Gelpí, J. L. Molecular dynamics simulations: advances and applications. *Adv. Appl. Bioinforma. Chem.* **8**, 37–47 (2015).
31. Archer, W. R. & Schulz, M. D. Isothermal titration calorimetry: practical approaches and current applications in soft matter. *Soft Matter* **16**, 8760–8774 (2020).
32. Breiten, B. *et al.* Water Networks Contribute to Enthalpy/Entropy Compensation in Protein−Ligand Binding. doi:10.1021/ja4075776.
33. Chodera, J. D. & Mobley, D. L. Entropy-enthalpy compensation: role and ramifications in biomolecular ligand recognition and design. *Annu. Rev. Biophys.* **42**, 121–142 (2013).
34. Fox, J. M., Zhao, M., Fink, M. J., Kang, K. & Whitesides, G. M. The Molecular Origin of Enthalpy/Entropy Compensation in Biomolecular Recognition. (2018) doi:10.1146/annurev-biophys.
35. Hall, M. D. *et al.* Fluorescence polarization assays in high-throughput screening and drug discovery: a review. *Methods Appl. Fluoresc.* **4**, 022001 (2016).
36. Vinegoni, C., Feruglio, P. F., Gryczynski, I., Mazitschek, R. & Weissleder, R. Fluorescence anisotropy imaging in drug discovery. *Adv. Drug Deliv. Rev.* **151**–**152**, 262 (2019).
37. Benhar, I. Biotechnological applications of phage and cell display. *Biotechnol. Adv.* **19**, 1–33 (2001).
38. Rami, A., Behdani, M., Yardehnavi, N., Habibi-Anbouhi, M. & Kazemi-Lomedasht, F. An overview on application of phage display technique in immunological studies. *Asian Pac. J. Trop. Biomed.* **7**, 599–602 (2017).
39. Ledsgaard, L., Kilstrup, M., Karatt-Vellatt, A., McCafferty, J. & Laustsen, A. H. Basics of Antibody Phage Display Technology. *Toxins (Basel).* **10**, (2018).
40. Chiu, M. L., Goulet, D. R., Teplyakov, A. & Gilliland, G. L. Antibody Structure and Function: The Basis for Engineering Therapeutics. *Antibodies 2019, Vol. 8, Page 55* **8**, 55 (2019).
41. Berg, J. M., Tymoczko, J. L. & Stryer, L. Stryer Biochemie. *Stryer Biochem.* (2013). doi:10.1007/978-3-8274-2989-6

42. Conway, K. A., Harper, J. D. & Lansbury, P. T. Accelerated in vitro fibril formation by a mutant α-synuclein linked to early-onset Parkinson disease. *Nat. Med.* **4**, 1318–1320 (1998).
43. Narhi, L. *et al.* Both familial Parkinson's disease mutations accelerate α-synuclein aggregation. *J. Biol. Chem.* **274**, 9843–9846 (1999).
44. Conway, K. A., Harper, J. D. & Lansbury, P. T. Fibrils formed in vitro from α-synuclein and two mutant forms linked to Parkinson's disease are typical amyloid. *Biochemistry* **39**, 2552–2563 (2000).
45. Goedert, M. Alpha-synuclein and neurodegenerative diseases. *Nat. Rev. Neurosci.* **2**, 492–501 (2001).

3.7 List of Figures

3.8 List of Tables

3.9 List of Abbreviations

°C	Degrees celsius
AD	Alzheimer's disease
$A\beta_{1-40}$	Amyloid beta 1-40
BBB	Blood-brain barrier
F_{ab}	Fragment antigen binding
F_C	Fragment crystallizable region
FP	Fluorescence polarisation
h	hour
HC	Heavy chain
HER2	Human epidermal growth factor receptor 2
HPLC system	High performance liquid chromatography
HTS	High throughput screening assay
IAPP	Islet amyloid polypeptide
IgG-type antibody	Immunoglobulin G antibody
ITC	Isothermal titration calorimetry
K	Kelvin
K_a	Association constant
K_D	Disassociation constant
kJ	kilo Joule
LC	Light chain
M	Molar
MD simulations	Molecular dynamics simulatioms
min	Minutes
mP	Millipolarization
NAC region	Non-amyloid-β-component
nm	Nano meter
nM	Nano molar
PD	Parkinson's disease
R	Gas constant
s	seconds
SEC	Size exclusion chromatography
T	Temperature
TAMRA	5-carboxytetramethylrodamin
ThT	Thioflavin T

TIID	Type II diabetes
ΔG	Free energy
ΔH	Enthalpy
ΔS	Entropy
αSyn CC	α-synuclein CC
αSyn	α-synuclein
µl	Mikro litre
µM	Mikro molar

Project 4: *Expression, purification, and aggregation of full length amyloidogenic variable light chains LEN and SMA*

Content

4 4.1 Introduction

Diseases involving amyloid deposits are mostly known from neurodegenerative diseases like Alzheimer's and Parkinson's disease, which could also be called brain-localized amyloidoses. There exist, of course, also amyloidoses where the brain is not affected but the rest of the body, either one specific organ in localized amyloidoses, or multiple ones in systemic amyloidoses. [19, 25, 29, 45] Systemic amyloidoses are not as common as the neurodegenerative ones; the most common type of the systemic amyloidoses is called light-chain amyloidosis. [8, 15, 25] The common feature of all amyloidoses is the deposition of proteins in the form of β-sheets stacked together in a way that forms fibrils. [18, 19] Those fibrils can be observed and quantified with different methods, the most common for tissues from patients being staining with the dye Congo red followed by imaging of the tissue under polarized light to detect apple-green birefringence. [8, 39] The most common way to observe amyloid and amyloid formation *in vitro* is the addition of the dye Thioflavin T and to track its fluorescence intensity during the formation of amyloid fibers.

Systemic amyloidoses are described as diseases where the protein that later causes the disease is produced at a different localization than where the deposition of fibrils later occurs. [32] As already mentioned above systemic amyloidoses are rare diseases and of these the light-chain (AL) amyloidosis is the most common one. [8, 25] In AL-amyloidosis the protein responsible for the disease and thus the one which forms the fibrils are the light chains of Ig antibodies. [19, 25, 32] The light chain or even only fragments of the light chain are, in short, produced in abundance and later released into the blood to deposit in most cases predominantly in the kidney and heart. [5, 8, 44] Still, every organ can be involved apart from the brain. In some cases, AL-amyloidosis occurs in combination with multiple myeloma. [8] In both cases, the plasma cells of the bone marrow are the problematic species. [19, 32, 43, 44] The first hints of AL-amyloidosis were described, even if the disease was not yet described as such, by Dr. Henry Bence Jones in 1845. [4] He received a urine sample with peculiar attributes. [4] The sample had an unusually high weight and viscosity, which could be boiled and with this turned opaque, and when nitric acid was added it apparently turned clear but returned to its former state when cooled again. [4] These boiling and cooling steps could apparently be repeated more than once with the same results. [4] These proteins found in the urine of certain patients were then named

‘Bence Jones proteins’ and became an indicator, among other things, for what is today known as multiple myeloma. [4, 5] It took another 100 years for these proteins to be identified as light chains form a human immunoglobulin. [4] AL-amyloidosis, along with being the most common of the systemic amyloidoses was also one of the first diseases described involving amyloids. [4, 32]

As already said, the starting point of AL-amyloidosis is within the plasma cells in the bone marrow. [19, 34, 43] Under normal conditions, these plasma cells are B cells or B lymphocytes that are fully differentiated, which manage the synthesis and, later, the secretion of immunoglobulins into the body. [19, 34, 43] In the case of AL-amyloidosis, one of these plasma cells starts to proliferate at an abnormal rate and thus produces an excess of, in almost all cases, monoclonal light chains and not the full antibody. [7, 19, 34, 43] An important note here is, that the secreted light chain is unique and only this one light chain will be produced by the abnormal plasma cell and all its clones. [25, 43] This means each patient with AL-amyloidosis has one unique light chain that they produce, meaning the light chain sequence of each patient is unique and thus makes therapeutic approaches complicated. [25, 43] In general, the diagnosis of AL-amyloidosis is not straightforward, as the symptoms are vague and not clearly defined. [25] An abundance of light chains in the urine can, for example, be a hint but there are also cases where there are light chains in the urine, but the patient is not suffering from AL-amyloidosis. [25] As urine can be a hint, a bone marrow biopsy is the surest way to diagnose the disease or at least to differentiate between AL-amyloidosis and multiple myeloma. [25] Often by the time there is organ dysfunction it is already too late for proper treatment. [25] AL-amyloidosis can affect every organ and tissue in the body apart from the brain; most affected are often the kidneys and the heart, with decreasing renal function in the kidneys and progressive heart failure as the ventricular walls of the heart thicken to a point where the heart can no longer pump the necessary volume of blood. [25] Also, there were cases described for the liver, the autonomic and peripheral nervous system, and soft tissue like the skin that can be affected by AL-amyloidosis. [25,34, 43]

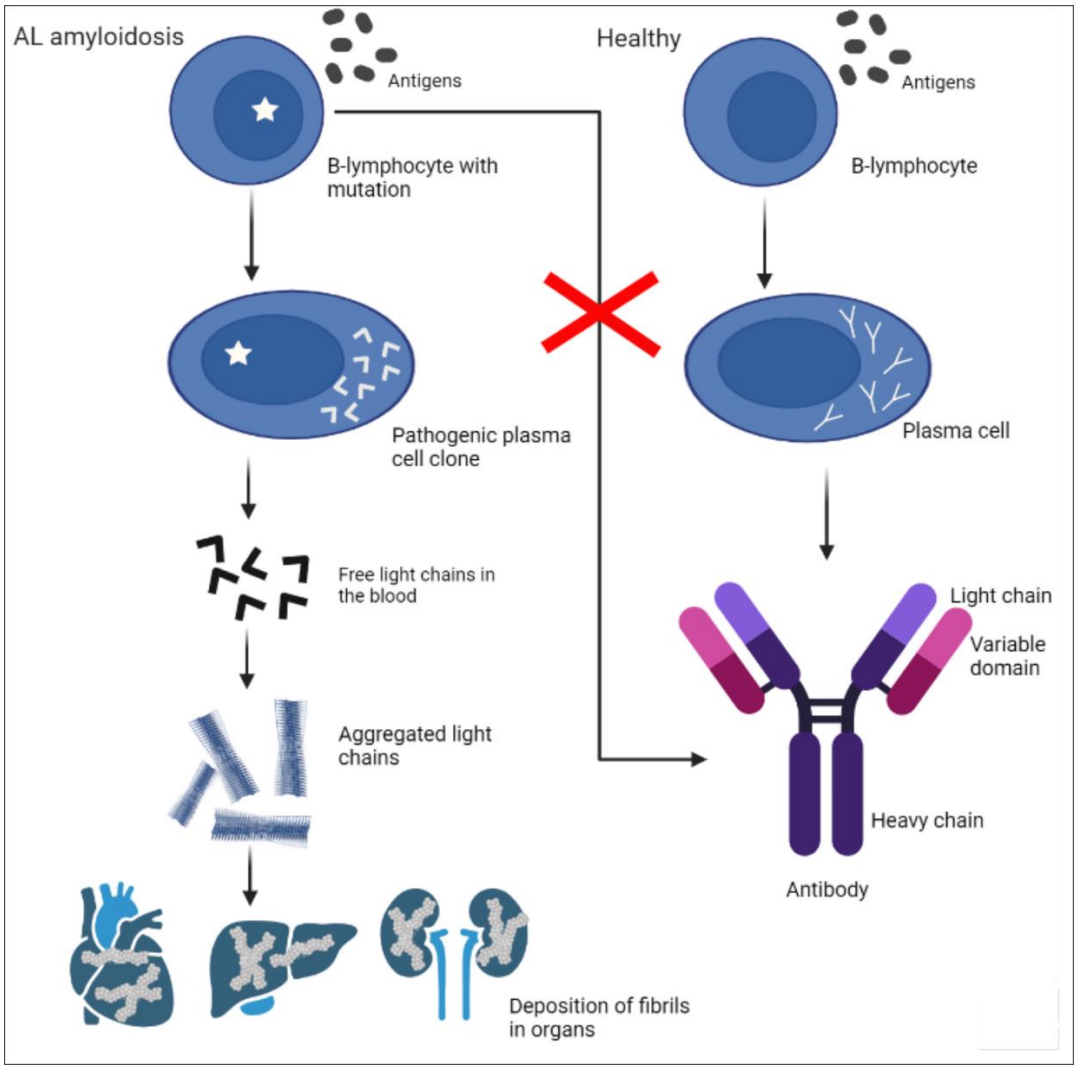

Figure 1: Schematic of the AL-amyloidosis B-cell pathway compared to a healthy B-cell, created with BioRender.com

As the diagnosis and, more importantly, the treatment of AL-amyloidosis is not straightforward, as each patient has a unique sequence of light chains involved in the disease, models for studying the light chains were developed. In general, the light chain is only a subunit of an antibody. An antibody consists of two heavy chains and two light chains. The light chain can be subdivided into a constant and variable region, where the constant region determines which type the light chain is. There are two types of light chains present in humans, the κ and λ light chains. [17, 45] The κ light chains are encoded on chromosome two by the immunoglobulin κ locus; the λ light chains, in turn, are encoded on chromosome 22 by the immunoglobulin λ locus. The genes encoding for both types of light chains are numerous. [43, 45] To form a light chain, a combination of three different gene segments is necessary; the variable gene of which

the humans have 73 in total (40 for the κ type, 33 for the λ type), a junction gene (five for the κ type, four for λ) and a constant gene with only one for the κ and five for the λ type. [43, 45] These three different genes can be combined in all ways as long there is one of each present in the final construct. [43, 45] In these combinations, mutations are typically occurring on a regular basis to be able to keep the immune system in working order. [43, 45] All this explains the large variety of different light chains that make it possible for each AL-amyloidosis patient to have its own unique sequence of light chain. If one were to look at the structure of the light chains it would be visible, that both the variable and constant regions are similar. [28] Both domains contain β-strands that form β-sheets which pack together in the form of a Greek key barrel, secured by a disulfide bond. [28] To come back to the above-mentioned models which were also used in this work. The model proteins used here are called LEN and SMA. [10, 44] Both comprise only the variable region of the light chain and are homologous apart from eight mutations in SMA. [10, 14] Both proteins are 144-residues long and belong to the κIV IgG family. [10] LEN was originally isolated from the urine of a patient who had ~50 g/day of Bence Jones protein present in his urine. [10, 12] The patient was suffering from multiple myeloma but showed no signs of amyloid aggregation or deposition. [10, 12] SMA was also isolated from a patient who was diagnosed with AL-amyloidosis and the protein was extracted post-mortem from a lymph node in the form of amyloid fibrils. [10, 14, 28] This allows for a comparison between an apparently benign variable light chain fragment (LEN) and an amyloidogenic one (SMA). [10, 12, 28, 44]

The first step in this work was to establish a way to express LEN and SMA in bacterial culture. Since the sequence of both is known the cloning and later transformation into bacterial cells was straightforward and already done in this case by Dr. Michael Wördehoff. To ensure that the light chains can be purified in their native fold or as closely as possible the so-called pelB leader sequence was added to the N-terminal ends of both variable light chains. [11, 33, 38] This leader sequence is responsible for proteins being shuttled to and into the periplasmic space of gram-negative *Escherichia coli* cells. [11, 30] The leader sequence gets cleaved off as soon as the proteins enter the periplasmic space of the bacterium. [11, 30, 44] The periplasmic space or periplasm can be found in gram-negative bacteria in between the inner cytosolic membrane and the outer bacterial membrane and has multiple positive aspects. [11, 30, 44] Proteins that get transported there with the help of leader sequences have the advantage, that those leader sequences (pelB, ompA) get cleaved off fully and automatically as soon as the protein reaches the periplasm. [11, 30, 44] Another benefit from this space is that proteins that are or could

potentially be cytotoxic can be expressed there without killing the whole cell. [11, 16, 35, 44] Most important for this work was, on one hand, the aspect that the periplasm contains an oxidizing space, meaning that disulfide bonds can be formed, and on the other hand, it contains two foldases to help the process of disulfide bridge formation (disulfide oxidoreductase DsbA, disulfide isomerase DsbC). [11, 16, 35] With this, if the protein extraction of the periplasm is successful, the refolding of proteins after the purification should not be necessary. [11, 16, 44]

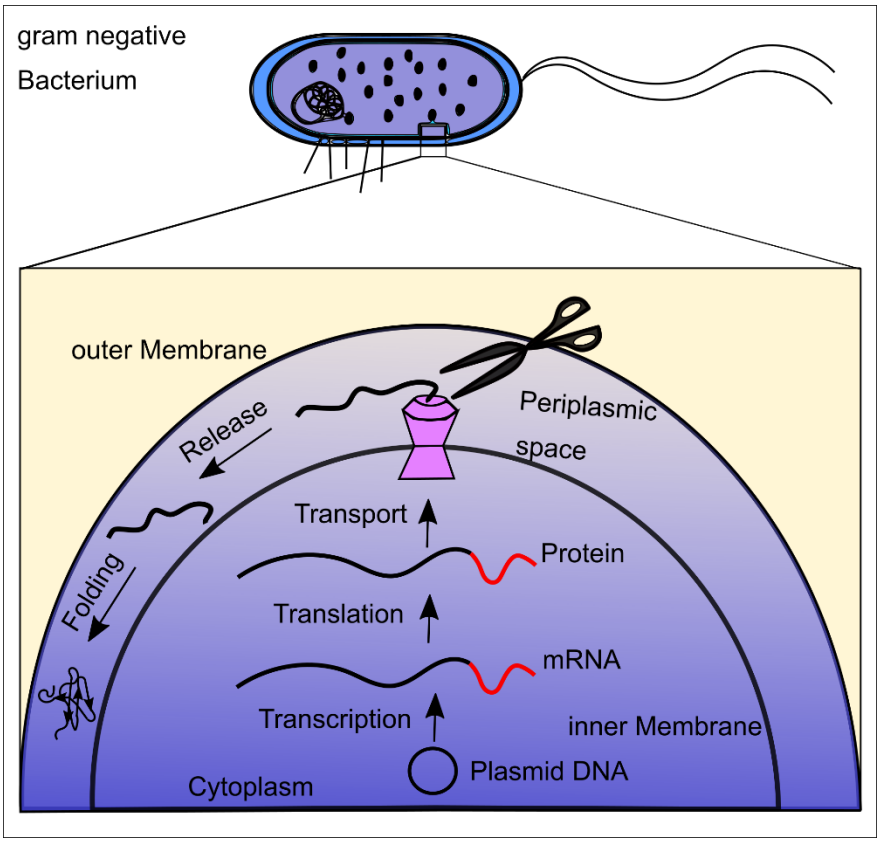

Figure 2: Schematic of a gram-negative bacterium and the pathway of a protein with the pelB leader sequence (red) attached from plasmid DNA to folded protein in the periplasmic space.

Other important aspects are the reduced proteolysis in this space; fewer other proteins and impurities are to be expected during purification; and that, as already been hinted above with the nonnecessity of refolding after purification, denaturing conditions during the extraction and purification are not necessary. [11, 30, 44] One has to be careful with the lysis of the cell for the purification, as ideally only the outer bacterial membrane should be broken, so that only the periplasmic proteins are released; different methods are available to achieve this. The fastest

method to release periplasmic proteins without destroying the whole cell is periplasmic extraction with chloroform. Here the cells are treated with chloroform and incubated with it for a short while before the buffer is added. [2] The resulting mixture is centrifuged carefully so as not to destroy the full cells and thus keep contamination with cell fragments to a minimum. [2] The supernatant, after the centrifugation, contains the proteins from the periplasm. [2] This is a rapid and easy method for the release of periplasmic proteins. [2] Another method is the usage of freeze and thaw cycles to extract the periplasmic proteins. [16] Here the harvested cells are resuspended in a buffer and subjected to cycles of freezing in liquid nitrogen followed by thawing. [16] Also, in this method, the periplasmic proteins are released into the supernatant. A third method is the usage of Lysozyme and Ethylenediaminetetraacetic acid (EDTA); as before the goal is to release only the periplasmic proteins into the supernatant. [44] In this method the Lysozyme is allowed to enter the periplasmic space to destroy the cell wall, EDTA is used to additionally weaken the outer bacterial membrane. [44] Important to note here is that also the Lysozyme stays in the supernatant and can lead to problems if the proteins to purify are close in size and attributes. [44] The maybe most classical method to release the periplasmic proteins is the osmotic or cold osmotic shock protocol. [2, 11, 44] Here the harvested cells are kept in a hypertonic solution, which with time and with increasing the concentration of the hypertonic solution, weakens the outer bacterial membrane. [2, 11, 44] After centrifuging the cells and removing the hypertonic solution, the cells are then rapidly resuspended in a hypotonic or cold hypotonic solution to break the weakened outer bacterial membrane. [2, 11, 44] These four methods were tested for this work. The purification of the released periplasmic proteins can be done with the widely known methods of ion exchange chromatography and size exclusion chromatography.

With expression and purification of LEN and SMA established the main interest was if an engineered protein made to inhibit the formation of fibrils in the amyloidogenic diseases Parkinson's and Alzheimer's disease and diabetes type II can also be used here. [54] The so-called β-wrapins are engineered homodimers based on the affibody sequence. [54] There are specific β-wrapins for the three above-mentioned diseases, called AS69 for Parkinson's disease, ZAβ_3 for Alzheimer's disease, and HI18 for diabetes type II. These β-wrapins were tailored to their specific protein (α-synuclein, Aβ, and IAPP) based on the observation that in each of the disease proteins, there are sequence stretches that can potentially form β-hairpins. [54] The engineered β-wrapins are able to bind to those β-hairpin stretches, and upon binding, the β-wrapin folds and wraps around the β-hairpin thus inhibiting the aggregation of the protein they

were tailored to. [54] LEN and SMA both also have a potential β-hairpin region and there exists a β-wrapin called AS10 that can bind α-synuclein, Aβ and IAPP and other β-hairpins that fulfill certain properties (see part 1 of this thesis). [54] It was shown via solution NMR that the fragments containing the potential β-hairpin region of LEN and SMA could be bound by AS10. It was also shown that for LEN and SMA to aggregate, their structure has to be slightly disturbed by denaturants like guanidinium hydrochloride which was used here. The β-wrapins were engineered to be highly stable. [54] It was not known at this point how much denaturant could be used before AS10 loses its structure and is no longer able to bind the β-hairpin region. This is to be done via Thioflavin-T assays. Thioflavin T (ThT) is a dye that is able to bind the β-structure that is typical for amyloid fibrils, since the fibrils of amyloidogenic diseases tend to have the same basic structure only with differences in morphology. [52, 53] The ThT signal changes in the bound stage, while free ThT has an excitation wavelength of 385 nm and emission of 445 nm, while bound ThT has a different excitation at 450 nm and emission at 482 nm. [52, 53]

4.2 Objective

The objective of this work was to establish a stable expression and purification protocol of the variable light chains LEN and SMA with a reasonably high yield. After the establishment of the protocol the next objective was to find the conditions in which both proteins aggregate reproducible enough to be sure that the possible influence of AS10 is visible. In accordance with this it was necessary to find out until which point the β-wrapin AS10 is able to withstand the presence of guanidinium hydrochloride. Which then brings it to the most important objective of the work, to test if AS10 is able to inhibit the aggregation of LEN and SMA.

4.3 Material and Methods

4.3.1 Material

Chemicals

Chemicals	Supplier
2YT (Yeast extract tryptone)	PanReac AppliChem, ITW Reagent
Lysogeny broth (LB)	PanReac AppliChem, ITW Reagent
Terrific broth (TB)	PanReac AppliChem, ITW Reagent
Bacto agar	Dickinson and Company, BD
Ampicillin sodium salt	Roth
Potassium dihydrogen phosphate (KH_2PO_4)	Fisher chemicals
Potassium chloride (KCl)	VWR chemicals
Magnesium sulfate ($MgSO_4$)	Fluka
Disodium hydrogen phosphate (Na_2HPO_4)	Honeywell
Sodium dihydrogen phosphate (NaH_2PO_4)	Applichem, Sigma-Aldrich
Tris(hydroxymethyl)-aminomethan (Tris)	VWR Chemicals
Hydrochloric acid (HCl)	Fisher Chemical
Ethylenediaminetetraacetic acid (EDTA)	Acros Organics
Sucrose	Roth
Glucose	Fisher chemicals
Sodium acetate	Applichem, Sigma Aldrich
Sodium chloride (NaCl)	Merck
Sodium azide (NaN_3)	Sigma aldrich
Imidazole	Honeywell
Thioflavin T (ThT)	Sigma
Sodium dodecyl sulfate (SDS)	Merck
Acrylamid/Bisacrylamid (Rotiphorese Gel 30 (37:1))	Roth

Glycerol	VWR Chemicals
Comassie Brillant Blue G-250	Sigma
Methanol	Merck
Acetic acid	Merck
Tetramethylethylenediamine (TEMED)	Merck
Ammonium persulfate (APS)	Roth
10x TGS-buffer (Tris-Glycin-SDS-buffer)	BioRad
Bromophenol Blau	Merck
β-Mercaptoethanol	Roth
Isopropyl-β-D-thiogalactopyranosid (IPTG)	Roth
Guanidinium hydrochloride	Roth
cOmplete^{TM}, Mini, EDTA-free Protease Inhibitor Cocktail	Roche
PageRuler^{TM} Plus Prestained Protein Ladder 10-250 kDa	ThermoFisher
Sealing tape (Polyolefin Acrylate)	Thermo Scientific

Plasmids

pET-22b(+)

pET 302 nt/HIS

Cells

BL21 (DE3) cells, chemically competent [in house]

Genotype: B F^{-} *ompT gal dcm lon hsdS$_B$*($r_B^- m_B^-$) λ(DE3 [*lacI lacUV5-T7p07 ind1 sam7 nin5*]) [*malB*$^+$]$_{K\text{-}12}$(λ^S) pLysS[*T7p20 ori*$_{p15A}$](Cm^R)

Jm109 (DE3), chemically competent [in house]

Genotype: endA1 glnV44 thi-1 relA1 gyrA96 recA1 mcrB+ Δ(lac-proAB) e14- [F' traD36 proAB+ lacIq lacZΔM15] hsdR17(rK-mK+) and λ(DE3 [lacI lacUV5-T7p07 ind1 sam7 nin5]) [malB+]K-12(λS)

Proteins and Peptides

LEN

-DIVMTQSPDS LAVSLGERAT INCKSSQSVL YSSNSKNYLA WYQQKPGQPP KLLIYWASTR ESGVPDRFSG SGSGTDFTLT ISSLQAEDVA VYYCQQYYST PYSFGQGTKL EIKR-

SMA

-DIVMTQSPDS LAVSLGERAT INCKSSQSVL YSSNNRNYLA WYQQKLGQPP KLLIYWASTR ESGVPDRFSG SGSGTDFTLT ISSLQAEDVA VYYCHQYYSH PQTFGQGTKL ELKR-

pelB leader sequence

-MKYLLPTAAA GLLLLAAQPA MAMG-

AS10

-MHHHHHHVDN KFNKEMASAG GEIVYLPNLN PDQLCAFFHS VHDDPSQSAN LLAEAKKLND AQAPK-

Media

LB (Lysogeny broth) -Agar for 1 L

5 g/L NaCl

10 g/L Tryptone

5 g/L Yeast extract

100 μg/ml Ampicillin

15 g/L Bacto agar

2YT (Yeast extract tryptone)

5 g/L NaCl

16 g/L Tryptone

10 g/L Yeast extract

100 μg/ml Ampicillin

TB (Terrific broth)

12 g/L Tryptone

24 g/L Yeast extract

1x TB phosphate

10x TB phosphate, 100 ml

2.31 g KH_2PO_4 (0.17 M)

12.54 g K_2HPO_4 (0.72M)

2YT (Yeast extract tryptone) for LEN and SMA expression

Dissolve everything in PBS, pH 7.4

5 g/L NaCl

16 g/L Tryptone

10 g/L Yeast extract

2 mM $MgSO_4$

0.2% Glycerol

0.4% Glucose

100 μg/ml Ampicillin

10x PBS 1 L, pH 7.4

80 g NaCl

2 g KCl

26.8 g Na_2HPO_4

2.4 g KH_2PO_4

autoclave

Buffers

AS10 purification

Loading buffer Ni-NTA

50 mM Tris-HCl, pH 8.0

500 mM NaCl

20 mM imidazole

Elution buffer Ni-NTA

50 mM Tris-HCl, pH 8.0

500 mM NaCl

500 mM imidazole

SEC-buffer

20 mM NaPi, pH 7.4

50 mM NaCl

LEN and SMA purification buffers

Periplasmic extraction via osmotic shock

Step 1

100 mM Tris-HCl, pH 8

1 mM EDTA

20% Sucrose

EDTA-free mini protease inhibitor tablet

Step 2

5 mM $MgSO_4$

Dialysis

20 mM Sodium acetate, pH 5.0

IEC

Loading buffer

10 mM Sodium acetate, pH 5.0

Elution buffer LEN

500 mM NaCl

Elution buffer SMA

10 mM Tris-HCl, pH 8.0

SEC buffer

20 mM NaPi, pH 7.4

50 mM NaCl

CD buffer

20 mM NaPi, pH 7.4

50 mM NaCl

0-2 M Guanidinium hydrochloride

ThT-assay buffer

20 mM NaPi, pH 7.4

50 mM NaCl

20 µM ThT

0.04% NaN_3

0-4 M Guanidinium hydrochloride

SDS-Page

Separating gel buffer

1.5 M Tris-HCl, pH 8.8

14 mM SDS

Stacking gel buffer

0.5 M Tris-HCl, pH 6.8

4% (w/v) SDS

Separating gel 15% (2 gels)

4000 µl Acrylamid/Bisacrylamid (Rotiphorese Gel 30 (37:1))

1600 µl ddH_2O

400 µl Glycerin (99%)

2000 µl separating gel buffer

4 µl TEMED

40 µl 10% APS

Stacking gel (2 gels)

532 µl Acrylamid/Bisacrylamid (Rotiphorese Gel 30 (37:1))

2468 µl ddH_2O

1000 µl stacking gel buffer

3.2 µl TEMED

32 µl 10% APS

4x Læmmli reducing loading buffer

16% (v/v) SDS

38% (v/v) Glycerin

200 mM Tris-HCl, pH 6.8

0.04% (w/v) Bromophenol Blau

8% (v/v) β-Mercaptoethanol

TGS buffer (10x)

25 mM Tris-HCl

192 mM Gylcin

0.1% (w/v) SDS

Coomassie Brilliant Blue

Coomassie Brillant Blue R-250

45% (v/v) Methanol

10% (v/v) Acetic acid

45% (v/v) ddH_2O

Kits

Kit	Supplier
Plasmid DNA purification NucleoSpin®Plasmid	Macherey-Nagel

Devices

Device	Supplier
Centrifuge 5415 R	Eppendorf
Nanodrop 2000 Spectrophotometer	Thermo Scientific
pH-meter PB-11	Sartorius
Innova 40	New Brunswick Scientific
Infors HT Multitron Standard	Infors
Beckman Coulter Avanti J-26S XP	Beckman Coulter
Rotor JLA 10.500	Beckman Coulter
Rotor JA-20	Beckman Coulter
Sonicator Sonoplus	Bandelin
Sonotrode MS72	Bandelin
Centrifuge 5804 R	Eppendorf
NGC	BioRad
5 ml HiTrap Q FF	Cytiva life science
5 ml HisTrap FF	GE-Healthcare
Superdex 200 increase 10/300 GL	GE-Healthcare
Superdex 75 increase 10/30 GL	GE Healthcare
SnakeSkin 3500 MWCO	Thermo scientific
Spectrophotometer V-650	Jasco
Jasco J-715 Spectropolarimeter	Jasco
Tilt/Roller Mixer CAT RM5	CAT
Mini Protean Tetra System	BioRad
Geldocumentation System	BioRad
BMG Labtech CLARIOstar	BMG

Software

Name	Supplier
CLARIOstar 5.40 R	BMG
CLARIOstar Mars Data Analysis 3.31	BMG
GeneSnap	Syngene
Image Lab	BioRad
Nanodrop 2000/2000s 1.5	Thermo scientific
NGC Software ChromLab	BioRad
Origin Pro 9.0G	Origin
Pymol 2.0.6	Schrödinger LLC
SnapGene Viewer 3.1.3	SnapGene

4.3.2 Methods

Expression of full-length LEN and SMA

2YT medium is prepared in PBS pH 7.4 with 2 mM $MgSO_4$ and 0.2% Glycerol. The preculture is grown in a standard 2YT medium without any additives apart from the corresponding antibiotic Ampicillin in this case. The cells (BL21 DE3) were taken from a glycerol stock frozen at -80°C in 40% glycerol (provided by Dr. Michael Wördehoff). The cells contained the pET22 plasmid with LEN or SMA encoded, without a tag but with the pelB leader sequence fused to the N-terminal end of the protein; so that it is transported to the periplasmic space of *E. Coli*. The preculture is grown over night at 37°C and at least 160 rpm. The next day the expression culture is grown in the 2YT medium with additives and ampicillin. The optical density ($O.D._{600}$) of the preculture is measured at 600 nm, and the main culture is inoculated at an $O.D._{600}$ of 0.1. Important here for the main culture is that only 40% of the total volume of the flask is used for expression. The main culture is grown at 37°C and 130 rpm until an $O.D._{600}$ of around 1 is reached. The expression is then induced with IPTG to a final concentration of 1 mM (stock 1 M) and 0.4% final concentration glucose is added (stock 40%). The culture is then grown for an additional 4 h at 30°C and 120 rpm and then finally over night at 20°C and 11 rpm. The cells are then harvested at 5000 xg at 4°C for 10 min.

Periplasmic extraction through osmotic shock

Cells are solubilized in 1/20 of the original culture volume with 100 mM Tris-HCl (tris(hydroxymethyl)aminomethane), pH 8, 1 mM EDTA (Ethylenediaminetetraacetic acid), 20% sucrose and an EDTA-free mini protease inhibitor tablet (Roche). After the cells are thoroughly thawed, they are left to incubate for 45 min at 10°C on a tilt/roller mixer (TAMIRO). The mixture is centrifuged at 20 000 xg for 30 min at 4°C (Rotor JA-20, Beckman), and the supernatant is decanted into a fresh falcon tube and kept on ice. The pellet is submerged and solubilized again in 1/20 of the original culture volume in 5 mM $MgSO_4$ (Magnesium sulfate) and put back on the TAMIRO at 10°C for 45 min. After incubation it is again centrifuged at 9 000 xg for 10 min at 4°C. The supernatant is decanted and kept on ice. For dialysis 20 mM Sodium acetate pH 5 is prepared, at least 10x the volume of the total volume of supernatant, together with an appropriate amount of SnakeSkin 3500 MWCO (molecular weight cut-off),

hydrated in ddH_2O. The dialysis is kept overnight in a cold room (4-10°C). If there is precipitate the next day the buffer is exchanged for fresh buffer and dialyzed for 2-3 h more.

Purification of full-length LEN and SMA

The dialyzed supernatant is removed from the dialysis and centrifuged at 12 000 xg (Centrifuge 5415 R, Eppendorf) at 4°C for 10 min and then decanted into fresh falcon tubes. Precipitate and the "gel" that forms at the bottom is to be removed before continuing with the ion exchange chromatography. The sample is loaded in steps of up to 50 ml on a 5 ml HiTrap SPFF column (Cytiva), equilibrated with 10 mM sodium acetate pH 5 with a flow rate of 1-2 ml/min (NGC BioRad, sample pump). The sample wash buffer (10 mM sodium acetate pH 5) is loaded until the baseline is reached again. Then, LEN is eluted with a NaCl (sodium chloride) gradient from 0-100 mM. SMA is eluted with 10 mM Tris-HCl pH 8.0. The corresponding fractions are pooled and slightly concentrated before the size exclusion chromatography (SEC). SEC is done on a Superdex Increase 75 10/300 GL column (GE Healthcare) into a 20 mM NaPi (Sodium phosphate) pH 7.4, 50 mM NaCl buffer. The loop is flushed for three sample loop volumes and, the chromatography is run at 1 ml/min with an isocratic elution of the protein. Purity and correctness of the peak is controlled by an 15%-Glycine SDS-Gel. The correct fractions are then pooled, concentrated and if not immediately used flash frozen in liquid nitrogen and stored at -80°C. (Purification and osmotic shock procedure is based on the following publication: Hand, K. et al., Isolation and purification of recombinant immunoglobulin light chain variable domains from the periplasmic space of *Escherichia coli*, PLoS One 13, 2018)

Expression of β-wrapin AS10

The expression of the β-wrapin AS10 is done in *E. coli* JM109 DE3 cells using 2YT supplemented with 100 µg/L ampicillin. An overnight 2YT preculture was grown at 37 °C and 180 rpm. The main culture is done in 2YT and inoculated from the preculture at an optical density of 0.05 and grown at 37 °C and 140 rpm until induction with Isopropyl-β-D-thiogalactopyranosid (IPTG) at an optical density of 0.6, then incubated at 37 °C, 130 rpm for an additional 4 hours before harvesting. The cells are harvested by centrifuging at 5000 rpm for 10 min at 4 °C.

Purification of β-wrapin AS10

Harvested cells are frozen overnight in loading buffer (50 mM Tris(hydroxymethyl)aminomethane (Tris), pH 8.0, 500 mM sodium chloride (NaCl), 20 mM imidazole) with a protease inhibitor (cOmplete^{TM}, Mini, EDTA-free Protease Inhibitor Cocktail, Roche). After thawing the cells, they are sonicated on ice twice for 5 min with the sonication probe MS-72, with an amplitude of 35 % and a cycle of 3 s pulse and 5 s pause. Next step is to spin down the cell debris at 10 000 xg for 20 min at 4°C and the supernatant is run over a NiNTA-column (GE-healthcare, 5 ml HisTrap FF, column) in the loading buffer. Protein is eluted with a mixture of loading buffer and elution buffer (50 mM Tris, pH 8.0, 500 mM NaCl, 500 mM imidazole) into a final concentration of 250 mM imidazole. The eluate is then concentrated and kept at 4°C over-night. Next day, the protein is run over a size exclusion chromatography column (SEC Superdex^{TM} 200 Increase 10/300 GL GE healthcare) in a sodium phosphate buffer (20 mM NaPi, pH 7.4, 50 mM NaCl). The correct fractions are then collected, and pooled, concentrated and the concentration of protein is measured with a spectrophotometer. Afterwards, the protein is aliquoted, frozen in liquid nitrogen and stored at -80 °C.

Circular Dichroism of β-wrapin AS10 with guanidinium hydrochloride

The secondary structure of β-wrapin AS10 with and without the presence of different concentrations of guanidinium hydrochloride is probed with circular dichroism. In our study, a Jasco J-715 Spectropolarimeter is used. A clear quartz cuvette with 200 µl volume and 0.01 cm width is used. 20 µM AS10 is used for each measurement with either 0, 0.5, 1, 1.5 or 2 M guanidinium hydrochloride. For each of the measurements a buffer scan is also added containing everything but the protein AS10. The parameters for the measurements are as follows, the sensitivity is kept on standard, each measurement is from 260 nm to 180 nm. The scan is continuous with a data pitch of 0.1 nm and a scanning speed of 50 nm/min, the response time is 1 sec and the bandwidth 1 nm. Each measurement contains 10 accumulations.

Thioflavin T-Assays with full length LEN and SMA

All Thioflavin T (ThT) aggregation assays are done in Greiner 96-well half-area, clear bottom, low-binding plates. The measurements themselves are done in a BMG CLARIOstar plate reader

at 37 °C. Shaking is continuous over the whole measurement but is varied between 300 and 500 rpm with a glass bead per well. The volume per well is 80 µl. The buffer composition is always the same not including the guanidinium hydrochloride concentration which is varied between 0 and 4 M. The buffer contains 20 mM NaPi, pH 7.4, 50 mM NaCl, 20 µM ThT and 0.04% NaN_3 (Natrium azide). Protein concentration is varied between 20 and 60 µM. Wells with the samples are surrounded by wells filled with 150 µl water to minimize evaporation over the measurement time. The plate is always sealed before putting into the machine; measurement is done with the bottom optic.

4.4 Results

Expression of full-length variable light chains LEN and SMA

In a first step the expression for full length LEN and SMA had to be established. Expression in standard medium is possible but the yield is low. To generate a higher yield, expression tests with different media, additives, shaking speedss, and temperatures was done. Precultures, on the other hand, were grown in standard 2YT medium. Both proteins were subjected to the same test conditions. Media tested were the standard media like LB, 2YT, TB, and 2YT with different additives like 2YT prepared in 70 mM Potassium phosphate, pH 7.2 with 2 mM Magnesium sulfate, 0.2% Glycerol, and 0.4% Glucose either added at the beginning or with induction. Another medium mixture that was tested was 2YT prepared in phosphate-buffered saline (PBS), pH 7.4, with 2 mM Magnesium chloride and 0.4% glucose added directly or with induction. The last mixture tested was also 2YT prepared in PBS, pH 7.4 with 2 mM Magnesium sulfate and 0.2% Glycerol and again 0.4% Glucose added either directly or with the induction. The culture volume was reduced to 40% of the total volume of the flask used. The expression cultures were inoculated at an optical density of 0.1 and first grown at 37°C and 130 rpm. All cultures were induced at an optical density between 0.6 and 1, and in some cases, 0.4% Glucose was added together with the IPTG. After induction the temperature and shaking were reduced to 30°C and 120 rpm for 4 h. After 4 h, the temperature and shaking were further reduced to 20°C and 110 rpm respectively, and the cultures were left to grow over-night. Samples were taken before induction, 4 h after induction, and the following day after approximately 18 h after the 4 h. The collected samples were put on 15% Tris-Glycine gels; the optical density was normalized for each sample. What was visible first for both proteins, is that there seems to be already some expression before induction with IPTG no matter which kind of medium was used, which was visible on the gel as a double band between 10 and 15 kDa, which shows the correct size as both proteins have a molecular weight of approximately 12 kDa. The double band arises from the fact that the proteins contain the pelB leader sequence for transport into the periplasmic space. The signal sequence is cut off when the protein passes the membrane into the periplasmic space. Thus, the higher band on the SDS-gels should be the uncut protein with the leader sequence still attached with a higher molecular weight, and the lower band the correctly cut proteins without the leader sequence in the periplasmic space. After 4 h at 30°C, there was a clear distinction between the different media on the gel. The double band on the gel between 10 and 15 kDa indicative of the protein of interest are clearly visible for all media but

the thickness of the bands varies with the medium used. For both proteins, LB showed the faintest band on the gel. For LEN LB was followed by TB while 2YT and the 2YT prepared with different buffers and additives showed the thickest bands. The same can be said for SMA except that here TB is as thick a band as 2YT and the rest. This does not really change in the gels showing the samples after the expression over-night at 20°C, the bands simply become thicker, in fact so much, that it is no longer distinguishable as a double band. Still the best result with seemingly the most protein expressed and used for all further expressions of both proteins was 2YT prepared in PBS, pH 7.4, supplemented with 2 mM Magnesium sulfate, 0.2% Glycerol and 0.4% Glucose added upon induction. Grown under 37°C and 130 rpm shaking until induction, followed by 4 h at 30°C and 120 rpm and finally 20°C and 110 rpm overnight expression. Though if comparing the gels of both proteins it seems the yield of SMA could be higher than that of LEN.

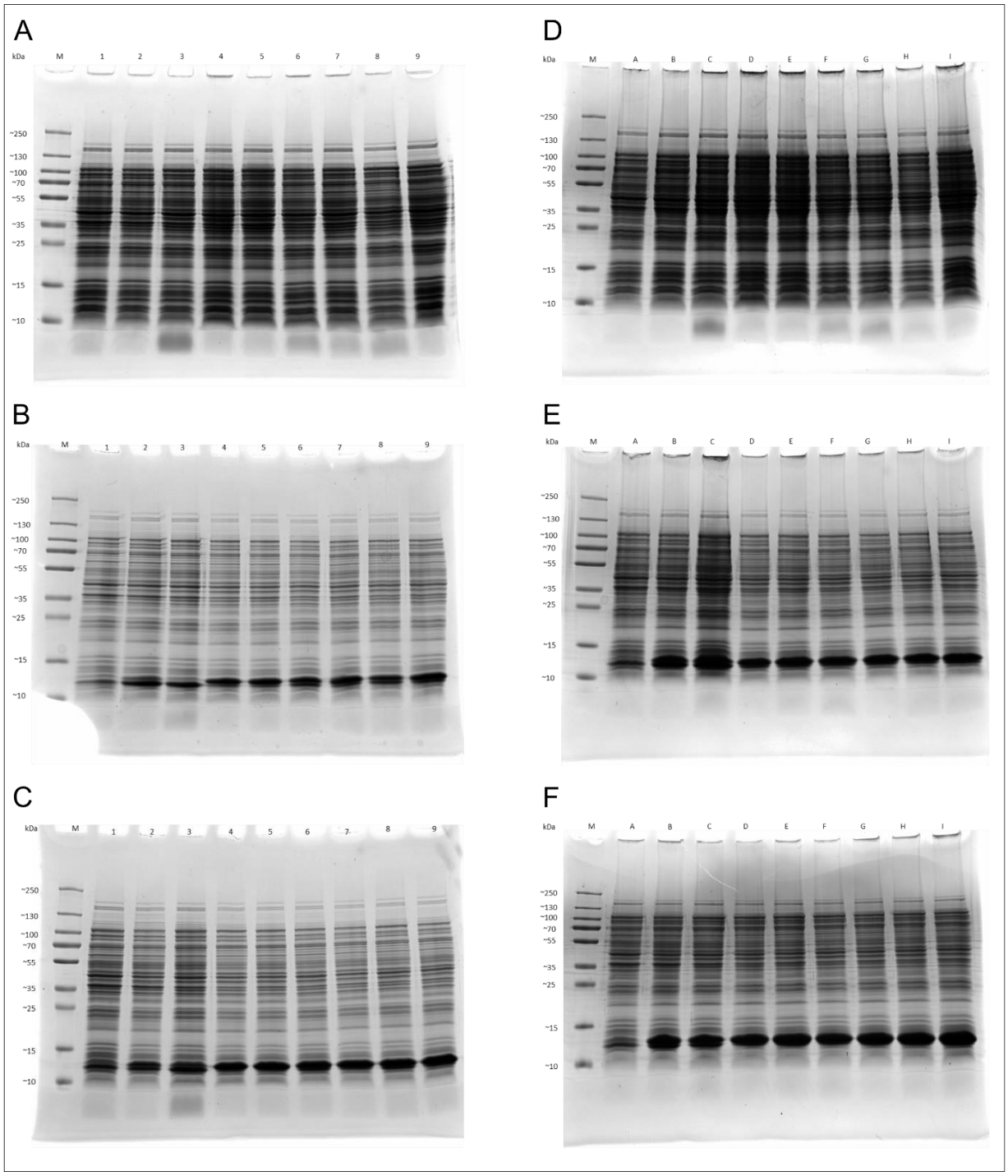

Figure 3: Glycine SDS-gels of full-length variable light chains LEN (A-C) and SMA (D-F) under different expression conditions. (A) and (D) show LEN and SMA before induction, (B) and (E) LEN and SMA 4 h, 30 °C after induction and, (C) and (F) LEN and SMA after overnight expression at 20 °C. Lanes in all SDS-gels were the following: marker (M); 1/A LB medium; 2/B 2YT medium; 3/C TBS medium; 4/D 2YT in 70 mM Potassium phosphate pH 7.2, 2mM $MgSO_4$, 0.2% Glycerol, 0.4% Glucose; 5/E 2YT in 70 mM Potassium phosphate pH 7.2, 2mM $MgSO_4$, 0.2% Glycerol, 0.4% Glucose added with induction; 6/F 2YT in PBS pH 7.4, 2 mM $MgCl_2$, 0.4% Glucose; 7/G 2YT in PBS pH 7.4, 2 mM $MgCl_2$, 0.4% Glucose added with induction; 8/H 2YT in PBS pH 7.4, 2 mM $MgSO_4$,

0.2% Glycerol, 0.4% Glucose; 9/I 2YT in PBS pH 7.4, 2 mM $MgSO_4$, 0.2% Glycerol, 0.4% Glucose added with induction.

Purification of full-length variable light chains LEN and SMA

To purify the proteins from the periplasmic space of E. coli four different approaches were tested. The methods tested were a freeze and thaw protocol in which the cells are repeatedly frozen and then thawed again and so supposed to release the proteins from the periplasmic space. This approach was not successful. Another method used was an approach with lysozyme. Here too, the proteins in the periplasmic space were supposed to be released into the resulting supernatant. This approach was not successful, as is visible in the gel, lysozyme (~ 14 kDa) is roughly the same size as LEN and SMA. A third approach was taken by a chloroform extraction which was also unsuccessful in releasing only the periplasmic proteins into the resulting supernatant. The fourth approach was an osmotic shock protocol done in two steps which showed the best results in releasing the periplasmic proteins from the bacterial cells. The osmotic shock protocol was carried out in two different ways, on the one hand all buffers and solutions were kept at 4°C to perform a cold osmotic shock and the samples kept on ice during incubation times, on the other hand everything was also tried at room temperature. Both approaches were successful, though the cold osmotic shock yield was slightly higher thus this protocol was kept for all further extractions. Before the resulting supernatant from the cold osmotic shock protocol could be run over an ion exchange column it needed to be dialyzed to lower the pH and to get rid of the sugar used in the osmotic shock as it would have been too viscous to load on a column. Different times were tested for the dialysis, the longest being three days with three buffer exchanges. This proved to be too much, as there were a lot of precipitates and barely any measurable protein left in the supernatant. The best solution proved to be over-night dialysis at 4 - 10°C with at least tenfold the volume of the supernatant with a buffer exchange in the morning for two more hours. At this point, there was barely any precipitate. After centrifugation to lose all possible precipitate, it was visible that instead of precipitate there was a viscous “jelly-like” liquid at the bottom of the falcon tube that could not be further identified and was not loaded on the ion exchange column. As an ion exchange column, a cation exchange column proved to be the best. Both LEN and SMA have a pI close to 8, and through the dialysis the pH was lowered to 5. This approach proved successful for both proteins. The supernatant loading had to be done in several steps; otherwise, the column would get clogged.

A maximum of 50 ml of supernatant could only be loaded onto the column before it had to be washed with the running buffer and the proteins had to be eluted. The elution of the light chain LEN was straightforwardly doable with a Sodium chloride gradient. This method could not be used for the light chain SMA. SMA was instead eluted with a Tris-HCl buffer with a pH of 8. After the elution, both LEN and SMA could be concentrated but not too high as the solutions with the proteins would turn into a "jelly-like", reddish solution, but it could be dissolved again when buffer was added. A size exclusion column followed the ion exchange column to put the proteins into the correct buffer for the aggregation assays and to lose more impurities.

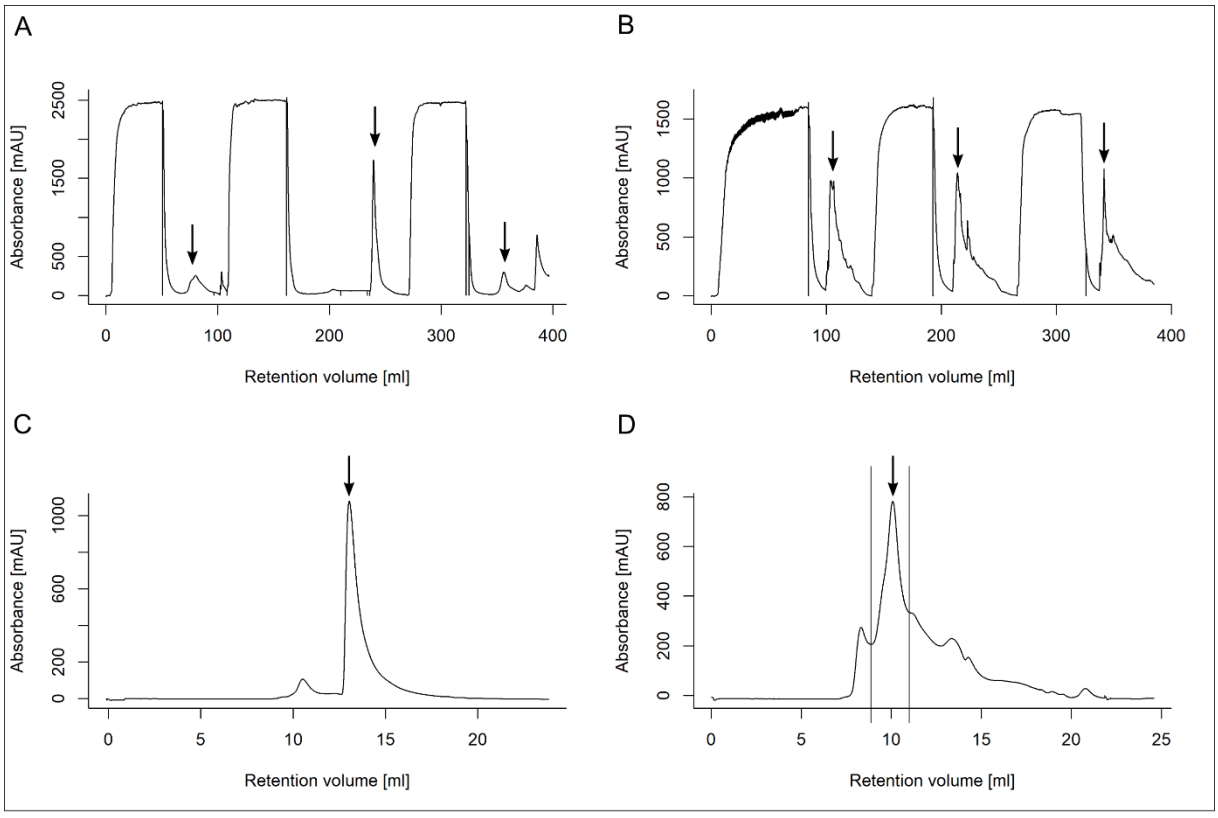

Figure 4: IEC and SEC of LEN and SMA. (A) and (B) show an IEC with LEN and SMA respectively, the arrows show the elution peaks. (C) and (D) show the corresponding SEC-profiles of LEN and SMA respectively, the arrows indicate which fractions were used in the experiments. For (D) SMA only a small part of the peak was used as indicated by the two straight lines. The shown wavelength for all profiles is 275 nm.

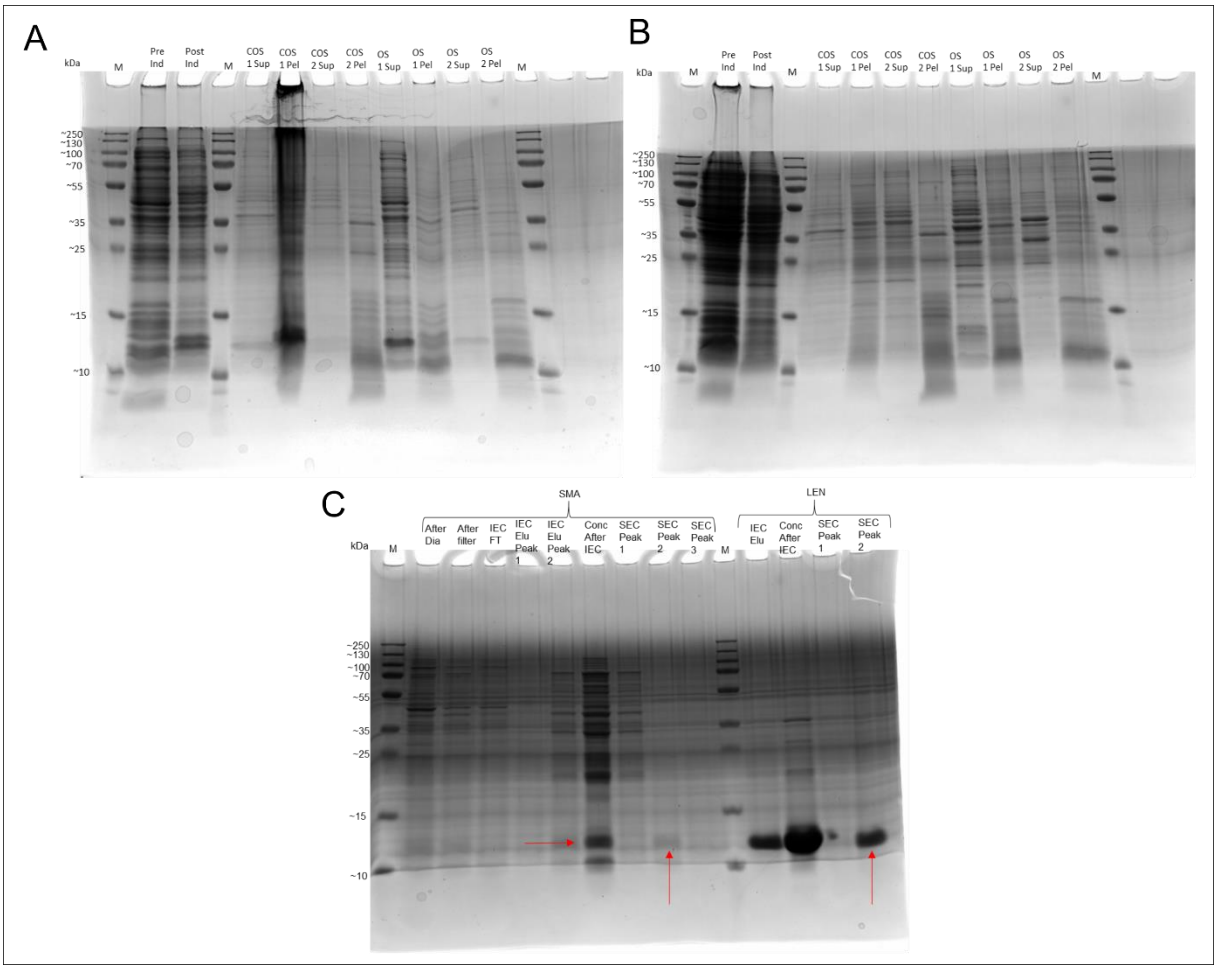

Figure 5: Periplasmic extraction of LEN (A) and SMA (B) and an exemplary purification of both (C). M depicts the marker. In (A) and (B), lanes two and three show the expression of LEN before and after induction. COS (Cold Osmotic Shock), OS (Osmotic shock), Sup (Supernatant) and Pel (remaining cell pellet). Lanes five to eight in (A) and (B) show the results of the cold osmotic shock procedure, while lanes nine to twelve show the osmotic shock procedure. In (C) lanes one to ten show a purification of SMA (Dia being dialysis, IEC being ion exchange column, FT the flow through, Elu being the elution, Conc. Concentrated sample, and SEC for size exclusion column). Lanes twelve to fifteen show purification of LEN. Both proteins were extracted using the cold osmotic shock protocol.

Circular dichroism spectroscopy of AS10 with guanidinium hydrochloride

To observe up to which point the β-wrapin AS10 can tolerate guanidinium hydrochloride without losing its secondary structure, circular dichroism (CD) spectroscopy measurements were performed. The guanidinium hydrochloride concentrations measured with AS10 were 0, 0.5, 1, 1.5, and 2 M. The first measurement without any guanidinium hydrochloride showed the typical secondary structure profile of a β-wrapin, with a lot of α-helical content matching the

known structure with two subunits containing three α-helices each. Though the noise level of the measurement is already quite high at 198 nm, the measurement is clear. Already at 0.5 M guanidinium hydrochloride it is visible that the measurement is only comparable to the one without guanidinium hydrochloride until 205 nm. From 205 to 260 nm, the measurement is clear and still shows a partly structured part, though the signal is less than for the first measurement. The signal in total continues to decrease in the following measurements of 1, 1.5, and 2 M guanidinium hydrochloride. Also, the data below 210 nm is not usable for any kind of analysis. The CD-signal from 210 to 260 nm on the other hand is high enough to be further analysed. Clearly visible is that the second negative peak at approximately 220 nm becomes less pronounced with increasing guanidinium hydrochloride concentration. This feature at 220 nm is one of the typical features in the measurements of β-wrapins; it indicates the presence of the two three-α-helices bundles that make up the homodimeric β-wrapin and can thus be used here to at least make estimations about the degree of denaturation. If the signal at 220 nm decreases with rising guanidinium hydrochloride concentration it means that the α-helices are denaturing and are thus losing their structure. From that knowledge it is possible to say that at 1 M guanidinium hydrochloride, a big part, if not the whole structure of AS10 is still intact, starting at 1.5 to 2 M guanidinium hydrochloride, the structure is lost.

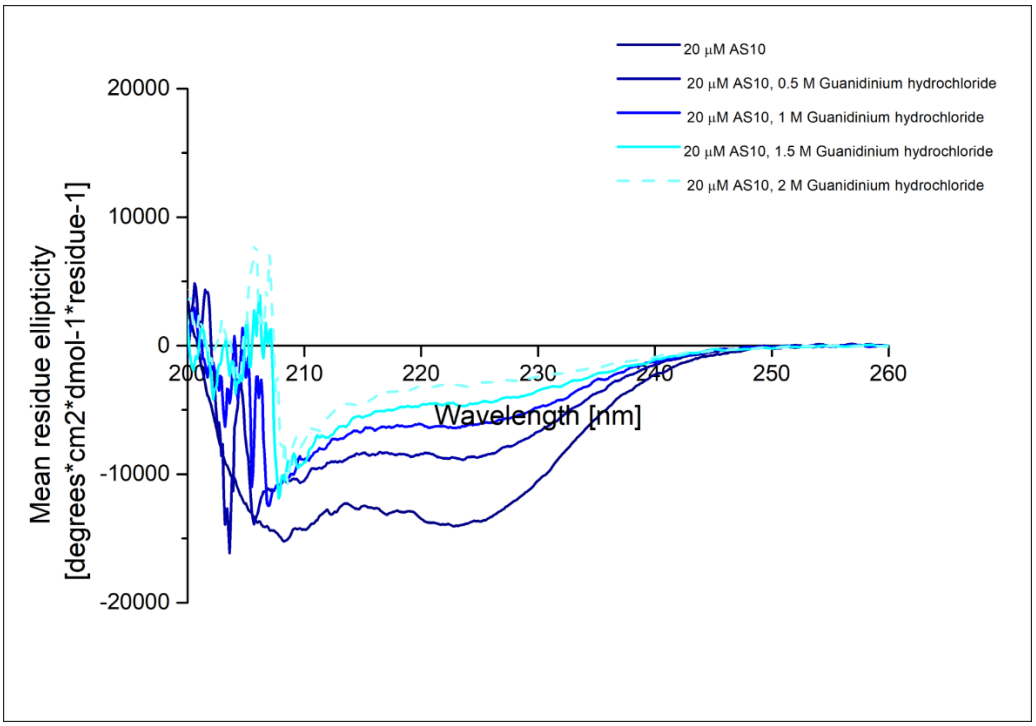

Figure 6: CD spectroscopy of AS10 with different concentrations of guanidinium hydrochloride from none to 2 M. To show up to which concentration AS10 remains in its native fold. The darkest blue shows the AS10 without guanidinium hydrochloride in its native fold, while the dotted brightest blue line shows AS10 with 2 M guanidinium hydrochloride.

Thioflavin-T aggregation assays of full-length variable light chains LEN and SMA

In the first assays, it was tested under which conditions the light chains LEN and SMA aggregate monitored by Thioflavin T (ThT) fluorescence. In a first trial both LEN and SMA were tested at concentrations of 20 µM in an assay with and without glass beads and guanidinium hydrochloride concentrations from 0-2 M and shaking. For LEN with shaking, a glass bead and 2 M guanidinium hydrochloride there was aggregation visible in two of the triplicates, after approximately 30 and 60 hours. At guanidinium hydrochloride concentrations below no aggregation was detected. There were also no aggregation curves visible for LEN at all without a glass bead per well, no matter the guanidinium hydrochloride concentration. For the first trial no aggregation was observed at all for SMA. In a second trial with 40 µM protein the same conditions were kept as in the first one, just that instead of 300 rpm shaking it was increased to 500 rpm shaking in-between measurements, also all wells were supplemented with a glass bead. Again, for LEN at 2 M guanidinium hydrochloride aggregation could be observed for the whole triplicate. The aggregation seemed to be faster with the increased shaking, as here

two wells took only 20-30 hours to aggregate, while the third showed a curve only after 70 hours. Nothing changed for SMA, there was no aggregation detectable. In a third attempt, this time is only done with SMA, higher concentrations of the denaturant on the one hand and a pH shift from 7.4 to 2 with the denaturant, on the other hand, were tested. Both attempts were not successful, there was still no aggregation of SMA. Since it was shown in CD experiments that AS10 is already mostly denatured at 2 M guanidinium hydrochloride and LEN needs this concentration to show aggregation in the ThT-assay, an addition of AS10 to LEN with this amount of denaturant was not attempted. It was seen as unlikely that the already denatured AS10 would have an effect, especially an inhibitory one, on LEN and thus further experiments were not carried out.

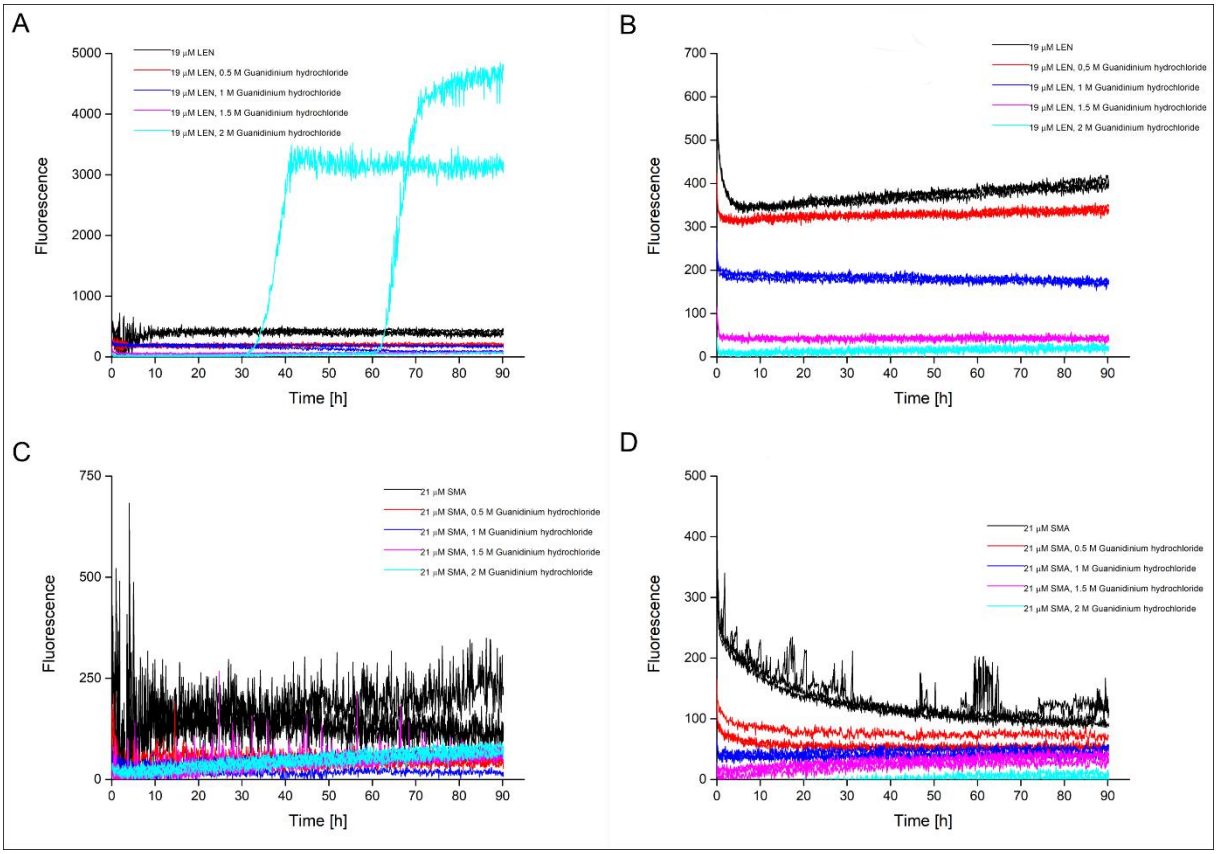

Figure 7: ThT-kinetics of LEN and SMA with different guanidinium hydrochloride concentrations. (A) 19 µM LEN with glass beads and no (black), 0.5 M (red), 1 M (dark blue), 1.5 M (magenta), and 2 M (cyan) guanidinium hydrochloride, with aggregation curves observable at 2 M only. (B) 19 µM LEN with the same concentrations of guanidinium hydrochloride but no glass beads. (C) and (D) show the same for 21 µM SMA with no (black), 0.5 M (red), 1 M (dark blue), 1.5 M (magenta), and 2 M (cyan) guanidinium hydrochloride, with glass beads (C) and without (D).

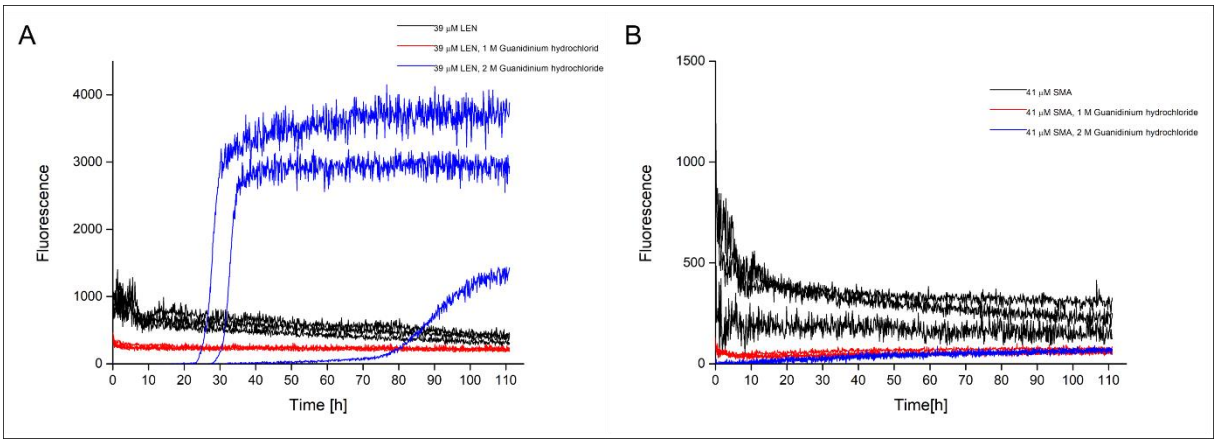

Figure 8: ThT-kinetic with higher concentrations of (A) LEN (39 µM) and (B) SMA (41 µM) with no (black), 1 M (red), and 2 M (blue) guanidinium hydrochloride.

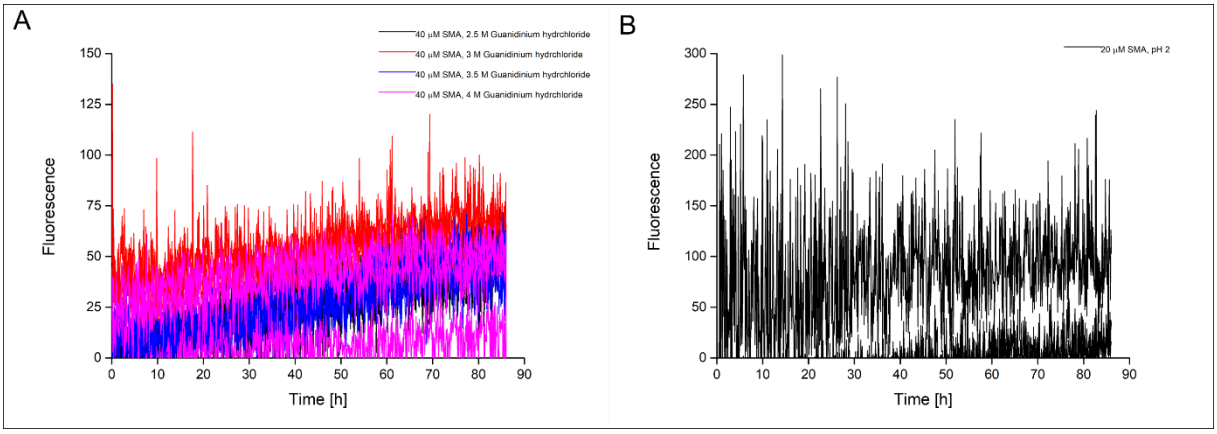

Figure 9: ThT-kinetics of SMA with more guanidinium hydrochloride (A) and at pH 2 without guanidinium hydrochloride (B).

4.5 Discussion

LEN and SMA are variable light chain fragments from two patients and can be used as model proteins for AL-amyloidosis. LEN was reported to be the more benign protein of the two concerning AL-amyloidosis, the patient suffered from multiple myeloma but showed no signs of amyloidogenic deposits. SMA on the other hand was isolated from a patient postmortem as amyloid fibril and reported to aggregate *in vitro*.

To establish a stable expression with a reasonably high yield and to have the proteins already as natively folded as possible in the cell, both proteins sequences were fused with the pelB leader sequence, which shuttles protein to the periplasm of *E. coli*, where it gets fully cleaved off. [11, 33, 38] The periplasm of gram-negative bacteria has the additional advantage, besides that the proteins stay soluble and can fold into their native fold there, with the help of an oxidizing environment and foldases which also allows for disulfide bridges to be formed, that there is little contamination in the form of other proteins and DNA to be found, which helps the purification later. [11, 16, 33, 38]

The cells grew in all tested media but with varying yields according to the SDS-PAGE glycine-gels, and in all media tested there was a double band visible on the height where the protein was to be expected. This can be explained by the fact that the pelB leader sequence that is used to transport the proteins to the periplasm gets fully cleaved off when the protein enters the periplasm. [11, 33, 38] The double band reflects the two different species of protein, one with the leader sequence and one without. It is striking that on the SDS-gels the upper band is thicker, which could mean that there is more protein in the cytosolic part of the bacterial cell and has not yet been shuttled to the periplasm and the pelB leader sequence has not yet been cleaved off. Albeit this levels out slightly with the change in medium. In the classical media LB, 2YT, and TB, the lower, possibly correct band, is thicker than the uncleaved band above. While the yield in total increases with 2YT in potassium phosphate or PBS buffer with the addition of magnesium chloride or sulfate plus sometimes glycerol and always glucose in the non-standard media, the upper noncleaved band grows thicker or seems to be at least equally as thick as the lower band. While it is published that the transport of proteins to the periplasm is upregulated if the bacterial cells experience osmotic stress while growing it also increases the total yield, maybe to a point where there is too much protein to easily shuttle into the periplasm. [16] Still, since the yield was seemingly the highest there, the medium 2YT in PBS with magnesium sulfate, glycerol and glucose was kept. Also, interesting to see is that the yield of the expression

of LEN and SMA among themselves is different, it seems the yield for SMA is higher than that for LEN but the overexpression is clearer for LEN (Figure 3). It seems that in general *E. coli* is able to express the amyloidogenic light chains but since most of the protein seems not be shuttled to the periplasm and thus not easily accessible for purification. The reason could be since they are amyloidogenic light chains that with the overexpression the proteins already aggregate intercellularly which could cause problems for the bacterial cells. Even if the same phenomenon could not be replicated with a ThT-assay later after purification of the proteins but this could be due to the vastly different environment between a bacterial cell and a ThT-assay.

The next step was the periplasmic extraction of the proteins. As already said, in the best case, if only the periplasm is extracted instead of the whole cell, there should barely be contamination with other proteins or other cell debris. There are several methods for periplasmic extraction, the ones tested here were the chloroform, EDTA/Lysozyme, freeze and thaw, and finally, the cold osmotic shock extraction. [2, 11, 16, 44] All methods are established, and protocols are available, although changes within the protocols are common. In all four protocols, the periplasmic proteins are supposed to be in the supernatant after the extraction, and there should not be much contamination. When tested here, all four protocols yielded a rather contaminated supernatant. When the pellet was checked via SDS-PAGE, it could be observed that there was still more protein left in the pellets than there was in the supernatant. More importantly, there were still the double bands visible at approximately 12 kDa, which would mean that not only the non-processed protein, which is still, and rightly so, in the cells and thus in the cell pellet, but also a part of the processed protein remains in the pellet. This could mean that the periplasmic extraction was not entirely successful. It is possible that the outer bacterial membrane was not perforated or destroyed enough for the proteins to be released. In the end, the cold osmotic shock procedure in two steps was done and kept for the periplasmic extraction as it provided, according to the SDS-PAGE, the highest yield as judged by the ratio of protein in the supernatant vs. protein in the cell pellet. After the extraction, the supernatant is surprisingly quite contaminated with other proteins; maybe in this two-step cold osmotic shock procedure, the inner cell membrane was also perforated, and so cytoplasmic components leaked into the supernatant. The rest of the purification is straightforward, with a cation exchange column followed by size exclusion chromatography. Albeit the dialysis before the two chromatography steps was challenging. Since the cold osmotic shock in two steps was used for the periplasmic extraction, it resulted in a high volume of supernatant that still had a too high

percentage of sugar to go smoothly over the ion exchange column. To lose the sugar, all possible salts and adjust the pH for the ion exchange to work different lengths of dialysis were tested. A dialysis protocol offered in the literature was to dialyze the supernatant over approximately three days with buffer exchanges in between. [44] This protocol was only used once as a lot of material precipitated and with it almost all of the protein. The dialysis time was thus shortened to over-night dialysis at 4°C with at least 10x higher dialysis buffer volume than the total volume of supernatant. This time frame showed less precipitate, and protein was still detectable in the supernatant, but another problem occurred. After the dialysis over-night, the remaining supernatant was centrifuged to pellet the precipitate so that it does not clog the column. After centrifugation there was not only a pellet of precipitate, but also a part of the supernatant that seemed a lot more viscous, more "jelly-like", than the rest. This part was carefully decanted and unused, as it clogged filters and the column. At first it was thought that the dialysis was too short, and the sugar was not fully removed, but longer dialysis with one buffer exchange after the overnight dialysis did not yield a better result. A likely possibility is that the gel-like material consists of amyloid aggregates of light chains or possibly fragments thereof, as amyloid fibrils have a tendency to associate leading to gelation. The nature of the jelly-like substance was not further investigated. Interestingly, when SMA and LEN were concentrated after the ion exchange chromatography for the size exclusion chromatography, both protein solutions turned more viscous and took on a reddish hue when concentrated further. This was reversible by adding buffer again to the solution. When the protein was concentrated to a point where the solution became "jelly-like" the process was only partially reversible with adding buffer. Some of the material seemed to dissolve again, but parts of it stayed in a "gel-like" state and seemed no longer soluble. This could already include aggregation, but it was not possible to gain further insight by SDS-PAGE or atomic force microscopy. The resulting protein at the end of the purification on the other hand could be loaded onto an SDS-PAGE glycine-gel and is in accordance with the band already shown in the expression tests and should be at the right height according to the marker, there were barely any contaminations left and it was possible to concentrate, though here it was concentrated no further as soon as slight reddish tint appeared.

With the purified protein, an aggregation test could be done. As is written in the literature variable light chains and both LEN and SMA seem to aggregate easier in slightly destabilizing conditions *in vitro*, with the usage of urea, guanidinium hydrochloride, or even with pH changes. [26] At this point, it was immensely important to check if the suspected inhibitor, in

this case, the engineered homodimer β-wrapin AS10, which is able to wrap around β-hairpin regions and stop the aggregation of other amyloid disease-related proteins, is still able to work under such conditions. [54] Since the denaturing agent used here was guanidinium hydrochloride, AS10 was checked with different denaturant concentrations. AS10, as other β-wrapins, has a characteristic CD spectrum that reflects the high content in α-helical structure. Therefore, circular dichroism was used to observe at which point the secondary structure of AS10 is unfolded, resulting in loss of any potential inhibitory activity. It could be shown that already at a concentration of 0.5 M guanidinium hydrochloride the CD signal decreases, meaning that AS10 is already starting to denature. At 2 M guanidinium hydrochloride an α-helical structure signal could no longer be detected. This means AS10 is completely denatured at 2 M guanidinium hydrochloride and thus the concept of coupled folding-binding of the β-wrapin inhibition cannot function properly anymore. As already mentioned, both proteins do not seem to aggregate in their native fold but need to be destabilized from this fold to form aggregates. According to the literature, there is not only one intermediate conformation or partially unfolded conformation in between correctly folded and fully unfolded and not all intermediates aggregate the same way. [26] SMA is, as was shown in different studies, relatively unfolded at pH 3 but seems to form fibrils at this point, but at pH 2 it seems to form amorphous aggregates as well as fibrils but on a much smaller timescale than at pH 3. [21, 23] In the ThT-assays done here SMA did not aggregate at all, as it showed no increasing ThT-signal at all, not for destabilizing conditions up to 4 M guanidinium hydrochloride nor after a pH change to pH 2. LEN on the other hand, the according to literature more benign variable light chain, showed an increase of ThT signal at 2 M guanidinium hydrochloride under shaking conditions. LEN forms a dimer at neutral pH which has to be disrupted for LEN to aggregate. [22] In other studies of LEN, it was shown that the aggregation is highly dependent on the protein concentration, in this case by decreasing the protein concentration and increasing the urea concentration the aggregation is accelerated. Since it was not successful to get SMA to aggregate at all and LEN only with 2 M guanidinium hydrochloride, a concentration where also AS10 loses its secondary structure and with it its function it was not possible to test the inhibitory effect AS10 could have on these two model proteins of AL-amyloidosis.

In conclusion, the expression and purification of the AL-amyloidosis model variable light chains LEN and SMA are possible in the periplasm of *E. coli* BL21 DE3 cells with the cleavable pelB leader sequence. The periplasmic extraction of both proteins should be further optimized, while the purification is straightforward as was established here. Both proteins have the correct

height in a glycine SDS-PAGE gel but sequencing via mass spectrometry could be used to be sure that the proteins have the correct sequence. Other denaturants could also be tried as long as AS10 stays stable with them and both variable light chains aggregate under the same conditions. All in all, this project could be further optimized.

4.6 References

1. Solomon, A., Frangione, B. & Franklin, E. C. Bence Jones proteins and light chains of immunoglobulins. Preferential association of the V(λVI) subgroup of human light chains with amyloidosis AL(λ). *J. Clin. Invest.* **70**, 453–460 (1982).
2. Ferro-Luzzi Ames,', G., Prody, C. & Kustu2, S. *Simple, Rapid, and Quantitative Release of Periplasmic Proteins by Chloroform*. *JOURNAL OF BACTERIOLOGY* vol. 160 http://jb.asm.org/ (1984).
3. Solomon, A. [6] Light chains of human immunoglobulins. *Methods Enzymol.* **116**, 101–121 (1985).
4. Stevens, F. J., Schiffer, M. & Solomon, A. Bence Jones Proteins: A Powerful Tool for the Fundamental Study of Protein Chemistry and Pathophysiology. *Biochemistry* **30**, 6803–6805 (1991).
5. Solomon, A., Weiss, D. T. & Kattine, A. A. Nephrotoxic Potential of Bence Jones Proteins. *N. Engl. J. Med.* **324**, 1845–1851 (1991).
6. Solomon, A., Weiss, D. T. & Pepys, M. B. Induction in mice of human light-chain-associated amyloidosis. *Am. J. Pathol.* **140**, 629–637 (1992).
7. Buxbaum, J. Mechanisms of disease: Monoclonal immunoglobulin deposition. *Hematology/Oncology Clinics of North America* vol. 6 323–346 (1992).
8. Myatt, E. A. *et al.* Pathogenic potential of human monoclonal immunoglobulin light chains: Relationship of in vitro aggregation to in vivo organ deposition. *Proc. Natl. Acad. Sci. U. S. A.* **91**, 3034–3038 (1994).
9. Bork, P., Holm, L. & Sander, C. The immunoglobulin fold: Structural classification, sequence patterns and common core. *Journal of Molecular Biology* vol. 242 309–320 (1994).
10. Stevens, P. W. *et al.* Recombinant immunoglobulin variable domains generated from synthetic genes provide a system for in vitro characterization of light-chain amyloid proteins. *Protein Sci.* **4**, 421–432 (1995).
11. Thorstenson, Y. R., Zhang, Y., Olson, P. S. & Mascarenhas, D. Leaderless polypeptides efficiently extracted from whole cells by osmotic shock. *J. Bacteriol.* **179**, 5333–5339 (1997).
12. Huang, D. Bin *et al.* Variable domain structure of κIV human light chain Len: High homology to the murine light chain McPC603. *Mol. Immunol.* **34**, 1291–1301 (1997).

13. Olsen, K. E., Sletten, K. & Westermark, P. Extended analysis of AL-amyloid protein from abdominal wall subcutaneous fat biopsy: Kappa IV immunoglobulin light chain. *Biochem. Biophys. Res. Commun.* **245**, 713–716 (1998).
14. Lonescu-Zanetti, C. *et al.* Monitoring the assembly of Ig light-chain amyloid fibrils by atomic force microscopy. *Proc. Natl. Acad. Sci. U. S. A.* **96**, 13175–13179 (1999).
15. Raffen, R. et al. Physicochemical consequences of amino acid variations that contribute to fibril formation by immunoglobulin light chains. *Protein Science 8:509–517* (1999).
16. Barth, S. *et al.* Compatible-solute-supported periplasmic expression of functional recombinant proteins under stress conditions. *Appl. Environ. Microbiol.* **66**, 1572–1579 (2000).
17. Stevens, F. J. Four structural risk factors identify most fibril-forming kappa light chains. *Amyloid* **7**, 200–211 (2000). DOI: 10.3109/13506120009146835.
18. Davis, D. P. *et al.* Inhibition of amyloid fiber assembly by both BiP and its target peptide. *Immunity* **13**, 433–442 (2000).
19. Bellotti, V., Mangione, P. & Merlini, G. Review: Immunoglobulin light chain amyloidosis - The archetype of structural and pathogenic variability. *Journal of Structural Biology* vol. 130 280–289 (2000).
20. Kim, Y. S. *et al.* Counteracting effects of renal solutes on amyloid fibril formation by immunoglobulin light chains. *J. Biol. Chem.* **276**, 1626–1633 (2001).
21. Khurana, R. *et al.* Partially folded intermediates as critical precursors of light chain amyloid fibrils and amorphous aggregates. *Biochemistry* **40**, 3525–3535 (2001).
22. Souillac, P. O. *et al.* Effect of association state and conformational stability on the kinetics of immunoglobulin light chain amyloid fibril formation at physiological pH. *J. Biol. Chem.* **277**, 12657–12665 (2002).
23. Khurana, R. *et al.* A model for amyloid fibril formation in immunoglobulin light chains based on comparison of amyloidogenic and benign proteins and specific antibody binding. *Amyloid* **10**, 97–109 (2003).
24. Souillac, P. O., Uversky, V. N. & Fink, A. L. Structural transformations of oligomeric intermediates in the fibrillation of the immunoglobulin light chain LEN. *Biochemistry* **42**, 8094–8104 (2003).
25. Sanchorawala, V. Light-chain (AL) amyloidosis: diagnosis and treatment. *Clinical journal of the American Society of Nephrology : CJASN* vol. 1 1331–1341 (2006).

26. Qin, Z., Hu, D., Zhu, M. & Fink, A. L. Structural characterization of the partially folded intermediates of an immunoglobulin light chain leading to amyloid fibrillation and amorphous aggregation. *Biochemistry* **46**, 3521–3531 (2007).
27. del Pozo Yauner, L. *et al.* Influence of the germline sequence on the thermodynamic stability and fibrillogenicity of human lambda 6 light chains. *Proteins Struct. Funct. Bioinforma.* **72**, 684–692 (2008).
28. Mukherjee, S., Pondaven, S. P., Höfer, N. & Jaroniec, C. P. Backbone and side-chain 1H, 13C and 15N resonance assignments of LEN, a human immunoglobulin κiV light-chain variable domain. *Biomol. NMR Assign.* **3**, 255–259 (2009).
29. Randles, E. G., Thompson, J. R., Martin, D. J. & Ramirez-Alvarado, M. Structural Alterations within Native Amyloidogenic Immunoglobulin Light Chains. *J. Mol. Biol.* **389**, 199–210 (2009).
30. Sockolosky, J. T. & Szoka, F. C. Periplasmic production via the pET expression system of soluble, bioactive human growth hormone. *Protein Expr. Purif.* (2012) doi:10.1016/j.pep.2012.11.002.
31. Rognoni, P. *et al.* A Strategy for Synthesis of Pathogenic Human Immunoglobulin Free Light Chains in E. coli. *PLoS One* **8**, e76022 (2013).
32. Ramirez-Alvarado, M. Amyloid Formation in Light Chain Amyloidosis. *Curr. Top. Med. Chem.* **999**, 1–7 (2013).
33. Singh, P. *et al.* Effect of Signal Peptide on Stability and Folding of Escherichia coli Thioredoxin. *PLoS One* **8**, 63442 (2013).
34. Blancas-Mejía, L. M. & Ramirez-Alvarado, M. Systemic Amyloidoses. *Annu. Rev. Biochem.* **82**, 745–774 (2013).
35. Goemans, C., Denoncin, K. & Collet, J. F. Folding mechanisms of periplasmic proteins. *Biochimica et Biophysica Acta - Molecular Cell Research* vol. 1843 1517–1528 (2014).
36. Singh, A., Upadhyay, V., Upadhyay, A. K., Singh, S. M. & Panda, A. K. Protein recovery from inclusion bodies of Escherichia coli using mild solubilization process. *Microbial Cell Factories* vol. 14 41 (2015).
37. Dispenzieri, A. *et al.* Treatment of Immunoglobulin Light Chain Amyloidosis Mayo Stratification of Myeloma and Risk-Adapted Therapy (mSMART) Consensus Statement. *Mayo Clin. Proc.* **90**, 1054–1081 (2015).

38. Dow, B. A., Tatulian, S. A. & Davidson, V. L. Use of the amicyanin signal sequence for efficient periplasmic expression in E. coli of a human antibody light chain variable domain. *Protein Expr. Purif.* **108**, 9–12 (2015).
39. Sipe, J. D. *et al.* Amyloid fibril proteins and amyloidosis: chemical identification and clinical classification International Society of Amyloidosis 2016 Nomenclature Guidelines. *Amyloid* **23**, 209–213 (2016).
40. Marin-Argany, M. *et al.* Cell damage in light chain amyloidosis fibril internalization, toxicity and cell-mediated seeding. *J. Biol. Chem.* **291**, 19813–19825 (2016).
41. Andrich, K. *et al.* Aggregation of full-length immunoglobulin light chains from systemic light chain amyloidosis (AL) patients is remodeled by epigallocatechin-3-gallate. *J. Biol. Chem.* **292**, 2328–2344 (2017).
42. Mukherjee, S., Pondaven, S. P., Hand, K., Madine, J. & Jaroniec, C. P. Effect of amino acid mutations on the conformational dynamics of amyloidogenic immunoglobulin light-chains: A combined NMR and in silico study. *Sci. Rep.* **7**, 10339 (2017).
43. Blancas-Mejia, L. M. *et al.* Immunoglobulin light chain amyloid aggregation. *Chem. Commun.* **54**, 10664–10674 (2018).
44. Hand, K., Wilkinson, M. C. & Madine, J. Isolation and purification of recombinant immunoglobulin light chain variable domains from the periplasmic space of Escherichia coli. *PLoS One* **13**, (2018).
45. Milani, P., Merlini, G. & Palladini, G. Light chain amyloidosis. *Mediterranean Journal of Hematology and Infectious Diseases* vol. 10 (2018).
46. Lecoq, L. *et al.* A Substantial Structural Conversion of the Native Monomer Leads to in-Register Parallel Amyloid Fibril Formation in Light-Chain Amyloidosis. *ChemBioChem* **20**, 1027–1031 (2019).
47. Misra, P., Blancas-Mejia, L. M. & Ramirez-Alvarado, M. Mechanistic Insights into the Early Events in the Aggregation of Immunoglobulin Light Chains. *Biochemistry* **58**, 3155–3168 (2019).
48. Rennella, E., Morgan, G. J., Kelly, J. W. & Kay, L. E. Role of domain interactions in the aggregation of full-length immunoglobulin light chains. *Proc. Natl. Acad. Sci. U. S. A.* **116**, 854–863 (2019).
49. Morgan, G. J. *et al.* Stabilization of amyloidogenic immunoglobulin light chains by small molecules. *Proc. Natl. Acad. Sci. U. S. A.* **116**, 8360–8369 (2019).

50. Kazman, P. *et al.* Fatal amyloid formation in a patient's antibody light chain is caused by a single point mutation. *Elife* **9**, (2020).
51. Nilsson, M. R. Techniques to study amyloid fibril formation in vitro. *Methods* **34**, 151–160 (2004).
52. Xue, C., Lin, T. Y., Chang, D. & Guo, Z. Thioflavin T as an amyloid dye: fibril quantification, optimal concentration and effect on aggregation. *R. Soc. open Sci.* **4**, 160696 (2017).
53. Levine, H. Thioflavine T interaction with synthetic Alzheimer's disease β-amyloid peptides: Detection of amyloid aggregation in solution. *Protein Sci.* **2**, 404–410 (1993).
54. Shaykhalishahi, H. *et al.* A β-Hairpin-Binding Protein for Three Different Disease-Related Amyloidogenic Proteins. *ChemBioChem* **16**, 411–414 (2015).

4.7 List of Figures

4.9 List of Abbreviations

°C	Degrees Celsius
AL amyloidosis	Light chain amyloidosis
CD	Circular dichroism
Conc	Concentrated
COS	Cold osmotic shock
Dia	Dialysis
EDTA	Ethylenediaminetetraacetic acid
Elu	Elution
FT	Flow-through
h	hour
IAPP	Islet amyloid polypeptide
IEC	Ion exchange chromatography
IgG	Immunoglobulin g antibody
IPTG	isopropyl-beta-D-thiogalactopyranoside
kDa	kilo Dalton
M	Molar
$MgCl_2$	Magnesium chloride
$MgSO_4$	Magnesium sulfate
mM	Milli molar
nm	Nano meter
OS	Osmotic shock
PBS	Phosphate buffered saline
rpm	revolutions per minute
SDS-PAGE	Sodium dodecyl sulfate – Polyacrylamid gel electrophoresis
SEC	Size exclusion chromatography
ThT	Thioflavin T
Tris	Tris(hydroxymethyl)aminomethan
Tris-HCl	Tris(hydroxymethyl)aminomethane-hydrochlorid acid
µM	Mikro molar

Project 5 [Publication]: *An engineered monomer binding-protein for α-synuclein efficiently inhibits the proliferation of amyloid fibrils*

Content

Article information

Title of manuscript: An engineered monomer binding-protein for *a*-synuclein efficiently inhibits the proliferation of amyloid fibrils

Authors: Emil Dandanell Agerschou[1†], Patrick Flagmeier[2,3†], Theodora Saridaki[4], Céline Galvagnion[5,6], Daniel Komnig[4], Laetitia Heid[1], Vibha Prasad[4], Hamed Shaykhalishahi[1], Dieter Willbold[1,7], Christopher M Dobson[2,3], Aaron Voigt[4], Bjoern Falkenburger[4,8,9]*, Wolfgang Hoyer[1,7]*, Alexander K Buell[1,10]*

Journal: eLife

Status: Published (August 2019)

[1]Institut für Physikalische Biologie, Heinrich Heine University Düsseldorf, Düsseldorf, Germany

[2]Department of Chemistry, University of Cambridge, Cambridge, United Kingdom

[3]Centre for Misfolding Diseases, University of Cambridge, Cambridge, United Kingdom

[4]Department of Neurology, RWTH Aachen University, Aachen, Germany

[5]RG Mechanisms of Neuroprotection, German Centre for Neurodegenerative Diseases (DZNE), Bonn, Germany

[6]Department of Pharmacology and Drug Design, University of Copenhagen, Copenhagen, Denmark

[7]Institute of Complex Systems (ICS-6), Structural Biochemistry, Forschungszentrum Jülich, Jülich, Germany

[8]Department of Neurology, Dresden University Medical Center, Dresden, Germany

[9]JARA BRAIN Institute II, Julich and Aachen, Germany

[10]Department of Biotechnology and Biomedicine, Technical University of Denmark, Kgs. Lyngby, Denmark

*For correspondence: bjoern.falkenburger@ukdd.de (BF)
wolfgang.hoyer@uni-duesseldorf. de (WH)
alebu@dtu.dk (AKB)

†These authors contributed equally to this work

Declaration of article contributions:

Emil Dandanell Agerschou, Software, Formal analysis, Investigation, Visualization, Writing—original draft, Writing—review and editing

Patrick Flagmeier, Investigation, Visualization

Theodora Saridaki, Daniel Komnig, Vibha Prasad, Formal analysis, Investigation, Writing—review and editing

Céline Galvagnion, Laetitia Heid, Investigation, Writing—review and editing

Hamed Shaykhalishahi, Resources, Investigation, Methodology

Dieter Willbold, Christopher M Dobson, Funding acquisition, Writing—review and editing; Aaron Voigt, Formal analysis, Investigation, Visualization, Writing—review and editing

Bjoern Falkenburger, Conceptualization, Formal analysis, Supervision, Funding acquisition, Methodology, Writing—original draft, Project administration, Writing—review and editing

Wolfgang Hoyer, Conceptualization, Supervision, Funding acquisition, Methodology, Writing—original draft, Project administration, Writing—review and editing

Alexander K Buell, Conceptualization, Data curation, Formal analysis, Supervision, Funding acquisition, Validation, Investigation, Visualization, Methodology, Writing—original draft, Project administration, Writing—review and editing

Abstract

Removing or preventing the formation of α-synuclein aggregates is a plausible strategy against Parkinson's disease. To this end, we have engineered the β-wrapin AS69 to bind monomeric α-synuclein with high affinity. In cultured cells, AS69 reduced the self-interaction of α-synuclein and formation of visible α-synuclein aggregates. In flies, AS69 reduced α-synuclein aggregates and the locomotor deficit resulting from α-synuclein expression in neuronal cells. In biophysical experiments in vitro, AS69 highly sub-stoichiometrically inhibited both primary and autocatalytic secondary nucleation processes, even in the presence of a large excess of monomer. We present evidence that the AS69-α-synuclein complex, rather than the free AS69, is the inhibitory species responsible for sub-stoichiometric inhibition of secondary nucleation. These results represent a new paradigm that high affinity monomer binders can lead to strongly substoichiometric inhibition of nucleation processes.

5.1 Introduction 5

Cytoplasmic aggregates of the protein α-synuclein are the pathological hallmark of Parkinson's disease (PD) and other synucleinopathies (Spillantini et al., 1997). Point mutations in the α-synuclein gene or triplication of the α-synuclein locus are associated with familial forms of PD, and the α-synuclein locus is a genetic risk factor for sporadic PD (Obeso et al., 2017). α-synuclein aggregate pathology was demonstrated to propagate from neuron to neuron (Desplats et al., 2009), and recent work has focused on understanding the cellular and molecular events in this process. From a therapeutic perspective, α-synuclein aggregation is thought to be the underlying cause of PD and remains the focus of causal therapeutic strategies. The link between α–synuclein aggregation and PD has been known for two decades (Spillantini et al., 1997; Conway et al., 1998); however, translation of this scientific discovery into a therapy has proven challenging. From the first description of small molecules that inhibit α-synuclein aggregation in 2006 (Masuda et al., 2006), the search for promising compounds has continued (Wagner et al., 2013; To´th et al., 2014; Wrasidlo et al., 2016; Perni et al., 2017; Kurnik et al., 2018). While the first small molecules also inhibited the aggregation of tau and amyloid-β, more recent compounds bind α-synuclein more selectively and show reduced α-synuclein toxicity in mouse models of PD (Wrasidlo et al., 2016). We have taken a different strategy by engineering a protein, the β-wrapin AS69, to induce formation of a β-hairpin in monomeric α-synuclein upon binding (Figure 1a) (Mirecka et al., 2014). AS69 was selected by phage display (Mirecka et al., 2014) from protein libraries based on $ZA\beta_3$, an affibody against the amyloid-β peptide (Hoyer et al., 2008; Hoyer and Härd, 2008; Luheshi et al., 2010). AS69 thus not only binds α-synuclein with high and approximately constant affinity throughout the pH range most relevant for α-synuclein aggregation (Buell et al., 2014a; Figure 1b,c), but also induces a specific conformational change - akin to molecular chaperones (Muchowski and Wacker, 2005).

AS69 induces local folding of the region comprising residues 37–54 into a β-hairpin conformation in the otherwise intrinsically disordered, monomeric α-synuclein (Figure 1a). The critical role of this region for α-synuclein aggregation is indicated by the cluster of disease-related mutation sites (Figure 1a). Accordingly, modification of the local conformation by, for example, introduction of a disulfide bond strongly modulates aggregation (Shaykhalishahi et

al., 2015). Sequestration of residues 37–54 of monomeric α-synuclein by AS69 inhibits the amyloid fibril formation of α-synuclein under conditions of vigorous shaking of the solution even at highly sub-stoichiometric ratios (Mirecka et al., 2014). Amyloid fibril formation, however, is not a one-step process but can be decomposed into different individual steps, including primary and secondary nucleation and fibril elongation. With vigorous shaking, for instance, primary nucleation can occur readily at the air-water interface (Campioni et al., 2014) and fibril fragmentation induced by the shaking amplifies the number of growth-competent fibril ends (Xue et al., 2009). To validate AS69 as a potential therapeutic

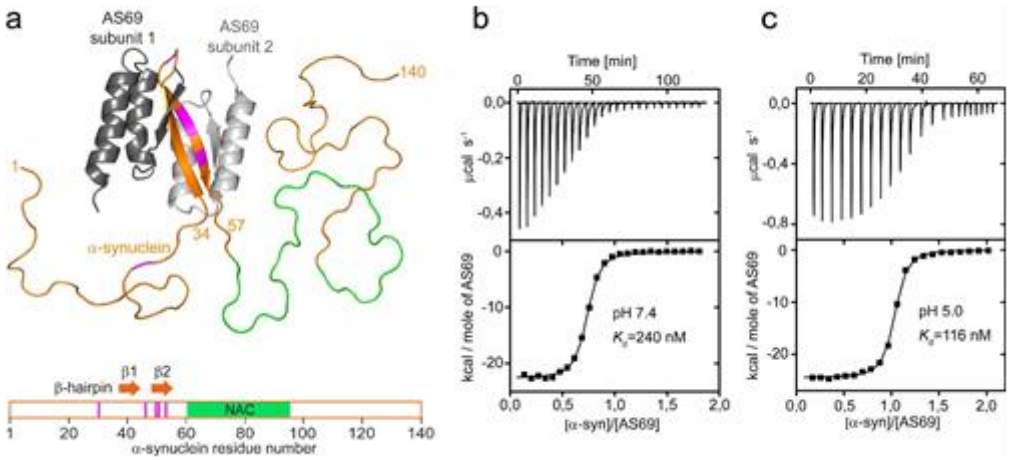

Figure 1: AS69 binds to monomeric α-synuclein, inducing local folding of the region comprising residues 37–54 into a β-hairpin conformation. (a) Structural model of the AS69: α-synuclein complex based on NMR (pdb entry 4BXL) (Mirecka et al., 2014), generated with PyMOL (The PyMOL Molecular Graphics System, 1.2; Schrödinger, LLC.). AS69 (grey) is a disulfide-linked homodimer. α-Synuclein (orange) locally adopts β-hairpin conformation, while the remainder of the molecule, including the hydrophobic NAC segment (green), remains intrinsically disordered (Mirecka et al., 2014). Positions at which disease-related mutations have been identified are given in magenta. (b,c) The affinity of AS69 to α-synuclein at pH 7.4 (b) and pH 5.0 (c) analyzed by isothermal titration calorimetry (ITC) experiments. Titration of 420 µM α-synuclein into 47 µM AS69 in 20 mM sodium phosphate, 50 mM NaCl, pH 7.4 (b), or 320 µM α-synuclein into 32 µM AS69 in 20 mM sodium acetate, pH 5.0 (c), at 30 ˚C. The upper panels show the baseline-corrected instrumental response. The lower panels show the integrated data (filled squares) and the fit to a 1:1 binding model (continuous line).

agent, we therefore tested its biological effects in cellular and animal models, and found it to be a highly efficient inhibitor of α-synuclein aggregation and associated toxicity. In addition, we designed a set of experimental conditions to measure selectively the effect of AS69 on specific steps of α-synuclein aggregation. We found that AS69 is able to efficiently interfere with both the lipid-induced formation and the auto-catalytic amplification of α-synuclein amyloid fibril formation. These inhibitory effects on nucleation are observed even in the presence of a large excess of α-synuclein monomer, which is expected to sequester AS69 into inhibitor-monomer complexes. We show evidence that the secondary nucleation of α-synuclein can be inhibited by the α-synuclein-AS69 complex and, therefore the inhibitory effect of AS69 on this crucial step of aggregate amplification is unaffected by even large excess concentrations of free α-synuclein monomer.

5.2 Results

Co-expression of AS69 reduces visible α-synuclein aggregates in cell culture

First, we explored the effect of the expression of AS69 on the viability of living cells and the association of α-synuclein in a cellular environment. In these model systems we not only expressed WT α-synuclein but also the A53T variant, which has been associated with familial PD and which produces aggregates more quickly than the WT protein (Conway et al., 1998; Flagmeier et al., 2016). We first used bimolecular fluorescence complementation (BiFC) to probe whether AS69 can interfere with formation of oligomeric α-synuclein species in living HEK293T cells (Falkenburger et al., 2016). Constructs of WT and A53T α-synuclein were tagged with the C-terminal segment of the fluorescent protein Venus (synuclein-VC) or with the complementary N-terminal segment of this protein (VN-synuclein) (Figure 2a). Neither of the two Venus fragments shows significant fluorescence by itself, but together they can generate a functional fluorescent protein (Bae et al., 2014) and hence function as a reporter for protein-protein interaction. We then transfected HEK293T cells with both synuclein-VC and VN-synuclein, in addition to AS69 (or LacZ as a control) and determined by flow cytometry the fraction of cells that displayed Venus fluorescence (Figure 2b, the raw data can be found in the table in Figure 2—source data 1). In the absence of AS69, the fraction of fluorescent cells was larger with the expression of A53T-α-synuclein than WT-α-synuclein (Figure 2b, $p<0.05$, two-way ANOVA). Co-expression of AS69 with both variants reduced the number and fraction of fluorescent cells (Figure 2b, $p<0.05$ for WT and $p<0.01$ for A53T, two-way ANOVA). AS69 did not, however, significantly affect the total quantity of α-synuclein in the cells, as determined from immunoblots (Figure 2c and d). This finding is consistent with the hypothesis that the effects of AS69 in this cellular model system result from inhibition of a direct interaction between α-synuclein molecules, and not from an enhanced clearance of α-synuclein. Despite the enhanced affinity for self-interaction which the fluorescence complementation tag might convey to α-synuclein compared to the untagged protein, the affinity for AS69 is high enough to sequester a significant proportion of the α-synuclein in living cells.

Having established that α-synuclein and AS69 can interact in cells, we next probed the effects of AS69 on the formation of larger, optically visible aggregates of α-synuclein by transfecting HEK293T cells with A53T-α-synuclein tagged with enhanced green fluorescent protein (EGFP) as previously described (Opazo et al., 2008; Karpinar et al., 2009; Dinter et al., 2016;

Figure 2e). The distribution of EGFP within transfected cells was classified as 'homogenous', 'containing particles' or 'unhealthy' (rounded cells that in time-lapse microscopy were observed to subsequently undergo apoptosis). Co-expression of AS69 with A53T α-synuclein led to an increase in the fraction of cells with a 'homogenous' distribution of EGFP and fewer cells showed α-synuclein particles relative to those cells without AS69 (Figure 2f). These findings indicate that the co-expression of AS69 reduces formation of visible aggregates in cultured human cells.

Co-expression of AS69 rescues A53T α-synuclein-dependent phenotype in *Drosophila melanogaster*

Subsequently, we tested the effects AS69 has in *Drosophila melanogaster* (fruit flies) expressing untagged A53T-α-synuclein in neurons (Figure 3). In the absence of AS69, these flies show a progressive reduction in the spontaneous climbing (i.e. neuronal impairment) between 15 and 25 days of age (Butler et al., 2012; Dinter et al., 2016; illustrated in Figure 3a). We then generated flies co-expressing either AS69 or GFP (as a control) with A53T α-synuclein in neurons. Flies expressing AS69 and A53T α-synuclein showed preserved climbing behaviour (Figure 3b, two-way ANOVA), demonstrating that neuronal expression of AS69 reduces the phenotype in this fly model of A53T α-synuclein toxicity. We further went on to determine whether or not the observed effect of AS69 on climbing behaviour could result from a reduction in the number of α-synuclein aggregates and used flies expressing in all neurons one copy of A53T-α-synuclein fused to VC, one copy of A53T-α-synuclein fused VN (Prasad et al., 2019), and, in addition, AS69 or 'always early RNAi' (see Materials and methods section) as a control. Aggregates of α-synuclein were quantified by a filter trap assay in which urea-treated lysates of fly heads were passed through a membrane and the quantity of α-synuclein aggregates retained in the membrane was detected by antibodies raised against α-synuclein (illustrated in Figure 3c). We found that the quantity of aggregates retained in the filter was significantly smaller in lysates from flies co-expressing AS69 and A53T-α-synuclein than in lysates from flies only expressing VN- and VC-tagged A53T-α-synuclein (Figure 3d and e). These findings confirm that AS69 reduces high molecular weight aggregates of α-synuclein in neuronal cells of *Drosophila melanogaster*.

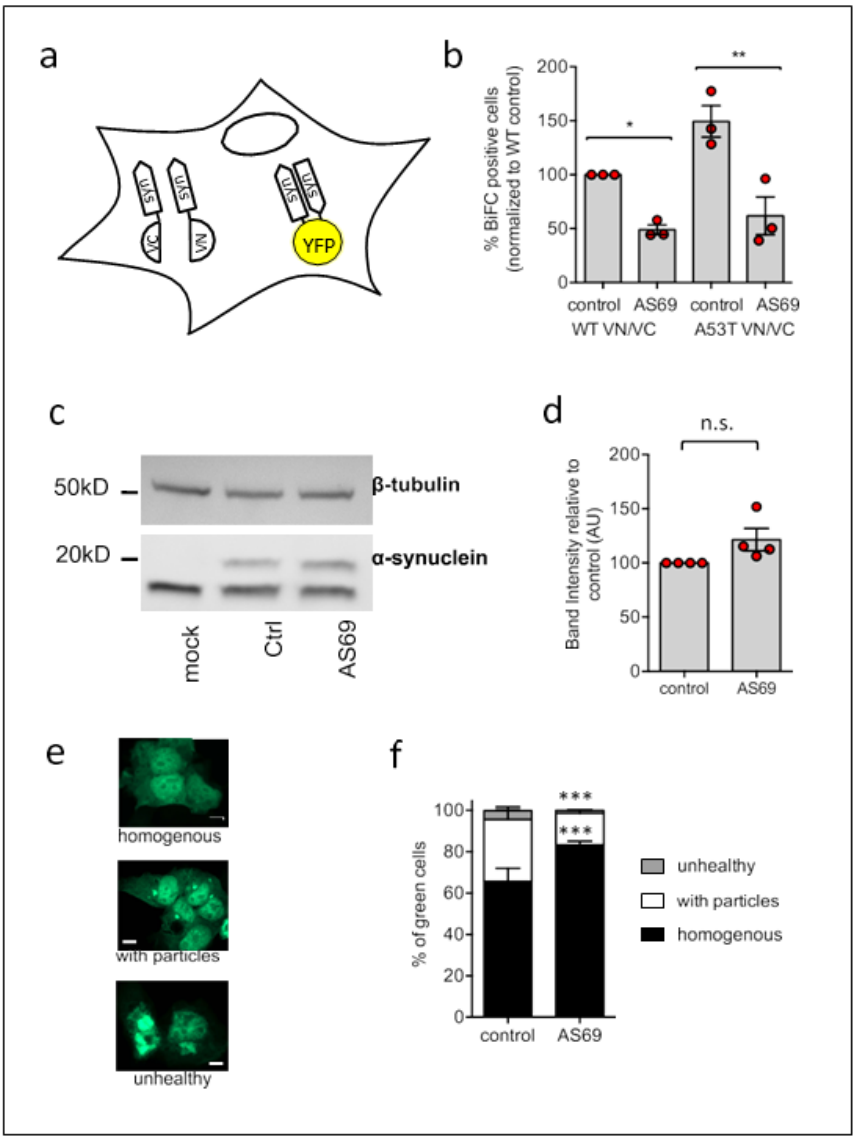

Figure 2. AS69 reduces aggregation of α-synuclein in cellular models. (a) Schematic representation of bimolecular fluorescence complementation where α-synuclein is tagged by either the C-terminal (VC) or the N-terminal (VN) fragment of the Venus protein. In dimers or larger oligomers of α-synuclein, the two Venus fragments can form a functional fluorescent protein. (b) The percentage of cells with BiFC fluorescence as determined by flow cytometry. HEK293T cells were transfected with α-synuclein (WT or A53T), fused to the VN or VC fragment and either LacZ (control) or AS69. Displayed are the results of n = 3 independent experiments and mean ± SEM. In each experiment, 75,000 cells were analyzed per group. Results were compared by one-way ANOVA, results of Sidak's posthoc test depicted. (c) Immunoblot of lysates of cells transfected with EGFP-tagged α-synuclein and, in addition, AS69 or LacZ (control), developed with antibodies against α-synuclein (band just below 20 kDa, note that only the upper band reports a-synuclein, *Dinter et al., 2016*) and β-tubulin (band just below 50 kDa), the latter as a loading control. (d) Quantification of n = 4

independent blots as described in (c). Results were compared by t-test. (e) HEK293T cells were transfected with EGFP-tagged α-synuclein and the distribution of fluorescence was classified into the depicted groups. (f) Summarized results of n = 3 independent experiments with n = 300 cells classified per group in each experiment (mean ± SEM). Results were compared by two-way ANOVA and Sidak's posthoc test.

The online version of this article includes the following source data and figure supplement(s) for figure 2:

Source data 1. Raw cell counts of cells from the three independent experiments shown in *Figure 2b*.

Figure supplement 1. Complete Western blot (*Figure 2c*) from cell culture lysates showing the loading control with β-tubulin at 50 kD, two nonspecific bands visible also in mock transfected cells, that is without α-synuclein expression, and one specific band just below 20 kD (*).

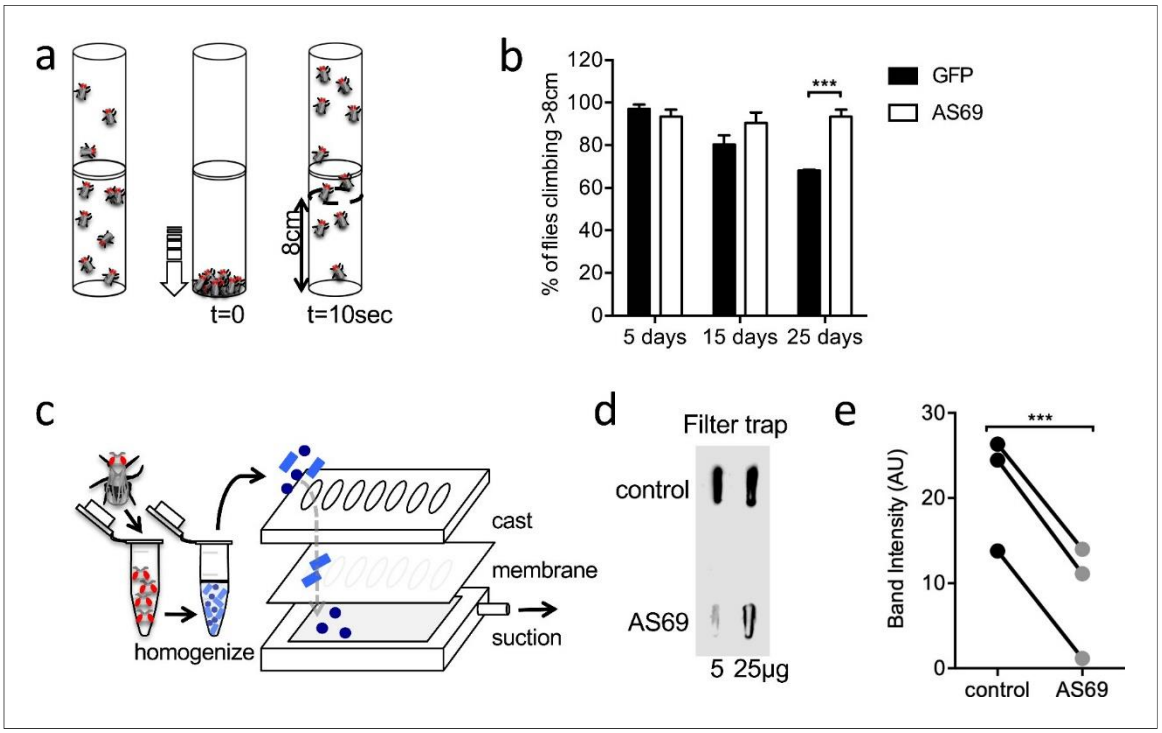

Figure 3: AS69 rescues the motor phenotype and reduces α-synuclein aggregation in *Drosophila melanogaster*. (a) Schematic representation of the climbing assay. The vials are tapped to move the flies to the base of the vial, and thereafter the flies climb towards the top of the vial; in this experiment the number of flies climbing 8 cm in 10 s was determined. (b) Performance in the climbing assay of *Drosophila melanogaster* expressing A53T-α-synuclein and either AS69 or GFP in neurons. At each time point, n = 30 flies were assayed per genotype; similar findings were observed for eight different lines expressing AS69. Results were compared by two-way ANOVA and Sidak's posthoc test. (c) Schematic representation of the filter trap assay in which aggregates in the protein lysate are retained by a membrane, which is subsequently developed in the same manner as an immunoblot. (d) Results of the filter trap assay from lysates of control flies and flies expressing AS69 in addition to A53T-α-synuclein in all neurons. Two different quantities of the protein lysate were applied in each case, 5 and 25 µg. (e) Summary of the quantification of n = 3 dot blots as in (d). Only the 25 µg band was quantified. Results were compared by t-test.

AS69 stoichiometrically inhibits the elongation of α-synuclein fibrils

We next set out to elucidate the origin of the remarkable ability of AS69 to inhibit α-synuclein aggregate formation in cells and in vivo (Figure 2, Figure 3), and amyloid fibril formation in vitro (Mirecka et al., 2014). To this end, we performed a detailed mechanistic analysis, where we examined the effect of AS69 on the growth (Buell et al., 2014a), autocatalytic amplification (Buell et al., 2014a; Flagmeier et al., 2016) and lipid-induced formation (Galvagnion et al., 2015) of α-synuclein amyloid fibrils. We first carried out experiments in the presence of micromolar concentrations (in

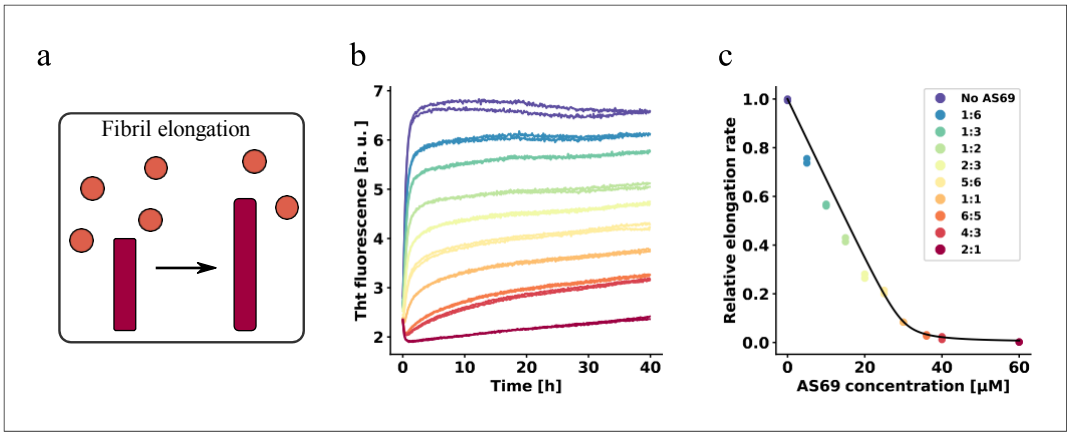

Figure 4: AS69 inhibits α-synuclein fibril elongation. (a) Schematic representations of fibril elongation. (b) Change in ThT fluorescence when a 30 mM solution of monomeric a-synuclein was incubated in the presence of 5 mM pre-formed fibrils under quiescent conditions with increasing concentrations of AS69. (c) Relative rates of fibril elongation with increasing concentrations of AS69. The solid line corresponds to a prediction based on the affinity of AS69 for monomeric a-synuclein (240 nM, Figure 1b [*Mirecka et al., 2014*], see Appendix 1 for details).

The online version of this article includes the following figure supplement(s) for figure 4:

Figure supplement 1. Characterisation of α-synuclein fibrils formed in the presence and absence of AS69 by AFM.

Figure supplement 2. Binding specificity determines the inhibitory activity.

monomer equivalents) of pre-formed seed fibrils of α-synuclein at neutral pH under quiescent conditions (Figure 4a,b). We have shown previously that under these conditions only fibril elongation through addition of monomeric α-synuclein to fibril ends occurs at detectable rates (Buell et al., 2014a), and that the rate of de novo formation of fibrils is negligible. We therefore examined the effects of AS69 on fibril elongation and analyzed these data by fitting linear functions to the early stages of the aggregation time courses (see Appendix 1 for details of the analysis). The results indicate that fibril elongation is indeed inhibited by AS69 in a stoichiometric concentration-dependent manner (Figure 4c). In this experiment, both the seed fibrils and the AS69 compete for the monomeric α-synuclein, and the relative affinities determine the kinetics and thermodynamics of the system.

To obtain an estimate of the affinity of monomeric α-synuclein for the ends of fibrils, we performed elongation experiments at low monomer concentrations in the absence of AS69. We found evidence that the fibrils are able to elongate in the presence of 0.5 μM monomeric α-synuclein (see Appendix 1), providing an upper bound of the critical concentration (which is formally equivalent to a dissociation constant, see Appendix 1). Despite the similar affinity of monomeric α-synuclein for both fibril ends and AS69, the timescales of the two types of interactions are very different; monomeric α-synuclein was found to interact on a timescale of seconds with AS69, as seen by isothermal titration calorimetry (ITC) experiments (Mirecka et al., 2014 and Figure 1b and c), but to incorporate on a timescale of minutes to hours into free fibril ends (see Figure 4b and Buell et al., 2014a; Wördehoff et al., 2015). The slow kinetics of the latter process is partly because the number of fibril ends is much smaller than the number of monomers (Buell et al., 2014a), such that each fibril sequentially recruits many α-synuclein molecules. Therefore, the equilibrium between AS69 and α-synuclein should be rapidly established and perturbed only very slowly by the presence of the fibrils.

Inhibition of fibril elongation is caused by monomer sequestration

The initial fibril elongation rate as a function of AS69 concentration was found to follow closely the predicted concentration of unbound α-synuclein across the entire range of concentrations of AS69 used in this study, as shown in Figure 4c, where the solid line corresponds to the predicted elongation rate, assuming fibrils can only be elongated by unbound α-synuclein. The inhibition of fibril elongation can therefore be explained quantitatively by the sequestration of

monomeric α-synuclein by AS69 and the assumption that the AS69:α-synuclein complex cannot be incorporated into the

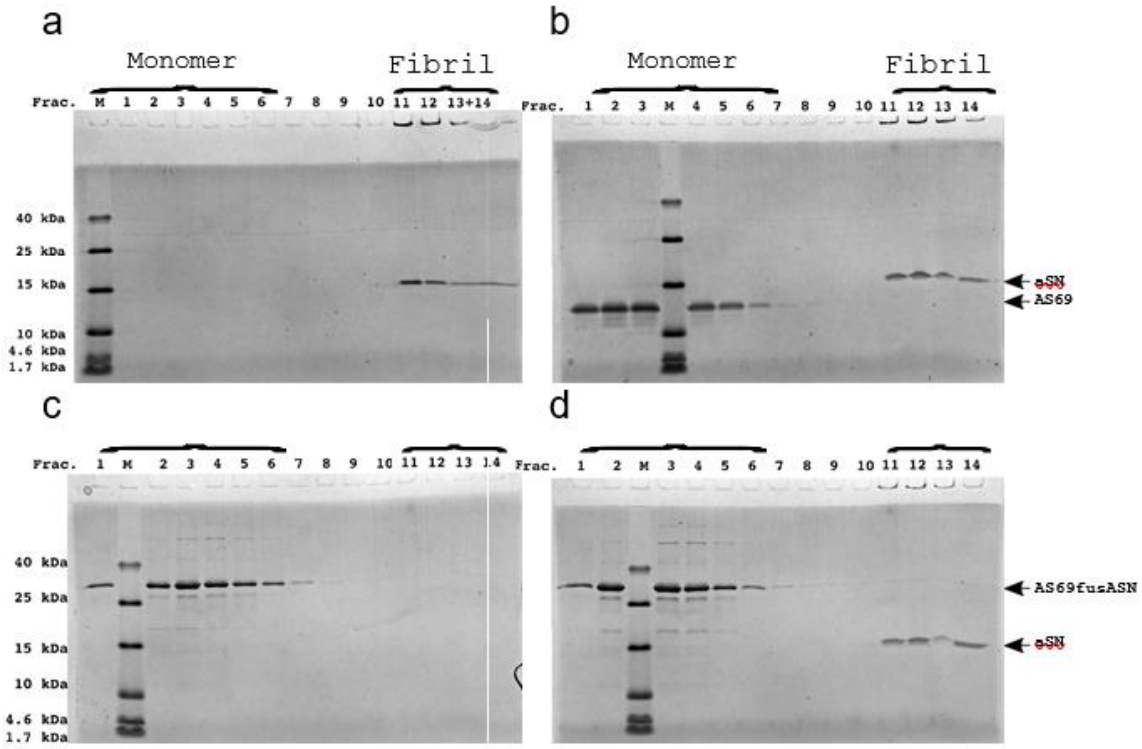

Figure 5: SDS-PAGE of density gradient centrifugation (DGC) experiments to probe the binding of AS69 to α-synuclein fibrils at pH 7.4 after elongation experiments. (a) 25 μM seeds, (b) 25 μM AS69 and 25 μM seeds, (c) 16.7 μM AS69fusASN, (d) 25 μM AS69fusASN and 25 μM seeds

growing fibril. This conclusion is supported by the finding that the fibrils formed in the presence of increasing concentrations of AS69 are morphologically indistinguishable from the fibrils formed in the absence of AS69 (as judged from AFM images, see Figure 4—figure supplement 1). Our kinetic analysis of fibril elongation in the presence of AS69 does not, however, suggest a preferential interaction with fibril ends, as such an interaction can be expected to lead to a sub-stoichiometric inhibition of fibril elongation, which is not observed in our experiments. Indeed, the finding that the effect on elongation can be quantitatively described by considering only the interaction of AS69 with monomeric α-synuclein (Appendix 1) suggests a weak, if any, interaction of AS69 with fibrils. Furthermore, density gradient centrifugation (DGC) of samples containing only seeds and AS69 (Figure 5a and b) did not show AS69 to co-migrate

with large species to any significant extent under conditions that favour elongation. In agreement with inhibition of fibril elongation by monomer sequestration, ZAβ3W, a binding protein for amyloid-β peptide (Grüning et al., 2013), which is a significantly weaker α-synuclein binder than AS69, correspondingly showed a considerably weaker inhibitory effect on α-synuclein fibril elongation (Figure 4—figure supplement 2).

AS69 sub-stoichiometrically inhibits amplification of α-synuclein fibrils

These findings clearly demonstrate that AS69 inhibits fibril elongation in a stoichiometric manner through monomer sequestration. Consequently, inhibition of fibril elongation cannot explain the previously observed sub-stoichiometric inhibition of α-synuclein fibril formation by AS69 (Mirecka et al., 2014). We therefore performed seeded experiments under mildly acidic solution conditions in the presence of very low concentrations of pre-formed fibrils (nM monomer equivalents) under quiescent conditions (Figure 6a,b) (Buell et al., 2014a; Gaspar et al., 2017). Under those solution conditions, seeded aggregation has been shown to consist of two processes in addition to fibril elongation, namely secondary nucleation, which increases the number of growth competent fibril ends, and higher order assembly ('flocculation', Figure 6—figure supplement 1b,c), which decreases the overall aggregation rate by reducing the number of accessible fibrils through their burial within higher order aggregates (Buell et al., 2014a). The de novo formation of amyloid fibrils through primary nucleation is suppressed if the solution is not agitated and if non-binding surfaces are used (Figure 6—figure supplement 1a). We find that under these solution conditions, where only growth and secondary nucleation contribute to the increase in fibril mass and number, respectively, the seeded aggregation is inhibited in a strongly sub-stoichiometric manner (Figure 6b,c). We analysed these data to determine the maximum rate of aggregation (see Appendix 2 for details) using the framework from Cohen et al. (2011) (Figure 6c). Based on recent results on the concentration-dependence of autocatalytic secondary nucleation of α-synuclein amyloid fibrils (Gaspar et al., 2017), we have calculated the predicted inhibitory effect from monomer sequestration by AS69 in Figure 6c (see Figure 6—figure supplement 2 and Appendix 2 for details). We find that, unlike the case of fibril elongation, monomer sequestration cannot explain the extent of inhibition, even by assuming a very high reaction order of 5 (i.e. a dependence of the rate of secondary nucleation on the 5th power of the free monomer concentration; $dP(t)/dt \propto m(t)^5$) which is not compatible with recent results, showing that secondary nucleation of α-synuclein amyloid

fibrils depends only weakly on the concentration of free monomer (Gaspar et al., 2017). However, even in this unlikely scenario, the very strong inhibitory effect of low AS69 concentrations cannot be explained by monomer depletion.

Sub-stoichiometric inhibition of fibril amplification is not caused by interaction with the fibril surface

We have previously been able to rationalise inhibition of the secondary nucleation of α-synuclein by the homologous protein β-synuclein through competition for binding sites on the surface of the fibrils (Brown et al., 2016). Here we find that AS69 is a significantly more efficient inhibitor of the autocatalytic amplification of α-synuclein amyloid fibrils than β-synuclein (a similar degree of inhibition is achieved with a 10-fold lower concentration ratio). This result is particularly interesting in the light of the fact that AS69 binds efficiently to monomeric α-synuclein under both neutral and mildly acidic solution conditions (Figure 1b,c), whereas we found no evidence for a relevant direct interaction between the monomeric forms of α- and β-synuclein, given the complete absence of any inhibitory effect of β-synuclein on the elongation of α-synuclein fibrils (Brown et al., 2016). Therefore, despite the vast majority of the AS69 being bound within a complex with monomeric α-synuclein, AS69 is an efficient sub-stoichiometric inhibitor of the secondary nucleation of α-synuclein. This finding suggests that in addition to inhibiting through competition for nucleation sites on the fibril surface, AS69 or its complex with α-synuclein could interact directly with intermediates of the secondary nucleation process. To investigate whether AS69 binds to the fibril surface under these secondary nucleation-inducing solution conditions, we performed additional DGC experiments. Co-migration in the density gradient of AS69 with fibrils, which would imply direct interactions between these species, was undetectable (Figure 7a–c). If AS69 was able to inhibit secondary nucleation through binding to the fibril surface in the presence of a large excess of monomer, its affinity to fibril surfaces would need to be much higher than to monomeric α-synuclein. This implies that under the conditions of the DGC experiments which were performed in the absence of monomeric α-synuclein, all binding sites on the fibrils should be occupied. Therefore, the absence of detectable binding implies either a weak affinity for fibrils or a very low stoichiometry, that is a very low density of binding sites for AS69 on the fibril surface.

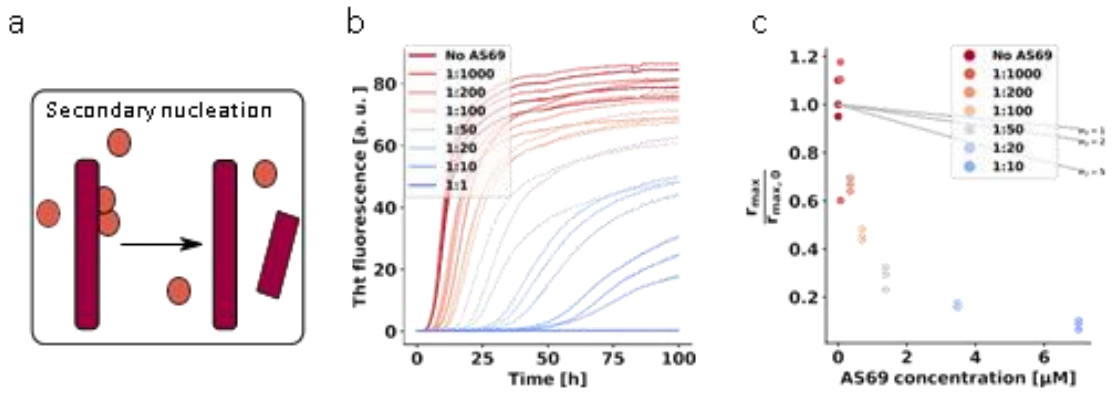

Figure 6: AS69 inhibits α-synuclein fibril amplification. (a) Schematic representation of fibril amplification through secondary nucleation Buell et al. (2014a). (b) Change in ThT fluorescence intensity when a 70 μM solution of monomeric α-synuclein was incubated with increasing concentrations of AS69 in acetate buffer (pH 5.0) under quiescent conditions and weak seeding. (c) Relative rate of fibril amplification as a function of the concentration of AS69. The solid lines correspond to simulations based on the assumption that AS69 acts only through monomer sequestration, for different values of the monomer dependence (reaction order) of secondary nucleation (see Appendix 2 for details).

The online version of this article includes the following figure supplement(s) for figure 6:

Figure supplement 1. Seeds are required for aggregation under quiescent conditions.

Figure supplement 2. Weakly seeded aggregation experiments at pH 5.0.

Figure supplement 3. AS69 interacts with two distinct a-synuclein species.

AS69 binds to stable α-synuclein oligomers with comparable affinity as to monomers

We next tested whether binding of AS69 to oligomeric states of α-synuclein could explain the efficient inhibition of secondary nucleation. The heterogeneous and often transient nature of oligomeric intermediates on the pathway to formation of amyloid fibrils makes any interaction between such species and AS69 difficult to probe. However, monomeric α-synuclein can be converted into kinetically stable oligomers that can be studied in isolation, because they do not readily convert into amyloid fibrils (Lorenzen et al., 2014). Despite it not being likely that these species are fibril precursors, they are intermediate in size and structure between monomeric and fibrillar α-synuclein and hence can serve as a model for AS69 binding to α-synuclein

oligomers. Using microscale thermophoresis (MST, Wolff et al., 2016) at neutral pH, we were able to confirm the binding of AS69 to both monomeric (Figure 6—figure supplement 3a) and oligomeric α-synuclein (Figure 6—figure supplement 3b) and provide estimates of the respective binding affinities (ca. 300 nM for monomeric and ca. 30 nM for oligomeric α-synuclein). The former value is in good agreement with results from ITC experiments under the same solution conditions (Figure 1b and Mirecka et al., 2014), whereas the affinity of AS69 to oligomeric α-synuclein has not previously been determined. The finding that AS69 is able to inhibit secondary nucleation in a highly sub-stoichiometric manner in the presence of a large excess of free monomer, to which it binds with high affinity, necessitates that the interactions of AS69 with aggregation intermediates must be of significantly higher affinity, if they are to explain the inhibition. Otherwise, the monomer would out-compete the aggregation intermediate for AS69 binding, because of the much lower concentration of the latter. An estimate (see Appendix 2 for details) suggests that the affinity of AS69 for aggregation intermediates would need to be several orders of magnitude higher than to α-synuclein monomer to explain an inhibitory effect of the observed magnitude. This required affinity is indeed much higher than the affinity we have determined here for an oligomeric state of α-synuclein.

A covalent complex of AS69 and α-synuclein efficiently inhibits secondary nucleation

The analysis described in the previous section suggests, therefore, that the α-synuclein:AS69 complex itself could be the inhibitory species. The population of this complex is sufficiently high, even at low ratios of AS69:α-synuclein, to interact with a considerable fraction of aggregation intermediates. It is possible, therefore, that while the AS69:α-synuclein complex is unable to incorporate into a fibril end (see section above on the stoichiometric inhibition of fibril elongation), it can interact with oligomeric fibril precursors and block their conversion into fibrils. We tested this hypothesis by producing a molecular construct whereby α-synuclein and AS69 are linked together with a flexible glycine tether that allows formation of an intramolecular complex (AS69fusASN). The formation of the intra-molecular complex was verified by performing CD spectroscopy at 222 nm over the temperature range from 10 to 90˚C and fitting the data to a two-state model (Pace et al., 1998) (see Figure 8— figure supplement 1). Both at neutral and mildly acidic pH, the fusion construct AS69fusASN has a higher thermal stability than the free AS69 and, indeed, as the stoichiometric mixture of AS69 and α-synuclein

(Table 1). The difference in melting temperatures between the covalent and non-covalent complex can be explained by the differences in the entropy of binding, which is more

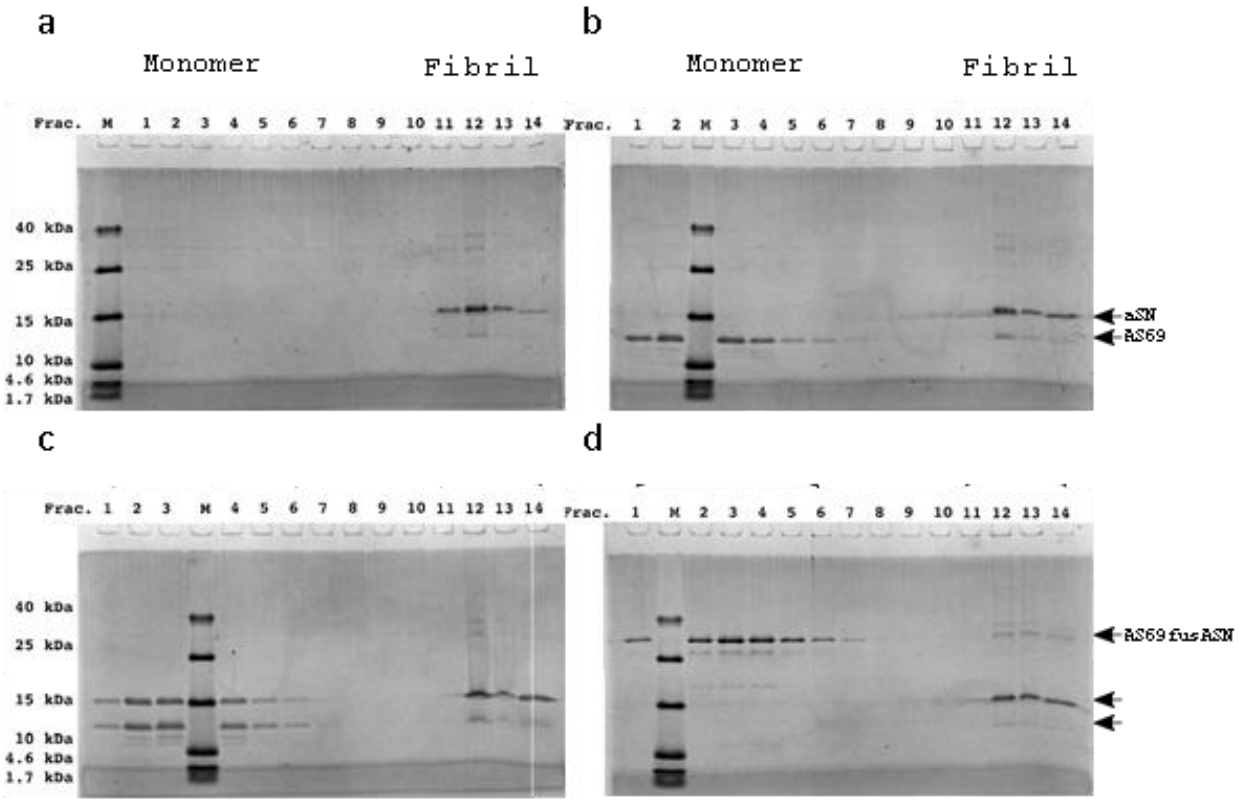

Figure 7: SDS-PAGE of density gradient centrifugation experiments to probe for binding of AS69 to fibril surfaces at pH 5.0. (a) 12.5 μM seeds, (b) 12.5 μM AS69 and 12.5 μM seeds, (c) 12.5 μM AS69, 12.5 μM seeds and 12.5 μM monomer, and (d) 12.5 μM AS69fusASN and 12.5 μM seeds.

unfavourable in the case of the non-covalent complex, given the loss of three degrees of freedom of translational motion upon binding.

We performed weakly seeded aggregation experiments under conditions where secondary nucleation leads to the amplification of the added seed fibrils (see above) at different concentrations of AS69 (Figure 8a,c), as well as AS69-α-synuclein complex (Figure 8b,d) We found that the pre-formed complex is a similarly efficient inhibitor as the free AS69 under secondary nucleation conditions (Figure 8e). These results provide strong support for our hypothesis that the AS69-α-synuclein complex, covalent or non-covalent, is the species that is

responsible for the sub-stoichiometric inhibition of secondary nucleation. Therefore, we propose a model whereby rather than requiring the binding of free AS69 to an aggregation intermediate, the AS69:α-synuclein complex is able to incorporate into a fibril precursor and efficiently prevent it from undergoing the structural rearrangement required to transform into a growth-competent amyloid fibril.

AS69 inhibits lipid-induced aggregation of α-synuclein

Having established and rationalised the high efficiency of AS69 to inhibit autocatalytic amplification of α-synuclein amyloid fibrils through secondary nucleation, we next investigated whether the de novo formation of α-synuclein amyloid fibrils is also efficiently inhibited. As experimental setup, we chose a recently developed paradigm of lipid-induced aggregation (Galvagnion et al., 2015), which allows analysis of the resulting kinetic data in a more quantitative manner compared to the widely employed conditions of strong mechanical agitation and high affinity multiwell plate surfaces. In the latter conditions, the dominant role of the air-water interface (Campioni et al., 2014) as well as of fragmentation have rendered challenging quantitative analysis of the resulting data. In the lipid-induced aggregation, under quiescent conditions and in non-binding plates, the nucleation on the lipid vesicles is the dominant source of new α-synuclein amyloid fibrils. We therefore probed the

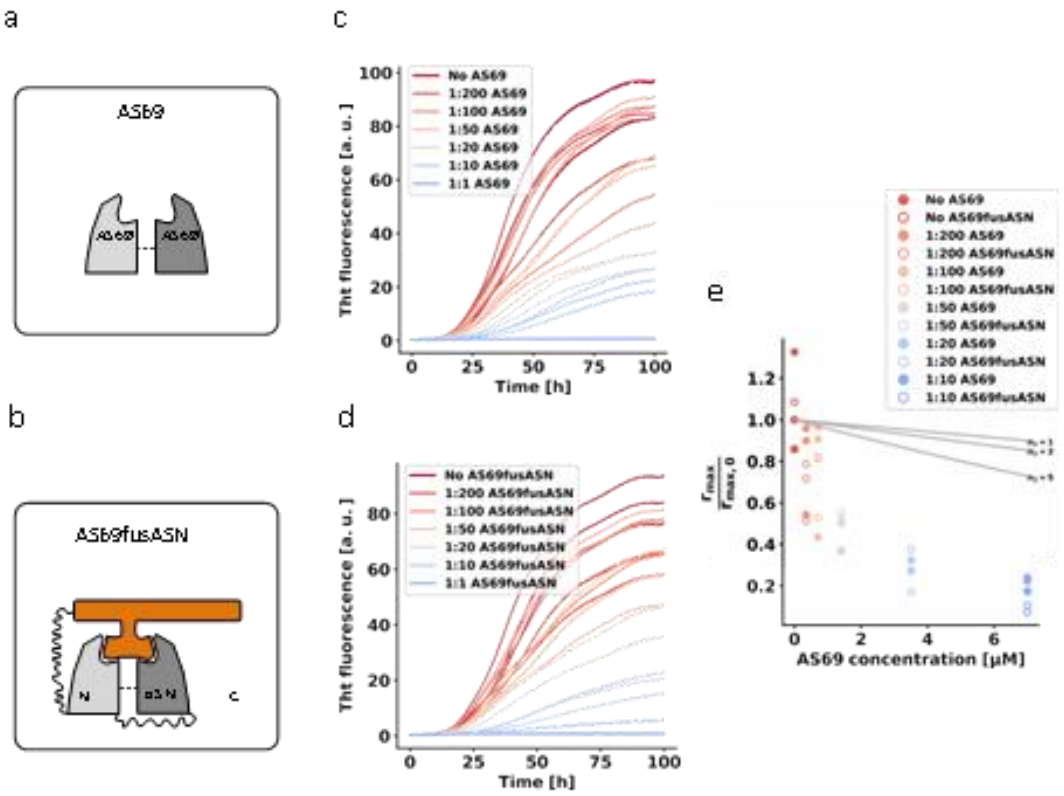

Figure 8: AS69 and AS69fusASN inhibit α-synuclein fibril amplification to similar extent. (a) and (b) Schematic representations of AS69 and AS69fusASN, respectively. (c), (d) Change in ThT fluorescence when a 70 μM solution of monomeric α-synuclein was incubated with increasing concentrations of AS69 or AS69fusASN, respectively, in sodium acetate buffer (pH 5.0) under quiescent conditions. (e) Relative maximum rate of aggregation as a function of the concentration of AS69 (closed circles) and AS69fusASN (open circles). The solid lines correspond to simulations based on the assumption that AS69 acts only through monomer sequestration, for different values of the monomer dependence (reaction order) of secondary nucleation (see Appendix 2 for details).

The online version of this article includes the following figure supplement(s) for figure 8:

Figure supplement 1. Determination of thermal stabilities of AS69 and its non-covalent and covalent complex with α-synuclein.

Figure supplement 2. Weakly seeded aggregation experiments at mildly acidic pH 5.

inhibitory effect of AS69 on lipid vesicle (DMPS-SUV)-induced aggregation of α-synuclein (Figure 9a, b). We then analysed the early times of the kinetic traces using a single-step nucleation model (Figure 9c) that includes only primary nucleation and fibril elongation (see

Appendix 3). The results reveal that AS69 inhibits lipid-induced aggregation at sub-stoichiometric concentrations to α-synuclein in a concentration-dependent manner (Figure 9c). To characterise the system α-synuclein-AS69-DMPS-SUV in more detail, we performed titration experiments where we varied the concentration of SUVs at constant α-synuclein:AS69 ratios of 10:1 and 1:1. We monitored the formation of α-helical structure, induced by binding of α-synuclein to the DMPS-SUV by circular dichroism (CD) spectroscopy (Figure 9—figure supplement 1a–c). We find that the system is well-described as a competition between the AS69 and the lipid vesicles for the monomeric α-synuclein (Figure 9—figure supplement 1d and see Materials and methods section for details of the mathematical analysis). We simulated the effects that AS69 has on the aggregation process of α-synuclein in the presence of lipids, assuming that sequestration of free monomer is the only mechanism through which AS69 inhibits the aggregation reaction (Figure 9c). The results show that the lipid-induced aggregation of α-synuclein is inhibited by AS69 significantly more strongly than predicted by monomer sequestration alone. However, before being able to conclude that AS69 inhibits the lipid-induced aggregation of α-synuclein through a mechanism similar to that defined above for secondary nucleation, it needs

Table 1. Melting temperatures, T_m, obtained from fitting of CD melting curves in *Figure 8—figure supplement 1*.
*Data from *Gauhar et al. (2014)* was refitted to obtain the numerical values listed in the table.

Construct	T_M [˚C] at pH 7.4	T_M [˚C] at pH
AS69	37.5(± 1.6)*	*36.5(± 1.8)
AS69 + a-synuclein	51.0(± 0.6)*	55.8(± 0.2)
AS69fusASN	66.5(± 0.3)	66.1 (± 0.2)

to be established whether or not AS69 can directly interact with the lipid vesicles and exert an inhibitory effect through this interaction. We have previously reported that this type of inhibition is displayed by β-synuclein, a homologous protein which directly competes with α-synuclein for binding sites on the lipid vesicles (*Brown et al., 2016*). To test for a direct interaction between AS69 and the DMPS-SUV, we performed both isothermal titration and differential scanning calorimetry (ITC and DSC, *Figure 9—figure supplement 2*). We find that

the melting temperature of DMPS vesicles is decreased in the presence of AS69 (*Figure 9—figure supplement 2a,b*) and, furthermore, titration of AS69 into DMPS-SUV reveals a complex signature of heat release and consumption (*Figure 9—figure supplement 2c,d*). While a detailed analysis of this interaction behaviour is beyond the scope of the present study, taken together these calorimetric experiments suggest indeed a direct interaction between AS69 and DMPS-SUV. Therefore, despite AS69 appearing to be a more potent inhibitor of lipid-induced aggregation than β-synuclein, with similar inhibitory effects for very different ratios of inhibitor to α-synuclein of 5:1 (β-synuclein) and 1:10 (AS69), it cannot be excluded that the same mechanism of inhibition contributes significantly to the overall inhibitory effect in lipid-induced aggregation.

5.3 Discussion

The β-wrapin AS69 is a small engineered monomer binding protein that upon coupled folding-binding induces a local β-hairpin conformation in the region comprising amino acid residues 37–54 of otherwise intrinsically disordered monomeric α-synuclein (Figure 1). AS69 shows strongly sub-stoichiometric inhibition of α-synuclein aggregation in vitro, which is remarkable for a monomer binding-protein (Mirecka et al., 2014). Here, we show that potent aggregation inhibition of AS69 can be recapitulated in cell culture as well as an animal model. In cell culture, AS69 interfered with the interaction between tagged α-synuclein molecules as judged by a fluorescence complementation assay and reduced the formation of visible aggregate particles of GFP-tagged α-synuclein (Figure 2). In fruit flies, co-expression of AS69 led to reduced abundance of large molecular weight aggregates of tagged α-synuclein and rescue of the motor phenotype resulting from neuronal expression of untagged A53T-α-synuclein (Figure 3). While the nature of the α-synuclein aggregates formed inside the cells and fly neurons remains elusive, these results show that AS69 is able to interact with different constructs and forms of α-synuclein in vivo, and hence its inhibition of α-synuclein amyloid fibril formation observed in vitro (Mirecka et al., 2014) warrants further in-depth analysis. Our detailed biophysical in vitro aggregation experiments under well-defined conditions enabled us to reveal several distinct modes of inhibition of α-synuclein amyloid fibril formation by AS69, as summarised in Figure 10. First, as expected for a monomer-binding species, AS69 inhibits fibril growth in a strictly stoichiometric manner, suggesting that the non-covalent AS69-α-synuclein complex is unable to add onto a fibril end and elongate the fibril. This is consistent with our results from DGC regarding the lack of a detectable interaction between AS69 and fibrils. Second, AS69 is found to be a very efficient inhibitor of secondary nucleation at highly sub-stoichiometric ratios. The overall result of our experimental and theoretical analysis is that this inhibitory effect is unlikely to stem from a direct interaction between the AS69 and either fibril surfaces or secondary nucleation intermediates. Such an interaction would need to be of an unrealistically higher affinity than the interaction between AS69 and α-synuclein monomer. A possible solution to this conundrum is presented by the hypothesis that the AS69-α-synuclein complex is the inhibitory species. This hypothesis gains strong support from our finding that a covalently linked complex is equally as efficient an inhibitor of secondary nucleation as the free AS69 molecule. It is important to note here that this proposed mode of action is very distinct from

other types of inhibitory behavior reported previously. For example, in the case of nanobodies raised against monomeric α-synuclein, at least stoichiometric amounts of the nanobodies are needed to interfere significantly with unseeded aggregation (Iljina et al., 2017). In the case of molecular chaperones, on the other hand, sub-stoichiometric inhibitory behaviour has been reported previously (Waudby et al., 2010; Ma˚nsson et al., 2014), but it is usually found that these molecules do not interact significantly with the monomer, but rather bind specifically to aggregated states of the protein. Therefore, the AS69 affibody represents a new paradigm in the inhibition of amyloid fibril formation: strongly sub-stoichiometric inhibition by a tight monomer-binding species. In this scenario, it is not the inhibitor itself that plays the role of a molecular chaperone, that is interacting with an on-pathway species and interfering with its further evolution, but rather the monomer-inhibitor complex acts as a chaperone. This mode of action represents a range of significant advantages over the other previously described modes of action (i.e. monomer sequestration and direct interaction with aggregation intermediates). First, it is rather straightforward to develop further molecules that bind to the monomeric forms of proteins, given that the latter are well-defined, reproducible and easy to handle. This simplicity is in contrast to the difficulty presented by targeting on-pathway aggregation intermediates which are difficult to isolate for the development of inhibitors. Second, binders of oligomeric aggregation intermediates can be expected to be less specific compared to binders of a well-defined monomeric state, as suggested by the existence of antibodies that interact with protofibrillar species independently of the protein from which they have formed (Kayed et al., 2003). This lack of specificity can potentially lead to cross-reactivity and side effects. And third, the mode of inhibition presented here avoids the need for stoichiometric amounts of inhibitors that are usually required in the case of monomer-sequestering species, resulting in a more efficient inhibition. Interestingly, we find that AS69 is a similarly potent inhibitor in a lipid-induced aggregation paradigm, whereby heterogeneous primary, rather than secondary, nucleation is the dominant source of new aggregates. However, we found the inhibitory effect in this case possibly

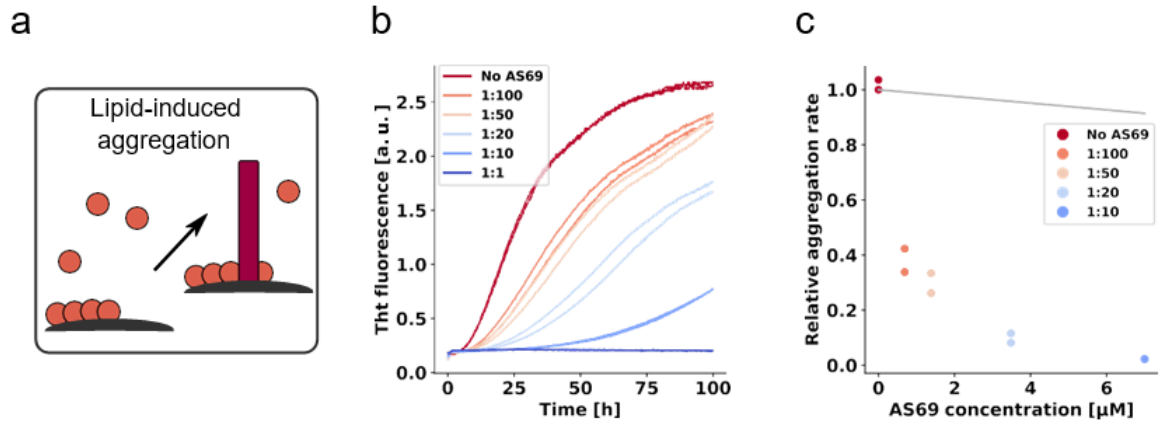

Figure 9: AS69 inhibits lipid-induced aggregation of α-synuclein. (a) Schematic representation of lipid-induced aggregation (Galvagnion et al., 2015). (b) Change in ThT fluorescence intensity when a 70 μM solution of monomeric α-synuclein was incubated with 100 μM DMPS-SUVs and increasing concentrations of AS69 in 20 mM phosphate buffer (pH 6.5) under quiescent conditions. (c) Relative rate of lipid-induced formation of α-synuclein amyloid fibrils as a function of the concentration of AS69. The solid line corresponds to a simulation based on the assumption that AS69 acts only through monomer sequestration (see Appendix 3 for details).

The online version of this article includes the following figure supplement(s) for figure 9:

Figure supplement 1. Influence of AS69 on the lipid-binding of α-synuclein monitored using circular dichroism.

Figure supplement 2. Calorimetric experiments designed to elucidate the molecular mechanism of inhibition of lipid-induced aggregation of α-synuclein by AS69.

also stemmed from a direct interaction between AS69 and the lipid vesicles. It is therefore not straightforward to decide whether the dominant mechanism of inhibition by AS69 in heterogeneous primary and secondary nucleation is closely related.

An inhibitor functioning according to this dual mode, that is being active both as a free molecule and as a complex with monomeric α-synuclein, is expected to efficiently reduce α-synuclein aggregation in vivo. This is in agreement with the cell culture and fly data we present in this manuscript. Further steps will be to test the effects of AS69 in cell-based fibril seeding assays, in mammalian dopaminergic neurons, and in PD models where synuclein aggregates are formed from endogenous a-synuclein.

In conclusion, high affinity monomer binders displaying strong sub-stoichiometric inhibition of fibril formation represent attractive agents to interfere with pathological protein aggregation, as a result of their multiple inhibitory action.

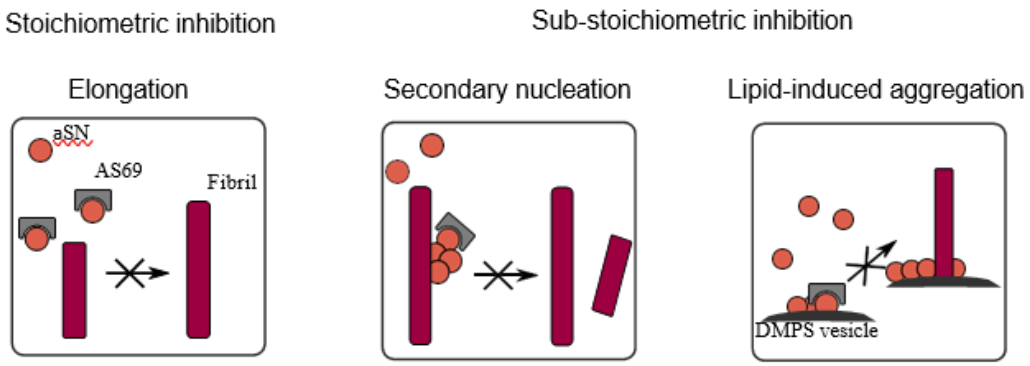

Figure 10. Summary of mechanisms by which AS69 inhibits amyloid fibril formation of α-synuclein in vitro.

5.4 Material and Methods

Reagents

Thioflavin T UltraPure Grade (ThT > 95%) was purchased from Eurogentec Ltd (Belgium). Sodium phosphate monobasic (NaH2PO4, BioPerformance Certified >99.0%), sodium phosphate dibasic (Na2HPO4, ReagentPlus, >99.0%) and sodium azide (NaN3, ReagentPlus, >99.5%) were purchased from Sigma Aldrich, UK. 1,2-Dimyristoyl-sn-glycero-3-phospho-L-serine, sodium salt (DMPS) was purchased from Avanti Polar Lipids, Inc, USA.

Protein preparation

α-synuclein was expressed and purified as described previously (Hoyer et al., 2002; Buell et al., 2014a). To determine the concentrations in solution, we used the absorbance value of the protein measured at 275 nm and an extinction coefficient of 5600 M-1cm-1. The protein solutions were divided into aliquots, flash-frozen in liquid N2 and stored at -80˚C, until used. A pET302/NT-His plasmid carrying AS69 with a N-terminal hexahistag (on each monomer) was expressed and purified as previously described (Mirecka et al., 2014) in E. coli JM109(DE3) with small modifications. Briefly, 20 µl cell culture from a glycerol stock was used to inoculate 50 ml 2YT (PanReac AppliChem) with 100 µg / ml ampicillin overnight culture, from which 5 ml was added per 500 ml 2YT medium with 100 µg / ml ampicillin. Expression was induced when OD600 reached 0.6, using IPTG to a final concentration of 1 mM, after which the cells were grown for an additional 4 h; the temperature of growth and expression was 37˚C and shaking was 110 RPM. Cells were harvested by centrifugation at 5000 g for 20 min at 4˚C, after which the cell pellets were resuspended in 50 mM Tris:Cl pH 8, 500 mM NaCl, 20 mM imidazole, and one protease inhibitor cocktail tablet (Roche) before being placed at -20˚C. Cells were thawed and lysed using a probe sonicator (Bandelin, Sonopuls UW 3200, Berlin, Germany) with a MS72 sonotrode, with pulses of 3 s with pauses of 5 s in between for a total of 5 min using 35% maximum power. Cell debris was removed by centrifugation at 13500 g for 20 min, before the supernatant was loaded on a 5 ml Histrap FF (GE Healtcare). A 50 mM imidazole- containing buffer (as opposed to 20 mM; see above) was loaded to remove unspecifically bound material before elution was performed using 250 mM imidazole. The eluate was placed on ice over-night before it was concentrated to a volume < 2.5 ml and then loaded onto a Hiload 16/600 Superdex 75 pg column, that had been

equilibrated in 20 mM NaPi, pH 7.4, 50 mM NaCl, for collection of the dimer peak. Protein concentration was measured at 275 nm with an extinction coefficient of 2800 M-1 cm-1 , protein solutions were aliquoted, flash-frozen in in liquid N2 and stored at -80˚C. AS69fusASN with a C-terminal hexahistag was expressed from a pET302/CT-His plasmid and purified identically to AS69 with the only exception that an anion exchange chromatography step was included (identical to the one used for α-synuclein). Protein concentration was measured at 275 nm with an extinction coefficient of 8400 M-1 cm-1, protein solutions were aliquoted, flash-frozen in in liquid N2 and stored at -80˚C.

Seed fibril formation

Seed fibrils were produced under different solution conditions, depending on which type of experiments they were needed for (see section on ThT experiments below).

Elongation assays

Seed fibrils were produced as described previously (Buell et al., 2014a). 500 µl samples of α-synuclein at concentrations from 500 to 800 µM were incubated in 20 mM phosphate buffer (pH 6.5) for 48–72 h at ca. 40˚C and stirred at 1500 rpm with a Teflon bar on an RCT Basic Heat Plate (IKA, Staufen, Germany). Fibrils were diluted to a monomer equivalent concentration of 200 µM, divided into aliquots, flash-frozen in liquid N2 and stored at -80˚C. For experiments at pH 6.5 and 5 µM fibril concentrations, the 200 µM fibril stock was sonicated between 30 s and 1 min using a probe sonicator (Bandelin, Sonopuls HD 2070, Berlin, Germany), using 10% maximum power and a 50% cycle.

Secondary nucleation assays

Seed fibrils were produced in 10 mM acetate buffer at pH 5.0. A 1.2 ml sample of α-synuclein at a concentration of 25 µM was prepared and aliquoted into 12 wells of a 96-well Half Area Black Flat Bottom Polystyrene NBS Microplate (Corning), where a single glass bead of 2.85–3.45 mm diameter (Carl Roth) had been added. The plate was incubated at 37˚C for 48–72 h at

500 RPM. Sonication was performed using a probe sonicator (Bandelin, Sonopuls UW 3200, Berlin, Germany) with a MS72 sonotrode five times for 1 s using 10% maximum power.

Lipid vesicle preparation

DMPS lipid powder was dissolved in 20 mM phosphate buffer (NaH2PO4/Na2HPO4), pH 6.5, 0.01% NaN3 and stirred at 45˚C for at least 2 h. The solutions were then frozen and thawed five times using dry ice and a water bath at 45˚C. Lipid vesicles were prepared by sonication (Bandelin, Sonopuls HD 2070, 3 x 5 min, 50% cycle, 10% maximum power) and centrifuged at 15000 rpm for 30 min at 25˚C. The average size of the vesicles was verified by dynamic light scattering (Zetasizer Nano ZSP, Malvern Instruments, Malvern, UK) to ensure a distribution centred at a diameter of 20 nm.

Circular dichroism (CD) measurements and data analysis of α-synuclein-lipid interactions in the presence of AS69

Samples were prepared as described before (Galvagnion et al., 2015) by incubating 20 μM α-synuclein with 2 or 20 μM AS69 and DMPS concentrations ranging from 0 to 1.2 mM in 20 mM phosphate buffer, pH 6.5, 0.01% NaN3. Far-UV CD spectra were recorded on a JASCO J-810 instrument (Tokyo, Japan) equipped with a Peltier thermally controlled cuvette holder at 30 ˚C. Quartz cuvettes with path lengths of 1 mm were used, and the CD signal was measured at 222 nm by averaging 60 individual measurements with a bandwidth of 1 nm, a data pitch of 0.2 nm, a scanning speed of 50 nm/min and a response time of 1 s. The signal of the buffer containing DMPS and different concen- trations of AS69 was subtracted from that of the protein. The data were then analysed as described previously (Galvagnion et al., 2015; Brown et al., 2016). First the fraction of protein bound to DMPS for the different [α-synuclein], [DMPS] and [AS69] used in our study was determined using the following equation:

$$x_b = \frac{CD_{mes} - CD_{free}}{CD_{bound} - CD_{free}} \quad (1)$$

where CDfree is the signal of α-synuclein measured in the absence of both DMPS and AS69, CDbound is the signal of the α-synuclein measured in the presence of DMPS only under saturating conditions and CDmes is the signal of the α-synuclein measured at a given [DMPS] and [AS69].

The values of xb obtained from our CD measurements were then compared to those estimated from a competitive binding model where both AS69 and DMPS compete for the binding to α-synuclein molecules using the binding constants of the systems AS69:α-synuclein and DMPS:α-synuclein, determined from previous studies (Mirecka et al., 2014; Galvagnion et al., 2015). We considered the following two equilibria:

$$\alpha + (\mathrm{DMPS})_{\mathrm{L}} \rightleftharpoons \alpha(DMPS)_{L}$$

$$\alpha + \mathrm{AS69} \rightleftharpoons \alpha\ \mathrm{AS69}$$

that are described by the following equations:

$$K_{D,\alpha-DMPS} = \frac{[\mathrm{DMPS_f}][\alpha_{\mathrm{f}}]}{L_{\alpha}[\alpha_{\mathrm{b}}]} \quad (2)$$

$$K_{D,\alpha-AS69} = \frac{[\alpha_{\mathrm{f}}][\mathrm{AS69_f}]}{[\mathrm{AS69_b}]} \quad (3)$$

with

$$[\alpha] = [\alpha_{\mathrm{f}}] + [\alpha_{\mathrm{b}}] + [\mathrm{AS69_b}] \quad (4)$$

$$[\mathrm{DMPS}] = [\mathrm{DMPS_f}] + L_{\alpha}[\alpha_{\mathrm{b}}] \quad (5)$$

$$[\mathrm{AS69}] = [\mathrm{AS69_f}] + [\mathrm{AS69_b}] \quad (6)$$

where $K_{D,\alpha}$-DMPS, $K_{D,\alpha}$-AS69 are the binding constants of the system DMPS:α-synuclein and AS69:α- synuclein, respectively; L_{α} is the stoichiometry in which DMPS binds to α-synuclein, that is the number of DMPS molecules interacting with one molecule of α-synuclein; [α],[α_f], [α_b] are the concentrations of total, free and DMPS-bound α-synuclein; [AS69], [AS69f], [$AS69_b$] are the concentrations of total, free and α-synuclein-bound AS69; and [DMPS] and [$DMPS_f$] are the concentrations of total and free α-synuclein. The change in the fraction of protein bound with increasing concentration of DMPS can be described using the standard solution of the cubic equation:

$$K_{D,\alpha-DMPS} = \frac{([DMPS] - L_\alpha[\alpha_b])([\alpha] - [\alpha_b] - [AS69_b])}{[\alpha_b]L_\alpha} \quad (7)$$

$$[AS69_b] = \frac{[AS69] - [\alpha_b] + [\alpha] + K_{D,\alpha-AS69} - \sqrt{4([\alpha_b][AS69] - [AS69][\alpha]) + ([AS69] - [\alpha_b] + [\alpha] + K_{D,\alpha-AS69})^2}}{2[\alpha]}$$

Its solution is not shown here because of its length. For each data point, the concentrations [a_b], [AS] and [DMPS] are known and the equilibrium constants and stoichiometry for the α-synuclein: DMPS and α-synuclein:AS69 systems were set to the values determined previously (Galvagnion et al., 2015; Mirecka et al., 2014).

DSC and ITC measurements

DSC experiments with lipid vesicles, α-synuclein and AS69 (Figure 9—figure supplement 2a and b) were performed as described previously (Galvagnion et al., 2016). We used a VP-DSC calorimeter (Malvern Instruments, Malvern, UK) at a scan rate of 1˚C per minute. The lipid concentration was 1 mM and the protein concentrations are indicated in the figure legend.

ITC binding experiments between AS69 and α-synuclein were performed on a Microcal iTC200 calorimeter (GE Healthcare) at 30˚C. The buffer was either 20 mM sodium phosphate, 50 mM NaCl, pH 7.4, or 20 mM sodium acetate, pH 5.0. AS69 was used as titrant in the cell at a concentration of approximately 40 μM, and α-synuclein at approximately 10-fold higher concentration as titrant in the syringe. The heat of post-saturation injections was averaged and subtracted from each injection to correct for heats of dilution and mixing. Data were processed using MicroCal Origin software provided with the calorimeter. Dissociation constants were obtained from a nonlinear least-squares fit to a 1:1 binding model.

ITC binding experiments between SUVs made from DMPS and AS69 (Figure 9—figure supplement 2c and d) were performed using an ITC200 instrument (Malvern Instruments, Malvern, UK). A solution of 0.47 mM AS69 was titrated into 0.5 mM DMPS in 20 mM phosphate buffer pH 6.5 at 30˚ C, corresponding to the conditions under which the lipid-induced aggregation of α-synuclein had been studied. An interaction between AS69 and DMPS vesicles can be clearly detected, and the binding behaviour is complex, with an initially exothermic interaction at low protein to lipid ratios, followed by an endothermic interaction at molar ratios higher than 0.05. Because of the complex binding signature, it is not straightforward to fit the

data and extract a binding affinity, but it can be estimated that the binding affinity is in the sub-micromolar range, comparable to that of a-synuclein to the same lipid vesicles (Galvagnion et al., 2015).

Thioflavin-T (ThT) fluorescence assays of amyloid formation kinetics

The ThT experiments were performed under two distinct sets of solution conditions. Firstly, we used phosphate buffer (PB) at pH 6.5, where we have previously shown that highly quantitative kinetic data of amyloid fibril growth can be obtained, and where under strongly seeded and quiescent conditions, all nucleation processes can be neglected (Buell et al., 2014a). Furthermore, we also employed mildly acidic solution conditions (acetate buffer at pH 5.0), where secondary nucleation is strongly enhanced and can be conveniently studied (Buell et al., 2014a; Gaspar et al., 2017). In most of the ThT experiments, samples of 100 μl were loaded into a 96-well Half Area Black Flat Bottom Polystyrene NBS Microplate (Corning, product number 3881). 150 μl of water was added into the wells directly surrounding the wells containing sample, and the outer most wells were not used for experimental measurements. These measures minimise sample evaporation during prolonged kinetic experiments. The plate was sealed using clear sealing tape (Polyolefin Acrylate, Thermo Scientific) and placed inside a platereader (CLARIOStar or FLUOStar Omega, BMG LABTECH, Germany) that had been equilibrated to 37˚C. Data points were obtained every 120–360 s, depending on the duration of the experiment. In some experiments, the fluorescence was read by averaging 12–20 points, measured in a ring with a diameter of 3 mm (orbital averaging mode). Excitation and emission in the CLARIOStar (monochromator) was 440 nm (15 nm bandwidth) and 485 nm (20 nm bandwidth), respectively. Excitation and emission in the FLUOStar Omega (filter) was 448 nm (10 nm bandwidth) and 482 nm (10 nm bandwidth), respectively. In addition to the proteins of interest and buffer, all samples contained 0.04% (w/v) NaN3 and 40 or 50 mM ThT.

Preparation of fluorescently labelled oligomers

Fluorescently labelled α-synuclein oligomers were prepared as described previously (Pinotsi et al., 2014; Wolff et al., 2016). In brief, we produced fluorescently labelled α-synuclein monomer by expressing and purifying the N122C cystein variant of α-synuclein, which was then labelled through an incubation with a 10-fold excess of Alexa 647 maleimide (Thermo Fisher Scientific,

Loughbor- ough, UK), followed by removal of the excess dye with a Superdex 200 10/300 Increase gel filtration column (GE Healthcare, Amersham, UK). Wild-type and fluorescently labeled N122C variant α-synuclein were combined at a ratio of 30:1, corresponding approximately to the stoichiometry of the oligomers (Lorenzen et al., 2014), at a total concentration of ca. 200 μM, dialysed against distilled water for 24 h and lyophilised. The dry protein was redissolved in PBS at concentrations between 500 and 800 μM and incubated at RT overnight under quiescent conditions. The oligomers were then separated from the monomeric protein and larger aggregates using a Superdex 200 10/300 Increase column that had been equilibrated with 20 mM phosphate buffer pH 7.4 and 50 mM NaCl, collecting fractions of 500 μl. The exact concentrations of the oligomer fractions are difficult to determine, because of the weak absorption signal. However, based on the absorptions at 275 nm and 647 nm, we estimated the oligomer concentration to be 3–6 μM in monomer equivalents, corresponding to an oligomer number concentration of 100–200 nM, which also corresponds roughly to the concentration of Alexa label.

AFM images

pH 6.5

Atomic force microscopy images were taken with a Nanowizard II atomic force microscope (JPK, Berlin, Germany) using tapping mode in air. Solutions containing fibrils were diluted to a concentration of 1 μM (in monomer equivalents) in water and 10 μl samples of the diluted solution were deposited on freshly cleaved mica and left to dry for at least 30 min. The samples were carefully washed with ~50 μl of water and then dried again before imaging.

pH 5

Atomic force microscopy images were taken with a Bruker Mulitmode 8 (Billerica, Massachusetts, USA) using ScanAsyst-Air cantilvers (Camarillo, California, USA) using the ScanAsyst PeakForce tapping in air. 15 μl of a 0.7 μM fibril-containing solution was deposited on freshly cleaved mica and incubated for 10 min before the sample was carefully rinsed by applying and removing 100 μl water three times before the sample was dried under a gentle stream of nitrogen.

DGC

The DGC experiments were performed as previously described (Rösener et al., 2018). We performed DGC experiments both under conditions of neutral pH (pH 7.4), where the reaction is elongation dominated, and under mildly acidic conditions (pH 5.0,) where secondary nucleation strongly contributes to the reaction. We find that under both sets of conditions there is no detectable binding between amyloid fibrils and AS69.

Thermophoresis experiments

The thermophoresis experiments with fluorescently labeled monomeric and oligomeric α-synuclein were performed as described previously (Wolff et al., 2016), using a Monolith instrument (Nanotemper, Munich, Germany) and glass capillaries (Nanotemper, Munich, Germany) with hydrophobic coating (oligomeric α-synuclein) or uncoated (monomeric α-synuclein). A two-fold dilution series of AS69 in 20 mM phosphate buffer pH 7.4 with 50 mM NaCl was prepared and then either 10 µl of 5x diluted oligomers (corresponding to 0.6–1.2 µM) or 1 µM labelled monomer was added to each sample of the dilution series. We performed the binding experiments under these buffer conditions for optimal comparability with previous ITC experiments of AS69 binding to monomeric α-synuclein (Mirecka et al., 2014).

MST experiments were performed at 40% laser power and 75% LED power (oligomers) or 60% laser power and 20% LED power (monomers). For calculation of the relative change in fluorescence from thermophoresis, the cursors were set before the temperature jump followed by 5 s after the temperature jump (oligomers) and 45 s after the temperature jump (monomers).

CD melting curves

CD melting curves were obtained as described in Gauhar et al. (2014), with the sole difference that slightly higher concentrations of protein were used, and the samples were heated to 90˚C rather than 80˚C. The CD data were fitted directly using a two-state model to obtain the melting tempera- ture, Tm, as described in Pace et al. (1998):

$$y = \frac{(y_f + m_f T) + (y_u + m_u T) \cdot \exp\left(\frac{\Delta H_m}{RT} \cdot \frac{T - T_m}{T_m}\right)}{1 + \exp\left(\frac{\Delta H_m}{RT} \cdot \frac{T - T_m}{T_m}\right)} \quad (8)$$

using least-square fitting from the Python packages scipy.optimize.curve_fit. y is the CD signal in mdeg, $y_f + m_f T$ and $y_u + m_u T$ describes linear change in CD signal of the folded and unfolded state with respect to temperature, respectively, T is the temperature in Kelvin, R is the ideal constant constant, and ΔH_m is the change in enthalpy at Tm.

Cell culture and transfections

HEK293 cells (RRID CVCL0063) were obtained from the Department of Biochemistry, RWTH Aachen University, Aachen, Germany, and were cultured and transfected using Metafectene as previously described (Dinter et al., 2016). Cell line authentication was performed by Eurofins Forensik, using PCR-single-locus-technology. Cell lines were tested for mycoplasma contamination. HEK293T cells were used because they are the established cell line for our protocol. A53T-α-synuclein flexibly tagged with EGFP by the interaction of a PDZ domain with its binding motif was previously described (Opazo et al., 2008; Dinter et al., 2016). WT and A53T-α-synuclein tagged by the C-terminal and N-terminal half of Venus was obtained from Prof. Tiago Outeiro (University of Goettingen, Germany).

Immunoblots

Immunoblots were carried out 24 h after transfection as previously described (Dinter et al., 2016) using NP40 lysis buffer containing protease inhibitors (Pierce, Thermo Fisher Scientific) and the following primary antibodies: rabbit anti-α-synuclein (1:500, No. 2642, Cell Signalling Technology, Danvers, USA), mouse anti-beta-tubulin (1:1000, E7, Developmental Studies Hybridoma Bank, Iowa, USA). Secondary antibodies were anti-mouse IgG (NXA931) and anti-rabbit IgG (NA934V) from GE Healthcare Life Sciences (1:10000). These antibodies produce several nonspecific bands that are also visible in cells not expressing a-synuclein. Among the bands around 20 kDa observed with the α-synuclein antibody, only the upper band is considered specific and was used for quantification (see Dinter et al., 2016 for details).

Flow cytometry

Cells were grown in six-well plates and used 24 h after transfection. Adherent cells were washed with phosphate buffer saline (PBS) three times and detached with trypsin. Subsequently, cells

were collected in FACS tubes, centrifuged for 5 min at 2000 rpm and washed again with PBS. Cell pellets were finally resuspended in 200 ml of PBS. Flow cytometry was carried out by a FACSCalibur (BD Bio- sciences) using forward and sideward scatter to gate cells and a fluorescence threshold of 300 AFU to detect cells with Venus (YFP) fluorescence. This threshold was determined from measurements with untransfected cells and cells expressing either the N-terminal or the C-terminal half of Venus only.

Microscopy

For classification of EGFP distribution patterns, cells were grown on coverslips and fixed 24 h after transfection. The distribution of EGFP fluorescence was classified manually by a blinded observer into the categories 'homogenous distribution', 'containing particles' and 'unhealthy' (round, condensed cells) using an Olympus IX81 fluorescence microscope (60x oil objective, NA 1.35). At least

100 cells per coverslip were classified. In each experiment, three coverslips were evaluated per group and the results averaged.

Drosophila stocks

Flies expressing A53T-α-synuclein in neurons, *w*[*]; ; *P*{*w*[+*m*C] = *GAL*4 - *elav:L*}, *P*{*w*[+*mC*] = *UAS* - *HsapSNCA:A*53*T*} and flies expressing GFP under control of GAL4 *w*[*]; *P*(*acman*)[*w*[+] = *UAS – GFP*}5 were previously described (Dinter et al., 2016). Flies expressing AS69 under control of GAL4, *w*[118]; ; *P*{*w*[+] = *UAS* - *AS69*}, were generated using standard P-element transformation (BestGene Inc). Expression of A53T-α-synuclein fused to VN and VC in neurons was achieved by genetically crossing and recombining flies carrying GAL4 under the elav promoter and VN and VC tagged A53T-α-synuclein under the UAS promoter. The resulting genotype of these flies is *P*{*w*[+*mW.hs*] = *GawB*}*elav*[*C*155]; *P*[*w*[+] = *UAS* - *Hsap SNCA*[*A*53*T*] : *VC*], *PBac*{*attB*[+*mC*] =*UAS* - *VN* : *Hsap SNCA*[*A*53*T*]}/*Cyo*. Flies expressing 'always early RNAi', w[1118];P{*GD*4261}v13673, were used as control in experiments conducted with the A53T-α-synuclein VN/VC expressing flies. These flies have been shown to have no effect in genetic screens for modifiers in

neurodegenerative disease models. Flies were raised and maintained at 25˚C under a 12 h dark/light cycle.

Climbing assay and fly head immunoblot

Virgins of the stock *w*[*]; ; *P*{*w*[+*mC*] = *GAL*4 - *elav:L*}, *P*{*w*[+*mC*] = *UAS* - *Hsap SNCA*:*A*53*T*} were either crossed to males *w*[118]; ; *P*{*w*[+] = *UAS* - *AS*69}, or *w*[*]; *P*(*acman*)]{*w*[+] = *UAS – GFP*}5 (control). In the F1-progeny we selected for males with pan neural [A53T]α-synuclein and either AS69 or GFP concomitant expression. Climbing analysis was performed 5, 15 and 25 days post eclosion as previously described (Dinter et al., 2016). For each time point and per genotype 10 flies were analyzed in 10 tapping experiments with 60 s resting interval and the results averaged. The crosses were repeated n = 3 times.

In parallel, 10 fly heads from the F1-progeny and also from male w[*]; P(acman)w[+]=UAS GFP flies were homogenized in 100 µl RIPA buffer using the Speedmil P12 (Analytik Jena AG). The lysates were centrifuged at 12000 rpm for 10 min and the supernatant collected and used for immunoblot analysis. The following primary antibodies were used: mouse anti-α-synuclein (1:500, syn204, ab3309, Abcam) and mouse anti-syntaxin (1:500, 8C3, Developmental Studies Hybridoma Bank, Iowa, USA). Secondary antibody was anti-mouse IgG (NXA931) from GE Healthcare Life Sciences (1:5000).

Fly head filter trap assay

Virgins of the stock *P*{*w*[+*mW.hs*] = *GawB*}*elav*[*C*155], PBac {*attB*[+*mC*] = *UAS* - *VN* : *Hsap SNCA*[*A*53*T*]}/*Cyo* were either crossed to *w*[118]; ; *P*{*w*[+] = *UAS* - *AS*69} or *w*[1118]; *P*{*GD*4261}*v*13673 (control) males. In the F1-progeny we selected for males with pan neural [A53T]α-synuclein and either AS69 or 'always early RNAi' concomitant expression. 10 fly heads were homogenized in 100 µl RIPA buffer using the Speedmill P12. The lysates were centrifuged at 12000 rpm for 10 min at 4˚C and the supernatant collected. For the filter trap assay, equal protein amounts of RIPA fly head lysates (30 µg) were adjusted to equal volumes. An equal volume of urea buffer (8 M) was subsequently added, samples were incubated rolling at 4˚C for 1 h and sonicated in a water bath for 10 min. SDS and DTT were added to a final concentration of 2% and 50 mM. Using a dot blot filtration unit,

the resulting solutions were filtered through a 0.2 mm nitrocellulose membrane (Whatman) previously equilibrated with 0.1% SDS in TBS and afterwards washed in TBS-T. Membranes were further treated as an immunoblot described previously.

Acknowledgements

AKB thanks the Leverhulme Trust and the Parkinson's and Movement Disorder Foundation (PMDF) for funding and the Novo Nordisk Foundation for support through a Novo Nordisk Foundation pro- fessorship. PF thanks the Böhringer Ingelheim Fonds and the Studienstiftung des Deutschen Volkes for support. CG thanks the Alexander von Humboldt Foundation and the European Commission (H2020-MSCA grant agreement No 706551) for support. This project has received funding from the European Research Council under the European Union's Horizon 2020 research and innovation program, grant agreement No. 726368 (to WH). We thank Nadine Rösener for help with the density gradient centrifugation and Sabine Hamm for excellent technical assistance.

Additional information

Funding

Funder	Grant reference number	Author
Leverhulme Trust		Alexander K Buell
Boehringer Ingelheim Fonds		Patrick Flagmeier
Studienstiftung des Deutschen Volkes		Patrick Flagmeier
Alexander von Humboldt-Stiftung		Céline Galvagnion
H2020 European Research Council	726368	Wolfgang Hoyer
Parkinson's and Movement Disorder Foundation		Alexander K Buell
Novo Nordisk Foundation		Alexander K Buell
H2020 Marie Skłodowska-Curie Actions	706551	Céline Galvagnion
RWTH Aachen University	START-Program of the Faculty of Medicine	Theodora Saridaki

The funders had no role in study design, data collection and interpretation, or the decision to submit the work for publication.

Author ORCIDs

Patrick Flagmeier https://orcid.org/0000-0002-1204-5340

Daniel Komnig https://orcid.org/0000-0002-6312-5236

Dieter Willbold https://orcid.org/0000-0002-0065-7366

Aaron Voigt https://orcid.org/0000-0002-0428-7462

Bjoern Falkenburger https://orcid.org/0000-0002-2387-526X

Wolfgang Hoyer https://orcid.org/0000-0003-4301-5416

Alexander K Buell https://orcid.org/0000-0003-1161-3622

Decision letter and Author response

Decision letter https://doi.org/10.7554/eLife.46112.sa1

Author response https://doi.org/10.7554/eLife.46112.sa2

Additional files

Supplementary files

- Transparent reporting form

Data availability

Numerical data represented in the graphs for cell culture and fly experiments will be made publicly available on osf.io as we did for previous publications. The numerical data for the biophysical experi- ments will be made publicly available within the same repository on osf.io. The raw images of the gels used in the publication will be made publicly available. All data have been deposited on osf.io: https://osf.io/6n2gs/.

The following dataset was generated:

Author(s)	Year	Dataset title	Dataset URL	Database and Identifier
Falkenburger BH, Buell AK, Agerschou ED	2019	An engineered monomer binding- protein for α-synuclein efficiently inhibits the nucleation of amyloid fibrils	https://osf.io/6n2gs/	Open Science Framework, 6n2gs

5.5 References

1. Bae EJ, Yang NY, Song M, Lee CS, Lee JS, Jung BC, Lee HJ, Kim S, Masliah E, Sardi SP, Lee SJ. 2014. Glucocerebrosidase depletion enhances cell-to-cell transmission of a-synuclein. Nature Communications 5: 4755. DOI: https://doi.org/10.1038/ncomms5755, PMID: 25156829
2. Brown JW, Buell AK, Michaels TC, Meisl G, Carozza J, Flagmeier P, Vendruscolo M, Knowles TP, Dobson CM, Galvagnion C. 2016. b-Synuclein suppresses both the initiation and amplification steps of a-synuclein aggregation via competitive binding to surfaces. Scientific Reports 6:36010. DOI: https://doi.org/10.1038/ srep36010, PMID: 27808107
3. Buell AK, Galvagnion C, Gaspar R, Sparr E, Vendruscolo M, Knowles TP, Linse S, Dobson CM. 2014a. Solution conditions determine the relative importance of nucleation and growth processes in a-synuclein aggregation. PNAS 111:7671–7676. DOI: https://doi.org/10.1073/pnas.1315346111, PMID: 24817693
4. Buell AK, Dobson CM, Knowles TP. 2014b. The physical chemistry of the amyloid phenomenon: thermodynamics and kinetics of filamentous protein aggregation. Essays in Biochemistry 56:11–39. DOI: https://doi.org/10.1042/bse0560011, PMID: 25131584
5. Butler EK, Voigt A, Lutz AK, Toegel JP, Gerhardt E, Karsten P, Falkenburger B, Reinartz A, Winklhofer KF, Schulz JB. 2012. The mitochondrial chaperone protein TRAP1 mitigates a-Synuclein toxicity. PLOS Genetics 8: e1002488. DOI: https://doi.org/10.1371/journal.pgen.1002488, PMID: 22319455
6. Campioni S, Carret G, Jordens S, Nicoud L, Mezzenga R, Riek R. 2014. The presence of an air-water interface affects formation and elongation of a-Synuclein fibrils. Journal of the American Chemical Society 136:2866– 2875. DOI: https://doi.org/10.1021/ja412105t, PMID: 24460028
7. Cohen SI, Vendruscolo M, Welland ME, Dobson CM, Terentjev EM, Knowles TP. 2011. Nucleated polymerization with secondary pathways. I. time evolution of the principal moments. The Journal of Chemical Physics 135: 065105. DOI: https://doi.org/10.1063/1.3608916, PMID: 21842954
8. Conway KA, Harper JD, Lansbury PT. 1998. Accelerated in vitro fibril formation by a mutant alpha-synuclein linked to early-onset parkinson disease. Nature Medicine 4:1318–1320. DOI: https://doi.org/10.1038/3311, PMID: 9809558
9. Desplats P, Lee HJ, Bae EJ, Patrick C, Rockenstein E, Crews L, Spencer B, Masliah E, Lee SJ. 2009. Inclusion formation and neuronal cell death through neuron-to-neuron

transmission of a-synuclein. PNAS 106:13010– 13015. DOI: https://doi.org/10.1073/pnas.0903691106, PMID: 19651612

10. Dinter E, Saridaki T, Nippold M, Plum S, Diederichs L, Komnig D, Fensky L, May C, Marcus K, Voigt A, Schulz JB, Falkenburger BH. 2016. Rab7 induces clearance of a-synuclein aggregates. Journal of Neurochemistry 138: 758–774. DOI: https://doi.org/10.1111/jnc.13712, PMID: 27333324
11. Falkenburger BH, Saridaki T, Dinter E. 2016. Cellular models for parkinson's disease. Journal of Neurochemistry 139:121–130. DOI: https://doi.org/10.1111/jnc.13618, PMID: 27091001
12. Flagmeier P, Meisl G, Vendruscolo M, Knowles TPJ, Dobson CM, Buell AK, Galvagnion C. 2016. Mutations associated with familial parkinson's disease alter the initiation and amplification steps of a-synuclein aggregation. PNAS 113:10328–10333. DOI: https://doi.org/10.1073/pnas.1604645113
13. Galvagnion C, Buell AK, Meisl G, Michaels TC, Vendruscolo M, Knowles TP, Dobson CM. 2015. Lipid vesicles trigger a-synuclein aggregation by stimulating primary nucleation. Nature Chemical Biology 11:229–234. DOI: https://doi.org/10.1038/nchembio.1750, PMID: 25643172
14. Galvagnion C, Brown JWP, Ouberai MM, Flagmeier P, Vendruscolo M, Buell AK, Sparr E, Dobson CM. 2016. Chemical properties of lipids strongly affect the kinetics of the membrane-induced aggregation of a-synuclein. PNAS 113:7065–7070. DOI: https://doi.org/10.1073/pnas.1601899113
15. Gaspar R, Meisl G, Buell AK, Young L, Kaminski CF, Knowles TPJ, Sparr E, Linse S. 2017. Secondary nucleation of monomers on fibril surface dominates a-synuclein aggregation and provides autocatalytic amyloid amplification. Quarterly Reviews of Biophysics 50:e6. DOI: https://doi.org/10.1017/S0033583516000172, PMID: 29233218
16. Gauhar A, Shaykhalishahi H, Gremer L, Mirecka EA, Hoyer W. 2014. Impact of subunit linkages in an engineered homodimeric binding protein to -synuclein. Protein Engineering Design and Selection 27:473–479. DOI: https://doi.org/10.1093/protein/gzu047
17. Grüning CS, Klinker S, Wolff M, Schneider M, Toksöz K, Klein AN, Nagel-Steger L, Willbold D, Hoyer W. 2013. The off-rate of monomers dissociating from amyloid-b protofibrils. Journal of Biological Chemistry 288:37104– 37111. DOI: https://doi.org/10.1074/jbc.M113.513432, PMID: 24247242

18. Hoyer W, Antony T, Cherny D, Heim G, Jovin TM, Subramaniam V. 2002. Dependence of alpha-synuclein aggregate morphology on solution conditions. Journal of Molecular Biology 322:383–393. DOI: https://doi. org/10.1016/S0022-2836(02)00775-1, PMID: 12217698

19. Hoyer W, Grönwall C, Jonsson A, Sta˚ hl S, Härd T. 2008. Stabilization of a b-hairpin in Monomeric alzheimer's amyloid-b peptide inhibits amyloid formation. PNAS 105:5099–5104. DOI: https://doi.org/10.1073/pnas.0711731105

20. Hoyer W, Ha¨ rd T. 2008. Interaction of Alzheimer's A beta peptide with an engineered binding protein– thermodynamics and kinetics of coupled folding-binding. Journal of Molecular Biology 378:398–411. DOI: https://doi.org/10.1016/j.jmb.2008.02.040, PMID: 18358490

21. Iljina M, Hong L, Horrocks MH, Ludtmann MH, Choi ML, Hughes CD, Ruggeri FS, Guilliams T, Buell AK, Lee JE, Gandhi S, Lee SF, Bryant CE, Vendruscolo M, Knowles TPJ, Dobson CM, De Genst E, Klenerman D. 2017.

22. Nanobodies raised against monomeric a-synuclein inhibit fibril formation and destabilize toxic oligomeric species. BMC Biology 15:57. DOI: https://doi.org/10.1186/s12915-017-0390-6, PMID: 28673288

23. Karpinar DP, Balija MB, Ku¨ gler S, Opazo F, Rezaei-Ghaleh N, Wender N, Kim HY, Taschenberger G, Falkenburger BH, Heise H, Kumar A, Riedel D, Fichtner L, Voigt A, Braus GH, Giller K, Becker S, Herzig A, Baldus M, Ja¨ ckle H, et al. 2009. Pre-fibrillar alpha-synuclein variants with impaired beta-structure increase neurotoxicity in Parkinson's disease models. The EMBO Journal 28:3256–3268. DOI: https://doi.org/10.1038/ emboj.2009.257, PMID: 19745811

24. Kayed R, Head E, Thompson JL, McIntire TM, Milton SC, Cotman CW, Glabe CG. 2003. Common structure of soluble amyloid oligomers implies common mechanism of pathogenesis. Science 300:486–489. DOI: https:// doi.org/10.1126/science.1079469, PMID: 12702875

25. Kurnik M, Sahin C, Andersen CB, Lorenzen N, Giehm L, Mohammad-Beigi H, Jessen CM, Pedersen JS, Christiansen G, Petersen SV, Staal R, Krishnamurthy G, Pitts K, Reinhart PH, Mulder FAA, Mente S, Hirst WD, Otzen DE. 2018. Potent a-Synuclein aggregation inhibitors, identified by High-Throughput screening, mainly target the monomeric state. Cell Chemical Biology 25:1389–1402. DOI: https://doi.org/10.1016/j.chembiol. 2018.08.005, PMID: 30197194

26. Lorenzen N, Nielsen SB, Buell AK, Kaspersen JD, Arosio P, Vad BS, Paslawski W, Christiansen G, Valnickova- Hansen Z, Andreasen M, Enghild JJ, Pedersen JS, Dobson CM, Knowles TP, Otzen DE. 2014. The role of stable a-synuclein oligomers in the molecular events underlying amyloid formation. Journal of the American Chemical Society 136:3859–3868. DOI: https://doi.org/10.1021/ja411577t, PMID: 24527756

27. Luheshi LM, Hoyer W, de Barros TP, van Dijk Ha¨ rd I, Brorsson AC, Macao B, Persson C, Crowther DC, Lomas DA, Sta˚ hl S, Dobson CM, Ha¨ rd T. 2010. Sequestration of the abeta peptide prevents toxicity and promotes degradation in vivo. PLOS Biology 8:e1000334. DOI: https://doi.org/10.1371/journal.pbio.1000334,PMID: 20305716

28. Ma˚ nsson C, Arosio P, Hussein R, Kampinga HH, Hashem RM, Boelens WC, Dobson CM, Knowles TP, Linse S, Emanuelsson C. 2014. Interaction of the molecular chaperone DNAJB6 with growing amyloid-beta 42 (Ab42) aggregates leads to sub-stoichiometric inhibition of amyloid formation. Journal of Biological Chemistry 289: 31066–31076. DOI: https://doi.org/10.1074/jbc.M114.595124, PMID: 25217638

29. Masuda M, Suzuki N, Taniguchi S, Oikawa T, Nonaka T, Iwatsubo T, Hisanaga S, Goedert M, Hasegawa M. 2006. Small molecule inhibitors of alpha-synuclein filament assembly. Biochemistry 45:6085–6094. DOI: https://doi. org/10.1021/bi0600749, PMID: 16681381

30. Meisl G, Kirkegaard JB, Arosio P, Michaels TC, Vendruscolo M, Dobson CM, Linse S, Knowles TP. 2016. Molecular mechanisms of protein aggregation from global fitting of kinetic models. Nature Protocols 11:252–272. DOI: https://doi.org/10.1038/nprot.2016.010, PMID: 26741409

31. Mirecka EA, Shaykhalishahi H, Gauhar A, Akgu¨ l S¸ , , Lecher J, Willbold D, Stoldt M, Hoyer W. 2014. Sequestration of a b-hairpin for control of a-synuclein aggregation. Angewandte Chemie International Edition 53:4227–4230. DOI: https://doi.org/10.1002/anie.201309001, PMID: 24623599

32. Muchowski PJ, Wacker JL. 2005. Modulation of neurodegeneration by molecular chaperones. Nature Reviews Neuroscience 6:11–22. DOI: https://doi.org/10.1038/nrn1587, PMID: 15611723

33. Obeso JA, Stamelou M, Goetz CG, Poewe W, Lang AE, Weintraub D, Burn D, Halliday GM, Bezard E, Przedborski S, Lehericy S, Brooks DJ, Rothwell JC, Hallett M, DeLong MR, Marras C, Tanner CM, Ross GW, Langston JW, Klein C, et al. 2017. Past, present, and future of Parkinson's disease: A special essay on the 200th Anniversary of the Shaking

Palsy. Movement Disorders 32:1264–1310. DOI: https://doi.org/10.1002/mds.27115, PMID: 28887905

34. Opazo F, Krenz A, Heermann S, Schulz JB, Falkenburger BH. 2008. Accumulation and clearance of alpha- synuclein aggregates demonstrated by time-lapse imaging. Journal of Neurochemistry 106:529–540. DOI: https://doi.org/10.1111/j.1471-4159.2008.05407.x, PMID: 18410502

35. Pace CN, Hebert EJ, Shaw KL, Schell D, Both V, Krajcikova D, Sevcik J, Wilson KS, Dauter Z, Hartley RW, Grimsley GR. 1998. Conformational stability and thermodynamics of folding of ribonucleases sa, Sa2 and Sa3. Journal of Molecular Biology 279:271–286. DOI: https://doi.org/10.1006/jmbi.1998.1760, PMID: 9636716

36. Perni M, Galvagnion C, Maltsev A, Meisl G, Mu¨ ller MBD, Challa PK, Kirkegaard JB, Flagmeier P, Cohen SIA, Cascella R, Chen SW, Limboker R, Sormanni P, Heller GT, Aprile FA, Cremades N, Cecchi C, Chiti F, Nollen EAA, Knowles TPJ, et al. 2017. A natural product inhibits the initiation of a-synuclein aggregation and suppresses its toxicity. PNAS 114:E1009–E1017. DOI: https://doi.org/10.1073/pnas.1610586114

37. Pinotsi D, Buell AK, Galvagnion C, Dobson CM, Kaminski Schierle GS, Kaminski CF. 2014. Direct observation of heterogeneous amyloid fibril growth kinetics via two-color super-resolution microscopy. Nano Letters 14:339–345. DOI: https://doi.org/10.1021/nl4041093, PMID: 24303845

38. Prasad V, Wasser Y, Hans F, Goswami A, Katona I, Outeiro TF, Kahle PJ, Schulz JB, Voigt A. 2019. Monitoring - synuclein multimerization in vivo. FASEB Journal 33. DOI: https://doi.org/10.1096/fj.201800148RRR, PMID: 30252534

39. Roösener NS, Gremer L, Reinartz E, König A, Brener O, Heise H, Hoyer W, Neudecker P, Willbold D. 2018. A d-enantiomeric peptide interferes with heteroassociation of amyloid-b oligomers and prion protein. Journal of Biological Chemistry 293 ::15748–15764. DOI: https://doi.org/10.1074/jbc.RA118.003116, PMID: 30131337

40. Shaykhalishahi H, Gauhar A, Wördehoff MM, Grüning CS, Klein AN, Bannach O, Stoldt M, Willbold D, Härd T, Hoyer W. 2015. Contact between the b1 and b2 segments of a-Synuclein that inhibits amyloid formation.

41. Angewandte Chemie International Edition 54:8837–8840. DOI: https://doi.org/10.1002/anie.201503018, PMID: 26119103

42. Spillantini MG, Schmidt ML, Lee VM, Trojanowski JQ, Jakes R, Goedert M. 1997. Alpha-synuclein in lewy bodies. Nature 388 :839–840. DOI: https://doi.org/10.1038/42166

43. Tóth G, Gardai SJ, Zago W, Bertoncini CW, Cremades N, Roy SL, Tambe MA, Rochet JC, Galvagnion C, Skibinski G, Finkbeiner S, Bova M, Regnstrom K, Chiou SS, Johnston J, Callaway K, Anderson JP, Jobling MF, Buell AK, Yednock TA, et al. 2014. Targeting the intrinsically disordered structural ensemble of a-synuclein by small molecules as a potential therapeutic strategy for parkinson's disease. PLOS ONE 9:e87133. DOI: https://doi. org/10.1371/journal.pone.0087133, PMID: 24551051

44. Wagner J, Ryazanov S, Leonov A, Levin J, Shi S, Schmidt F, Prix C, Pan-Montojo F, Bertsch U, Mitteregger- Kretzschmar G, Geissen M, Eiden M, Leidel F, Hirschberger T, Deeg AA, Krauth JJ, Zinth W, Tavan P, Pilger J, Zweckstetter M, et al. 2013. Anle138b: a novel oligomer modulator for disease-modifying therapy of neurodegenerative diseases such as prion and Parkinson's disease. Acta Neuropathologica 125:795–813. DOI: https://doi.org/10.1007/s00401-013-1114-9, PMID: 23604588

45. Waudby CA, Knowles TP, Devlin GL, Skepper JN, Ecroyd H, Carver JA, Welland ME, Christodoulou J, Dobson CM, Meehan S. 2010. The interaction of alphaB-crystallin with mature alpha-synuclein amyloid fibrils inhibits their elongation. Biophysical Journal 98:843–851. DOI: https://doi.org/10.1016/j.bpj.2009.10.056, PMID: 201 97038

46. Wolff M, Mittag JJ, Herling TW, Genst ED, Dobson CM, Knowles TP, Braun D, Buell AK. 2016. Quantitative thermophoretic study of disease-related protein aggregates. Scientific Reports 6:22829. DOI: https://doi.org/ 10.1038/srep22829, PMID: 26984748

47. Wördehoff MM, Bannach O, Shaykhalishahi H, Kulawik A, Schiefer S, Willbold D, Hoyer W, Birkmann E. 2015. Single fibril growth kinetics of a-synuclein. Journal of Molecular Biology 427:1428–1435. DOI: https://doi.org/ 10.1016/j.jmb.2015.01.020, PMID: 25659910

48. Wrasidlo W, Tsigelny IF, Price DL, Dutta G, Rockenstein E, Schwarz TC, Ledolter K, Bonhaus D, Paulino A, Eleuteri S, Skjevik A˚ A, Kouznetsova VL, Spencer B, Desplats P, Gonzalez-Ruelas T, Trejo-Morales M, Overk CR, Winter S, Zhu C, Chesselet MF, et al. 2016. A de novo compound targeting a-synuclein improves deficits in models of Parkinson's disease. Brain : A Journal of Neurology 139:3217–3236. DOI: https://doi.org/10.1093/ brain/aww238, PMID: 27679481

49. Xue WF, Hellewell AL, Gosal WS, Homans SW, Hewitt EW, Radford SE. 2009. Fibril fragmentation enhances amyloid cytotoxicity. Journal of Biological Chemistry 284:34272–34282. DOI: https://doi.org/10.1074/jbc. M109.049809, PMID: 19808677

5.6 Appendix

Appendix 1

Analysis of strongly seeded aggregation data at neutral pH

In the case of aggregation experiments at high concentrations (μM) of pre-formed seeds under quiescent conditions, primary nucleation and fragmentation of α-synuclein amyloid fibrils can be neglected (***Buell et al., 2014a***). The aggregation kinetics were analysed as previously reported by fitting a linear function to the early times of the kinetic traces (***Buell et al., 2014a***), with the exception that fitting was only performed after the initial decrease in fluorescence intensity, which is due to the temperature dependence of ThT fluorescence and a consequence of the thermal equilibration of the multiwell-plate prepared at room temperature. The fit was performed through five time points starting from the point of minimal fluorescence intensity (see ***Appendix 1—figure 1***). The temperature-induced decrease in fluorescence intensity is superimposed to the increase in fluorescence due to fibril elongation. Therefore, using the initial growth rates likely leads to a small but systematic underestimation of the elongation rates. This fitting procedure was performed to obtain the values of $2k_+P(0)m(0)$, where k_+ is the fibril elongation rate constant, $m(0)$ the initial monomer concentration and $P(0)m(0)$ the initial number concentration of fibrils. For the comparison of the rates at different concentrations of AS69, we then calculate the ratios r:

$$r = \frac{\left(\frac{dM(t)}{dt}\right)_{AS69}\Big|_{t\approx 0}}{\left(\frac{dM(t)}{dt}\right)\Big|_{t\approx 0}} = \frac{k_+P(0)m(0,[AS69])}{k_+P(0)m(0)} \tag{9}$$

r is the ratio of the initial gradient fitted to the kinetic trace for monomer elongating fibrils in the presence of AS69 and the initial gradient fitted to the kinetic trace for monomer elongating fibrils in the absence of AS69. $P(0)$ is the initial number concentration of fibrils, which is constant, as the same stock solution of seeds was used, and $m(0)$ is the initial monomer concentrations. For the prediction in ***Figure 4*** of the main manuscript, we calculated the equilibrium concentrations of unbound α-synuclein, $m(0,[AS69]) = [m]_{free}$ as:

$$[m]_{free} = \frac{-([AS69]_{tot} + K_D - [m]_{tot}) + \sqrt{([AS69]_{tot} + K_D - [m]_{tot})^2 + 4K_D[m]_{tot}}}{2} \tag{10}$$

where the values obtained at different $[AS69]_{tot}$ were then used for $m(0,[AS69])$ in ***Equation 9***. This procedure corresponds to the assumption that the only effect of the AS69 is to sequester soluble α-synuclein.

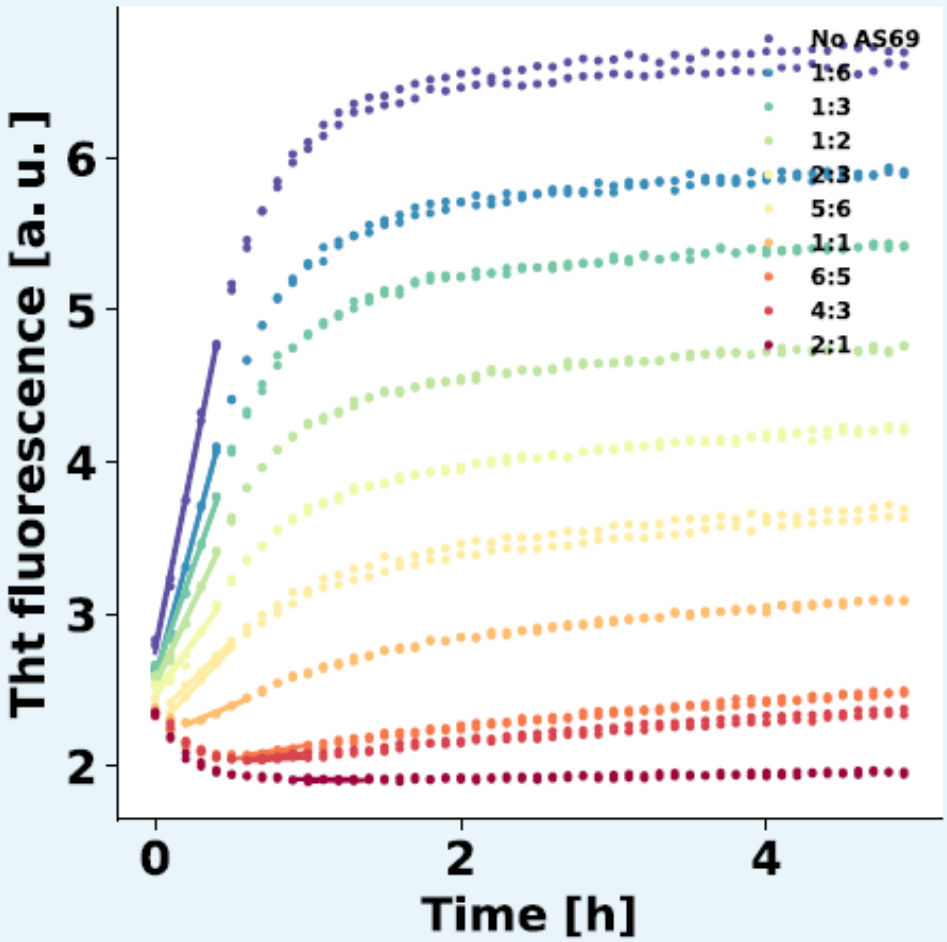

Appendix 1—figure 1. Linear fitting of the early times of strongly seeded aggregation kinetics. Solid lines show the fits. These data were used to produce the plot in ***Figure 4c***. At the highest inhibitor concentrations, the rates were so low that the temperature increase upon introduction of the plate into the platereader led to an initial decrease in fluorescence intensity. Therefore, the data was fitted once the fluorescence intensity had started to increase.

Seeded aggregation experiments at very low monomer concentrations (0.75 µM seeds) were performed in order to test whether a concentration could be determined at which no net elongation is observed (***Appendix 1—figure 2***). The concentration of free monomer at which the rates of fibril elongation and dissociation are equal corresponds to the equilibrium concentration (***Buell et al., 2014b***):

$$k_+[m]_{eq}[P] = k_-[P] \tag{11}$$

where k_+ is the elongation rate constant and k_- is the dissociation rate constant. The equilibrium constant of monomer addition to fibril ends therefore corresponds to the inverse of the monomer concentration at equilibrium:

$$K_{eq} = \frac{k_-[P]}{k_+[m]_{eq}[P]} = \frac{1}{[m]_{eq}} \tag{12}$$

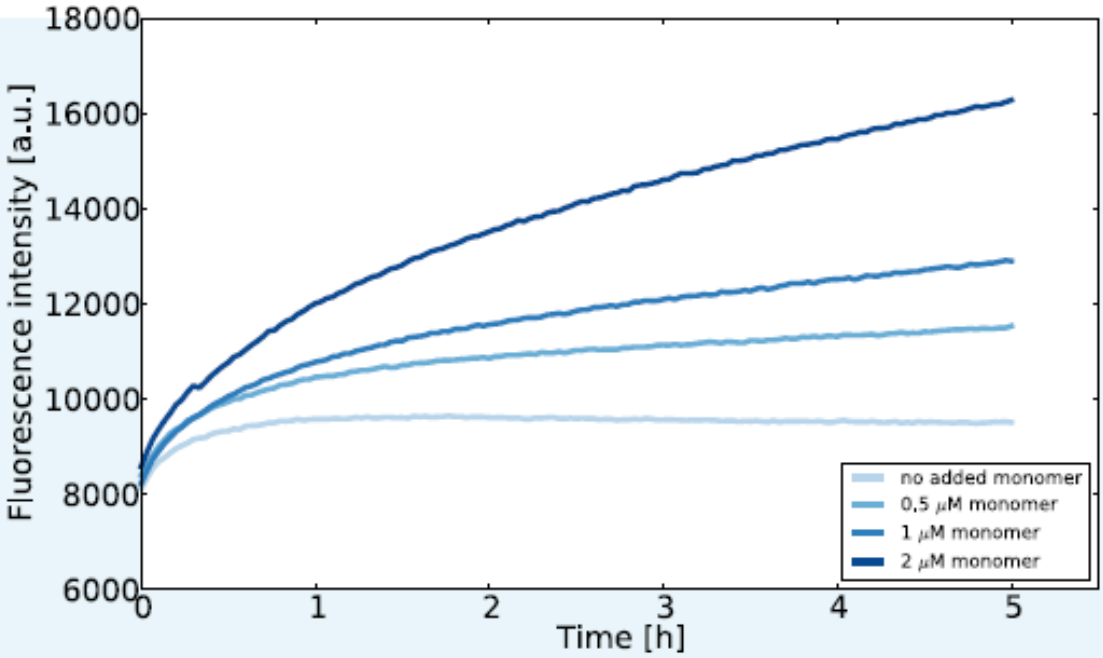

Appendix 1—figure 2. Seeded aggregation experiments at low monomer concentrations designed to estimate the concentration of monomeric α-synuclein in equilibrium with fibrils. The seed concentration is in all cases 0.75 µM and the ThT concentration is 10 µM. The experiment was performed at room temperature in order to slow the reaction down and avoid temperature effects on the fluorescence upon introduction of the multiwell plate into the fluorescence platereader.

The results of these experiments are shown in ***Appendix 1—figure 2***. We find that even at a concentration as low as 0.5 µM, the slight increase over time of Thioflavin-T fluorescence suggests that the fibril mass increases. This result is significant, given that the ThT fluorescence in a sample that contains only fibrils decreases over time. The fact that all samples, including that measured in the absence of added α-synuclein monomer, show an increase in ThT fluorescence during the first hour could be explained through sedimentation processes. We have shown previously that the sedimentation of fibrils can lead to an increase in detected ThT signal if the fluorescence is read from the bottom of the multiwell plate (***Buell et al., 2014a***). However, the subsequent increase in fluorescence intensity over several hours at concentrations of 0.5 μM or higher suggests an increase in fibril mass, and hence that the critical concentration under these conditions is lower than 0.5 μM.

Appendix 2

Analysis of weakly seeded aggregation data at mildly acidic pH

Aggregation experiments were also performed at very low (nM) seed concentrations at mildly acidic pH and under quiescent conditions, where it has been shown that autocatalytic secondary nucleation of α-synuclein amyloid fibrils plays an important role (***Buell et al., 2014a***). In the present study, we performed these aggregation experiments in 20 mM sodium acetate buffer at pH 5.0, well below the threshold for secondary nucleation (***Buell et al., 2014a***).

In order to quantitatively analyse the effects that AS69 and AS69fusASN exert on secondary nucleation, we started with the following equation describing the maximum aggregation rate in the presence of autocatalytic secondary nucleation (***Cohen et al., 2011***):

$$r_{\max} = \frac{M(\infty)\kappa}{e} \qquad \kappa = \sqrt{2m(0)^{n_2}[m(0)k_+ - k_{\text{off}}]k_2} \tag{13}$$

Where $M(\infty)$ is the long time limit of the fibrillar mass concentration, $m(0)$ is the starting concentration of monomeric α-synuclein, n_2 is the effective nucleus size of secondary nucleation, k_+ and k_{off} are the rate constants of elongation and de-polymerisation respectively, and k_2 is the rate constant of secondary nucleation. For our analysis, we assumed the rate of de-polymerisation to be negligible and that $M(\infty)$ was not altered by the presence of AS69. Furthermore we use the upper limit of how much monomer the AS69 could possibly sequester, which is equal to the AS69 concentration. Under these assumptions, the maximum rates relative to the case where no inhibitor was present can be described as:

$$\frac{r_{\max,I}}{r_{\max,0}} = \left(1 - \frac{I}{m(0)}\right)^{\frac{n_2+1}{2}} \tag{14}$$

Where $r_{\max,0}$ is the maximal aggregation rate in the absence of inhibitor, $r_{\max,I}$ is the maximal aggregation rate at inhibitor concentration I . The values of $r_{\max,I}$ for each kinetic trace were found by applying the gradient function from numpy and smoothing the resulting curves using a ten-point sliding average. The maxima of the resulting curves were taken to be $r_{\max,I}$. For the simulations, n_2 was varied in order to test whether the sequestration of monomer in conjunction with a higher reaction order of secondary nucleation can explain the observed strong inhibitory effect. However, even a value of n_2 as high as five was not able to explain the strong decrease in aggregation rate as a function of increasing inhibitor concentration. Therefore, we conclude that monomer sequestration cannot explain the highly efficient inhibition of secondary nucleation by AS69.

In the main manuscript, we discuss that the efficient inhibition of secondary nucleation by AS69 is likely to stem either from an interaction of AS69 alone or of the AS69:α-synuclein complex with an oligomeric aggregation intermediate. Given the low population of nuclei/oligomers compared to monomers during the aggregation time course, as well as the high affinity of the AS69 for monomeric α-synuclein, its affinity for such intermediate species would have to be significantly higher than that to monomers. This can be illustrated with a simple argument. At the end of an aggregation experiment, the fibrils typically are up to several micrometers in length, corresponding to thousands of protein molecules per fibril. Therefore, the total number of 'on pathway' oligomers that has formed during the aggregation process is three to four orders of magnitude smaller than the initial monomer concentration. In order to trap a significant fraction of these intermediates in the presence of a large excess of monomer, the affinity of AS69 to these intermediates would therefore have to be at least three orders of magnitude higher than that for monomer and hence be in the picomolar regime.

The alternative explanation, the binding of the AS69:α-synuclein complex to the aggregation intermediate, is more plausible. A clear inhibitory effect is still observed at a ratio

α-synuclein:AS69 of 100:1, which according to the estimate above corresponds to at least one order of magnitude more AS69:α-synuclein complex than 'on pathway'-intermediate, rendering an efficient interference with the nucleation process plausible. Therefore, we propose a model whereby rather than requiring the binding of free AS69 to an aggregation intermediate, the AS69:α-synuclein complex is able to incorporate into a fibril precursor and efficiently prevent it from undergoing the structural rearrangement required to transform into a growth-competent amyloid fibril.

Appendix 3

Determination of the lipid-induced aggregation rate

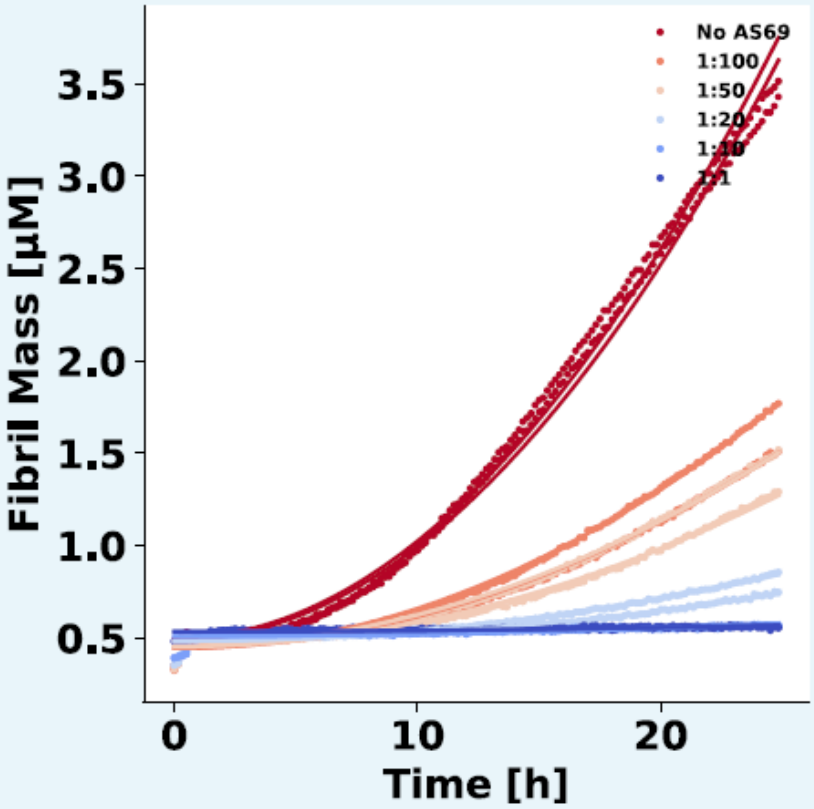

Appendix 3—figure 1. Analysis of the inhibition of the lipid-induced aggregation of α-synuclein by AS69.

The change in mass concentration of fibrils with time M(t) during the early time points of the lipid-induced aggregation of α-synuclein aggregation was fitted using the single-step nucleation model described previously (***Galvagnion et al., 2015***) and the following equation (***Meisl et al., 2016***):

$$M(t) = \frac{K_M k_+ m(0)^{n+1} k_n b t^2}{2(K_M + m(0))} \quad (15)$$

where k_+ is the elongation rate constant of fibrils from lipid vesicles, k_n is the heterogeneous primary nucleation rate constant, n is the reaction order of the heterogeneous primary nucleation reaction relative to the free monomer m, b is the total mass concentration of the protein bound to the lipid at 100% coverage ($b = \frac{[\mathrm{DMPS}]}{L}$, with L the stoichiometry) and K_M is the Michaelis constant which defines the concentration of soluble protein above which the elongation rate no longer increases linearly (fixed at 125 μM; ***Galvagnion et al., 2015***). The data was normalised such that the final amount of fibril mass was set to $2b$ for the traces where no AS69 was present as it was previously shown that the fibril mass is proportional to the concentration of DMPS (***Galvagnion et al., 2015***). A quadratic equation of the form $M(t) = at^2$, was fitted to the early time points of the normalised aggregation data (see Appendix 3 subsection 3) where $a = \frac{(K_M k_+ k_n)_{AS69} bm(0,[AS69])^{nAS69+1}}{2(K_{M\,AS69} + m(0,[AS69]))}$. The aggregation rate, $\frac{dM(t)}{dt}$ in the presence of

AS69 normalised by the rate in the absence of AS69, for the same initial concentrations of free monomer and monomer bound to the lipid, can be computed according to:

$$r = \frac{\left(\frac{dM(t)}{dt}\right)_{AS69}}{\left(\frac{dM(t)}{dt}\right)} = \left(\frac{(K_M k_n k_+)_{AS69} m(0,[AS69])^{n_{AS69}+1}}{K_{M,AS69} + m(0,[AS69])}\right) \times \left(\frac{K_M + m(0)}{K_M k_n k_+ m(0)^{n+1}}\right) \quad (16)$$

In order to test whether the lipid vesicle induced aggregation of α-synuclein in the presence of AS69 can be explained by monomer sequestration alone, we simulated the ratio r for different concentrations of AS69. Starting from ***Equation 15*** and assuming values of $k_n k_+$, K_M, b and n independent of AS69 (which amounts to the assumption that the presence of AS69 does not change the mechanism of aggregation, but merely inhibits through depleting the free monomer) and using $n+1 = 1.2$ (see ***Galvagnion et al., 2015*** for justification of $n = 0.2$) it can be shown that r takes the form:

$$r = \left(\frac{m(0,[AS69])^{1.2}}{m(0)^{1.2}}\right) \times \left(\frac{K_M + m(0)}{K_M + m(0,[AS69])}\right) \quad (17)$$

Where $m(0,[AS69])$ was calculated using ***Equation 10***. The result of this simulation is shown in ***Figure 9c***.

5.7 List of Figures

5.8 List of Tables

5.9 List of Abbreviations

°C	Degrees Celsius
BiFC	Bimolecular fluorescence complementation
CD	Circular dichroism
cm	centimeter
DGC	Density gradient centrifugation
DMPS	1,2-dimyristoyl-sn-glycero-3-phospho-L-serine
DSC	Differential scanning calorimetry
EGFP	Enhanced green fluorescent protein
h	hour
i.e.	that is
ITC	Isothermal titration calorimetry
mM	Millimolar
NAC region	Non-amyloid-β-component
nm	Nanometer
nM	Nanomolar
PD	Parkinson's disease
RNAi	RNA-Interference
s	second
SUV	Small unilamellar vesicles
synuclein-VC	Synuclein with the C-terminal segment of fluorescent protein Venus
T_m	Melting Temperature
VN-synuclein	Synuclein with the N-terminal segment of fluorescent proteinVenus
WT	Wildtype
µg	Mikrogramm
µM	Mirkomolar

Conclusions & Outlook 6

β-hairpins are a stable but simple secondary structure motif in proteins and gained interest in the field of amyloid diseases. There they seem to play an important role in the generation of fibrils the hallmarks of the most prominent neurodegenerative amyloid disease like Alzheimer's disease, Parkinson's disease, and Type II Diabetes. In this work the different projects look at the importance of β-hairpins from different viewpoints.

The first project aims to look at the potential of β-hairpins to be found throughout the whole human proteome and if the found sequences can be bound by the β-wrapin AS10 in the same way as the proteins from Alzheimer's disease, Parkinson's disease, and Type II Diabetes. With a bioinformatic approach fixed on the aggregation propensity and criteria derived from where α-synuclein, Aβ and IAPP have the same properties the human proteome could be successfully filtered. Looking at a test set of proteins it could be shown that despite being very different in sequence, properties, and not necessarily being in a β-hairpin structure when in the full protein some can be bound by AS10. It turns out that one of the tested sequences is involved in amyloid though in this case in functional amyloid, the semen amyloids. The found fragment is able to accelerate the aggregation of another fragment of the same protein and another both involved in the semen amyloids. According to literature and our own experiments the two protein fragments involved in semen amyloids are needed in high concentrations to aggregate by themselves, if the found β-hairpin fragment is added the concentration needed to aggregate is much lower. In conclusion to this project, it could be shown it is possible to find β-hairpin fragments with specific criteria in the human proteome and in turn a fragment was found that is able to accelerate the aggregation of functional amyloid in the way that lower concentrations of the involved proteins are needed.

In a second project two β-hairpin fragments, also filtered from the human proteome with the above mentioned bioinformatic approach, were used on α-synuclein to see if there is a difference in the aggregation behaviour. The fragments themselves are from two proteins used as model in the disease AL-amyloidosis a systemic amyloid disease. α-synuclein, the protein involved in Parkinson's disease, usually aggregates *in vitro* only with shaking, additional surfaces, like a glass bead, and also an air-water interface helps the aggregation and still it takes usually a few hours for the aggregation to occur. The kinetics of the aggregation can be

monitored by the dye thioflavin-T. Upon the addition of the two fragments, never at the same time, in different concentrations under the "classic" α-synuclein aggregation conditions no difference could be detected in the kinetics. When changing the conditions and for example removing the shaking or the glass bead or both, conditions where α-synuclein normally does not aggregate by itself, aggregation is possible again depending on the concentration of the fragments. In addition, when the N- or C-terminus of α-synuclein is removed and under the same conditions the aggregation behaviour changes depending on which part of α-synuclein is removed. When looking at the endpoint of the aggregation kinetics under the AFM the samples look different, from α-synuclein alone, depending on the fragment, the concentration of the fragment, the α-synuclein version and salt concentration used. In conclusion, in this project it was shown that β-hairpin fragments can accelerate aggregation or can even make aggregation possible in conditions where the amyloidogenic protein does not aggregate on its own. Specifically, here it seems that the primary cause is the difference in electrostatics between peptide fragment and protein, as shown by one of the truncated α-synuclein versions that has close to the same pI as the two fragments and only aggregates when the salt concentrations are clearly elevated.

In the third project the focus was more on the β-wrapin AS69. AS69 is able to bind the β-hairpin region in the α-synuclein sequence and through this can inhibit the aggregation of α-synculein. The goal of this project was to optimize the β-wrapin AS69 to be an even better binder to α-synuclein. To attain this goal two different ways were used one the one hand through phage display and on the other hand molecular simulations. The cloning and purification of the new AS69 constructs was straightforward. The method to test if the binding is better than the wildtype isothermal titration calorimetry (ITC) was used. Neither the constructs from phage display nor the constructs from the molecular dynamic simulations were better binders to a-synuclein than the wildtype AS69. Concerning the molecular dynamic simulations, the simulated binders may have not been better than the wildtype but other simulated characteristics like the enthalpy and entropy and their calculated values were similar in the simulations and in the experiments which is a great success. It seems that in experiments entropy and enthalpy seem to overcompensate each other. In another part of this project first steps towards a high throughput screening assay to scan for small molecules as inhibitors against α-synuclein were taken. Here fluorescence polarization was used to get first answer if a compound is a positive or negative hit. In conclusion the optimization of AS69 for α-synuclein was not successful in

this case but especially concerning the molecular dynamic simulations there are other properties of the simulations could be replicated in *in vitro* experiments.

The fourth project deals with the full-length proteins LEN and SMA which are variable light chains and can be used as a model system for the systemic amyloidosis AL amyloidosis. These two proteins also carry β-hairpin sequences that have the same criteria as α-synuclein, Aβ and IAPP and the β-hairpin sequences were also found by the bioinformatic approach from project one and used as β-hairpin peptides with α-synuclein in project two. Here the objective was to establish a protocol for the expression and purification of the two variable light chains in way that they are, in the best case, correctly folded at the end of the purification. Both expression and purification could be developed for both proteins but can surely be further optimized. In a second step the aggregation behaviour of both proteins was studied and if the β-wrapin AS10 can bind and inhibit the aggregation of both proteins. The structure of both proteins must first be destabilized for them to aggregate. In this case it was tried with guanidinium hydrochloride and in one case with a drastic pH shift. Both attempts were only successful in one case for LEN and not at all for SMA. Furthermore, it was tested in which of those destabilizing conditions the β-wrapin AS10 was still stable enough to be functional and while it was surprisingly stable the conditions in which LEN aggregated it was not functional anymore. In conclusion it was possible to find establish a protocol to express both full variable light chains in *Escherichia coli* and purify them, although this protocol can surely be further optimized to get a better yield. The aggregation of LEN and SMA was not reliably reproducible but only guanidinium hydrochloride and in the case of SMA a pH shift was tried, other denaturants could yield more reliable results and find conditions were also the β-wrapin AS10 stays functional.

All in all, this thesis looked at β-hairpins from different points of view and showed that in the field of amyloids and not only in the most common neurodegenerative diseases but also in the functional amyloid and systemic amyloids the role of β-hairpins should not be underestimated and overlooked. β-hairpins, as shown, can accelerate aggregation or even make aggregation possible in different ways, be it by making it possible for a protein to aggregate at lower concentrations or aggregate without specific conditions that are normally necessary for the aggregation and all that without having sequence similarity between the aggregating protein and the β-hairpin. They can be used to inhibit aggregation by being a binding motif for example for the β-wrapins used in thesis or later be targeted by small molecules. Despite having no sequence familiarity between them the known β-hairpin motifs in the proteins from the most common neurodegenerative diseases α-synuclein, Aβ and IAPP share enough characteristics

that it is possible to develop a bioinformatic approach to find more β-hairpins throughout the whole human proteome. Of course, this thesis only looked at β-hairpins in *in vitro* studies, but it could be interesting if some aspects can be transferred to more *in vivo* related studies. Finally, β-hairpins are a topic that still deserves some attention especially in combination with amyloid and not only amyloid diseases but also concerning functional amyloid.